Copy 280

[redacted]

NASA MEMO 4-27-59L

NASA MEMO 4-27-59L

NASA

MEMORANDUM

INVESTIGATION OF THE AERODYNAMIC CHARACTERISTICS OF A 0.067-SCALE MODEL OF THE X-15 AIRPLANE (CONFIGURATION 2) AT MACH NUMBERS OF 2.29, 2.98, 3.96, AND 4.65

By Arthur E. Franklin and H. Norman Silvers

Langley Research Center
Langley Field, Va.

CLASSIFIED DOCUMENT - TITLE UNCLASSIFIED

This material contains information affecting the national defense of the United States within the meaning of the espionage laws, Title 18, U.S.C., Secs. 793 and 794, the transmission or revelation of which in any manner to an unauthorized person is prohibited by law.

NATIONAL AERONAUTICS AND SPACE ADMINISTRATION
WASHINGTON
May 1959

[redacted]

288

2 cds removed 20 Jan 64 fa

[redacted]

NATIONAL AERONAUTICS AND SPACE ADMINISTRATION

MEMORANDUM 4-27-59L

INVESTIGATION OF THE AERODYNAMIC CHARACTERISTICS OF A 0.067-SCALE MODEL OF THE X-15 AIRPLANE (CONFIGURATION 2) AT MACH NUMBERS OF 2.29, 2.98, 3.96, AND 4.65*

L
2
2
9

By Arthur E. Franklin and H. Norman Silvers

SUMMARY

An investigation was made in the Langley Unitary Plan wind tunnel to determine the drag, static longitudinal and lateral stability characteristics, and control-surface bending- and torsion-moment characteristics of a 0.067-scale model of the X-15 airplane (configuration 2). The investigation was made at Mach numbers of 2.29, 2.98, 3.96, and 4.65 at a Reynolds number of about 2.6×10^6. In addition, the effect of Reynolds number was shown at Mach numbers of 2.98 and 4.65 by results obtained at Reynolds numbers of about 1.0×10^6 and 4.2×10^6.

INTRODUCTION

The development of the X-15 research airplane is a coordinated effort between the United States Air Force, the United States Navy, and the National Aeronautics and Space Administration. As part of the development program, an investigation of the aerodynamic characteristics and surface bending- and torsion-moment characteristics of a 0.067-scale model of the X-15 (configuration 2) has been made in the Langley Unitary Plan wind tunnel. The results of this investigation are presented herein without analysis. Some results obtained in an investigation of the low-speed stability and control characteristics of the configuration of the present tests are presented in reference 1.

*Title, Unclassified.

[redacted]

280

[redacted]

SYMBOLS

The longitudinal characteristics of the model are referred to the stability system of axes. The lateral characteristics of the model are referred to the body system of axes. The systems of axes used and the positive directions of forces, moments, and angles are shown in figure 1. The moments of the model are presented about a point located at the 0.25-chord point of the mean geometric chord and on the fuselage reference line (chord plane of the wing mean geometric chord). The control-surface bending moments are presented about the root chord of the surface and the torsion moments are presented about the hinge line of the surface.

I 2 2 9

b — wing or panel span, in.

c — chord, in.

$\bar{c}$ — wing or panel mean geometric chord, in.

C_D — drag coefficient, $\frac{\text{Drag}}{qS}$

C_{D_b} — base drag coefficient, $\frac{\text{Base drag}}{qS}$

C_L — lift coefficient, $\frac{\text{Lift}}{qS}$

C_m — pitching-moment coefficient, $\frac{\text{Pitching moment}}{qS\bar{c}}$

C_l — rolling-moment coefficient, $\frac{\text{Rolling moment}}{qSb}$

C_n — yawing-moment coefficient, $\frac{\text{Yawing moment}}{qSb}$

C_Y — side-force coefficient, $\frac{\text{Side force}}{qS}$

C_{L_α} — lift-curve slope ($\alpha \approx 0^\circ$), $\frac{\partial C_L}{\partial \alpha}$

$C_{m_{C_L}}$ — pitching-moment-curve slope (C_L at $\alpha \approx 0^\circ$), $\frac{\partial C_m}{\partial C_L}$

$C_{m_{i_t}}$ — stabilizer effectiv[redacted]er ($i_t \approx 0^\circ$), $\frac{\partial C_m}{\partial i_t}$

[redacted]

[redacted]

C_{l_β} effective-dihedral parameter $(\beta \approx 0^\circ)$, $\frac{\partial C_l}{\partial \beta}$, per degree

$C_{l_{\delta_r}}$ roll-control effectiveness parameter $(\delta_r \approx 0^\circ)$, $\frac{\partial C_l}{\partial \delta_r}$

$C_{l_{\delta_v}}$ rolling-moment parameter due to yaw-control deflection $(\delta_v \approx 0^\circ)$, $\frac{\partial C_l}{\partial \delta_v}$

C_{n_β} directional stability parameter $(\beta \approx 0^\circ)$, $\frac{\partial C_n}{\partial \beta}$, per degree

$C_{n_{\delta_r}}$ yawing-moment parameter due to roll-control deflection $(\delta_r \approx 0^\circ)$, $\frac{\partial C_n}{\partial \delta_r}$

$C_{n_{\delta_v}}$ yaw-control effectiveness parameter $(\delta_v \approx 0^\circ)$, $\frac{\partial C_n}{\partial \delta_v}$

C_{Y_β} side-force parameter $(\beta \approx 0^\circ)$, $\frac{\partial C_Y}{\partial \beta}$, per degree

C_B root-bending-moment coefficient on the surface panel, $\frac{\text{Bending moment}}{q(Sb)_{surface}}$

C_T torsion-moment coefficient on the surface panel about the surface hinge line, $\frac{\text{Torsion moment}}{q(S\bar{c})_{surface}}$

i_t pitch-control angle (positive as shown in figure 1(c)), $\frac{\delta_{H_R} + \delta_{H_L}}{2}$, deg

$(L/D)_{max}$ maximum lift-drag ratio

M free-stream Mach number

q free-stream dynamic pressure, lb/sq ft

[redacted]

[redacted]

R	Reynolds number
S	wing or panel area (includes body intercept for wing area only), sq ft
α	angle of attack referred to fuselage reference line, deg
β	angle of sideslip referred to model plane of symmetry, deg
δ_s	speed-brake deflection, deg
δ_r	roll-control angle $\left(\text{positive when trailing edge of } \delta_{H_R} \text{ is down with respect to trailing edge of } \delta_{H_L}\right)$, $\delta_{H_R} - \delta_{H_L}$, deg
δ_v	yaw-control angle (positive as shown in fig. 1(c)), deg

Subscripts:

H	horizontal tail
L	left
min	minimum
R	right
v	vertical tail
w	wing
O	value taken at zero lift coefficient

Configuration component designation:

F	fuselage
H	horizontal tail
S	speed brakes open 45° with respect to closed position
V	vertical tail
W	wing

[redacted]

[redacted]

APPARATUS AND MODELS

The tests were conducted in the high Mach number test section of the Langley Unitary Plan wind tunnel. This tunnel is a variable-pressure, continuous, return-flow type. The test section is 4 feet square and approximately 7 feet in length. The nozzle leading to the test section is of the asymmetric sliding-block type. Mach numbers may be varied continuously through a Mach number range from approximately 2.29 to 4.65 without tunnel shutdown.

L
2
2
9

Photographs of the model are presented as figure 2. Details of the test model and model components are shown in figures 3, 4, and 5. Geometric characteristics are presented in table I.

The basic model has a wing with 25.6° sweepback of the quarter chord, an aspect ratio of 2.50, a taper ratio of 0.20, dihedral angle of 0°, and a modified NACA 66-005 airfoil section. The aspect ratio and taper ratio of the control surfaces are based on the exposed portions of the surfaces and are referred to as panel characteristics. The horizontal tail, shown in figure 4, has 45.0° sweepback of the quarter chord, an aspect ratio of 2.80, a taper ratio of 0.21, dihedral angle of -15°, and a modified NACA 66-005 airfoil section. The vertical tail, shown in figure 5, has a sweepback of 22.0° at the quarter chord, a panel aspect ratio of 1.24, a taper ratio of 0.28, and a double-wedge airfoil section with a blunt trailing edge and an area ratio between the vertical tail area and total wing area of 0.193. The ventral fin, shown in figure 5, has 52.4° sweepback of the quarter chord, a panel aspect ratio of 0.28, a taper ratio of 0.64, and a double-wedge airfoil section with a blunt trailing edge, and an area ratio between the ventral fin and total wing area of 0.056. The speed brakes, shown in figure 5, are formed by wedges which simulate hinged panels of the rear wedge surfaces of both the ventral-fin and vertical-tail surfaces. The speed brakes extend from the tip chord to the root chord of the tail surfaces and from the speed-brake hinge line to trailing edges of the vertical tail. The speed brakes open 45° relative to their closed position.

Model forces and moments were measured by means of a six-component, electrical strain-gage balance. This balance was attached by means of a sting to the tunnel central support system.

An additional component of the model support system was a remotely operated adjustable coupling that enabled tests to be performed at variable sideslip angles concurrently with variable angles of attack. This coupling was placed between the model sting and the tunnel central support system.

[redacted]

[redacted]

The vertical tail and both horizontal-tail panels were independently remotely actuated. Position indication of control-surface angles was accomplished by a differential transformer attached to the control-surface linkage. Both horizontal-tail panels and the vertical tail were equipped with strain gages to measure the root bending moments and torsional moments of the panels. The left wing panel was equipped with a strain gage to measure wing root bending moment.

TESTS

Tests were made through an angle-of-attack range from approximately L
-4° to 20° at about 0°, -5°, and -10° angles of sideslip. All basic 2
model tests were made with a horizontal-tail deflection angle of 0°. 2
9

The Mach numbers, stagnation and dynamic pressures, and Reynolds numbers of the tests are listed in the following table:

M	Stagnation pressure, lb/sq in. abs	Dynamic pressure, lb/sq ft	Reynolds number
2.29	20.34	910	2.64×10^{6}
2.98	11.52	290	1.04
	28.35	705	2.56
	46.38	1,150	4.18
3.96	47.80	510	2.60
4.65	39.45	248	1.46
	67.62	425	2.50
	101.22	630	3.75

The Reynolds numbers are based on the mean geometric chord of the wing. The dewpoint for all tests was maintained below -30° F to prevent adverse condensation effects. The stagnation temperature was maintained at 150° F for all Mach numbers except 4.65, for which it was 175° F.

[redacted]

CORRECTIONS AND ACCURACY

The calibration of the flow in the test section which was completed subsequent to this investigation has shown that flow angularity exists. The values of flow angularity are 0.17°, 0.17°, 0.30°, and 0.75° for the test Mach numbers of 2.29, 2.98, 3.96, and 4.65, respectively. The results presented herein have been reduced to coefficients in which test-section flow angularity has been neglected. Moreover, the angles of attack presented do not include the increment in angle due to flow angularity.

L
2
2
9

The maximum deviation of local Mach number in the portion of the tunnel occupied by the model is ±0.015 from the average values listed in the preceding section.

The angles of attack and sideslip of the model have been corrected for the deflection of the model sting and balance under load. The control-surface angles were maintained at the desired deflection during the test by means of remotely operated electrically driven motors. Pretest calibration of the control-surface systems, however, revealed a certain amount of mechanical slop. The slop leads to the angular uncertainty of the control-surface deflections which are the values quoted in the table of accuracy presented in this section.

Pressure measurements were made at the base of the fuselage and at the base of the fuselage side fairings over the angle-of-attack range and Mach number range investigated. The base pressures have been used to adjust the level of drag coefficients presented herein to a condition of free-stream static pressure at the base of the fuselage and at the base of both side fairings of the fuselage. The drag coefficients used to make the adjustments are shown in figure 6. It will be noted (fig. 6) that a single value of fuselage-side-fairing base drag coefficient is used to adjust the results at every test Mach number, which indicates that angle of attack did not affect the level of fuselage-side-fairing base drag coefficient. This procedure was adopted subsequent to examination of the pressure measurements over the base of the fuselage side fairings for reasons of expediency in the reduction of data.

The estimated accuracy of the force and moment coefficients and angles based on calibration and repeatability of the data is as follows:

C_L	±0.0020
C_D	±0.0010
C_m	±0.0010
C_l	±0.0002

C_n	±0.0005
C_Y	±0.0015
$C_{T,v}$	±0.0015
$C_{B,v}$	±0.0015
$C_{B,H}$	±0.002
$C_{T,H}$	±0.002
$C_{B,w}$	±0.003
[1]α, deg	±0.10
β, deg	±0.10
δ_{H_L} and δ_{H_R}, deg	±0.20
δ_v, deg	±0.20

L
2
2
9

RESULTS

The results of an investigation of the aerodynamic and surface moment loading characteristics of an 0.067-scale model of the X-15 airplane (configuration 2) are presented in the figures and are organized as follows:

	Figures
Schlieren photographs of the model	7 to 11
Longitudinal stability characteristics:	
Effect of various model components	12
Effect of Reynolds number	13 and 14
Effect of various deflections of the horizontal-tail panels:	
Pitch-control deflections	15
Roll-control deflections	16
Effect of various deflections of the vertical tail	17 and 18
Summary of the longitudinal stability characteristics	19 and 20
Lateral stability characteristics:	
Effect of various model components	21
Effect of the vertical tail	22
Effect of Reynolds number	23 and 24
Effect of various deflections of the horizontal-tail panels:	
Pitch-control deflections	25
Roll-control deflections	26 and 27
Effect of various deflections of the vertical tail	28 and 29

[1]Values quoted do not include effect of test-section flow angularity.

It will be noted that the drag coefficients for the model with speed brakes open 45° are presented at a scale of 0.04 per inch, whereas the drag coefficients for the model with speed brakes closed are presented at a scale of 0.02 per inch.

The lateral stability coefficients were obtained at constant nominal angles of sideslip, whereas the model angle of attack was varied. As indicated, the angles of sideslip and attack have been corrected for deflection of the balance sting support under load. The corrected angles of sideslip are not presented in this paper. The lateral stability parameters C_{n_β}, C_{l_β}, and C_{Y_β} are, however, based on the coefficients presented and the corrected angles of sideslip. The lateral parameters were obtained by measurement of the slope near $\beta = 0^\circ$ of the lateral coefficients presented herein cross plotted as a function of angle of sideslip at constant angle of attack.

Langley Research Center,
National Aeronautics and Space Administration,
Langley Field, Va., February 9, 1959.

REFERENCE

1. Boisseau, Peter C.: Investigation of the Low-Speed Stability and Control Characteristics of a 1/7-Scale Model of the North American X-15 Airplane. NACA RM L57D09, 1957.

L
2
2
9

TABLE I

GEOMETRIC CHARACTERISTICS OF THE 0.067-SCALE MODEL

OF THE X-15 AIRPLANE (CONFIGURATION 2)

L
2
2
9

Wing[1]:	
Total area, sq ft	0.88
Exposed area, sq ft	0.46
Span, in.	17.87
Aspect ratio	2.50
Taper ratio	0.20
Sweepback of quarter-chord line, deg	25.6
Dihedral, deg	0.0
Incidence, deg	0.0
Geometric twist, deg	0.0
Airfoil section:	
Root	NACA 66-005 (modified)
Tip	NACA 66-005 (modified)
Root chord, in.	11.91
Tip chord, in.	2.38
Mean geometric chord:	
Length, in.	8.20
Distance, from the model center line, in.	3.47
Fuselage:	
Length, in.	39.16
Width (including side fairing), in.	5.90
Depth, in.	3.50
Frontal area, sq in.	9.90
Overall fineness ratio	11.17
Side area, sq in.	124.65
Canopy length, in.	10.84
Fineness ratio of canopy	9.61
Base area, sq in.	7.95
Side fairing base area, sq in.	2.14

[1]Total values unless otherwise noted.

TABLE I.- Concluded

GEOMETRIC CHARACTERISTICS OF THE 0.067-SCALE MODEL

OF THE X-15 AIRPLANE (CONFIGURATION 2)

Horizontal tail[2]:	
Total area, sq ft	0.49
Exposed area, sq ft	0.23
Span, in.	14.11
Aspect ratio	2.80
Taper ratio	0.21
Root chord, in.	8.01
Mean geometric chord:	
Length, in.	4.01
Distance from root chord, in.	1.96
Sweepback of quarter-chord line, deg	45.0
Dihedral, deg	-15.0
Geometric twist, deg	0.0
Airfoil section:	
Root	NACA 66-005 (modified)
Tip	NACA 66-005 (modified)
Tip chord, in.	1.68
Vertical tail[2]:	
Exposed area, sq ft	0.17
Span, in.	5.52
Aspect ratio	1.24
Taper ratio	0.28
Root chord, in.	6.91
Airfoil section:	
Root	10° double wedge (modified)
Tip	10° double wedge (modified)
Tip chord, in.	1.95
Ventral fin[2]:	
Exposed area, sq ft	0.05
Span, in.	1.40
Aspect ratio	0.28
Taper ratio	0.64
Root chord, in.	6.80
Airfoil section:	
Root	15° double wedge (modified)
Tip	15° double wedge (modified)

[2]Exposed values unless otherwise noted.

L
2
2
9

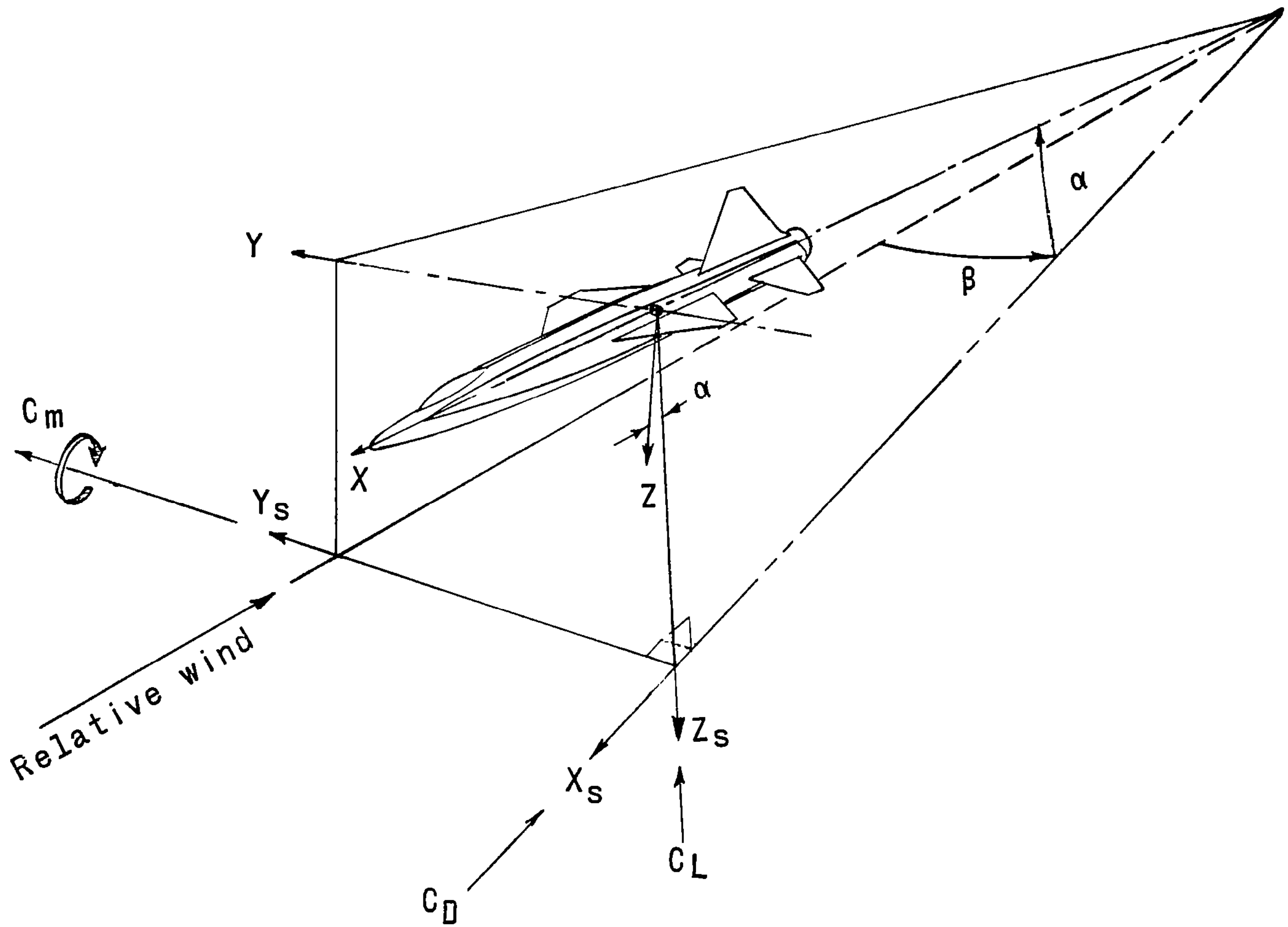

(a) Stability axes.

Figure 1.- Axes systems. Positive directions of forces, moments, and angles are indicated by arrows.

[redacted]

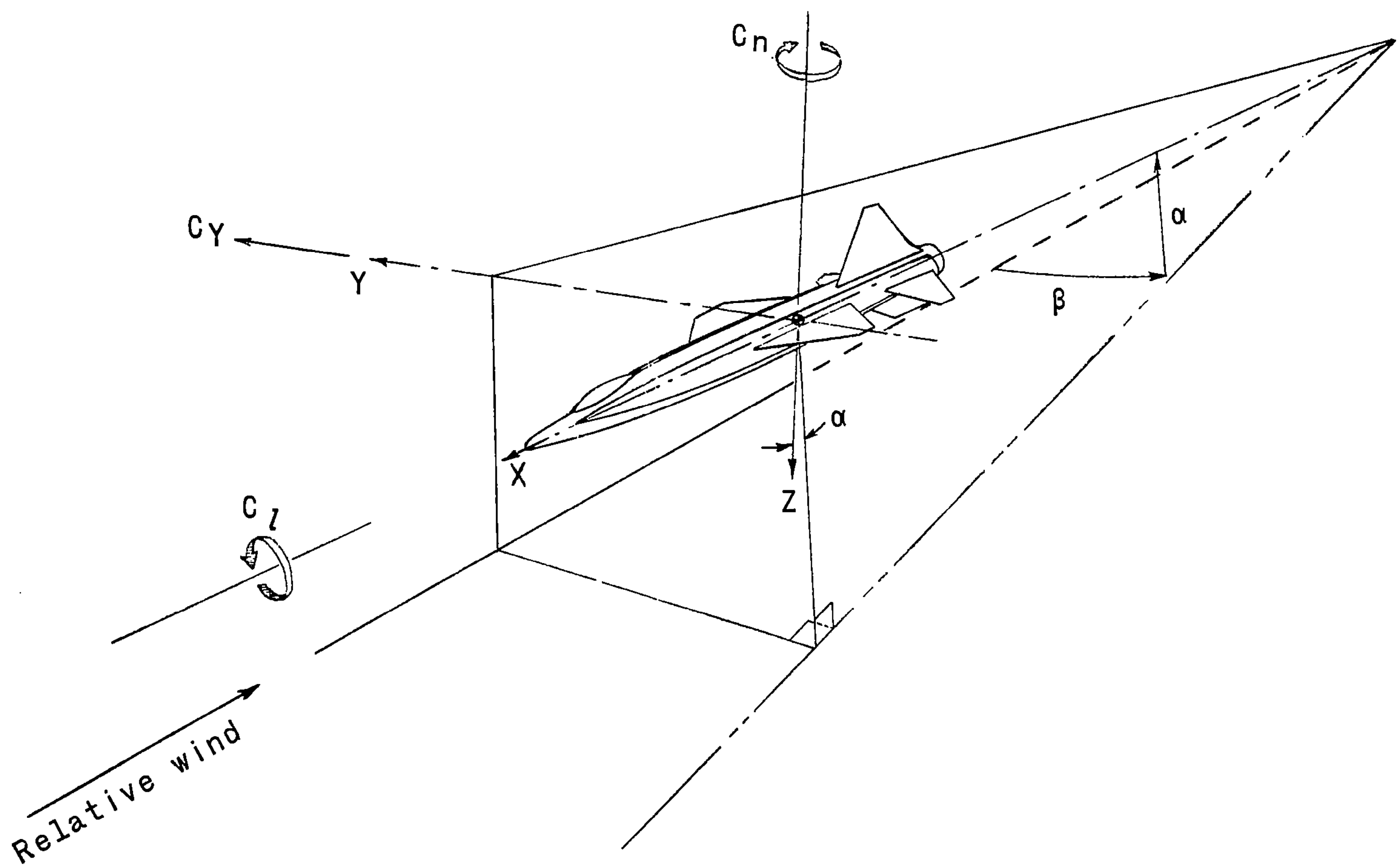

(b) Body axes.

Figure 1.- Continued.

[redacted]

L-229

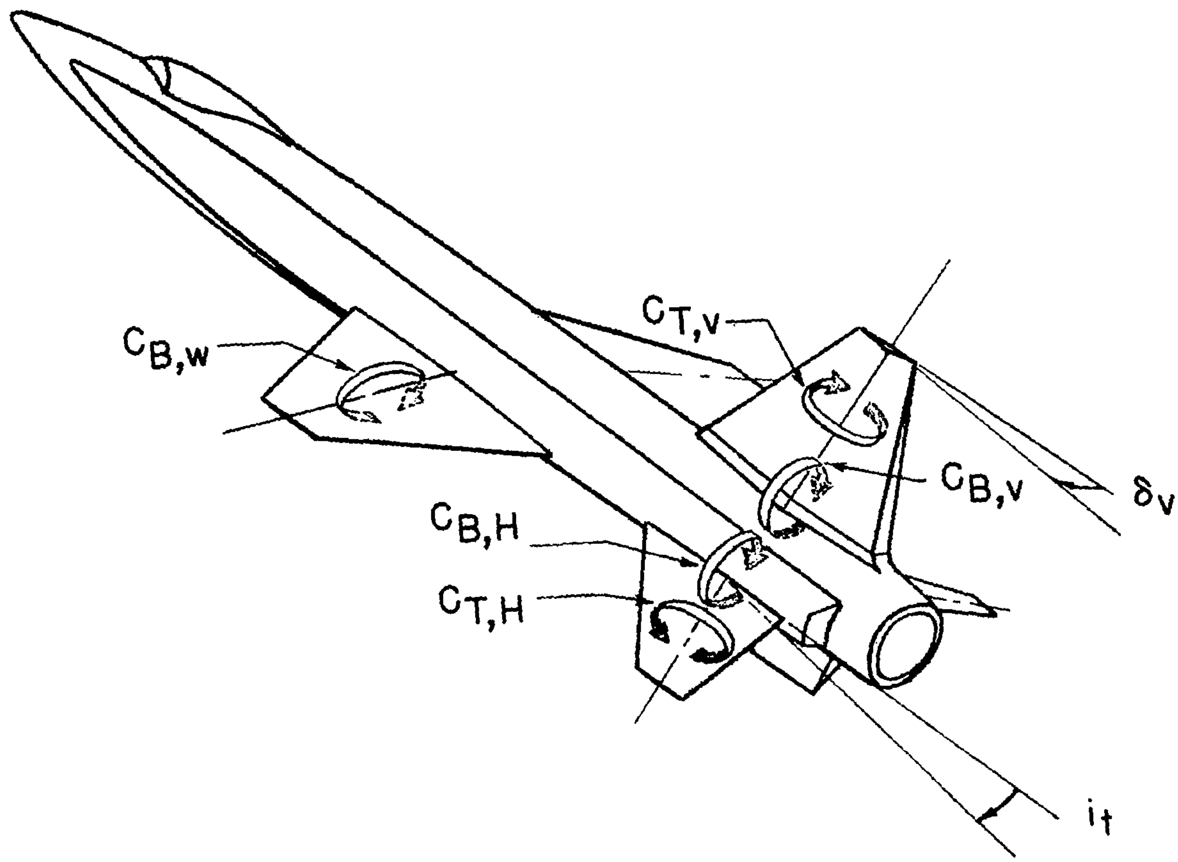

$$i_t = \frac{\delta_{H_R} + \delta_{H_L}}{2}$$

(c) Control-surface moments.

Figure 1.- Concluded.

[redacted]

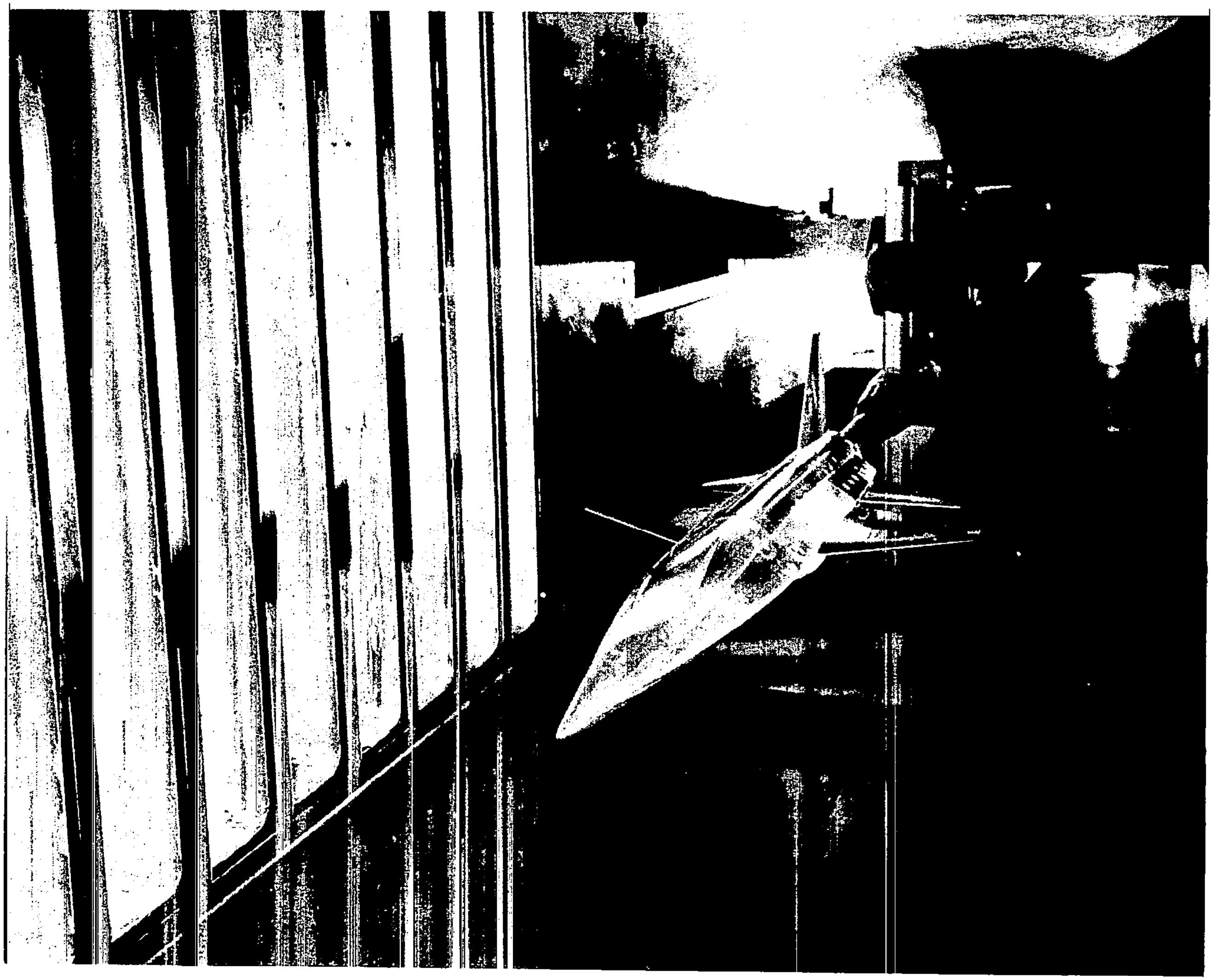

L-96458

Figure 2.- A 0.067-scale model of the X-15 airplane at the Langley Unitary Plan wind tunnel.

[redacted]

[redacted]

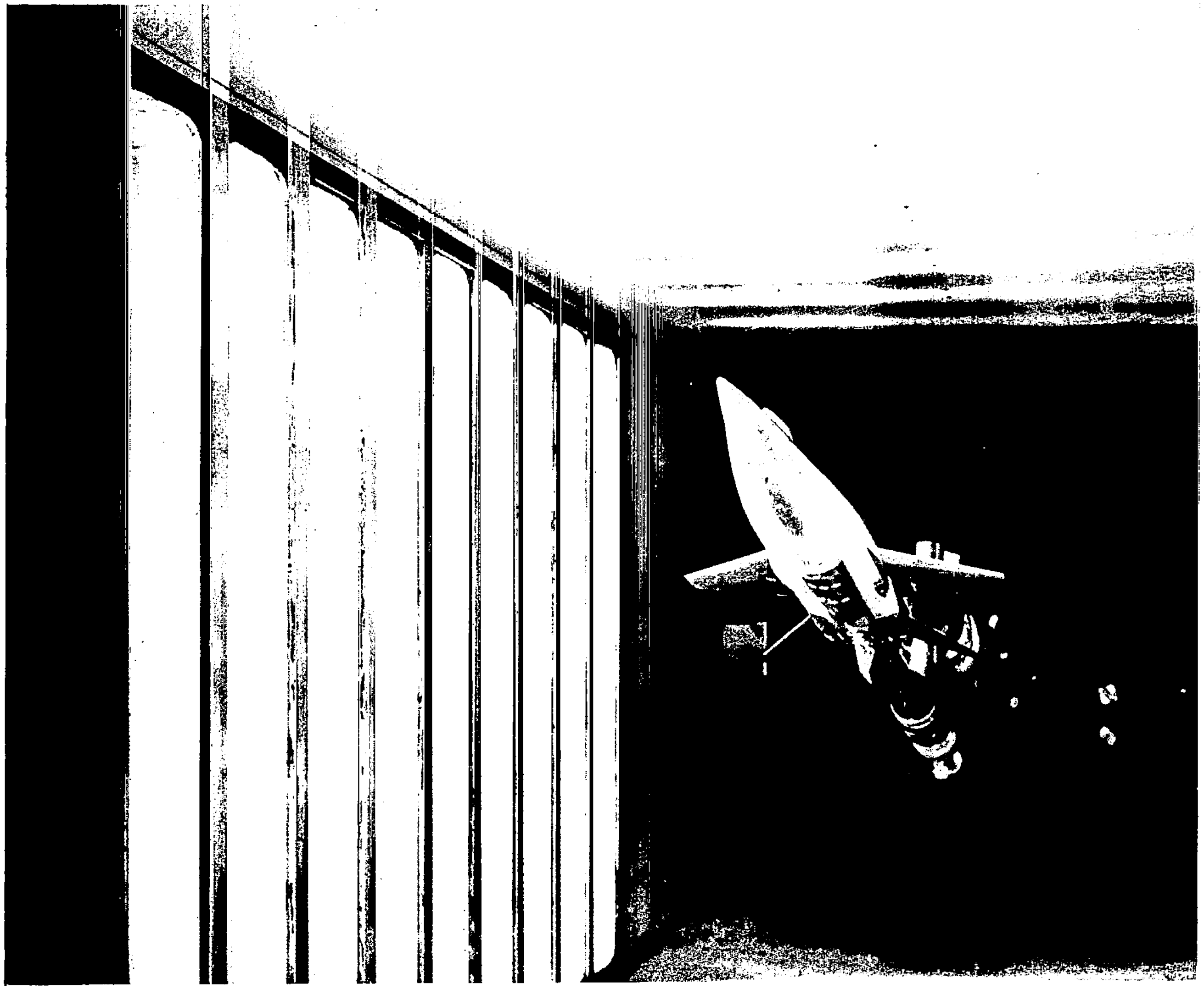

Figure 2.- Concluded. L-96459

[redacted]

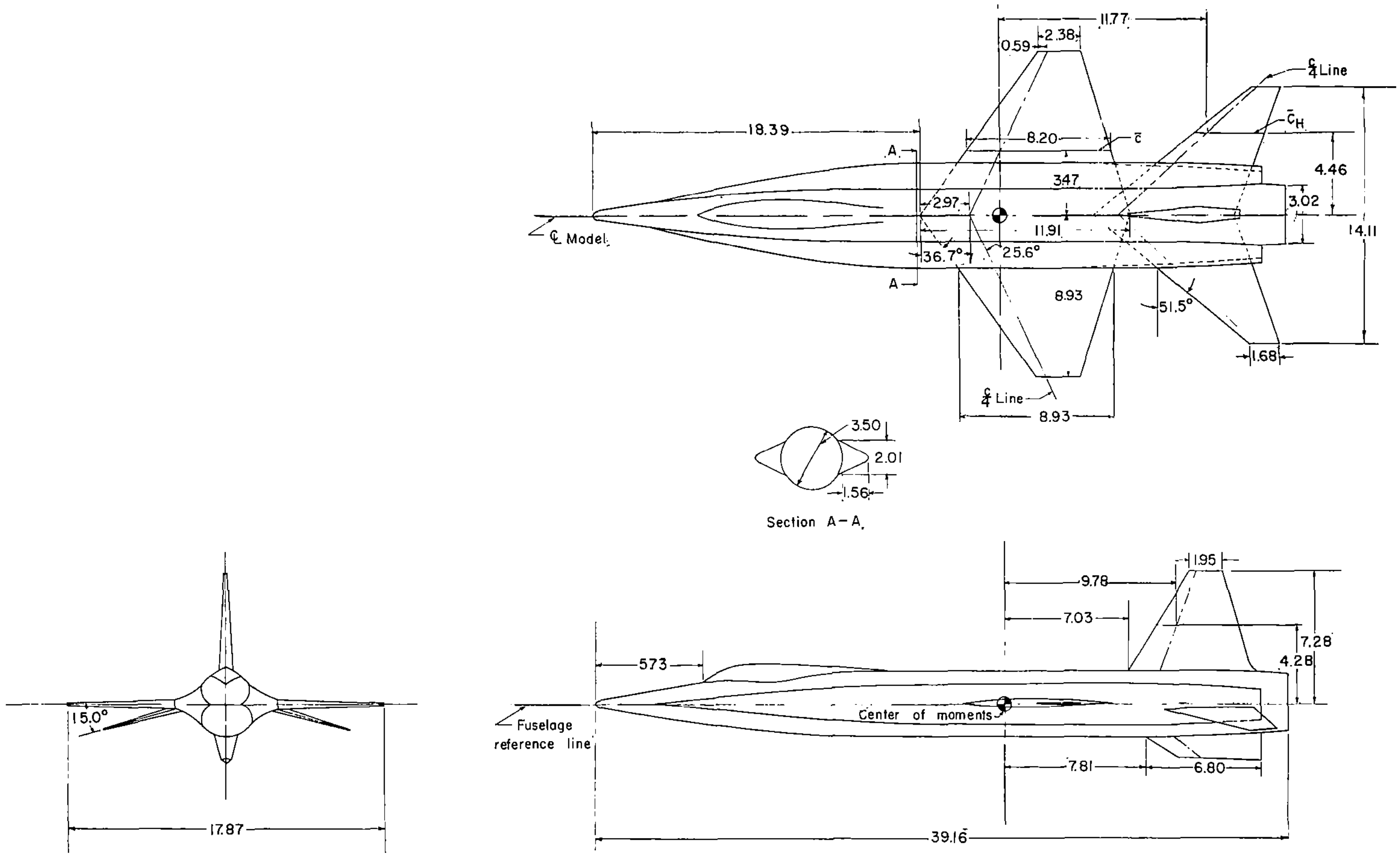

Figure 3.- Details of the 0.067-scale model of the X-15 airplane. Dimensions are in inches unless otherwise noted.

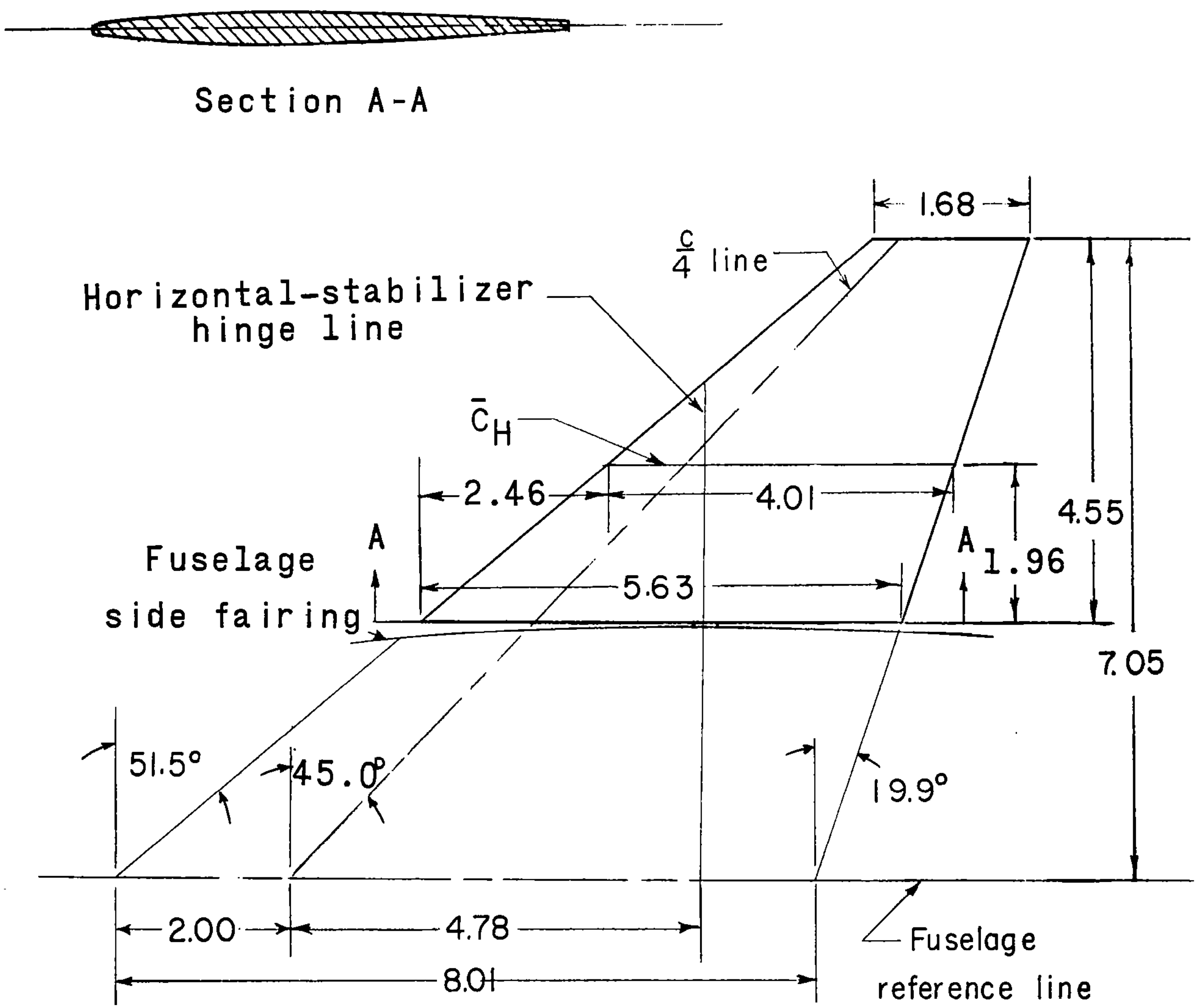

Figure 4.- Drawing of the horizontal stabilizer. Dimensions are in inches unless otherwise noted.

[redacted]

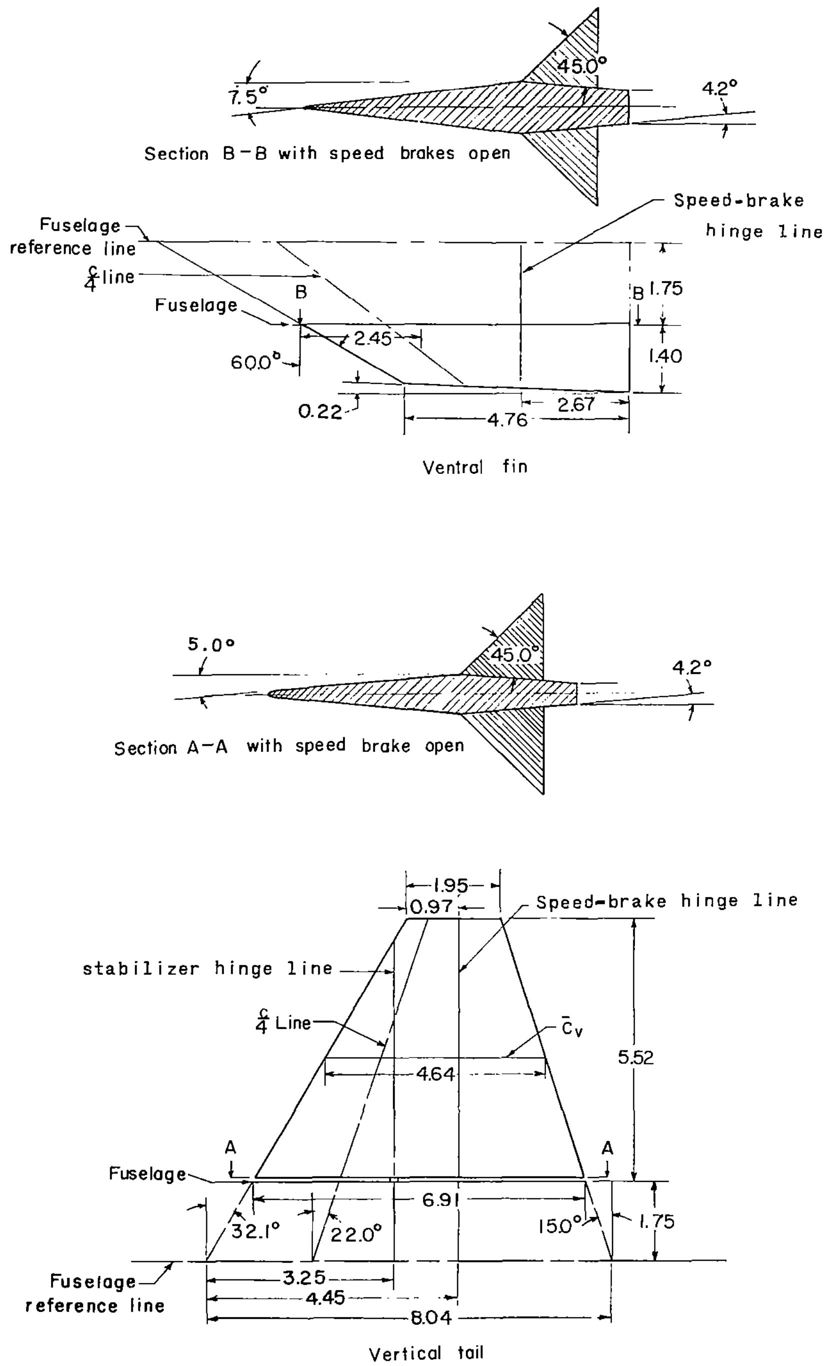

Figure 5.- Drawing of the vertical stabilizer of a 0.067-scale model of the X-15 airplane. Dimensions are in inches unless otherwise noted.

L-229

[redacted]

L-229

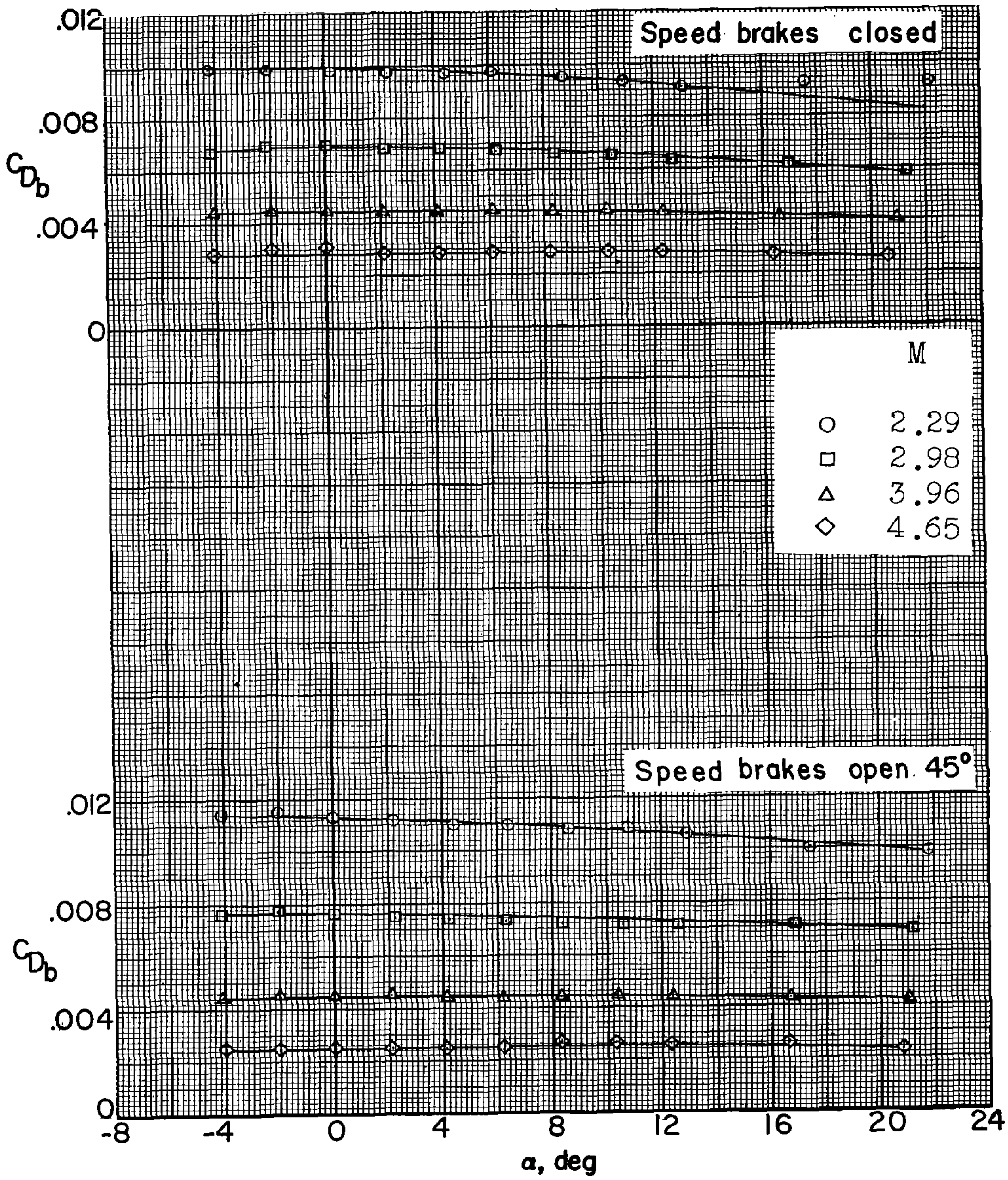

(a) Fuselage base drag coefficients.

Figure 6.- Base drag coefficients of a 0.067-scale model of the X-15 airplane at a nominal Reynolds number of 2.6×10^6.

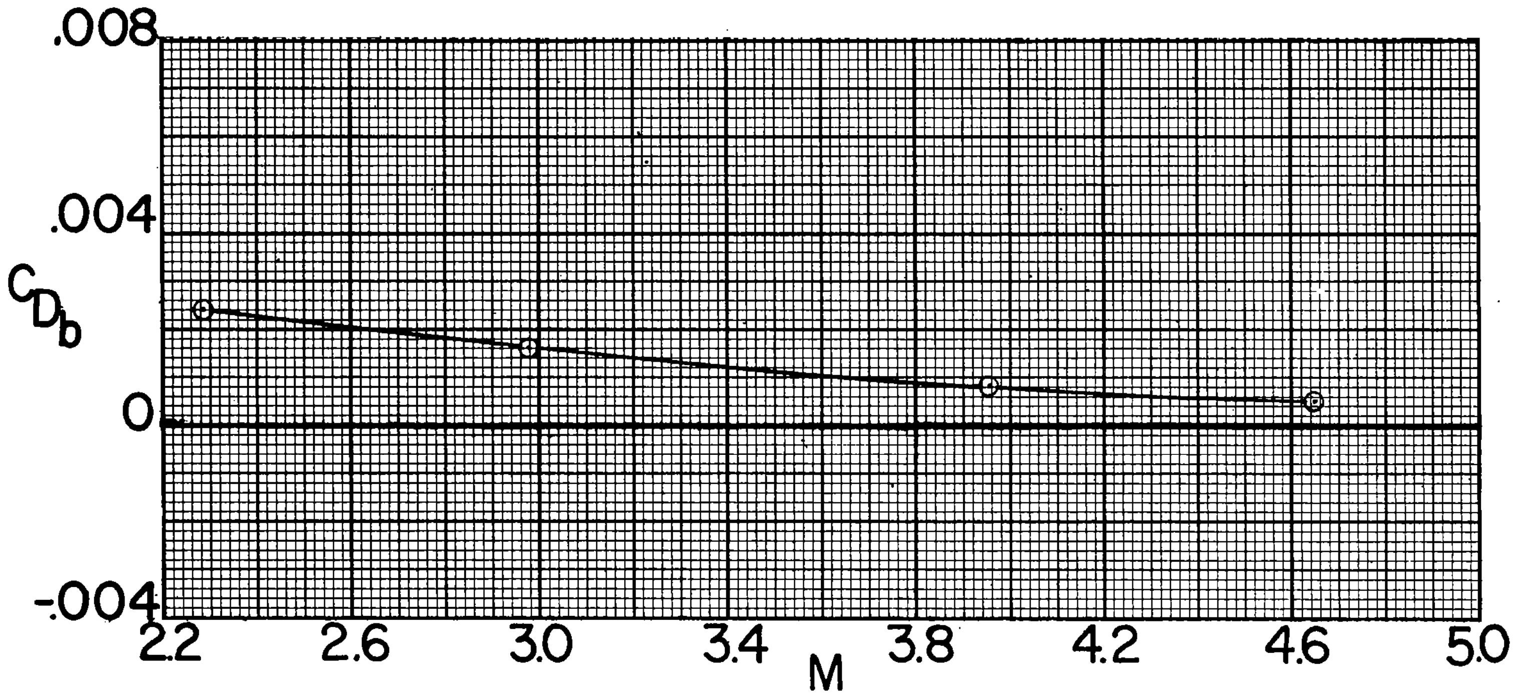

(b) Fuselage-side-fairing base drag coefficients.

Figure 6.- Concluded.

L-229

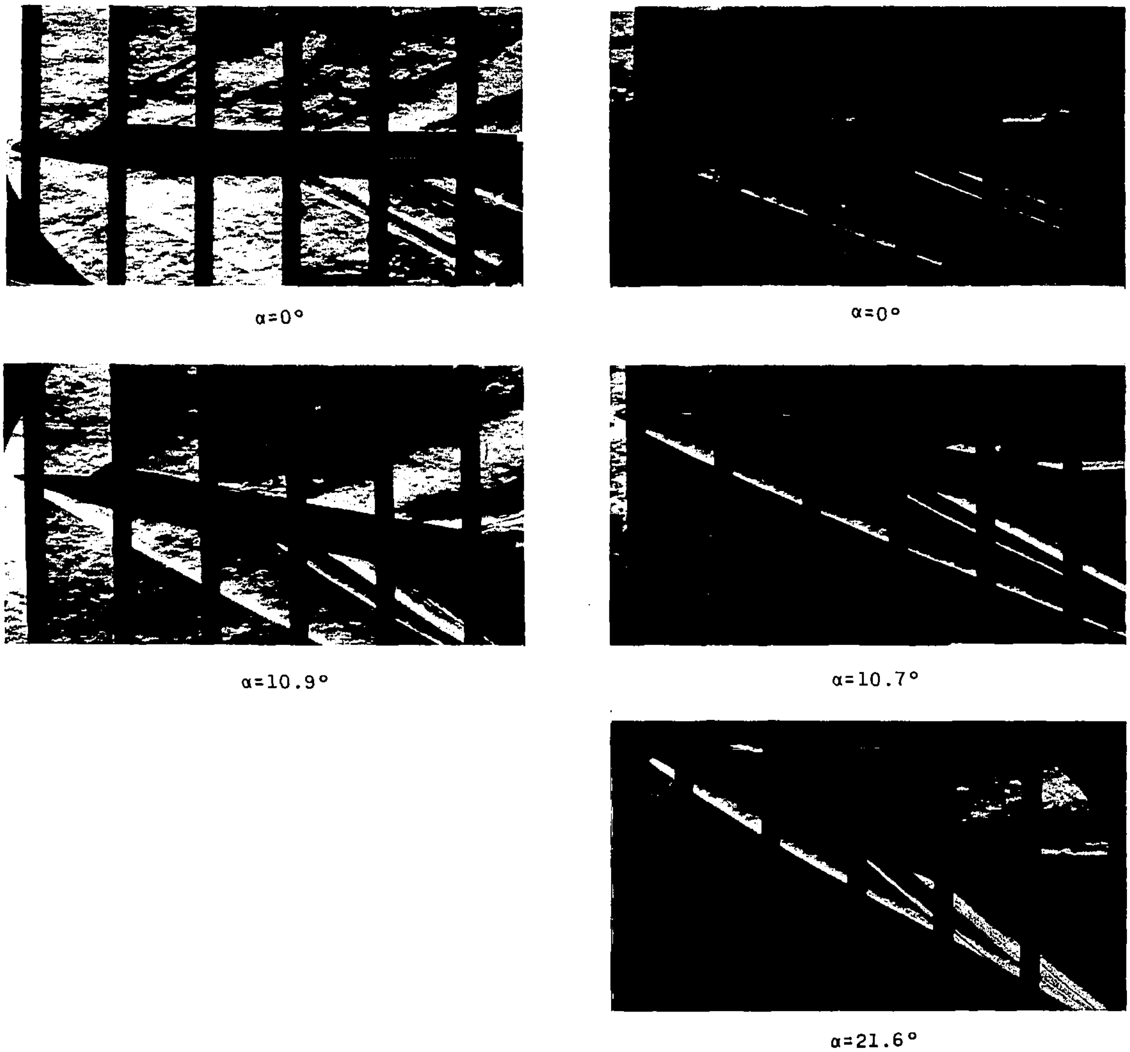

(a) M = 2.29.

(b) M = 2.98.

L-59-215

Figure 7.- Schlieren photographs of the wing-fuselage combination of a 0.067-scale model of the X-15 airplane in the Langley Unitary Plan wind tunnel. Nominal Reynolds number, 2.6×10^6.

α=0°

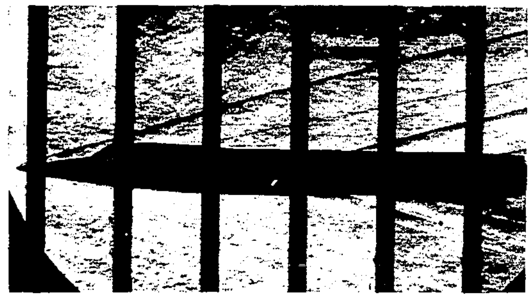

α=0.1°

α=10.4°

α=10.3°

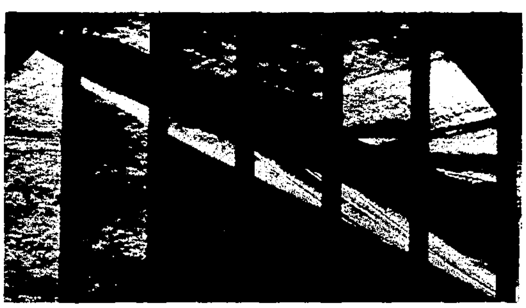

α=21.2°

α=21.0°

(c) M = 3.96. (d) M = 4.65.

Figure 7.- Concluded. L-59-216

L-229

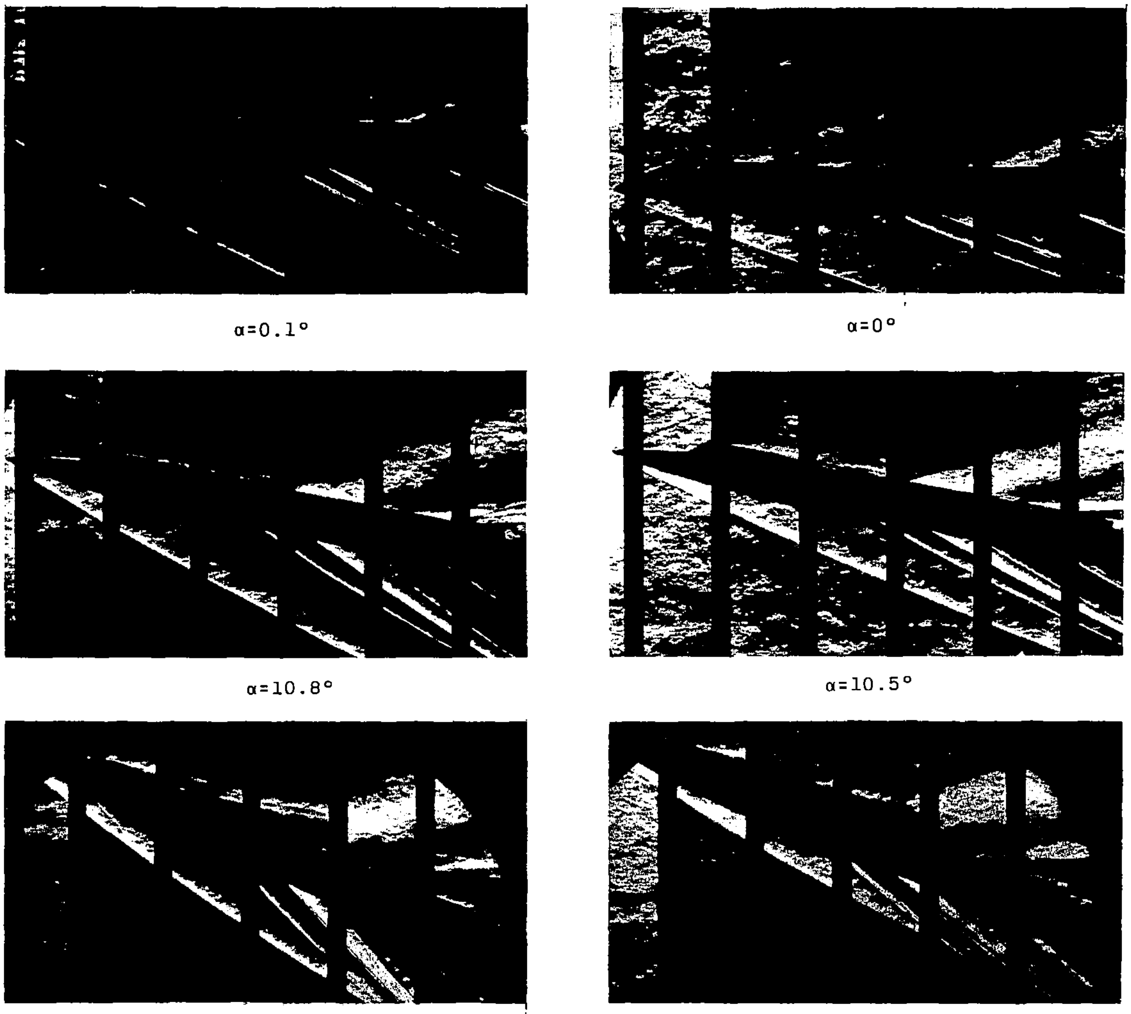

α=0.1° α=0°

α=10.8° α=10.5°

α=22.2° α=21.5°

(a) M = 2.29. (b) M = 2.98.

L-59-217

Figure 8.- Schlieren photographs of the wing—fuselage—horizontal-tail combination of a 0.067-scale model of the X-15 airplane in the Langley Unitary Plan wind tunnel. Nominal Reynolds number, 2.6×10^6.

[redacted]

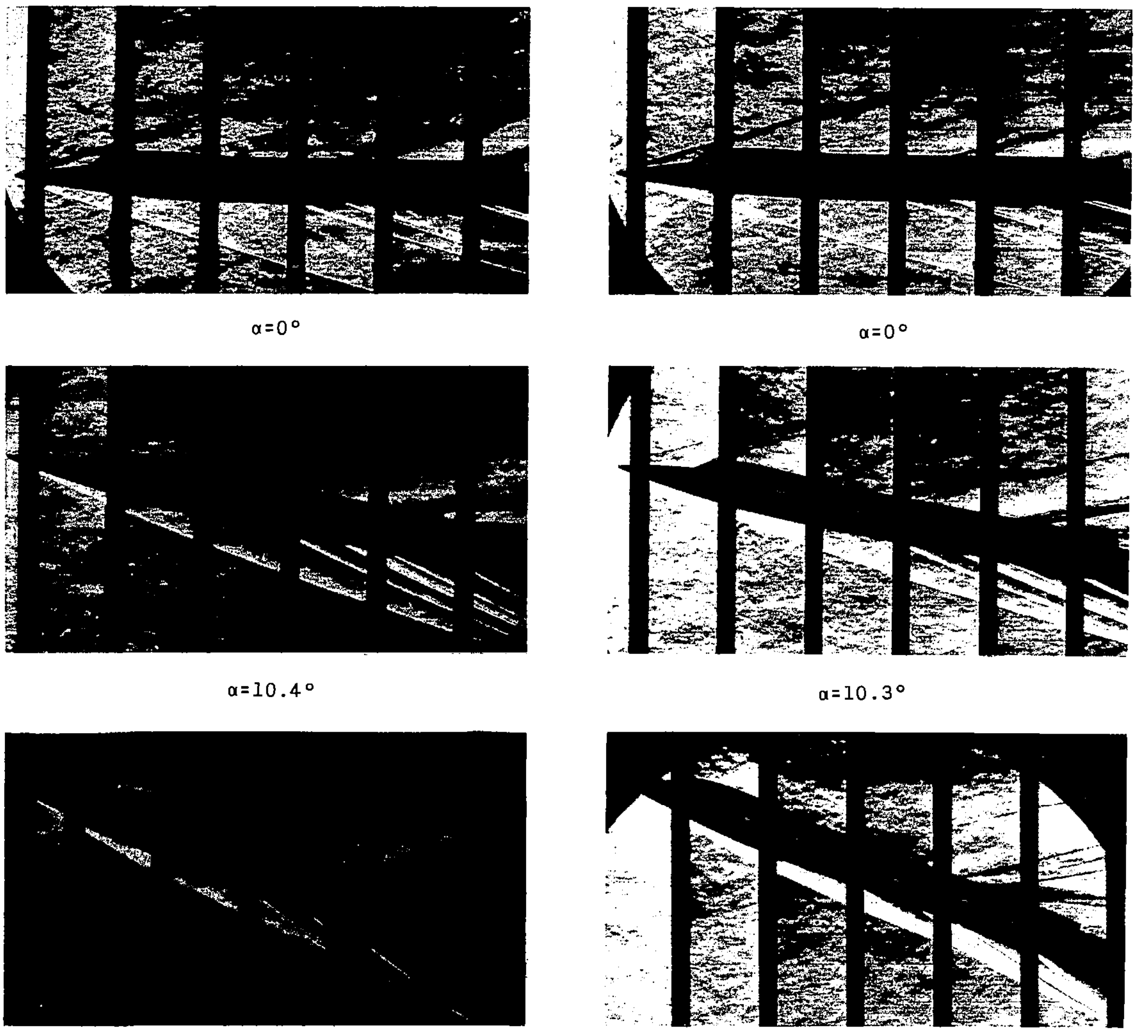

α=0°   α=0°

α=10.4°   α=10.3°

α=21.1°   α=20.9°

(c) M = 3.96.   (d) M = 4.65.

Figure 8.- Concluded.   L-59-218

L-229

[redacted]

[redacted]

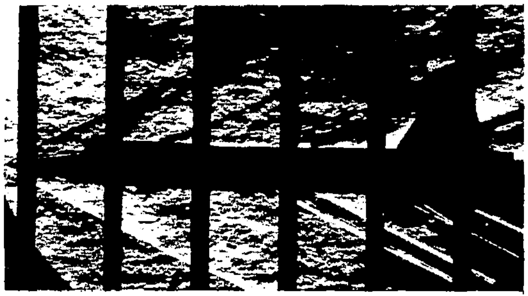

α=0.2°

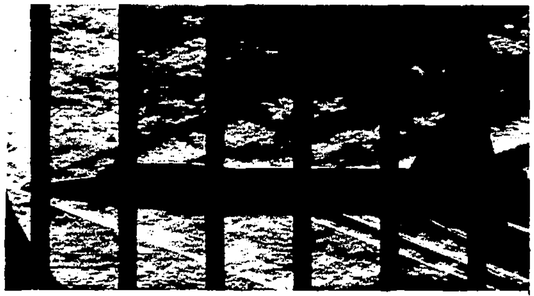

α=0°

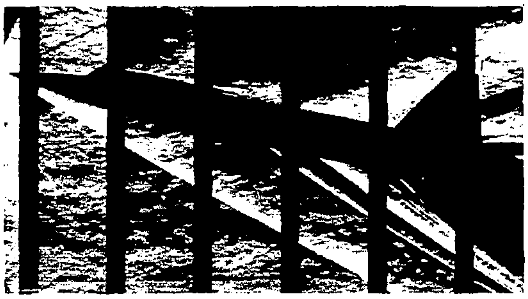

α=10.9°

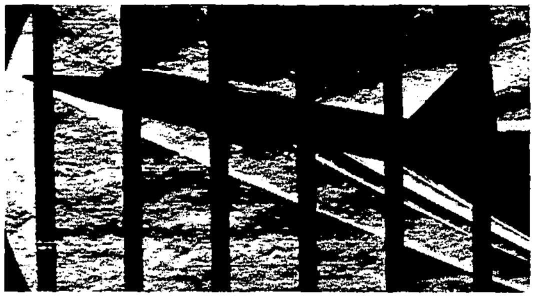

α=10.6°

α= 21.7°

(a) M = 2.29.

(b) M = 2.98.

L-59-219

Figure 9.- Schlieren photographs of the wing—fuselage—vertical-tail combination of a 0.067-scale model of the X-15 airplane in the Langley Unitary Plan wind tunnel. Speed brakes closed; nominal Reynolds number, 2.6×10^6.

[redacted]

[redacted]

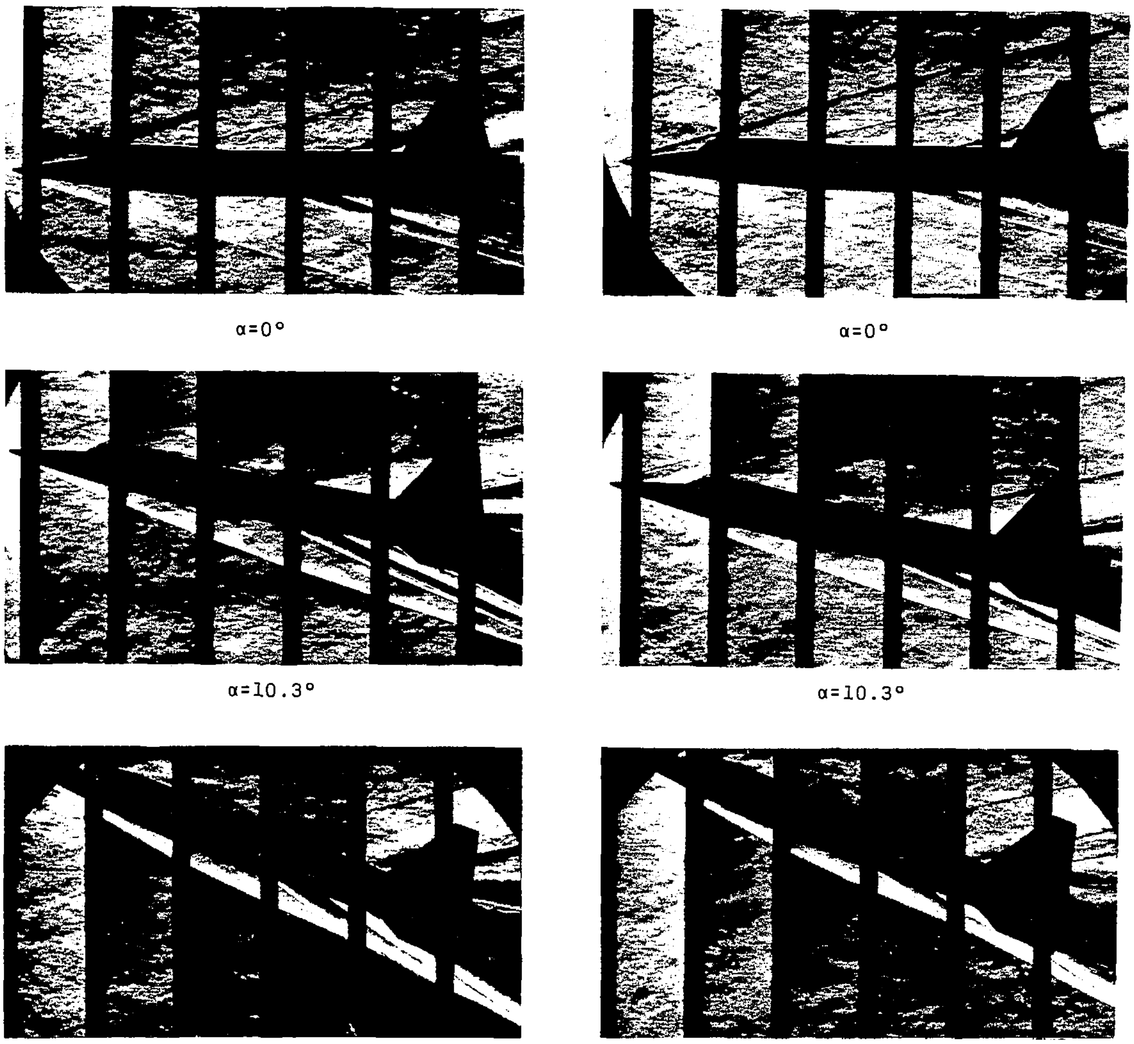

α=0° α=0°

α=10.3° α=10.3°

α=20.9° α=20.6°

(c) M = 3.96. (d) M = 4.65.

Figure 9.- Concluded. L-59-220

L-229

L-229

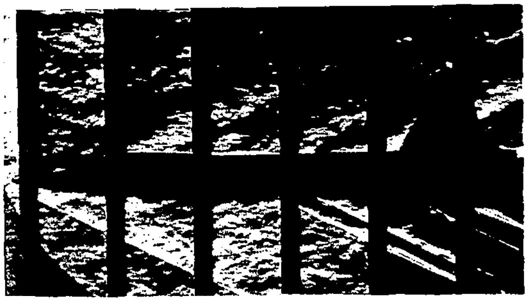

α=0.1°

α=0°

α=10.9°

α=10.5°

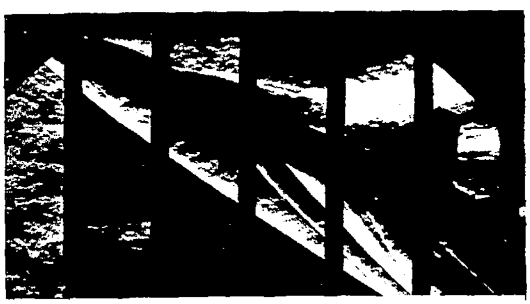

α=22.5°

α=21.3°

(a) M = 2.29. (b) M = 2.98.

L-59-221

Figure 10.- Schlieren photographs of the complete configuration of a 0.067-scale model of the X-15 airplane in the Langley Unitary Plan wind tunnel. Speed brakes closed; nominal Reynolds number, 2.6×10^6.

[redacted]

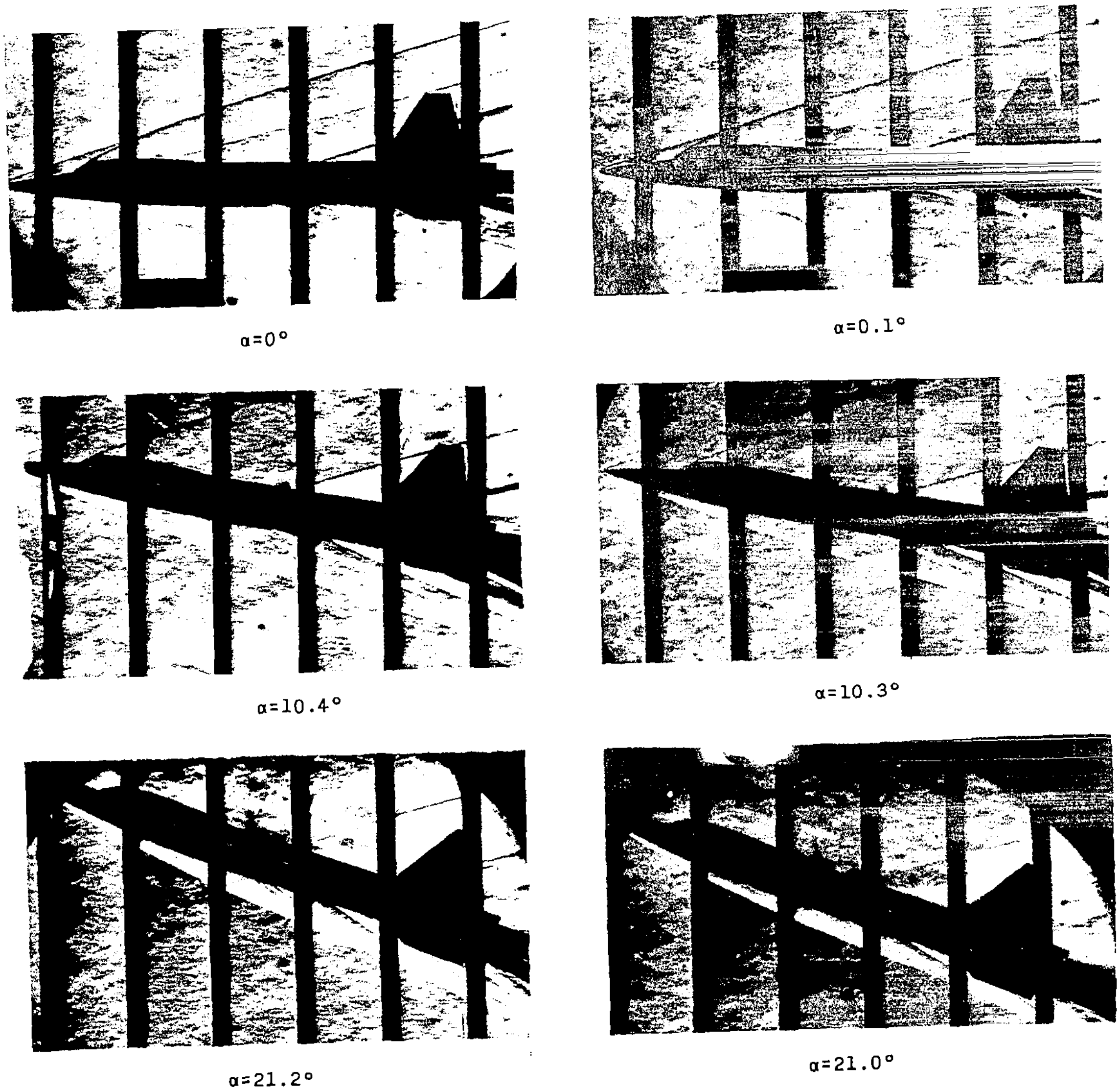

(c) M = 3.96.

(d) M = 4.65.

Figure 10.- Concluded.

L-59-222

L-229

[redacted]

[redacted]

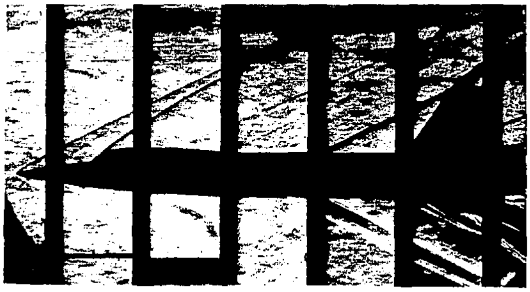

α=0.1°

α=0.1°

α=10.8°

α=10.6°

α=21.9°

α=21.2°

(a) M = 2.29.

(b) M = 2.98.

L-59-223

Figure 11.- Schlieren photographs of the complete configuration of a 0.067-scale model of the X-15 airplane in the Langley Unitary Plan wind tunnel. Speed brakes open; nominal Reynolds number, 2.6×10^6.

L-229

[redacted]

[redacted]

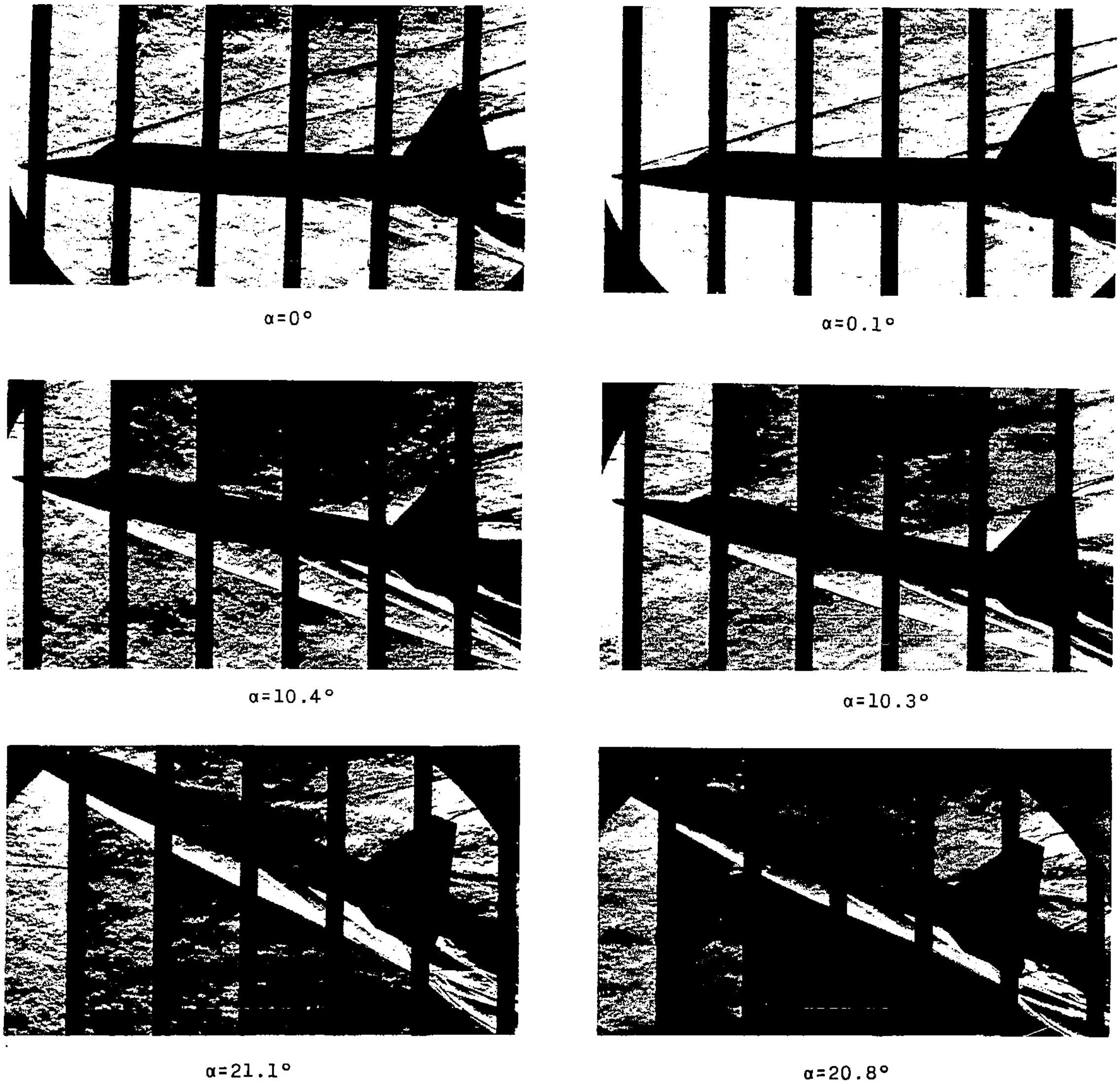

(c) $M = 3.96$. (d) $M = 4.65$.

Figure 11.- Concluded. L-59-224

L-229

[redacted]

[redacted]

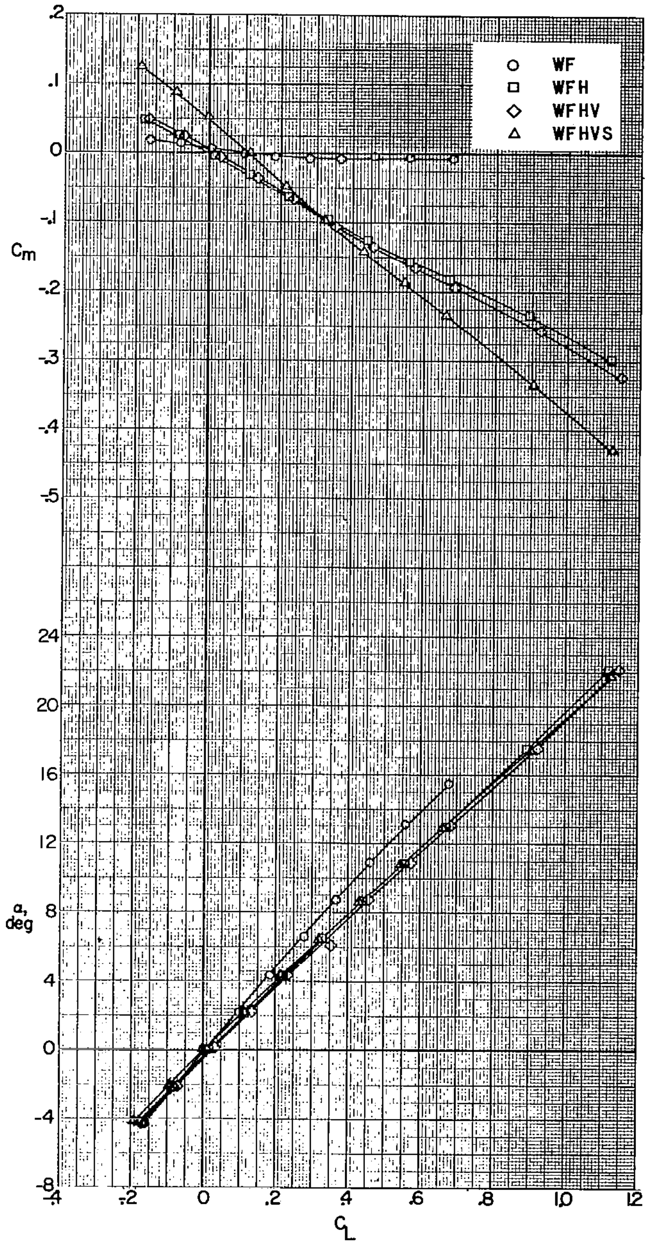

(a) M = 2.29.

Figure 12.- Longitudinal stability characteristics of a 0.067-scale model of the X-15 airplane with various combinations of model components.

[redacted]

[redacted]

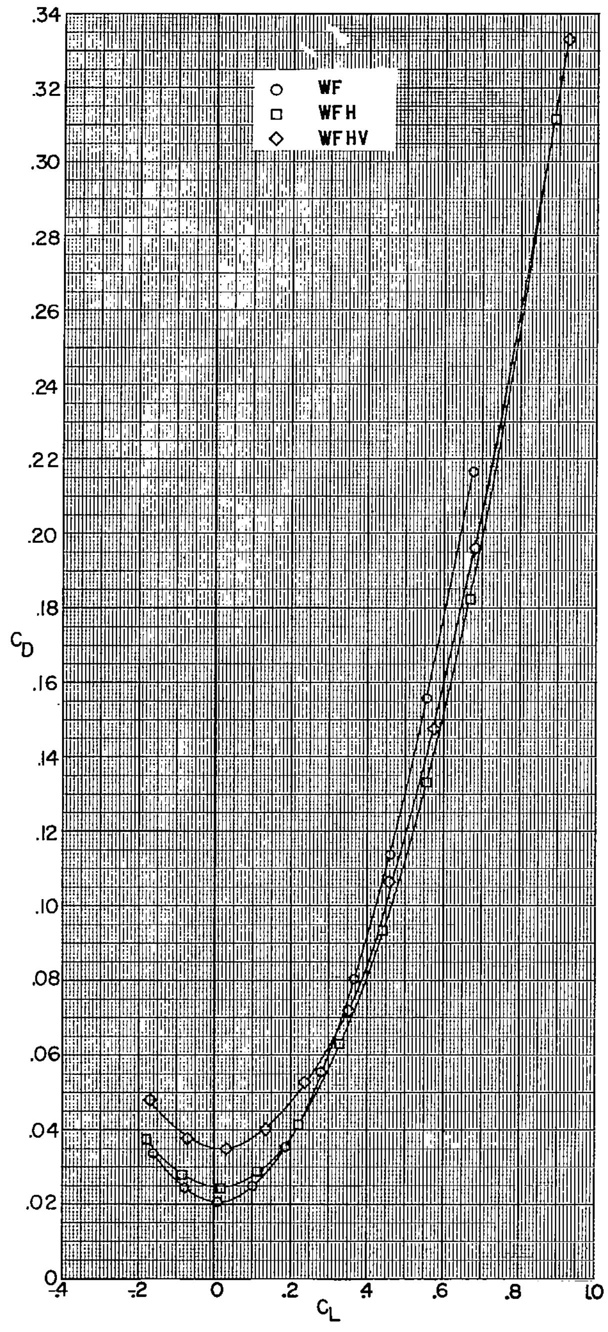

(a) Continued.

Figure 12.- Continued.

L-229

[redacted]

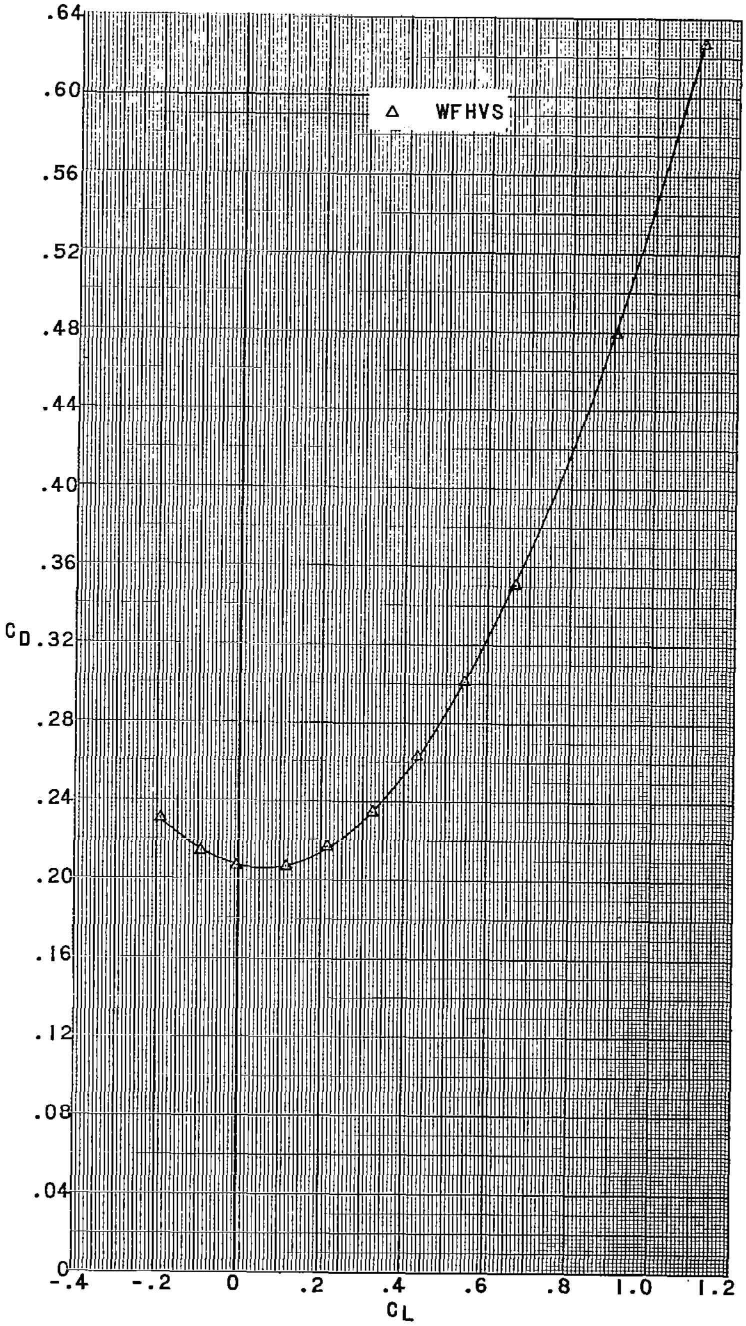

(a) Concluded.

Figure 12.- Continued.

[redacted]

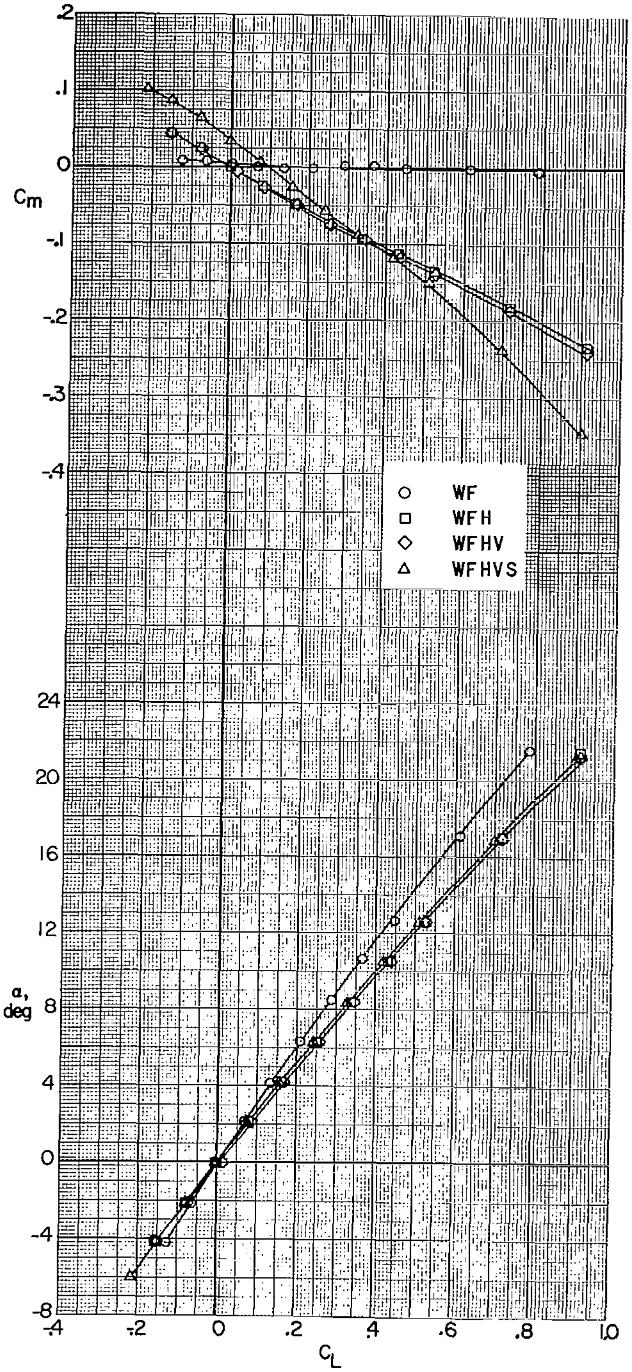

(b) M = 2.98.

Figure 12.- Continued.

[redacted]

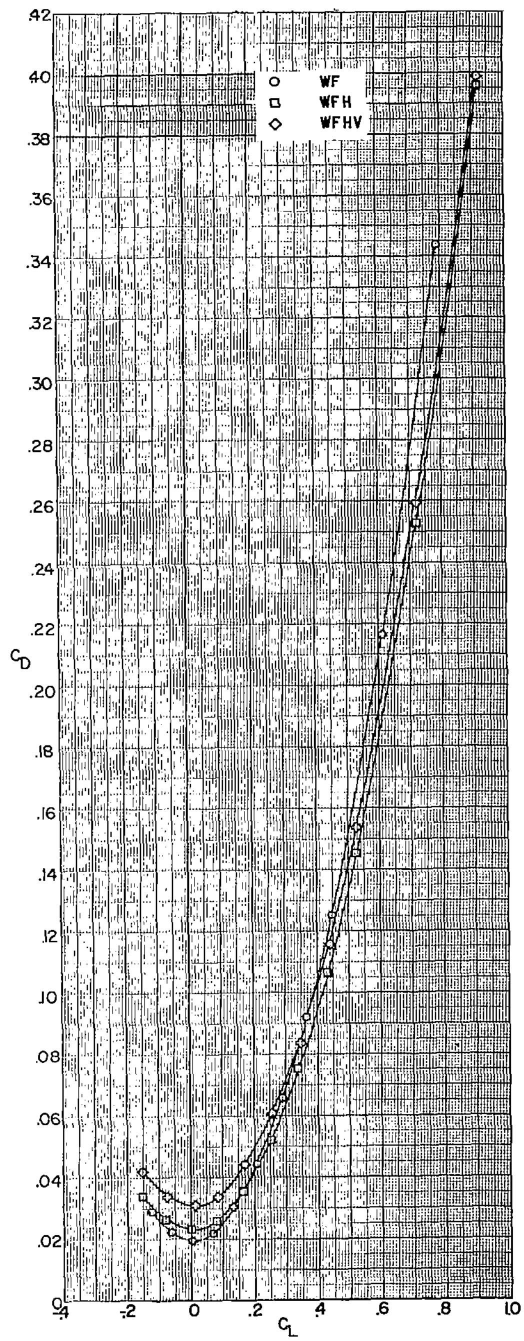

(b) Continued.

Figure 12.- Continued.

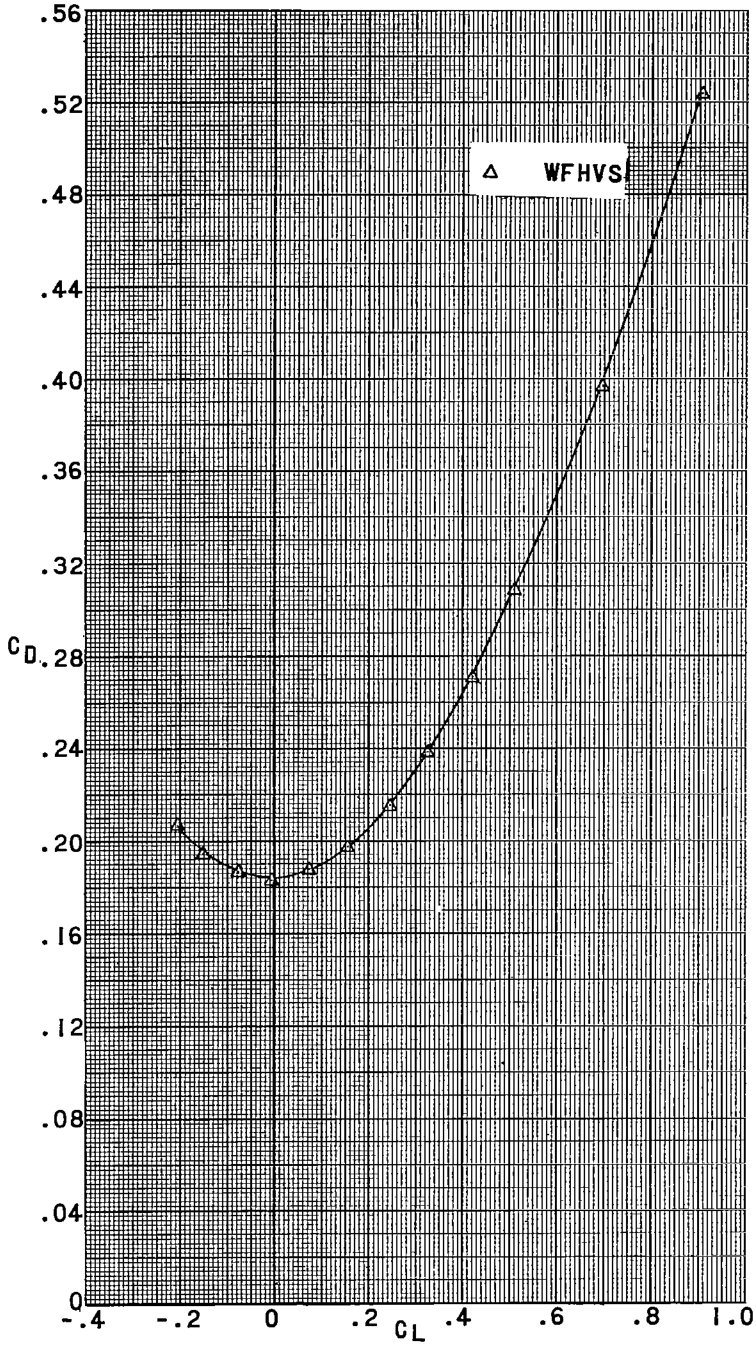

L-229

(b) Concluded.

Figure 12.- Continued.

[redacted]

L-229

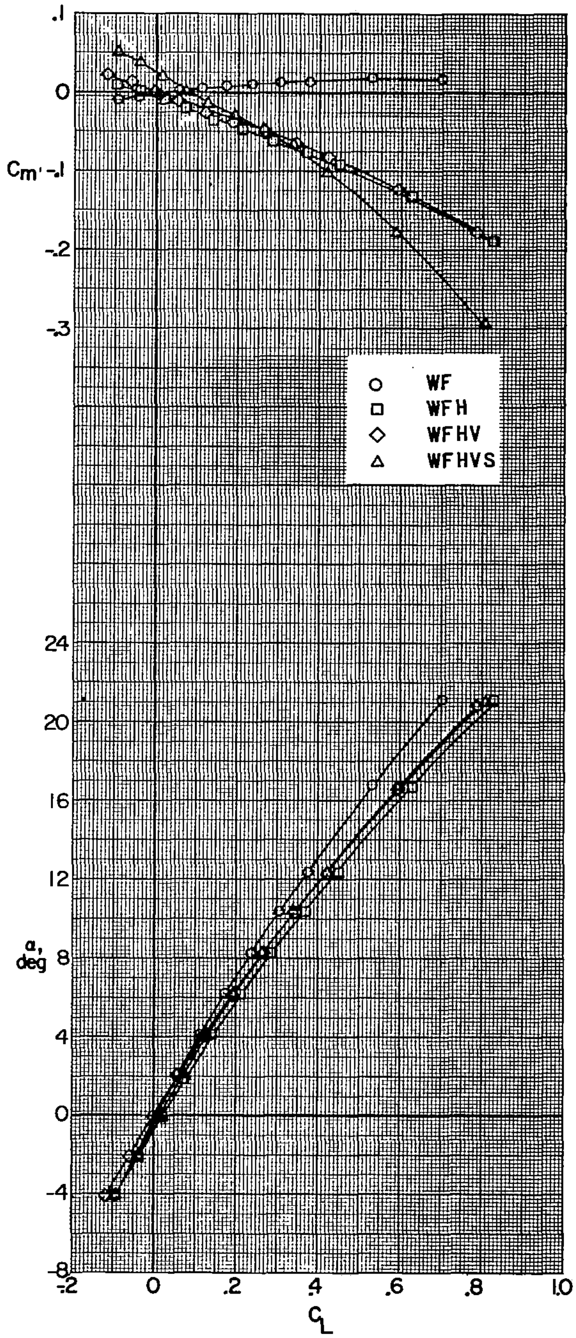

(c) M = 3.96.

Figure 12.- Continued.

[redacted]

[redacted]

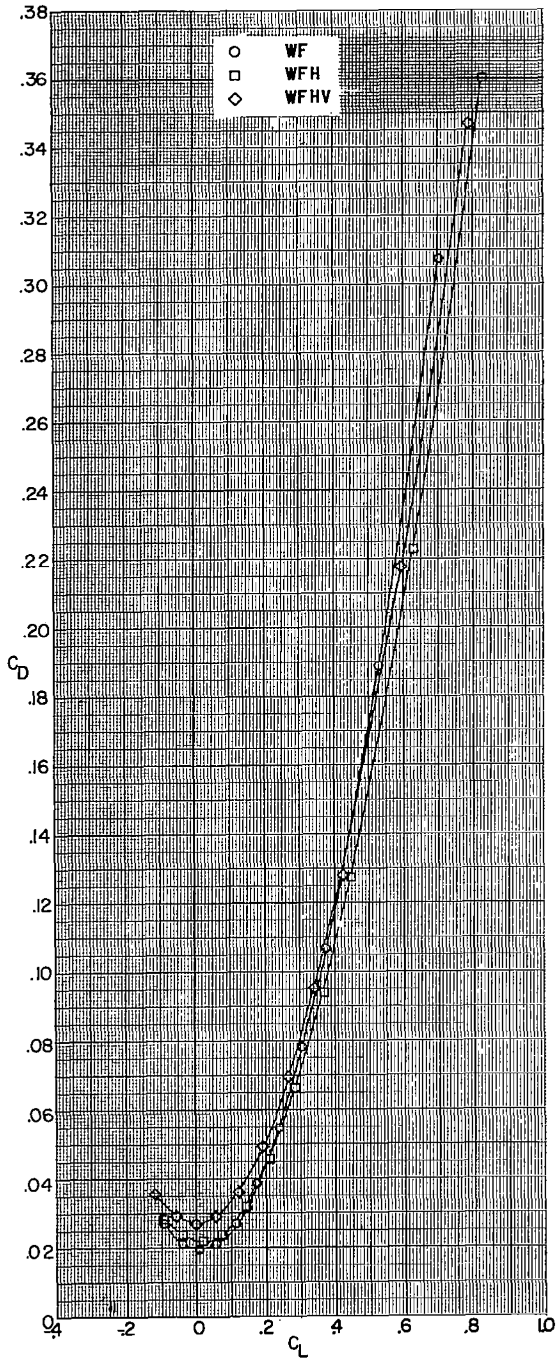

(c) Continued.

Figure 12.- Continued.

L-229

[redacted]

L-229

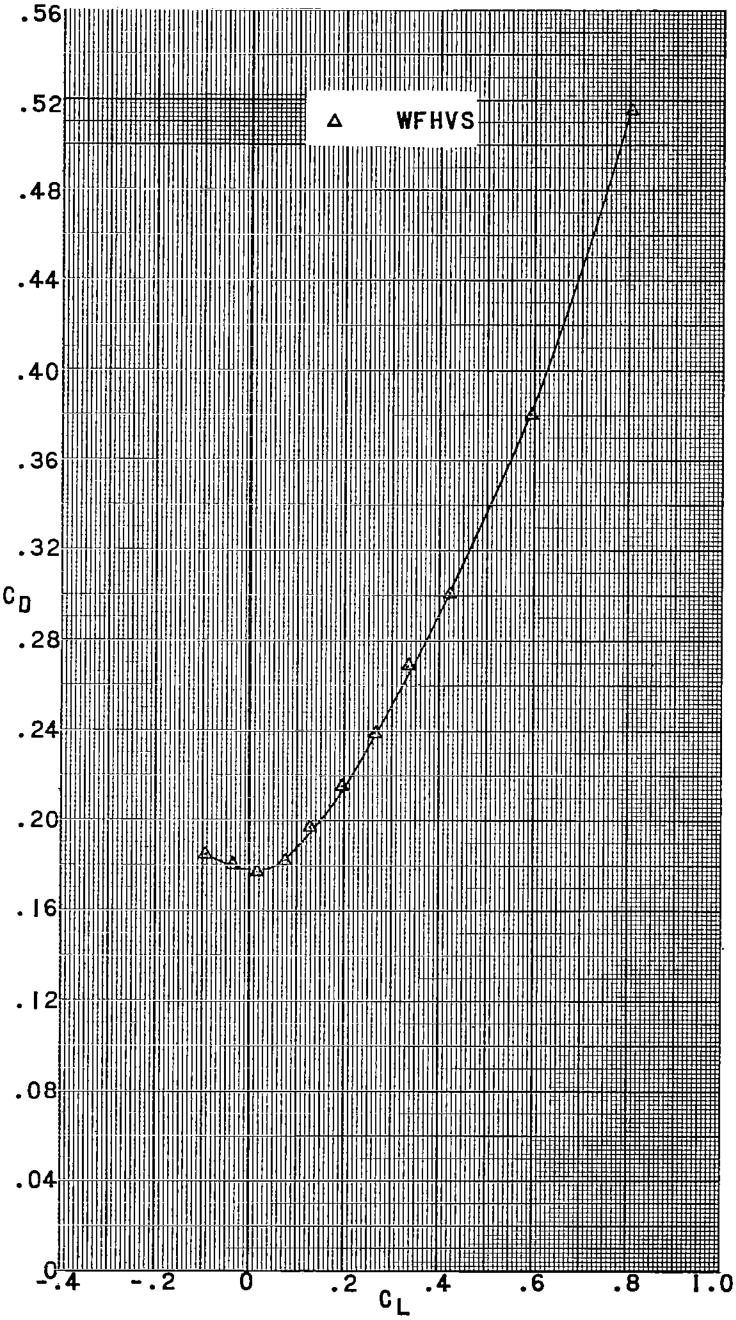

(c) Concluded.

Figure 12.- Continued.

[redacted]

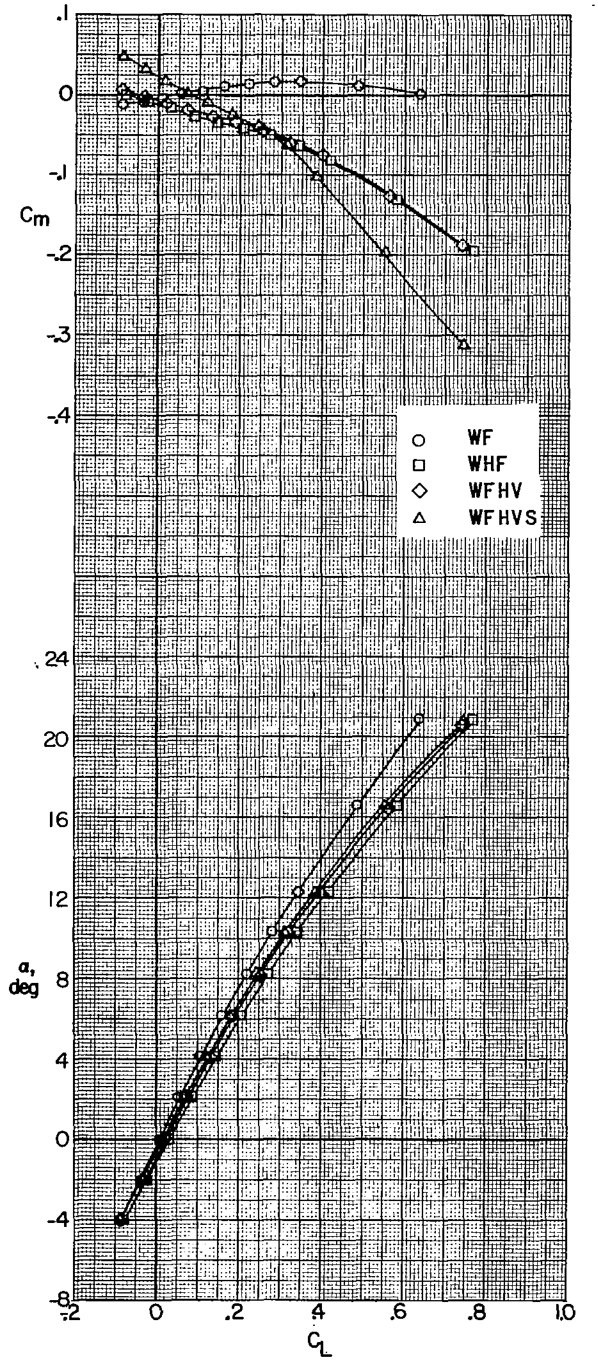

(d) M = 4.65.

Figure 12.- Continued.

L-229

[redacted]

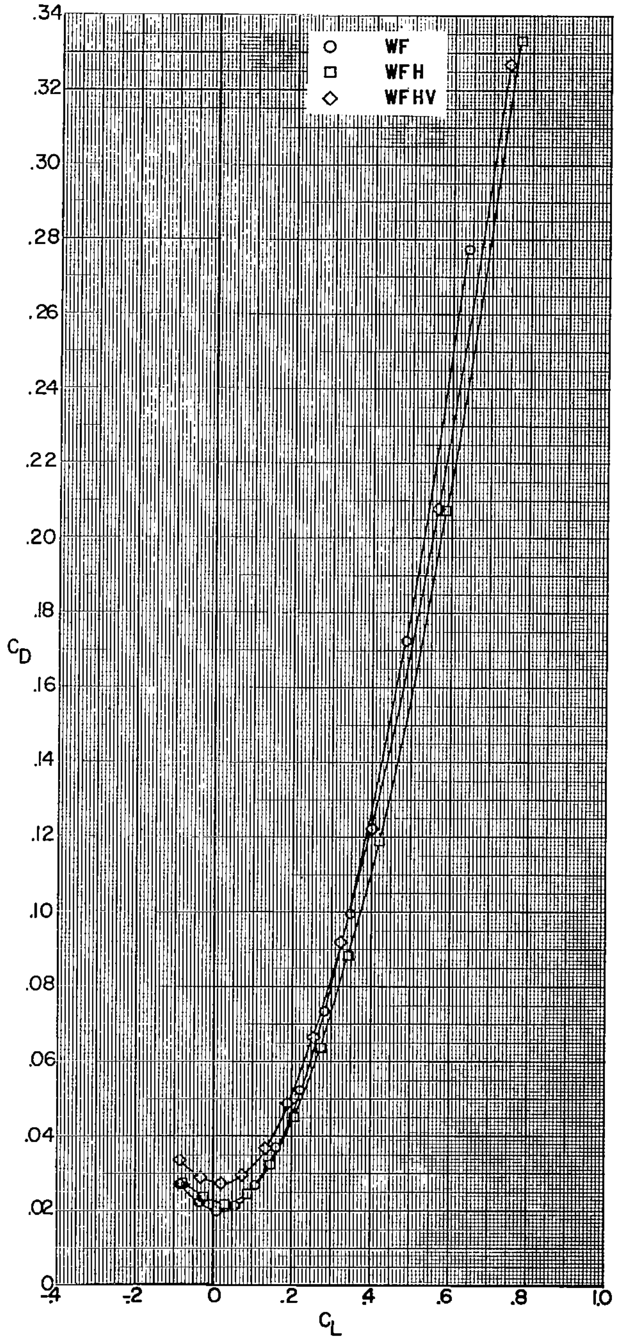

(d) Continued.

Figure 12.- Continued.

[redacted]

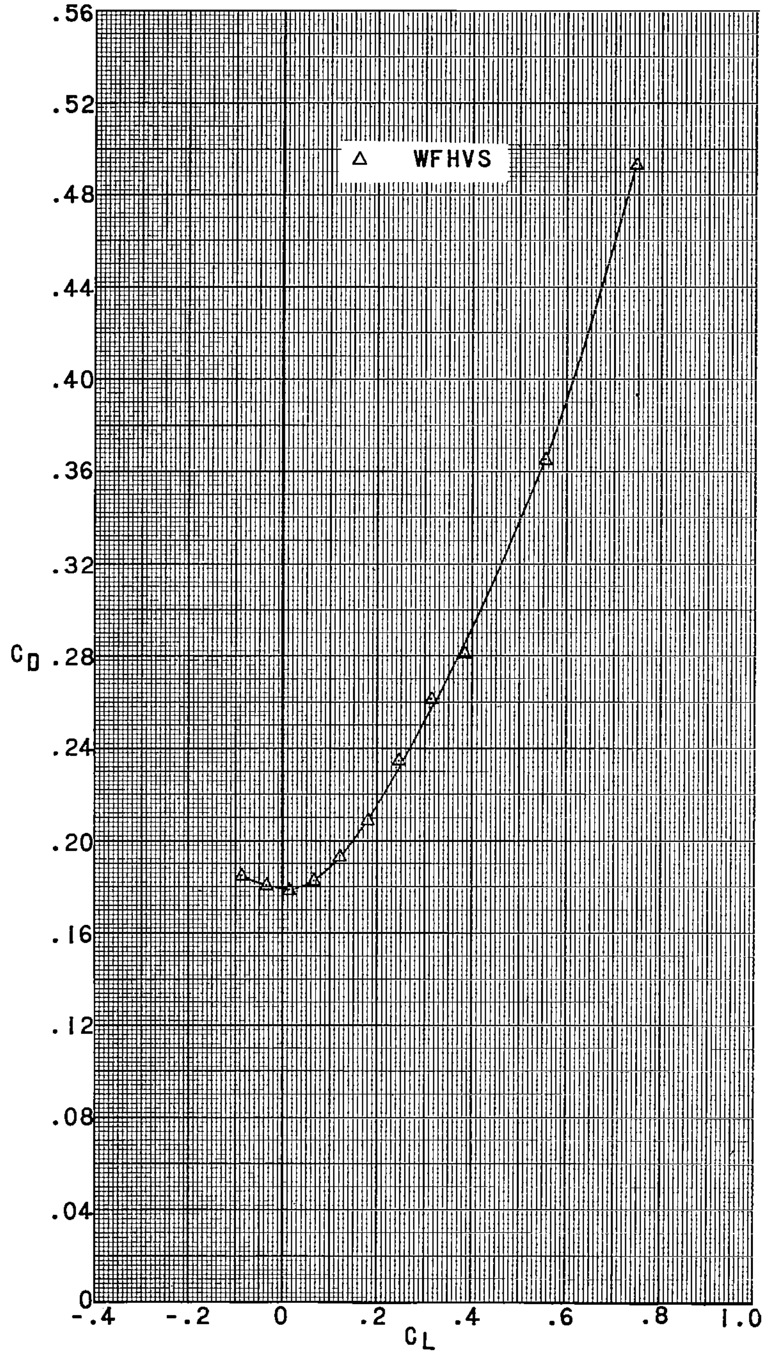

L-229

(d) Concluded.

Figure 12.- Concluded.

[redacted]

[redacted]

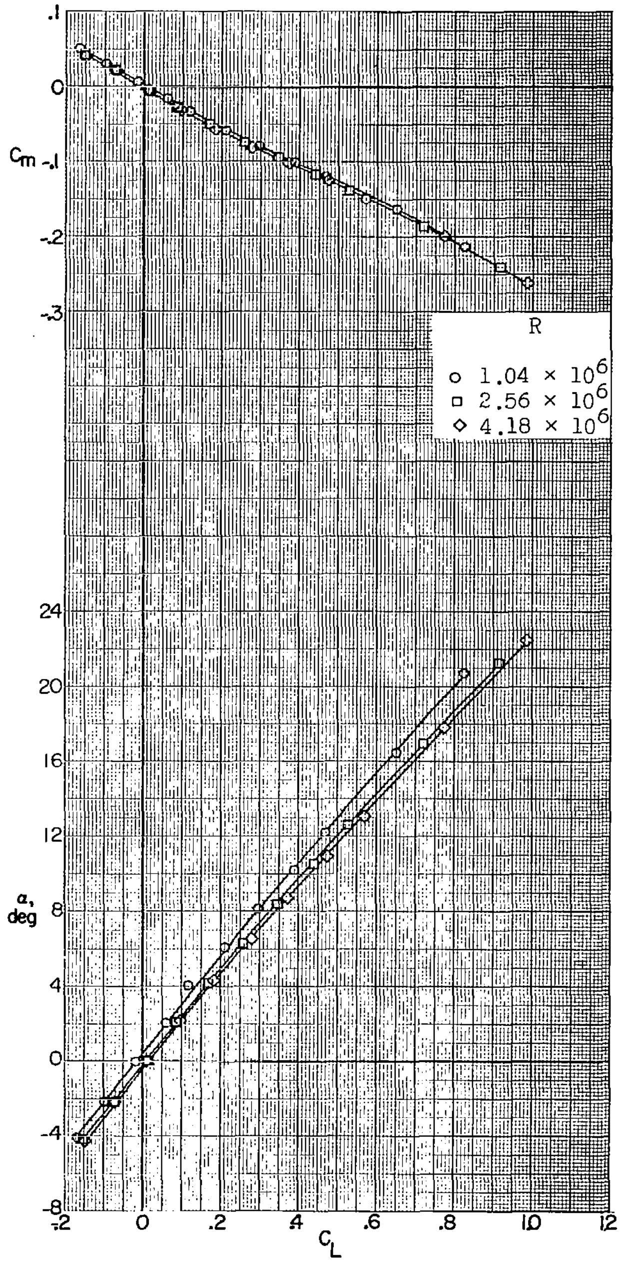

(a) M = 2.98.

Figure 13.- Longitudinal stability characteristics of a 0.067-scale model of the X-15 airplane at various Reynolds numbers. Speed brakes closed.

[redacted]

[redacted]

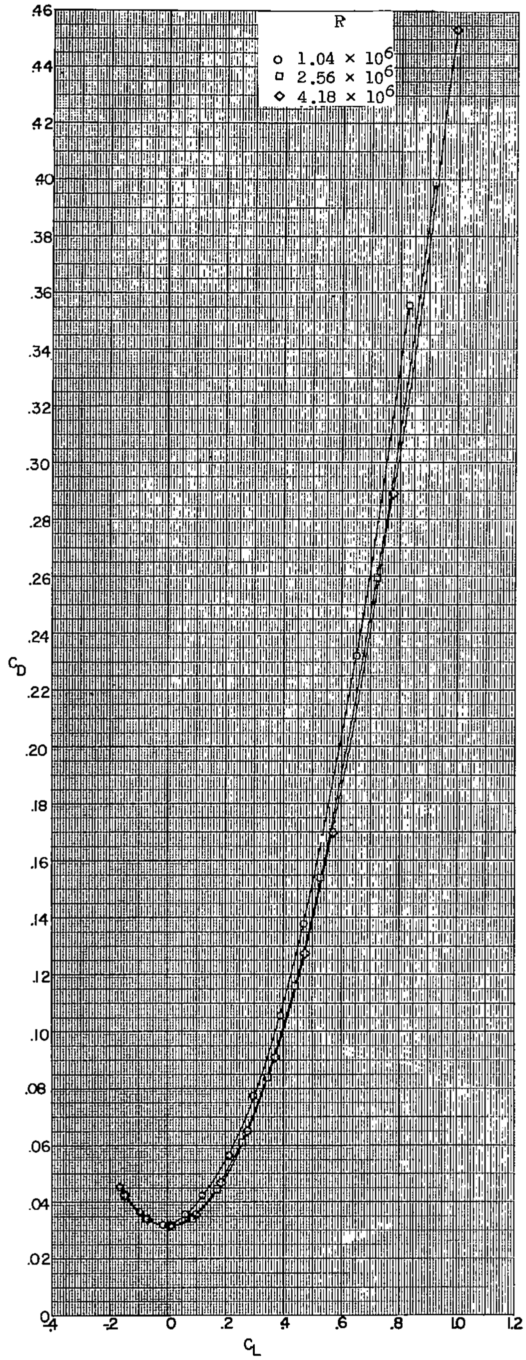

(a) Concluded.

Figure 13.- Continued.

L-220

[redacted]

[redacted]

L-229

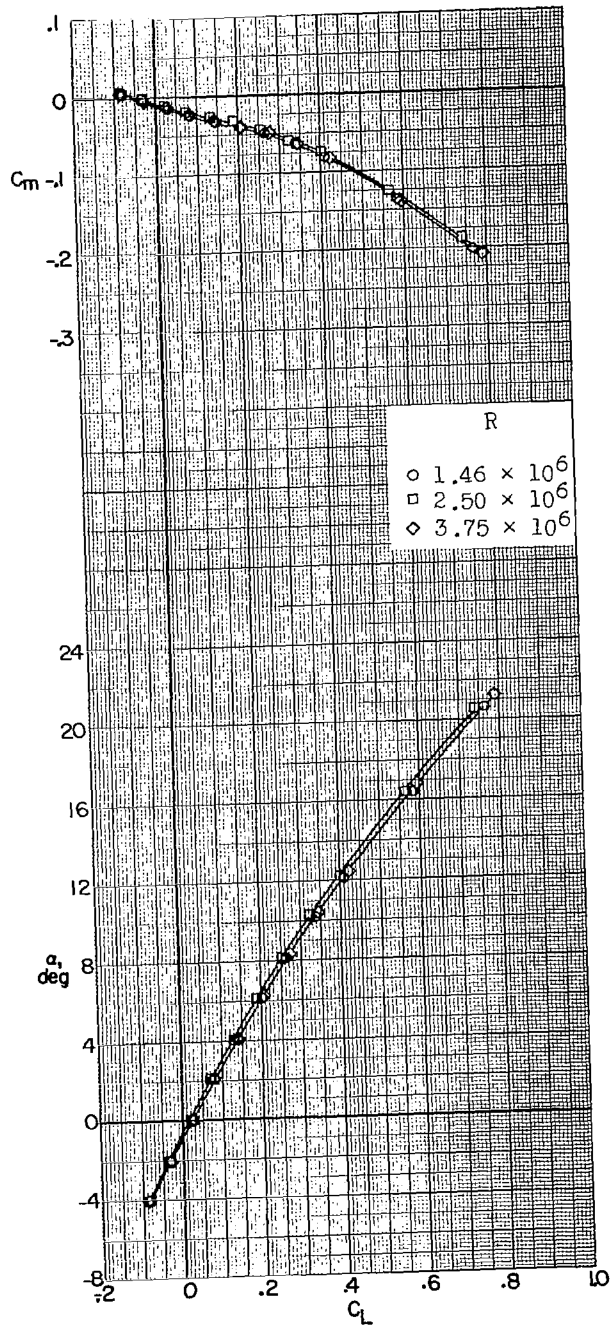

(b) M = 4.65.

Figure 13.- Continued.

[redacted]

[redacted]

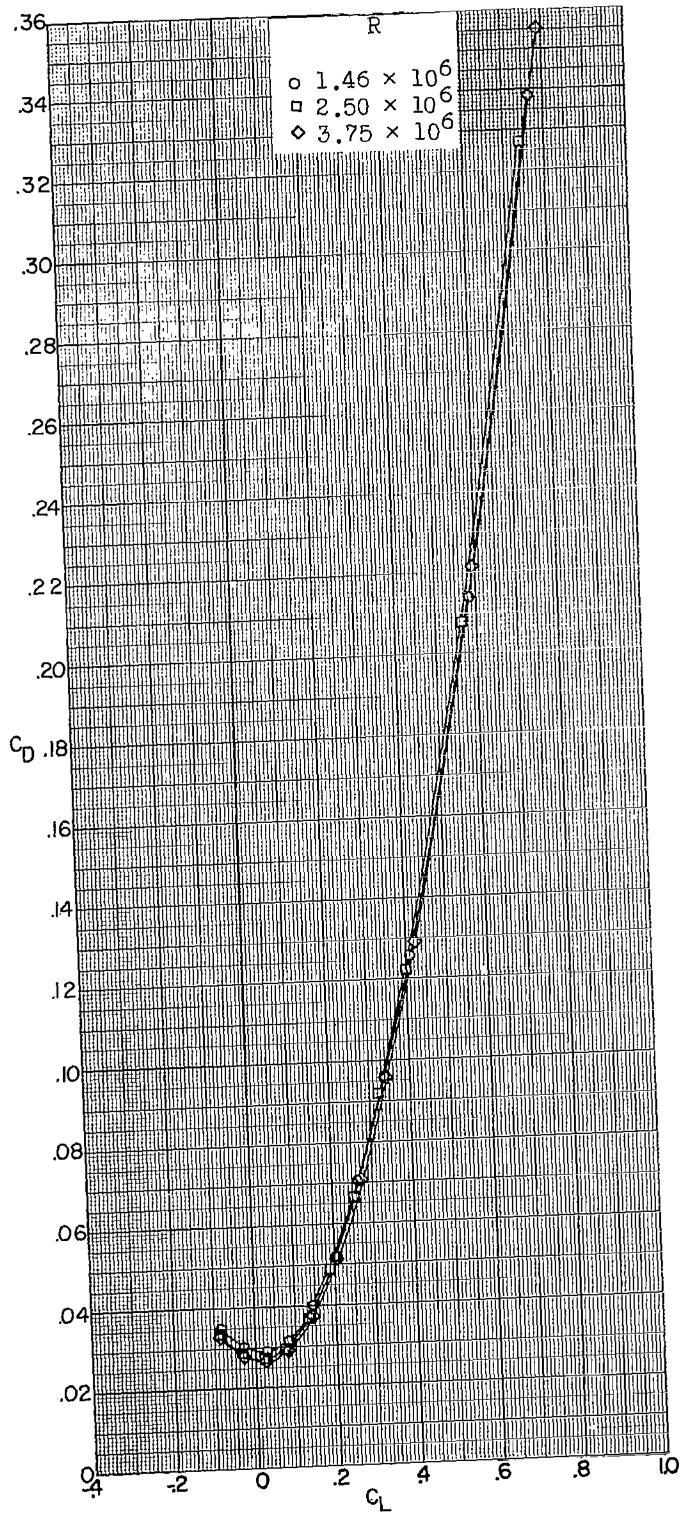

(b) Concluded.

Figure 13.- Concluded.

[redacted]

L-229

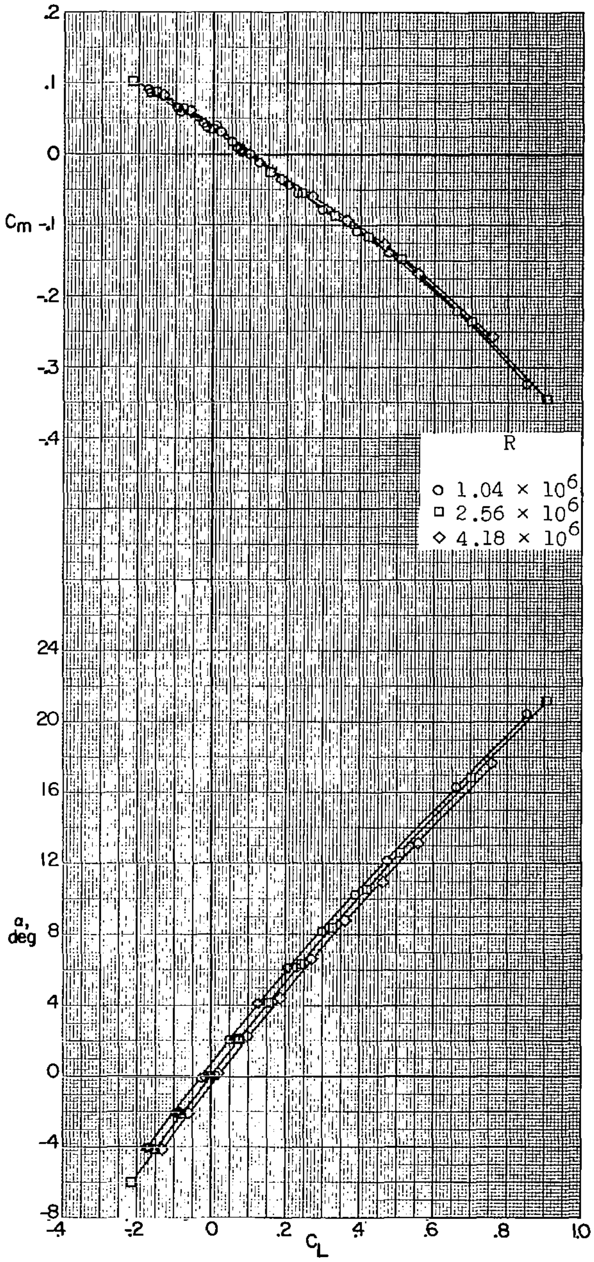

(a) M = 2.98.

Figure 14.- Longitudinal stability characteristics of a 0.067-scale model of the X-15 airplane at various Reynolds numbers. Speed brakes open 45°.

[redacted]

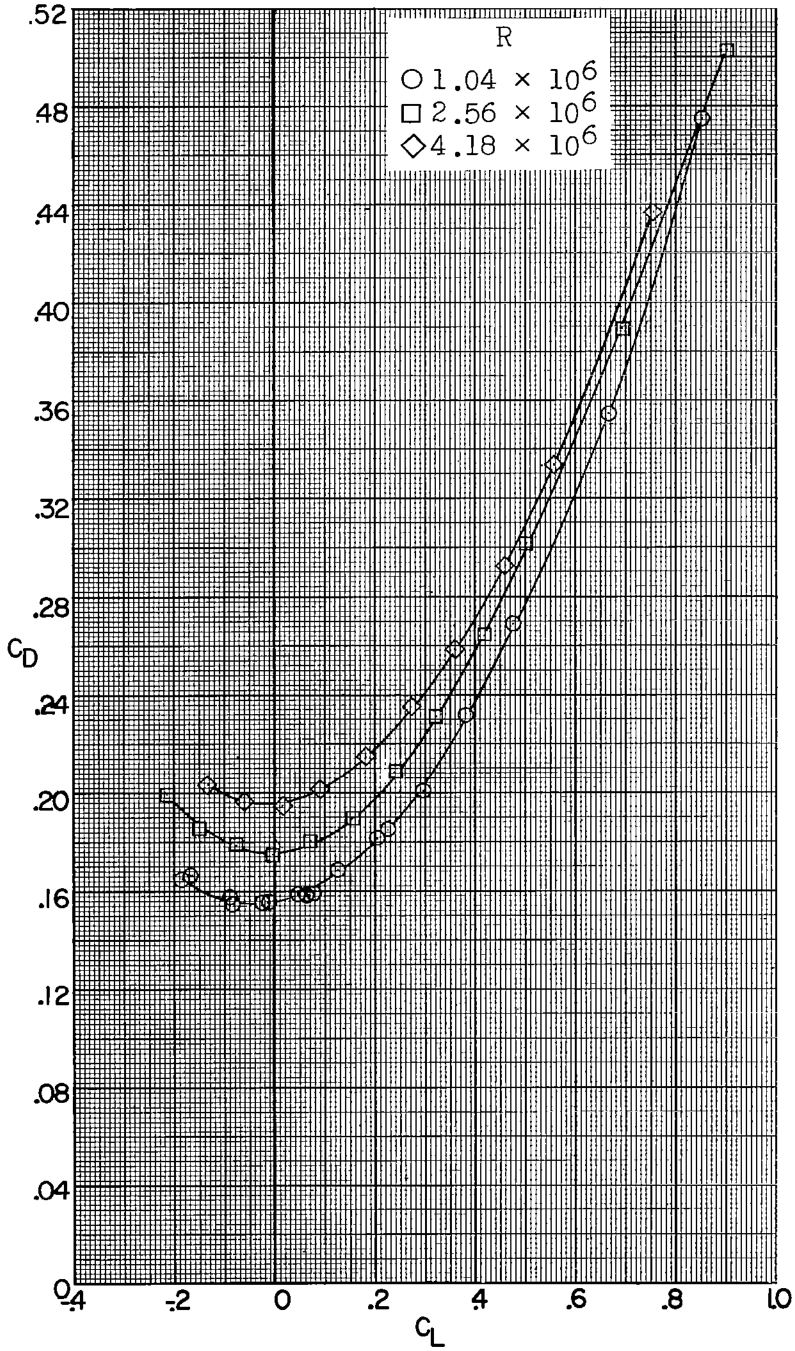

(a) Concluded.

Figure 14.- Continued.

[redacted]

L-229

[redacted]

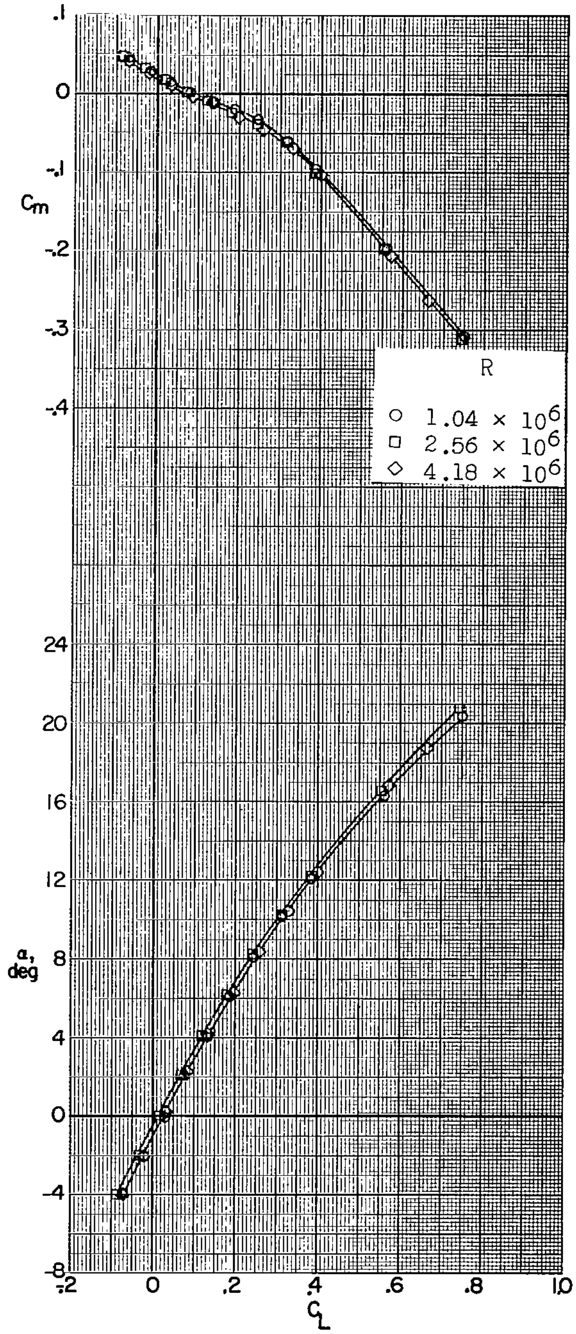

(b) M = 4.65.

Figure 14.- Continued.

[redacted]

[redacted]

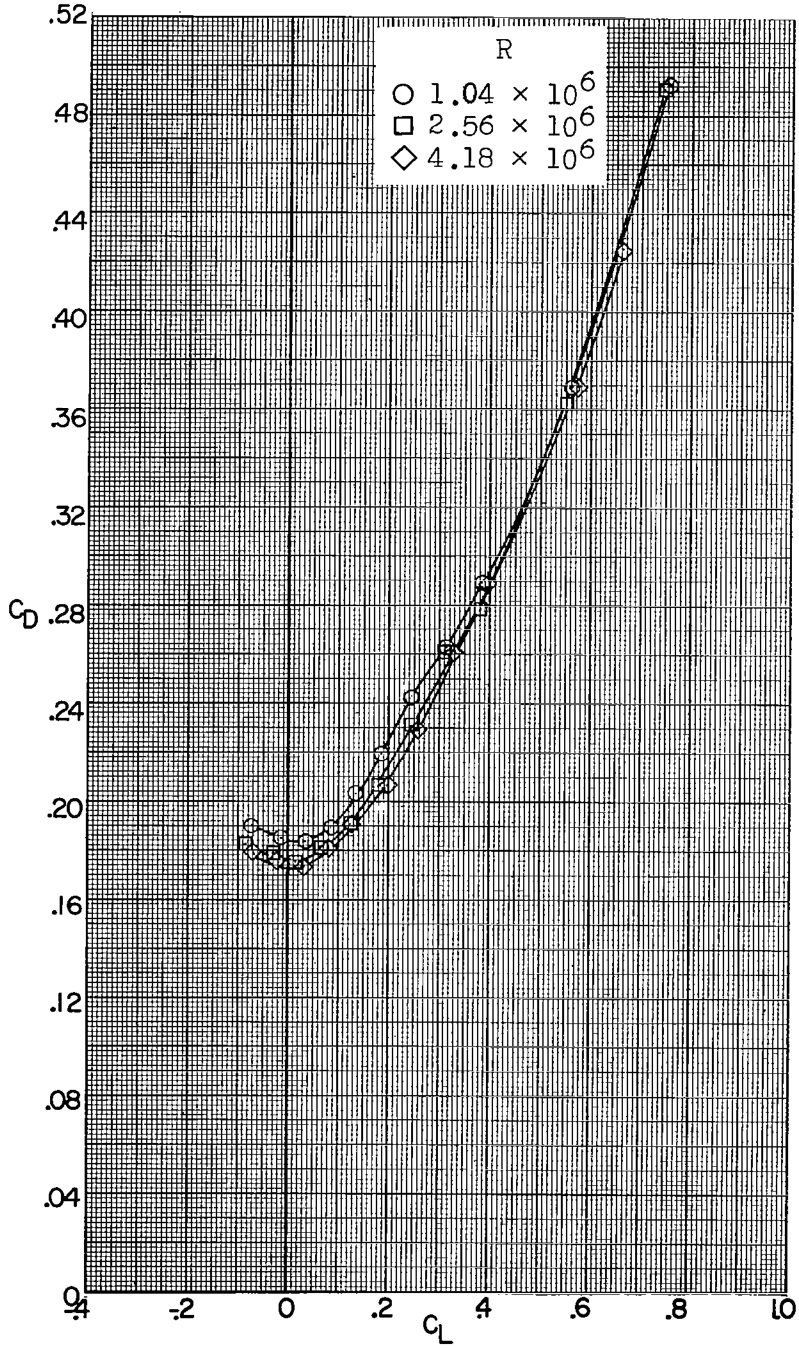

(b) Concluded.

Figure 14.- Concluded.

L-229

[redacted]

[redacted]

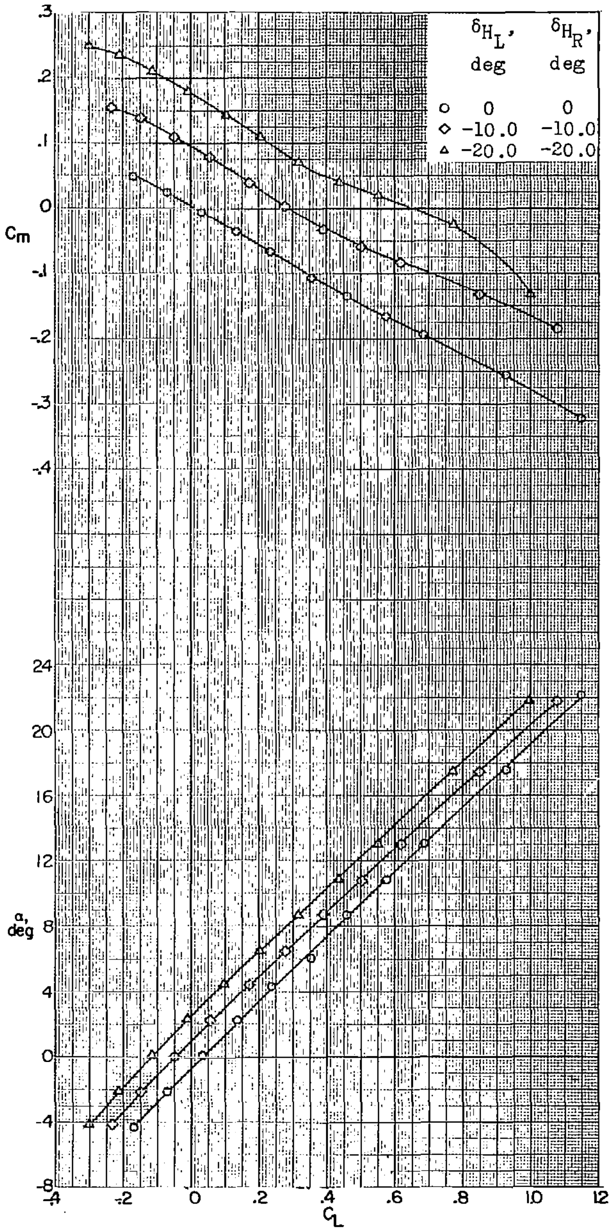

(a) M = 2.29.

Figure 15.- Longitudinal stability characteristics of a 0.067-scale model of the X-15 airplane with various pitch-control deflections of the horizontal tail. Speed brakes closed.

[redacted]

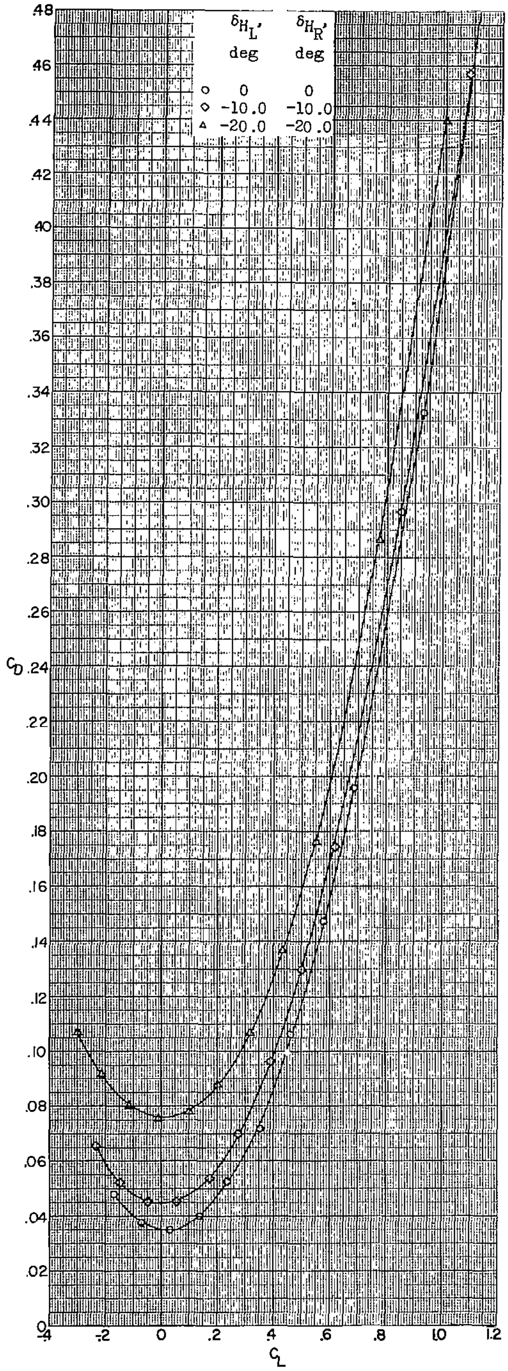

(a) Concluded.

Figure 15.- Continued.

L-229

L-229

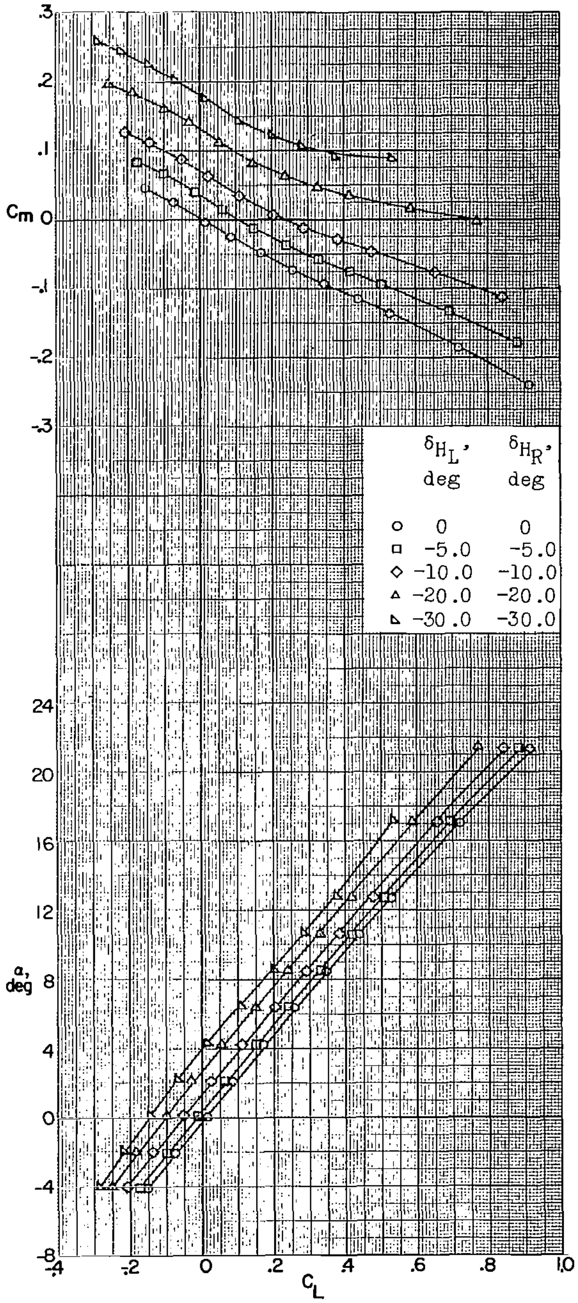

(b) M = 2.98.

Figure 15.- Continued.

[redacted]

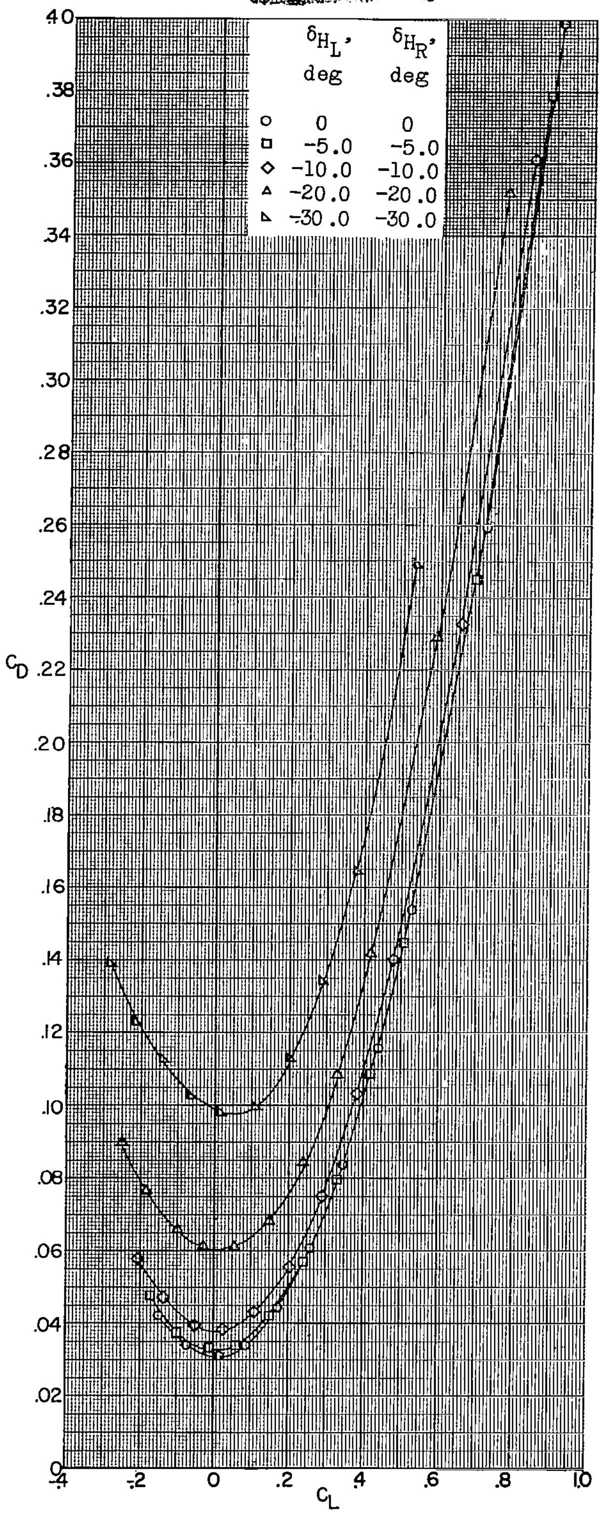

(b) Concluded.

Figure 15.- Continued.

[redacted]

L-229

[redacted]

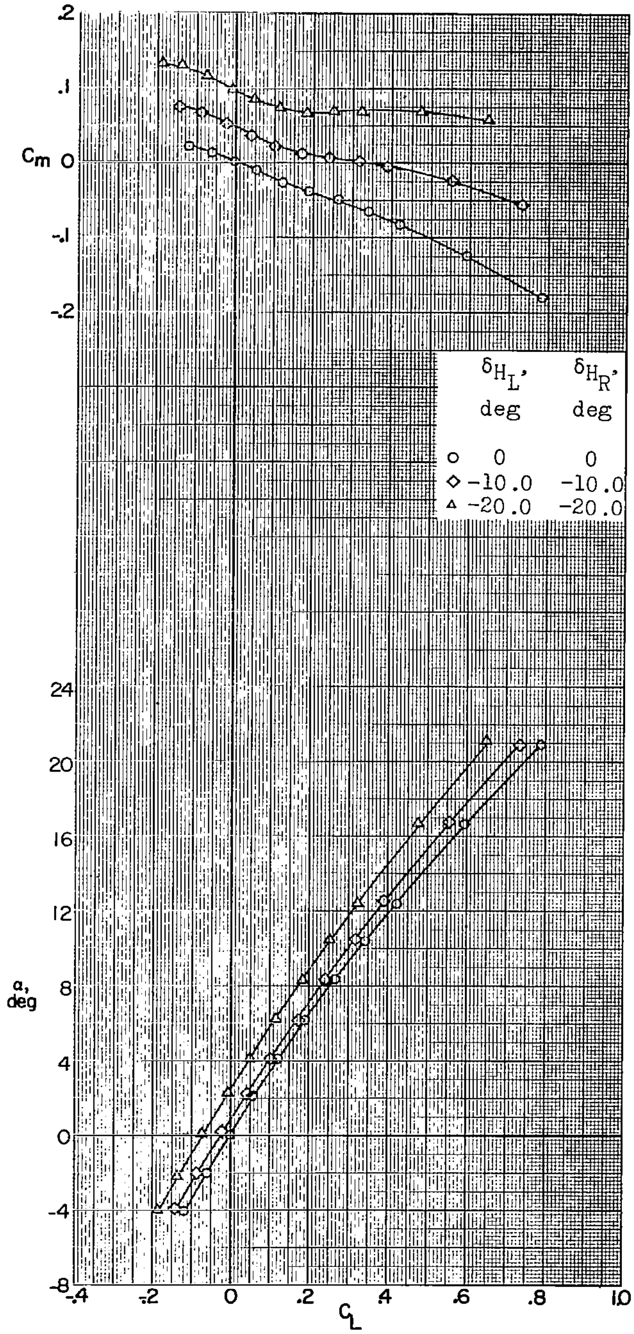

(c) M = 3.96.

Figure 15.- Continued.

[redacted]

[redacted]

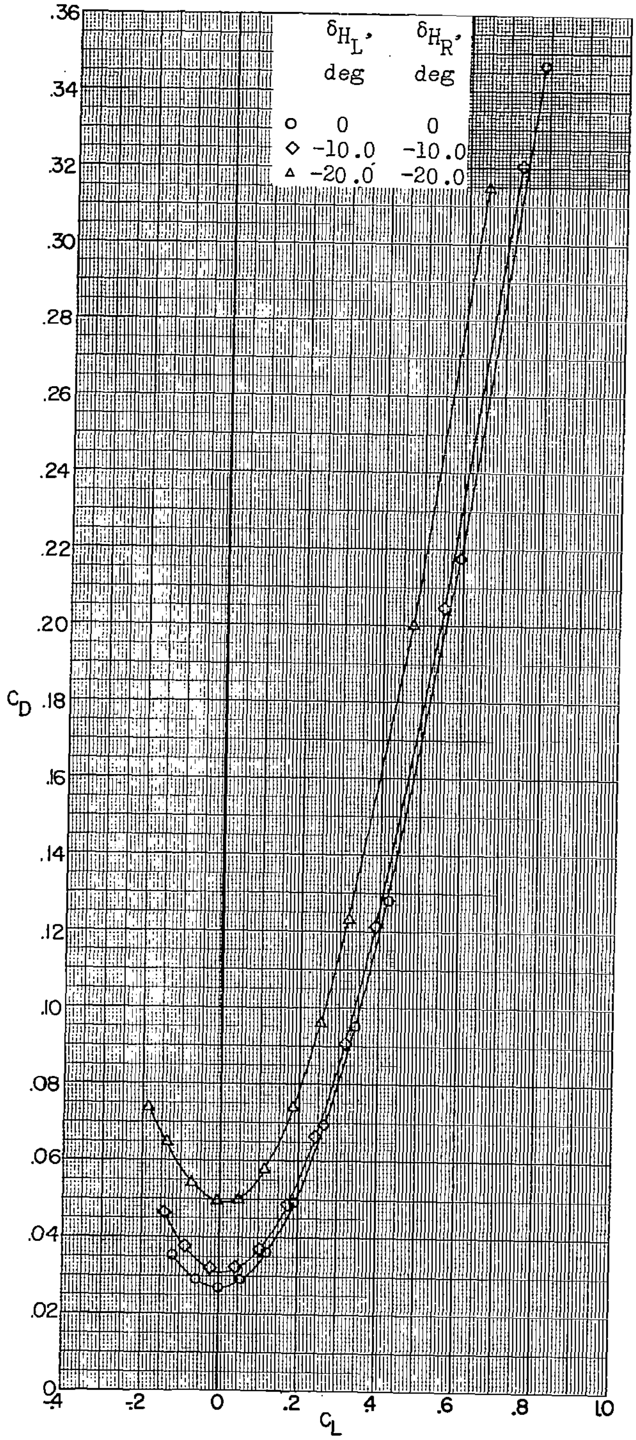

(c) Concluded.

Figure 15.- Continued.

L-229

[redacted]

L-229

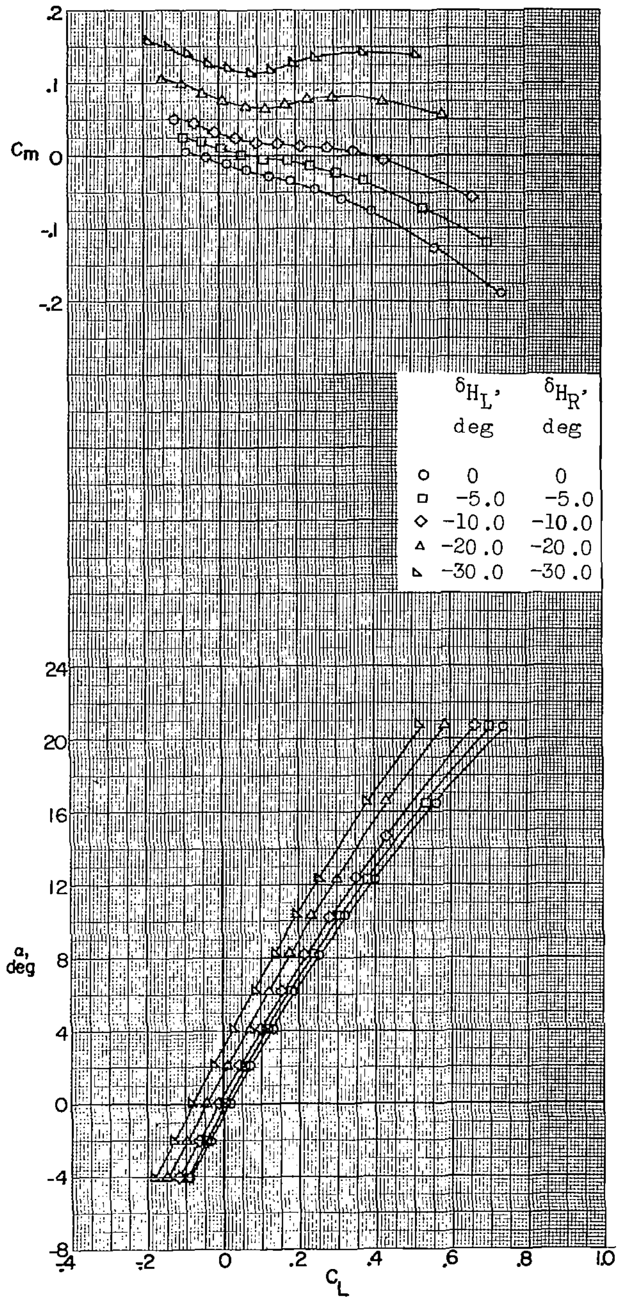

(d) M = 4.65.

Figure 15.- Continued.

[redacted]

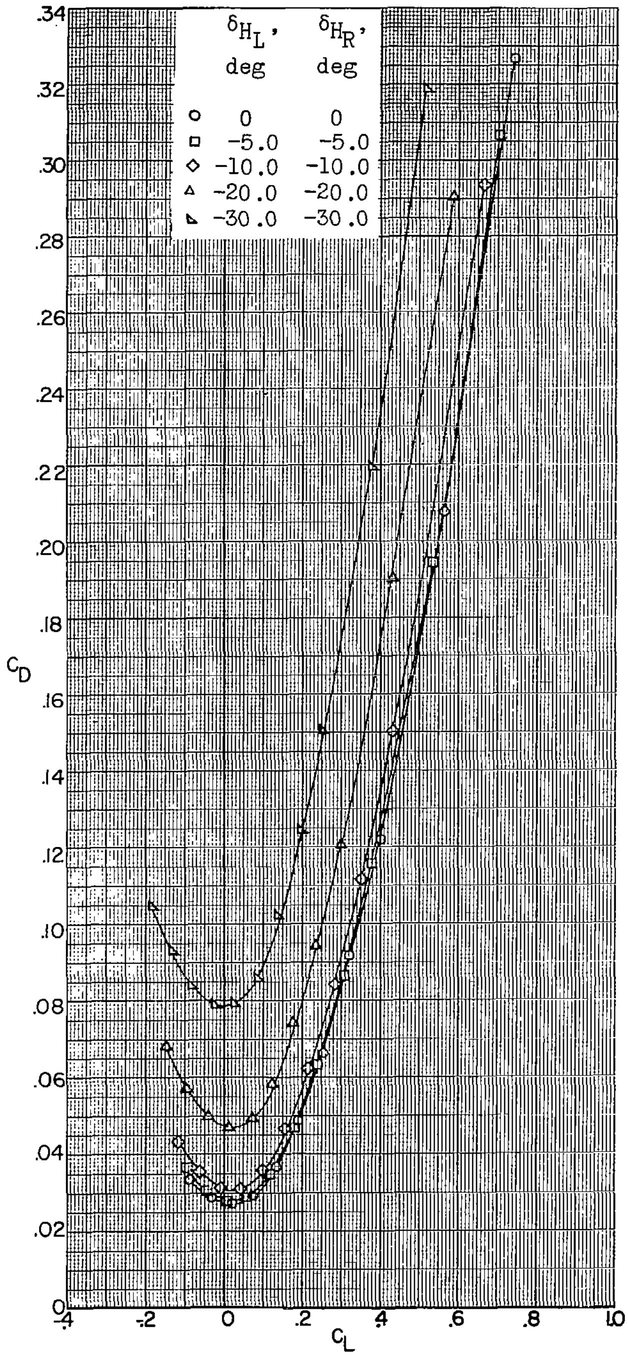

(d) Concluded.

Figure 15.- Concluded.

L-229

[redacted]

[redacted]

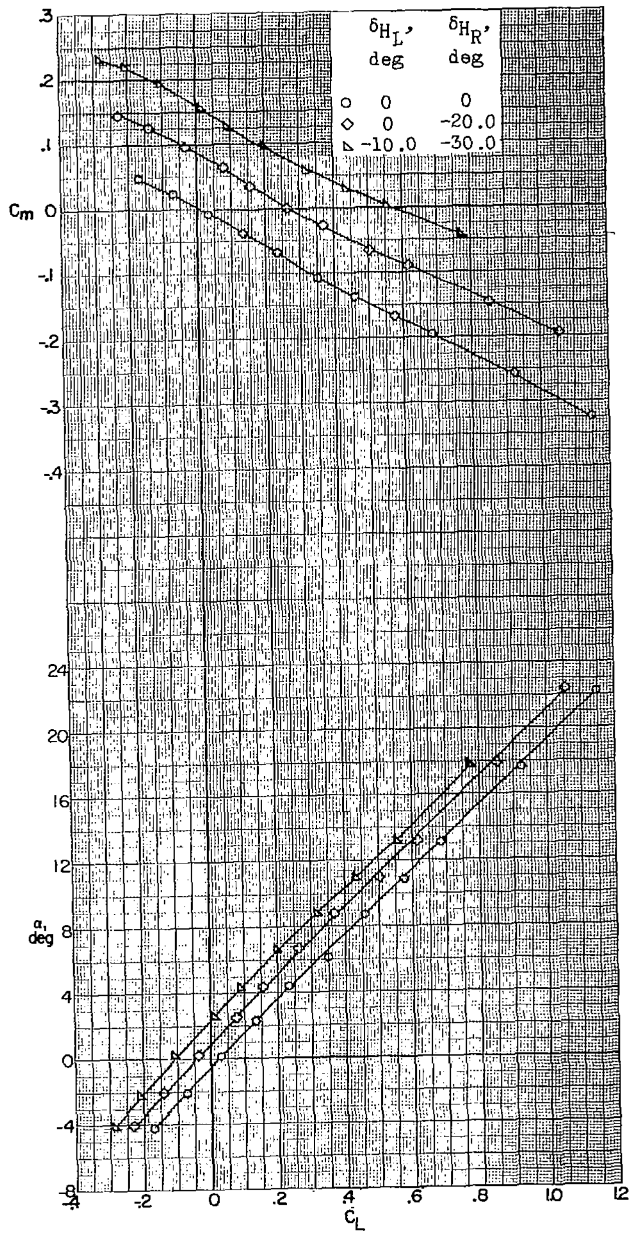

(a) M = 2.29.

Figure 16.- Longitudinal stability characteristics of a 0.067-scale model of the X-15 airplane with various roll-control deflections of the left and right panels of the horizontal tail. Speed brakes closed.

[redacted]

[redacted]

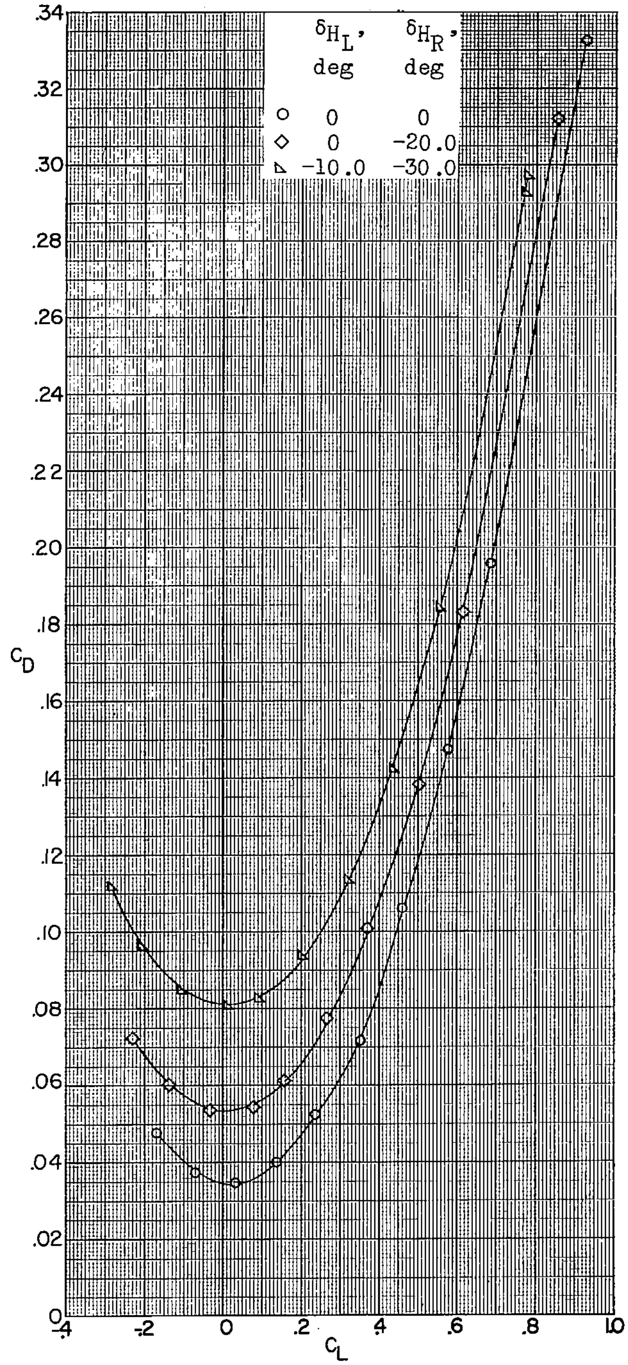

(a) Concluded.

Figure 16.- Continued.

L-229

[redacted]

L-229

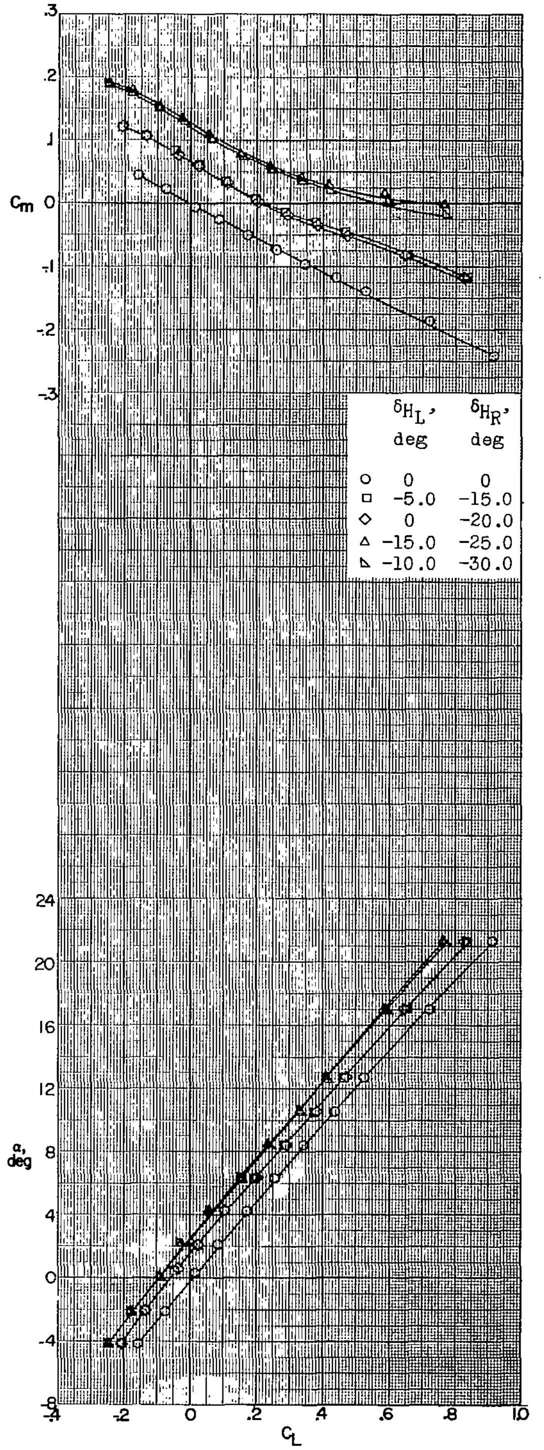

(b) M = 2.98.

Figure 16.- Continued.

[redacted]

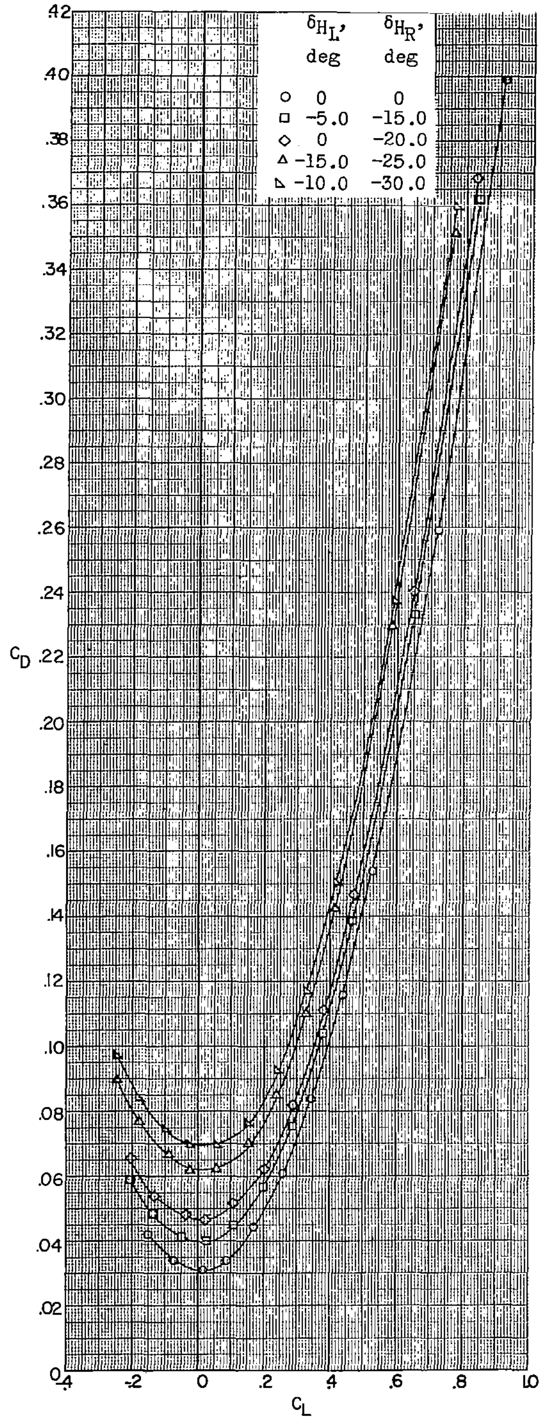

(b) Concluded.

Figure 16.- Continued.

L-229

[redacted]

[redacted]

L-229

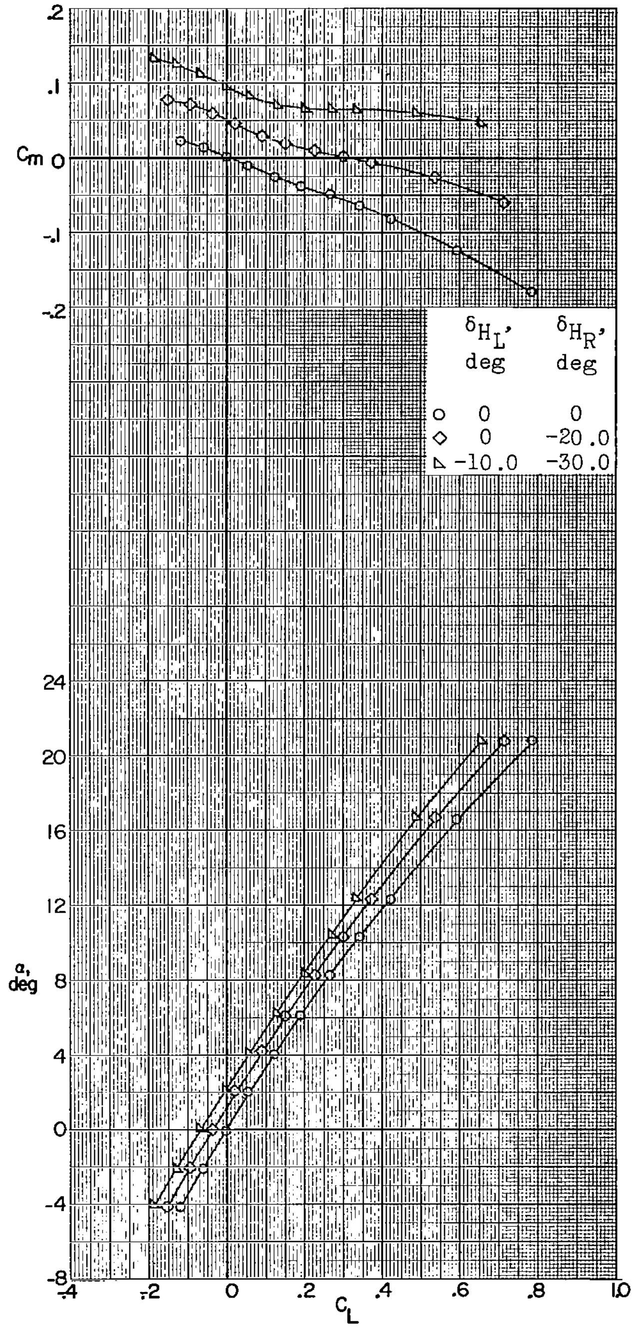

(c) M = 3.96.

Figure 16.- Continued.

[redacted]

[redacted]

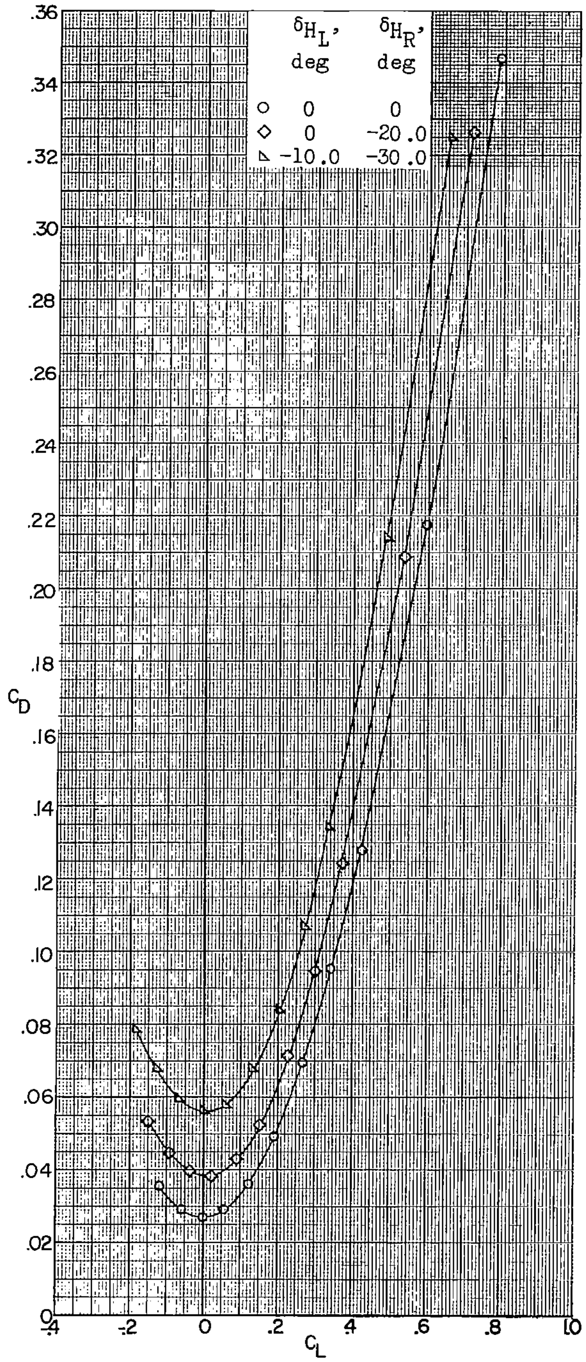

(c) Concluded.

Figure 16.- Continued.

[redacted]

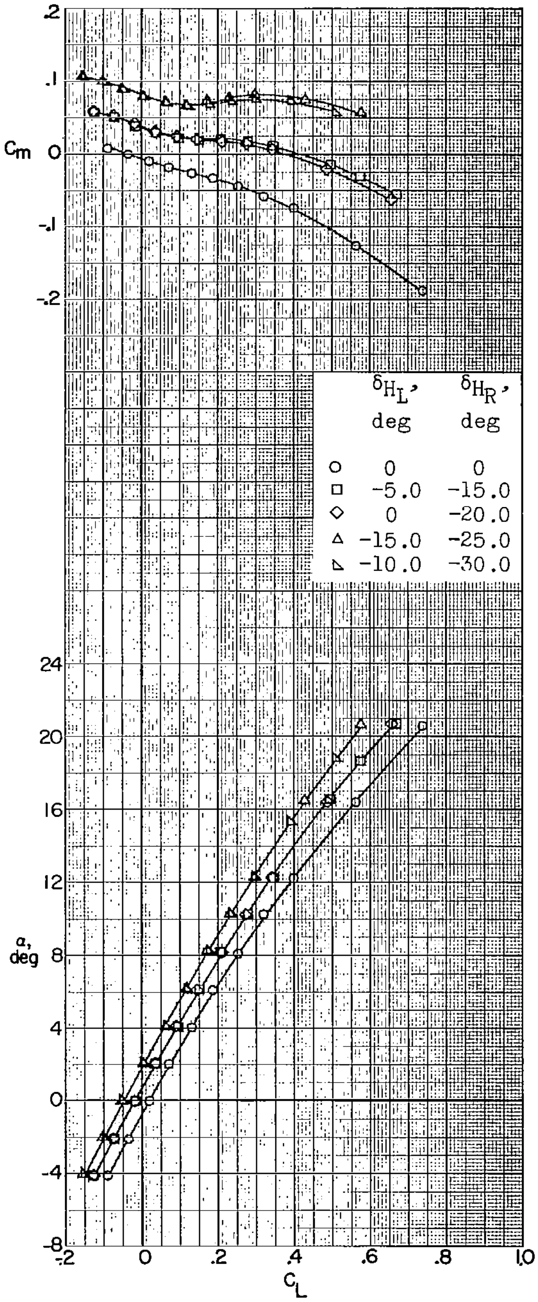

(d) M = 4.65.

Figure 16.- Continued.

[redacted]

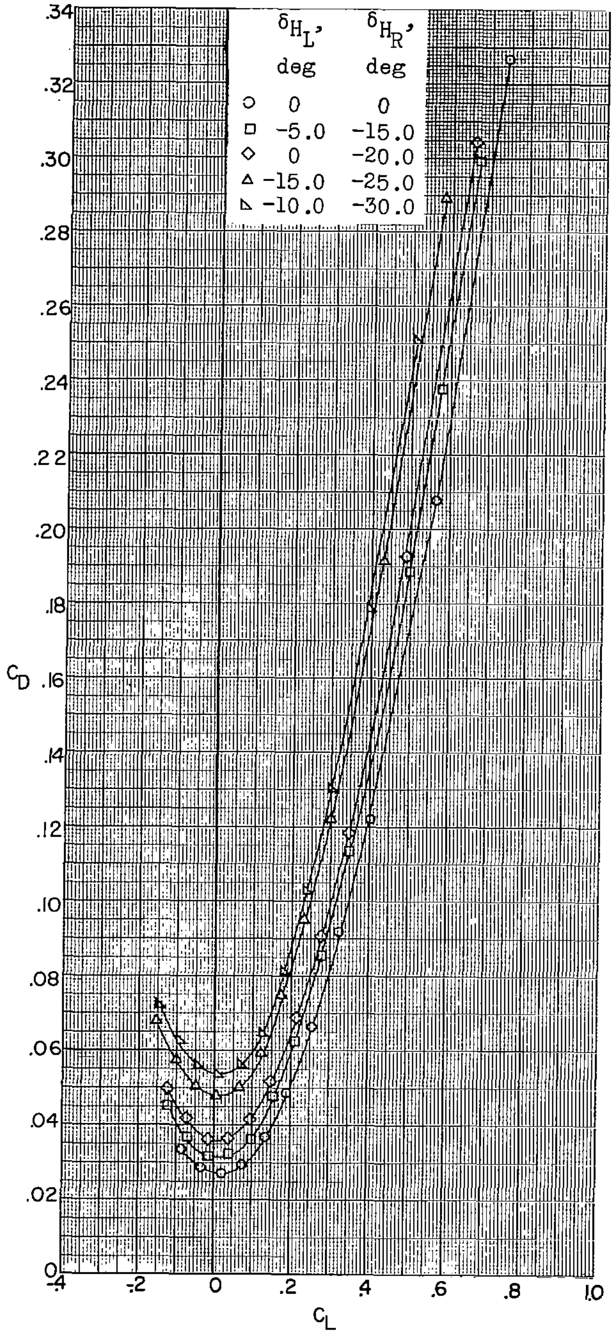

(d) Concluded.

Figure 16.- Concluded.

L-229

[redacted]

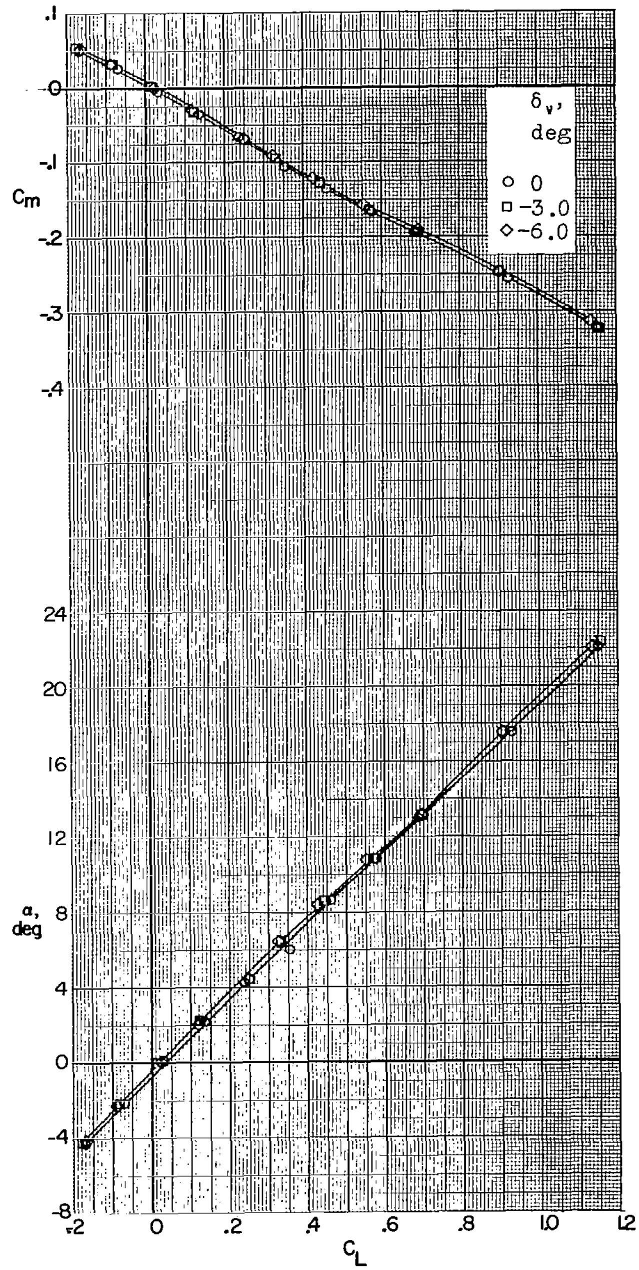

(a) M = 2.29.

Figure 17.- Longitudinal stability characteristics of a 0.067-scale model of the X-15 airplane with various deflections of the vertical tail. Speed brakes closed.

L-229

[redacted]

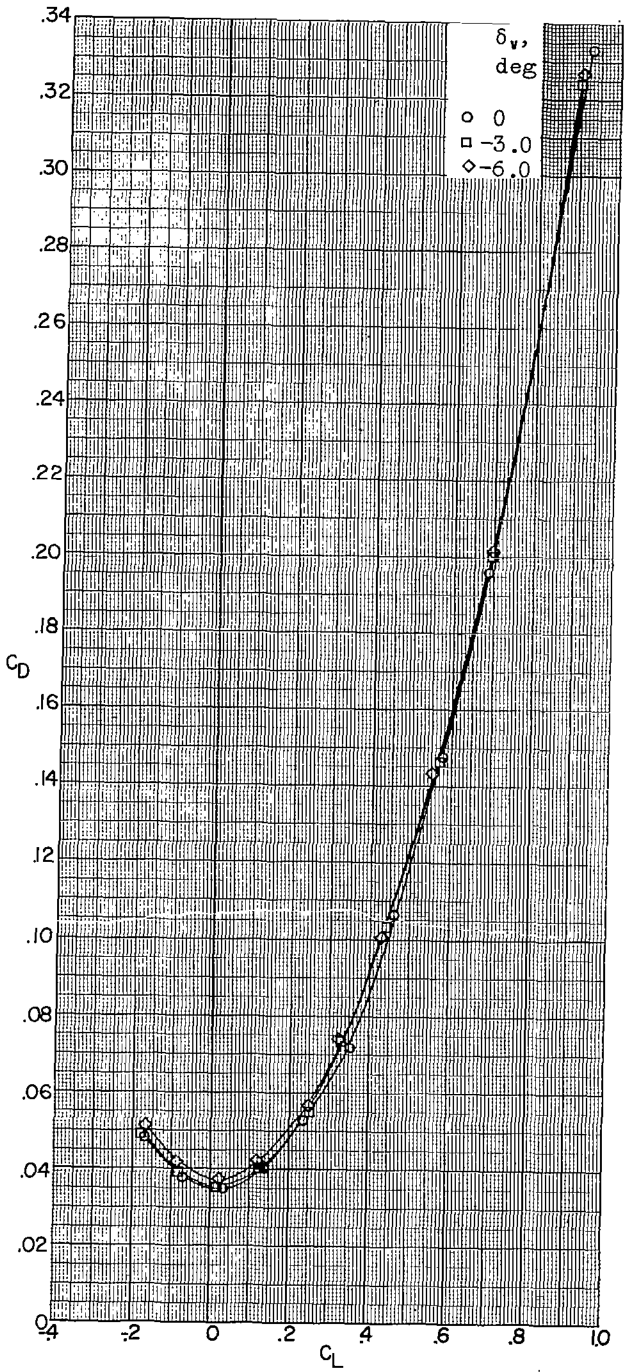

(a) Concluded.

Figure 17.- Continued.

L-229

[redacted]

[redacted]

L-229

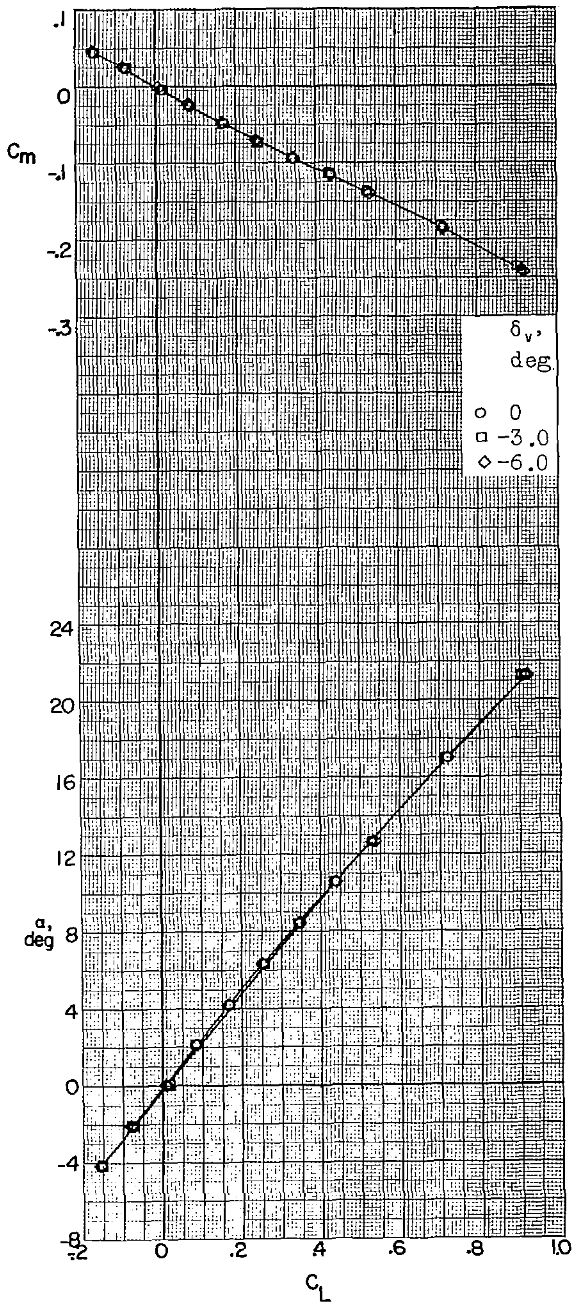

(b) M = 2.98.

Figure 17.- Continued.

[redacted]

[redacted]

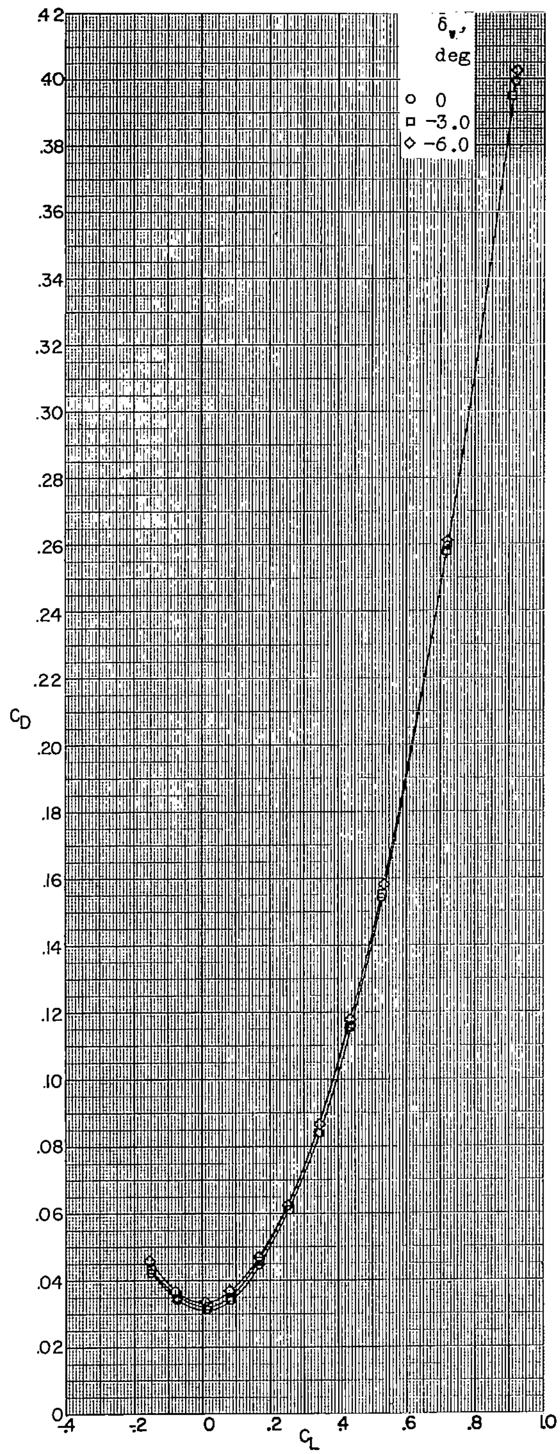

(b) Concluded.

Figure 17.- Continued.

[redacted]

L-229

[redacted]

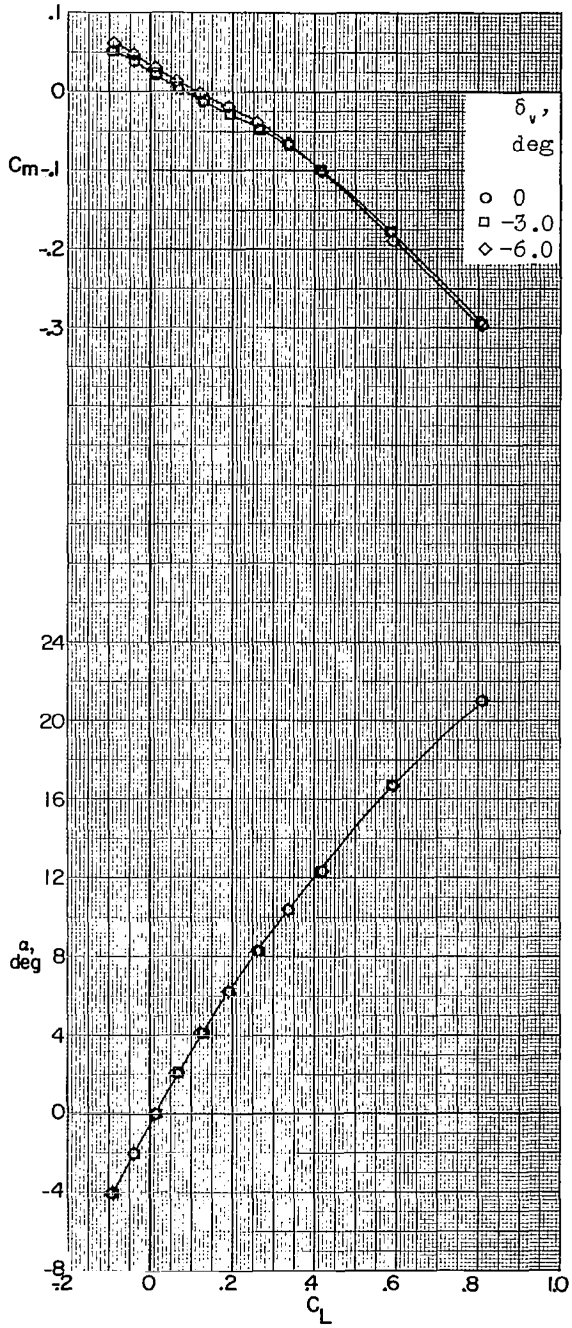

(c) $M = 3.96$.

Figure 17.- Continued.

[redacted]

[redacted]

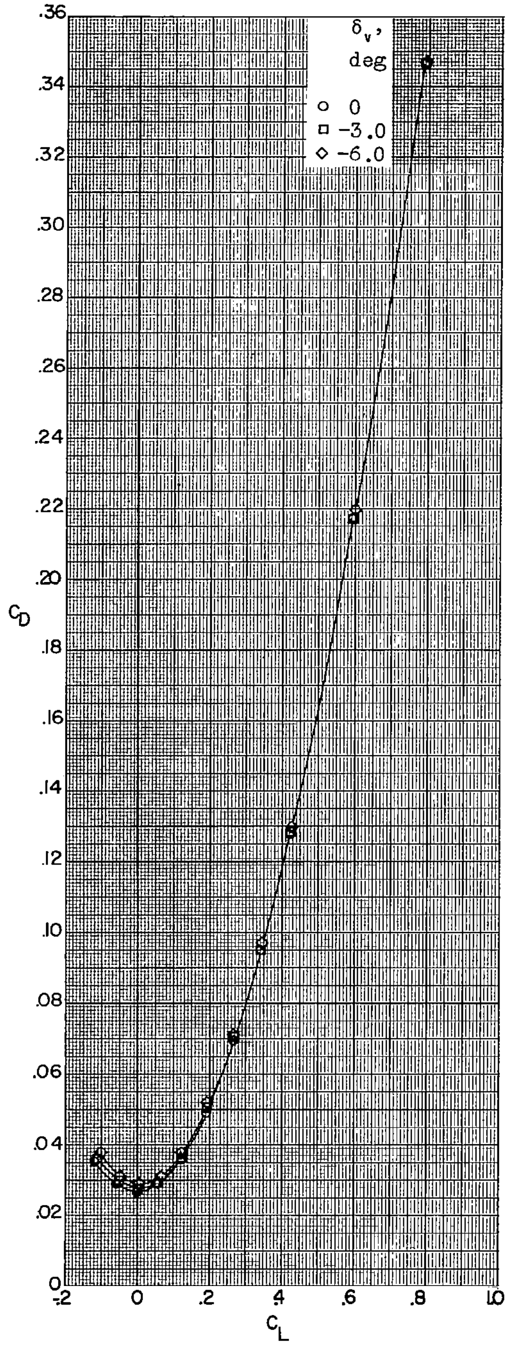

(c) Concluded.

Figure 17.- Continued.

L-229

[redacted]

[redacted]

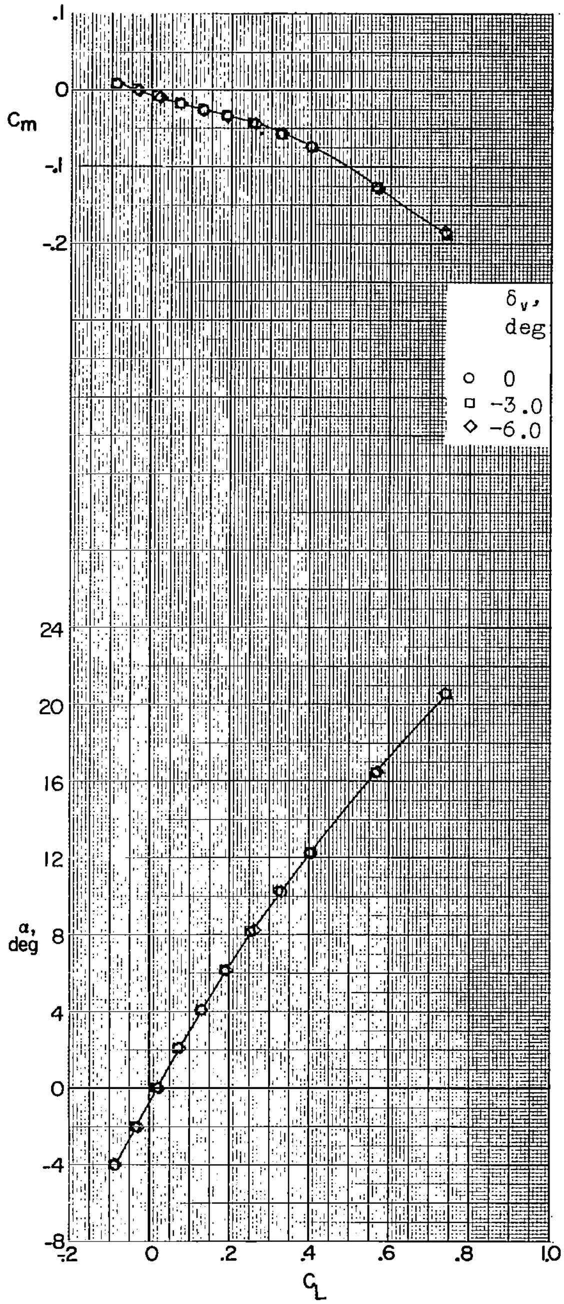

(d) M = 4.65.

Figure 17.- Continued.

[redacted]

[redacted]

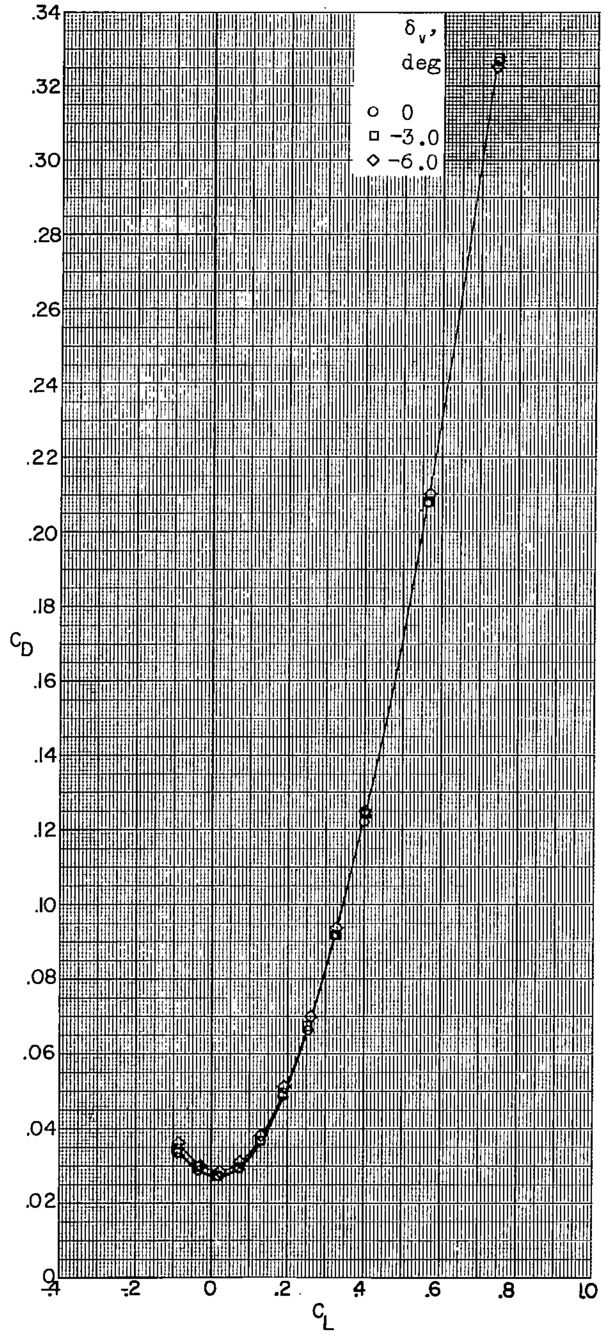

(d) Concluded.

Figure 17.- Concluded.

L-229

[redacted]

[redacted]

L-229

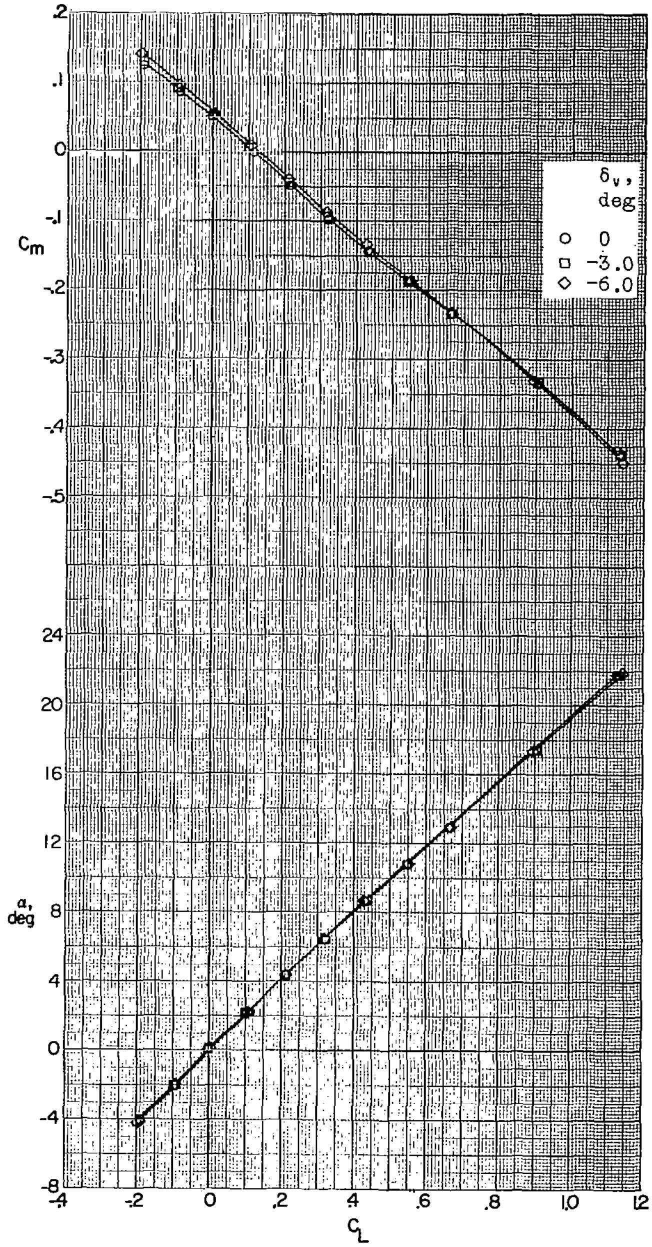

(a) M = 2.29.

Figure 18.- Longitudinal stability characteristics of a 0.067-scale model of the X-15 airplane with various deflections of the vertical tail. Speed brakes open 45°.

[redacted]

[redacted]

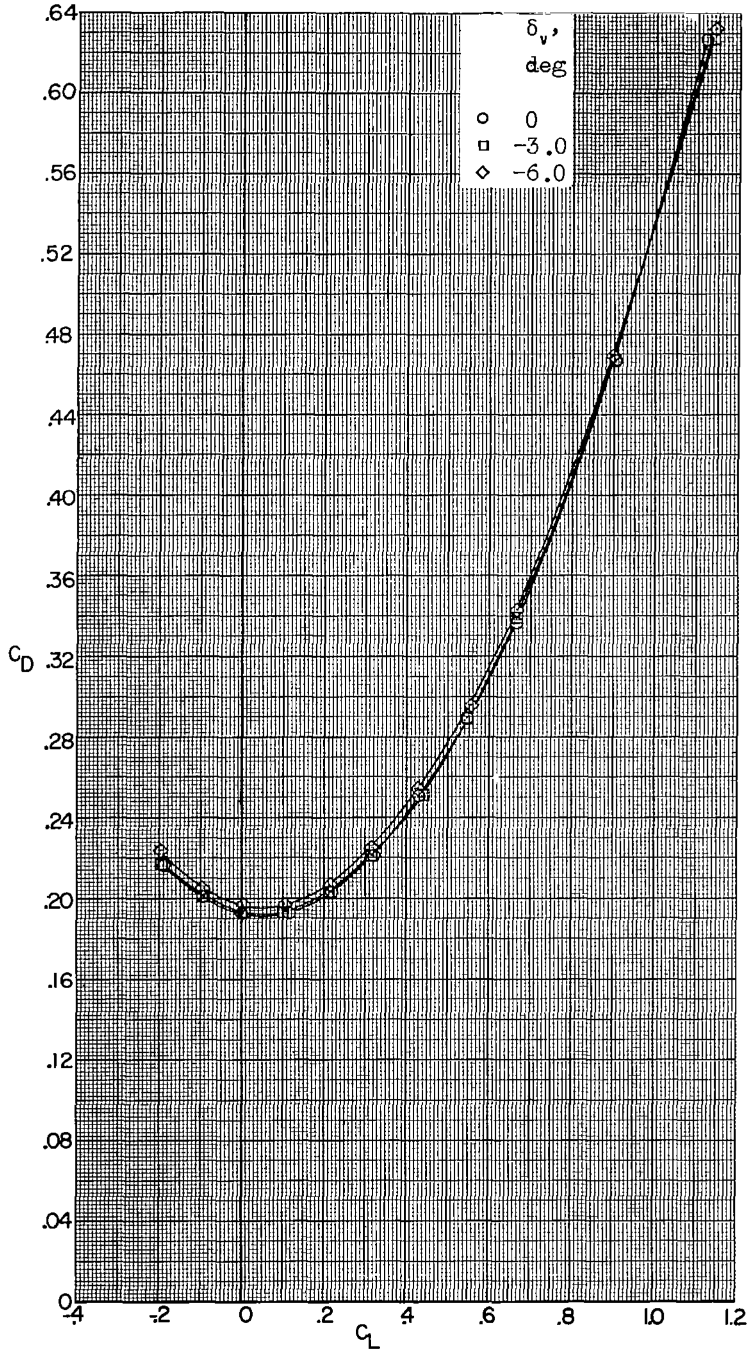

(a) Concluded.

Figure 18.- Continued.

L-229

[redacted]

[redacted]

L-229

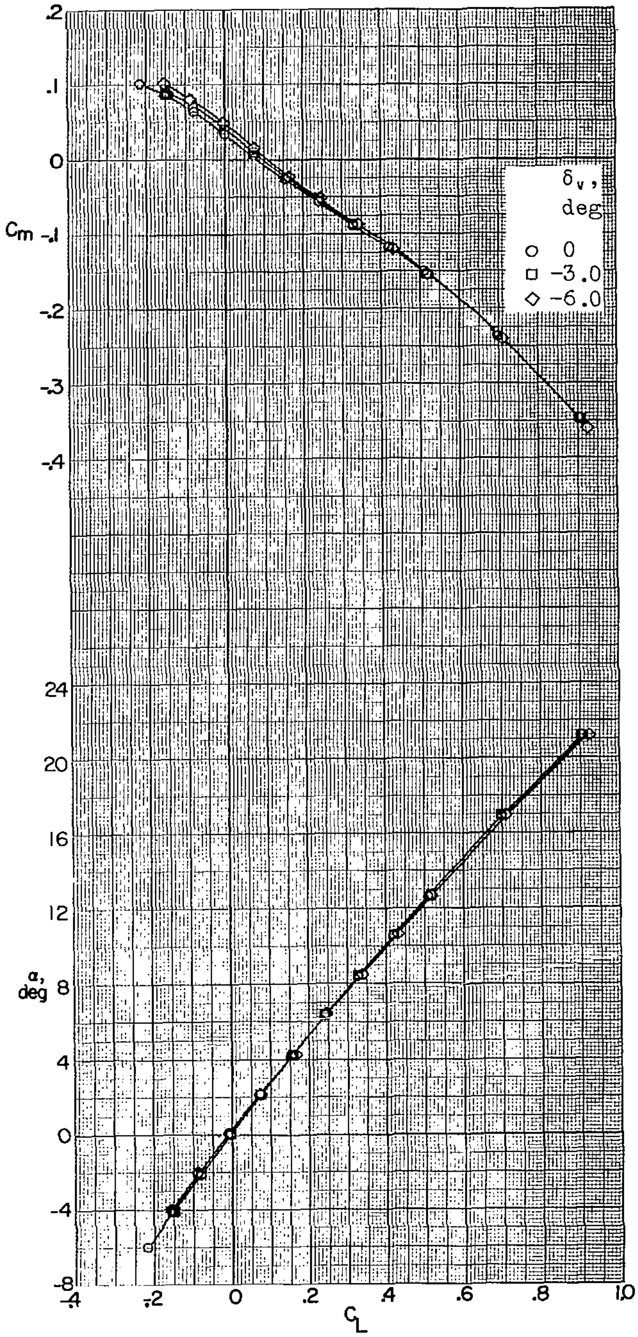

(b) M = 2.98.

Figure 18.- Continued.

[redacted]

[redacted]

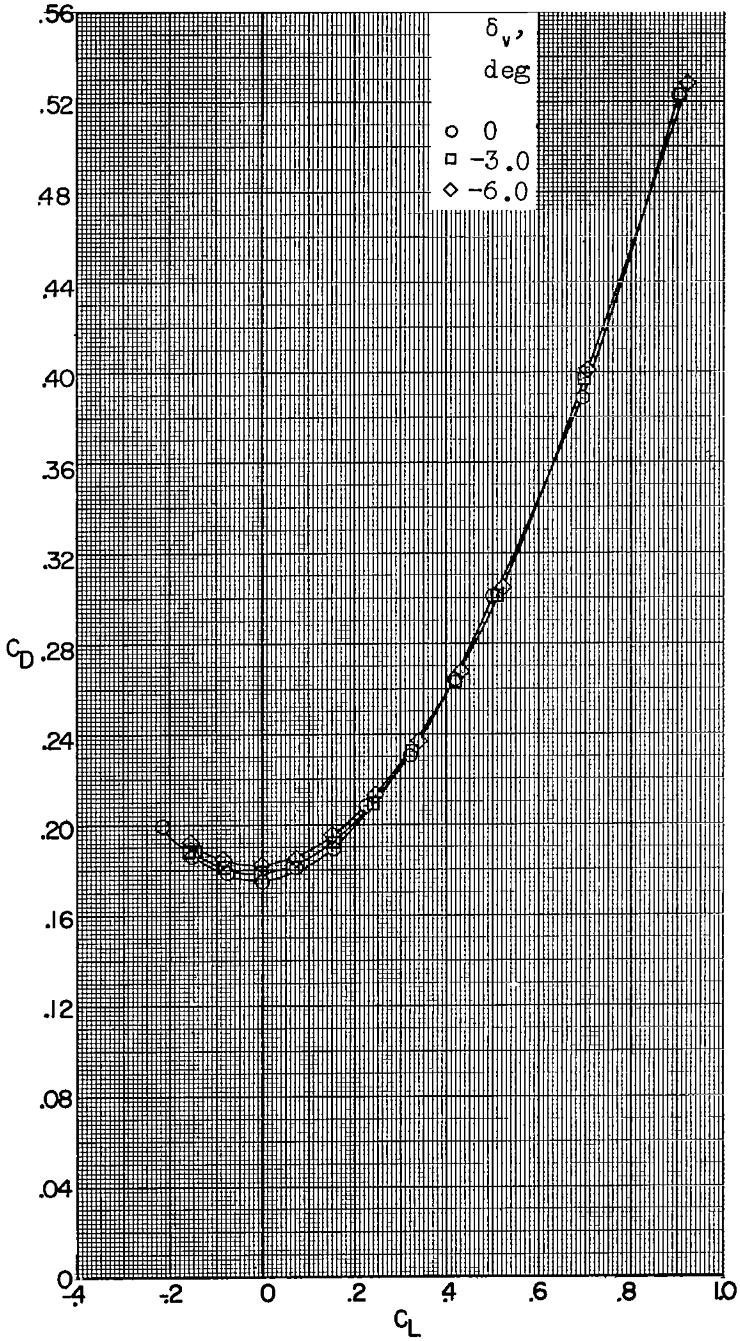

(b) Concluded.

Figure 18.- Continued.

L-229

[redacted]

L-229

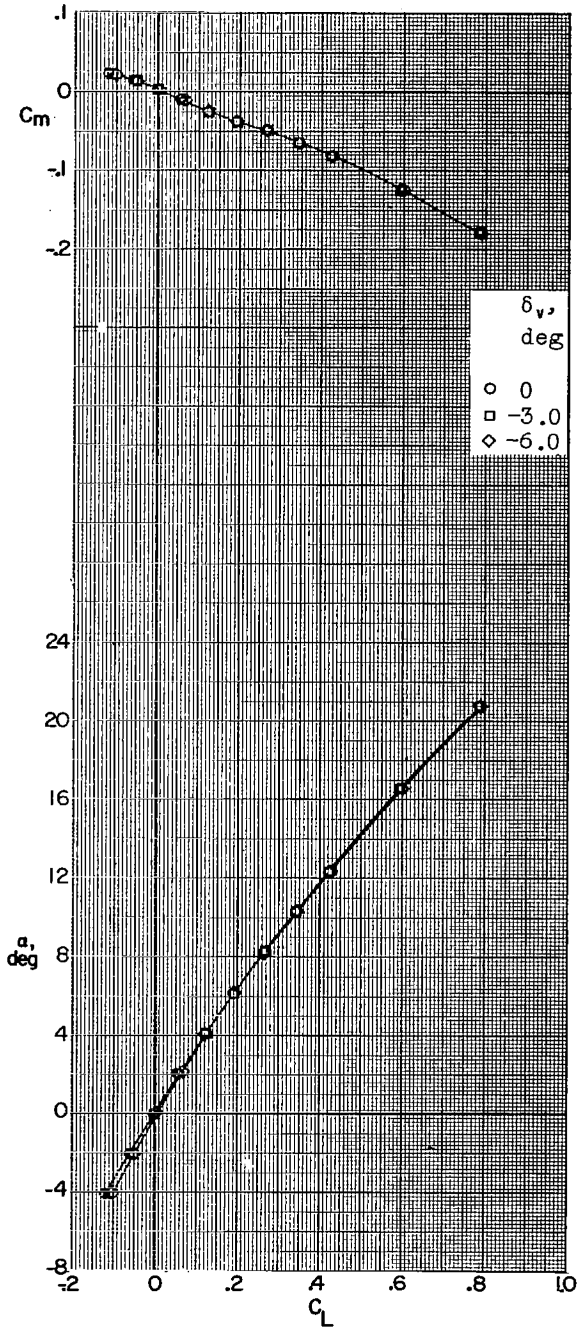

(c) M = 3.96.

Figure 18.- Continued.

[redacted]

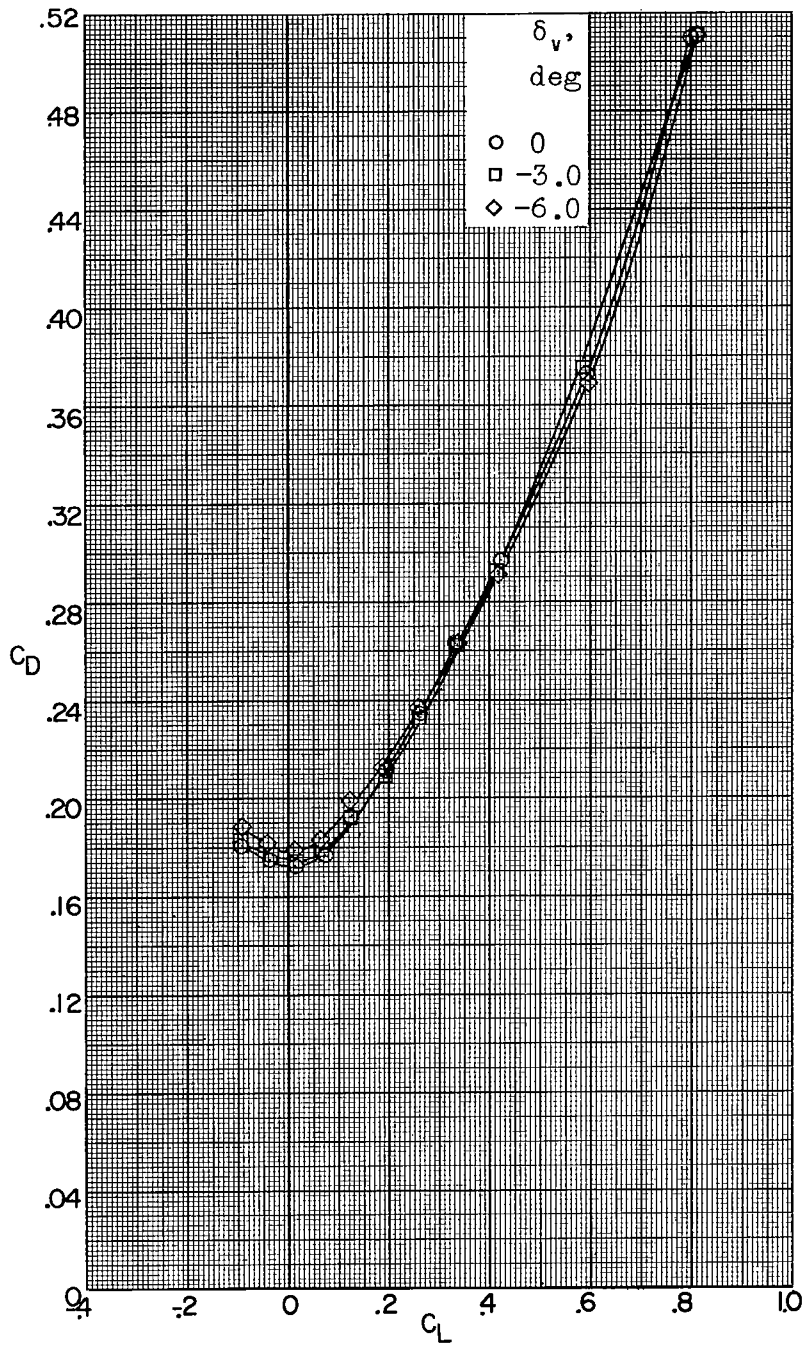

(c) Concluded.

Figure 18.- Continued.

[redacted]

[redacted]

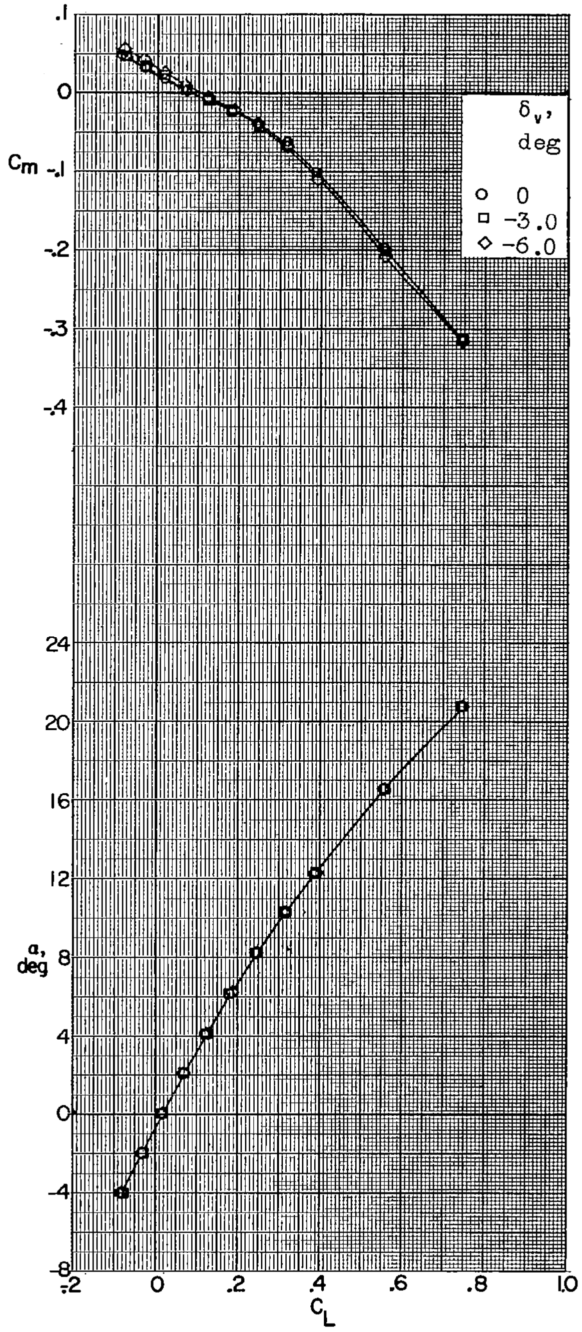

(d) M = 4.65.

Figure 18.- Continued.

L-229

[redacted]

[redacted]

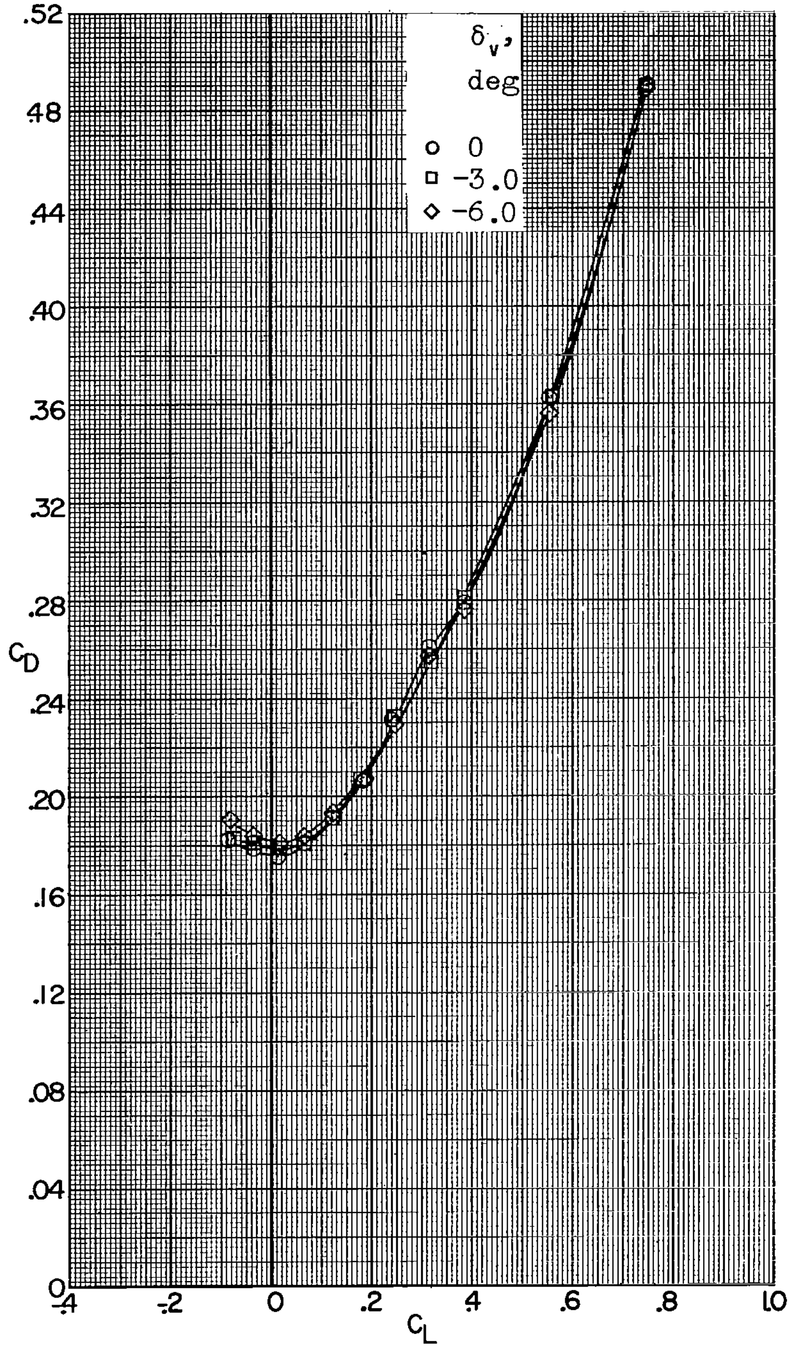

(d) Concluded.

Figure 18.- Concluded.

L-229

[redacted]

[redacted]

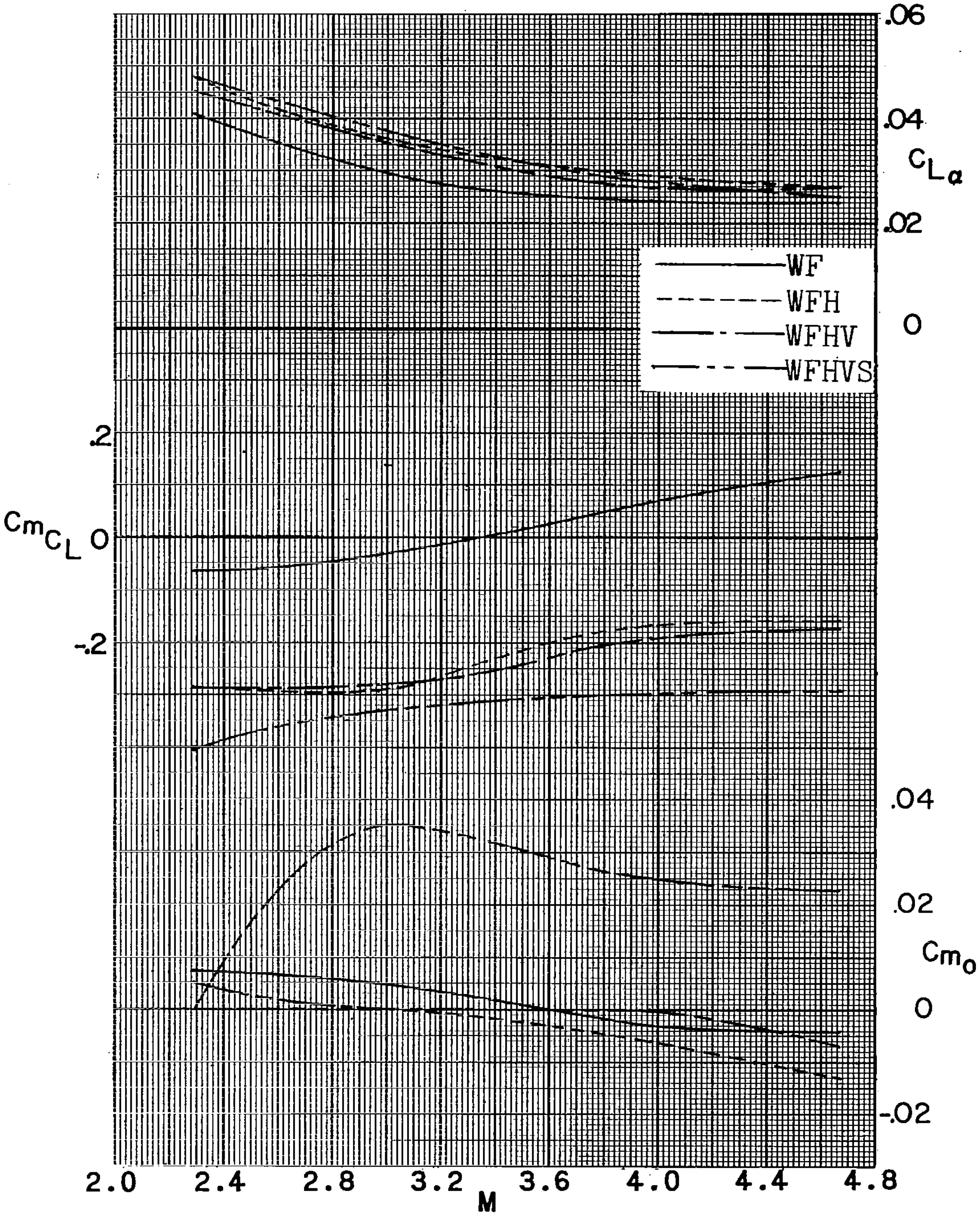

Figure 19.- Summary of longitudinal aerodynamic characteristics of a 0.067-scale model of the X-15 airplane.

[redacted]

L-229

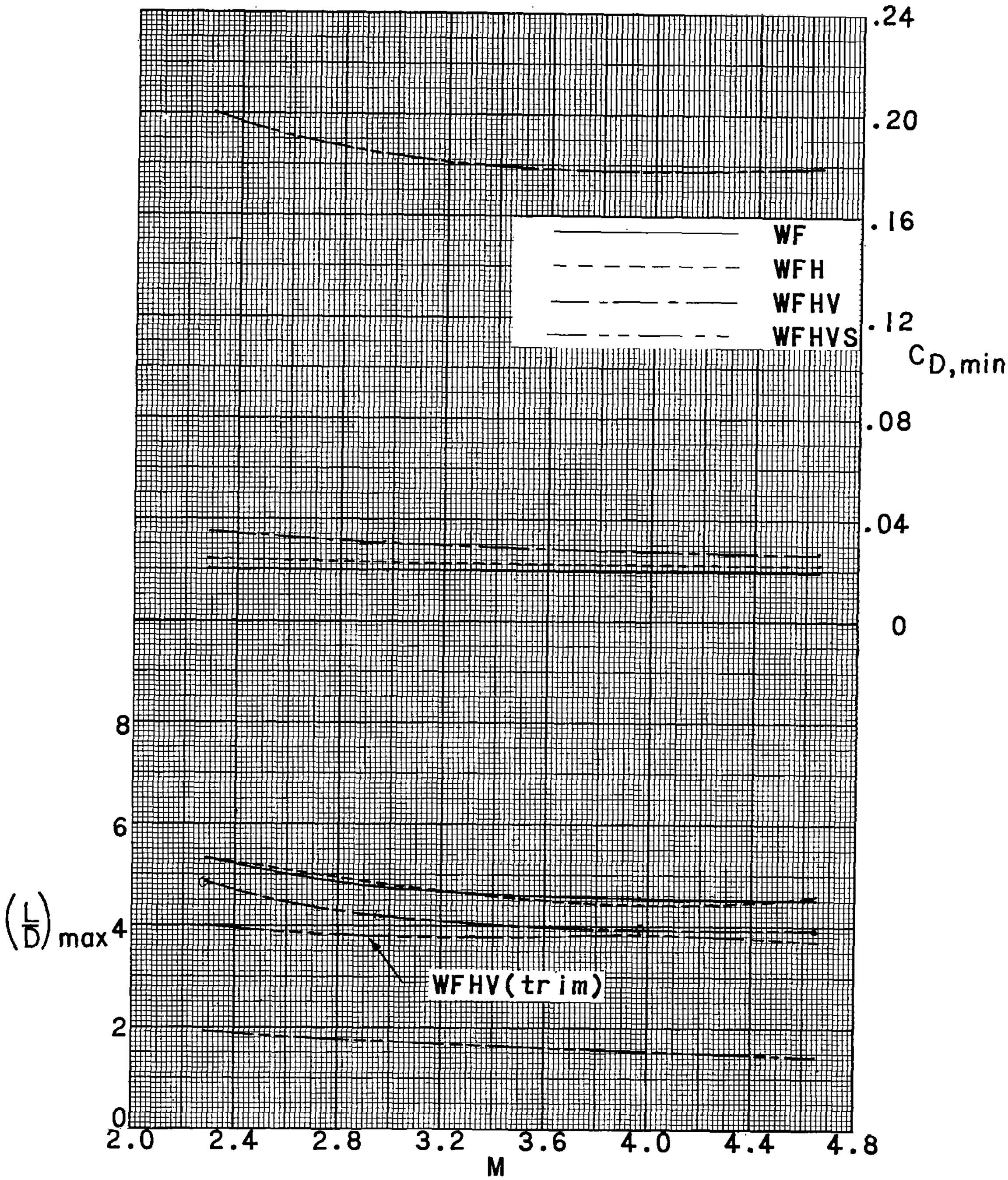

Figure 19.- Continued.

L-229

[redacted]

L-229

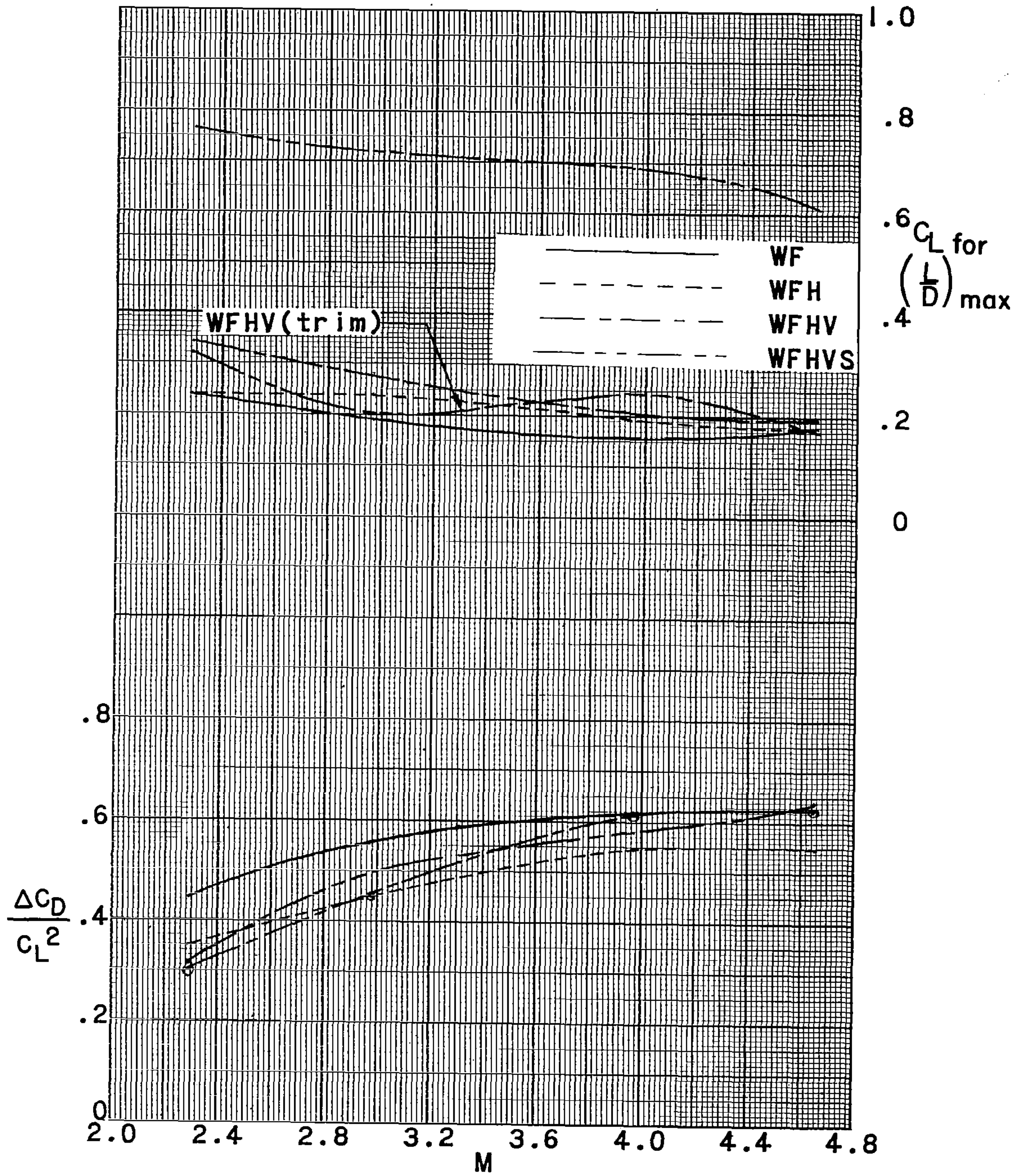

Figure 19.- Concluded.

[redacted]

[redacted]

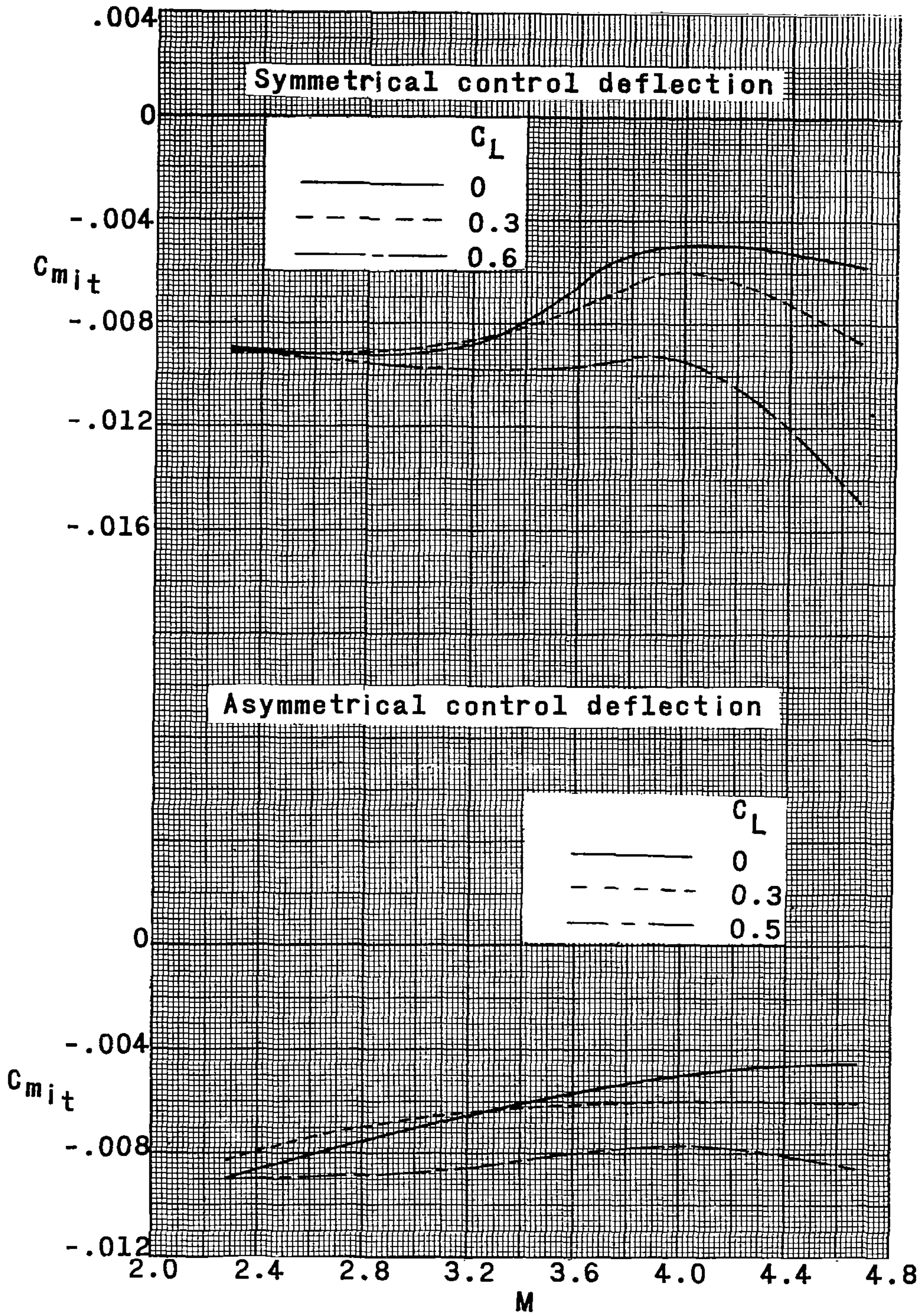

L-229

Figure 20.- Summary of the stabilizer effectiveness of a 0.067-scale model of the X-15 airplane. Speed brakes closed.

[redacted]

L-229

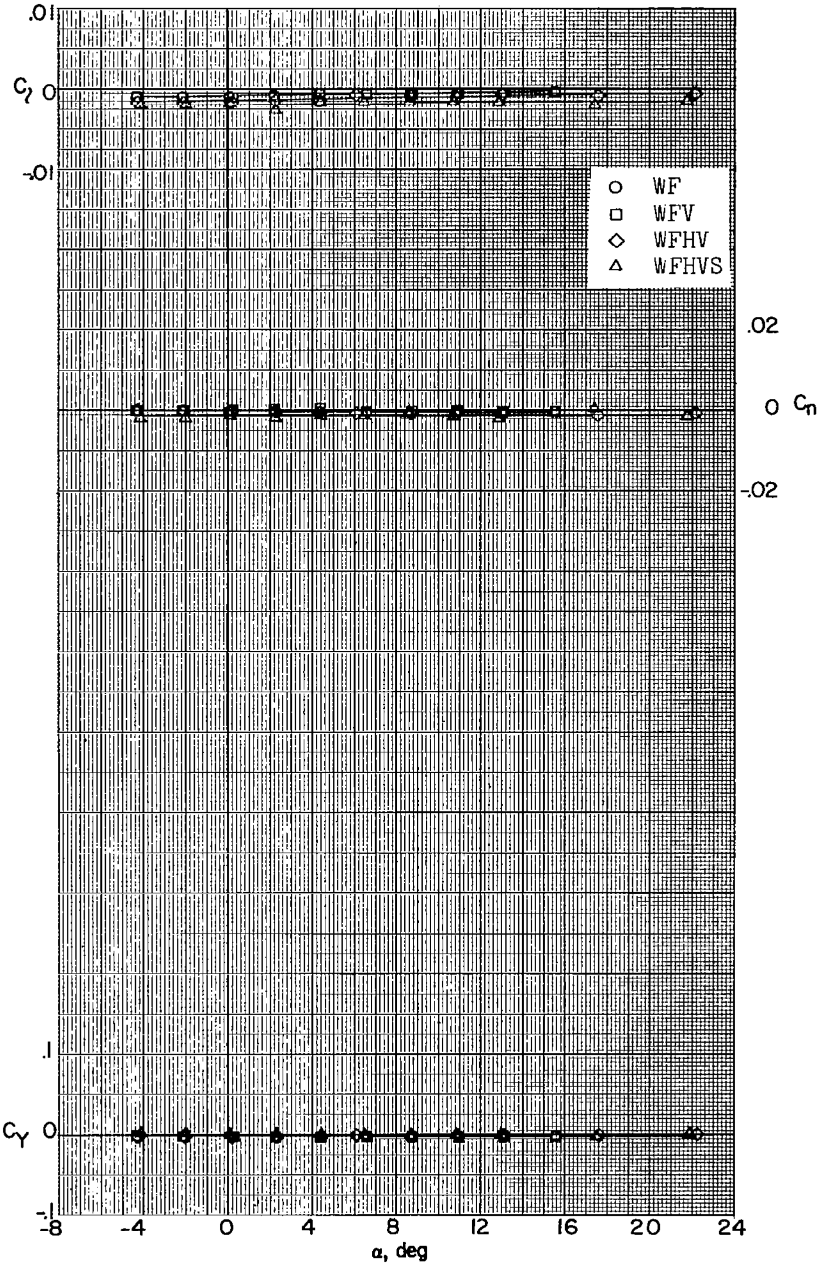

(a) M = 2.29; β = 0°.

Figure 21.- Lateral stability characteristics of a 0.067-scale model of the X-15 airplane with various combinations of model components.

[redacted]

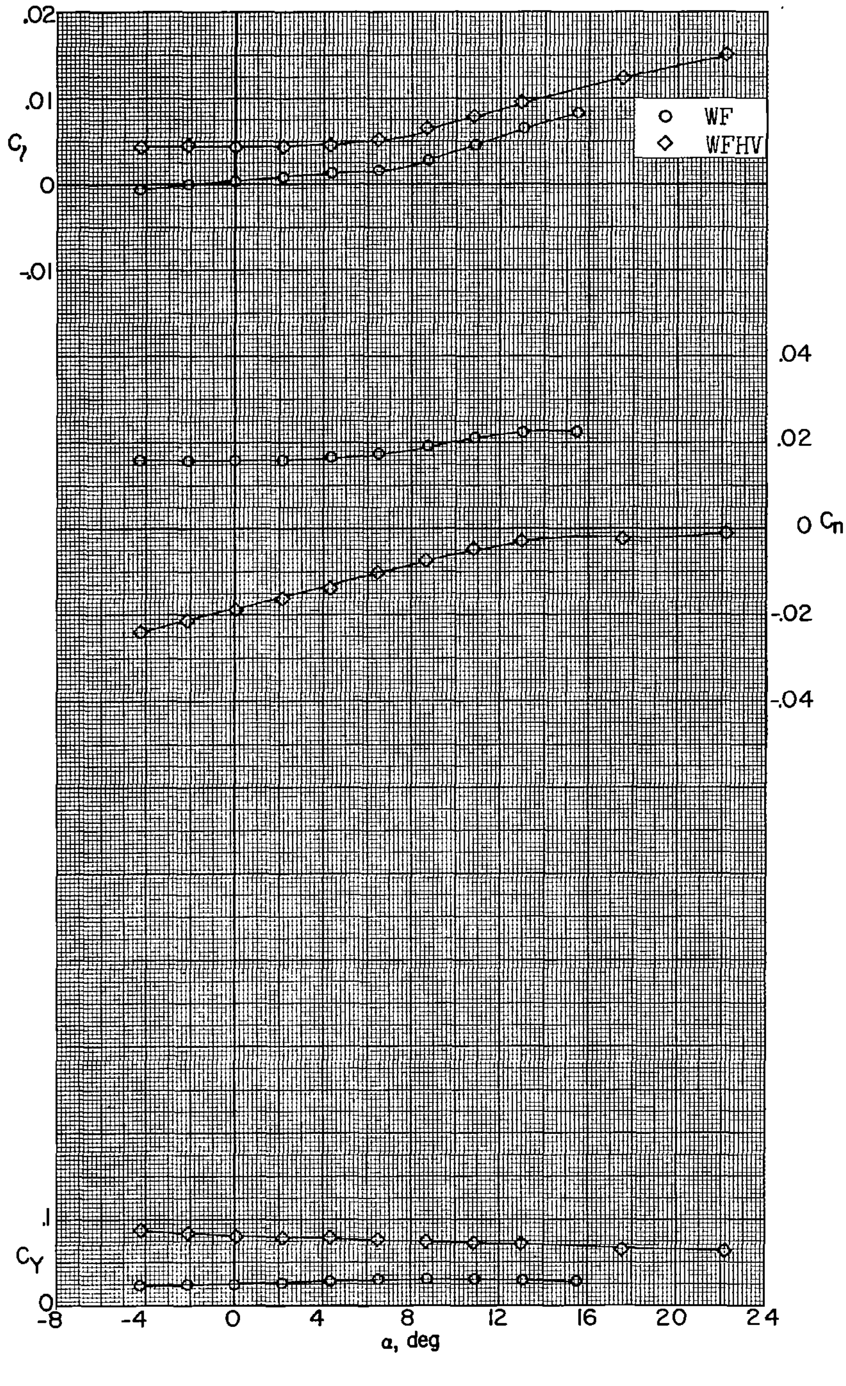

(b) M = 2.29; β = -5.2°.

Figure 21.- Continued.

[redacted]

[redacted]

L-229

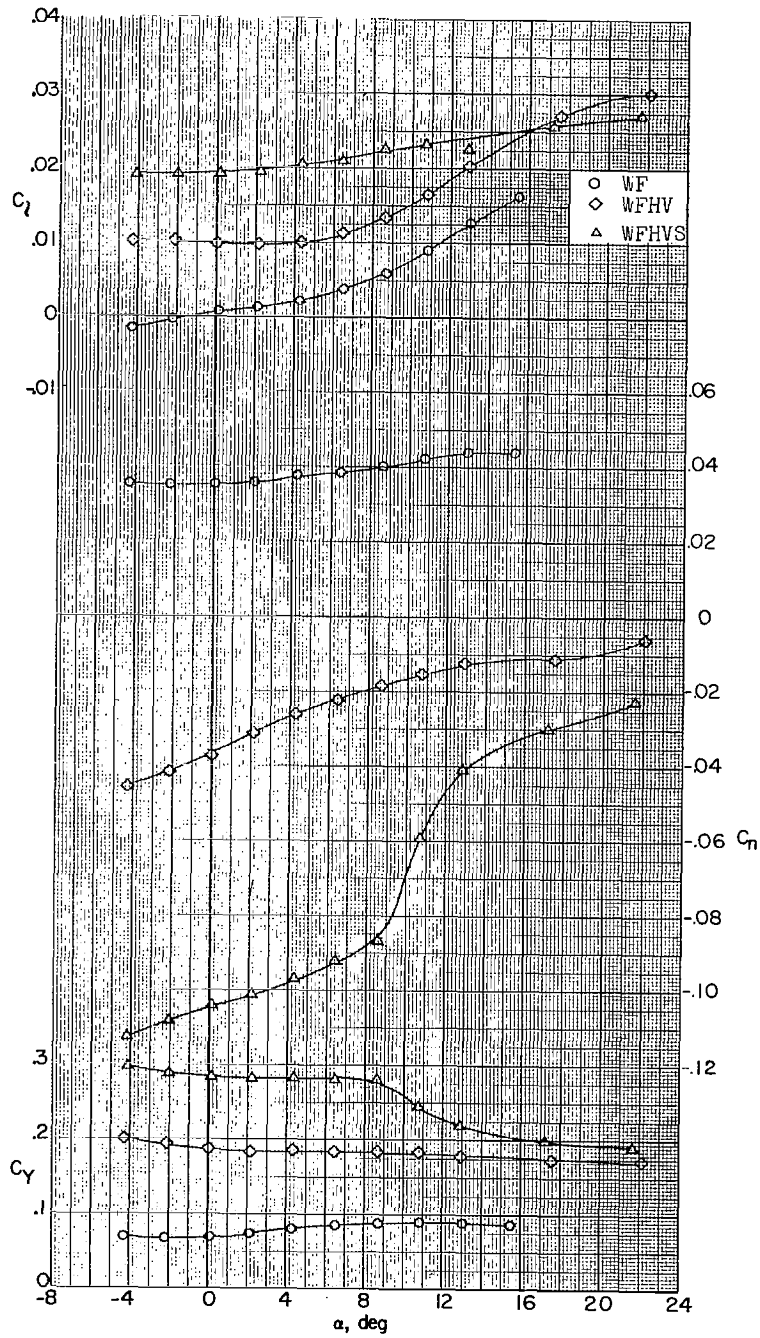

(c) M = 2.29; β = -10.7°.

Figure 21.- Continued.

[redacted]

[redacted]

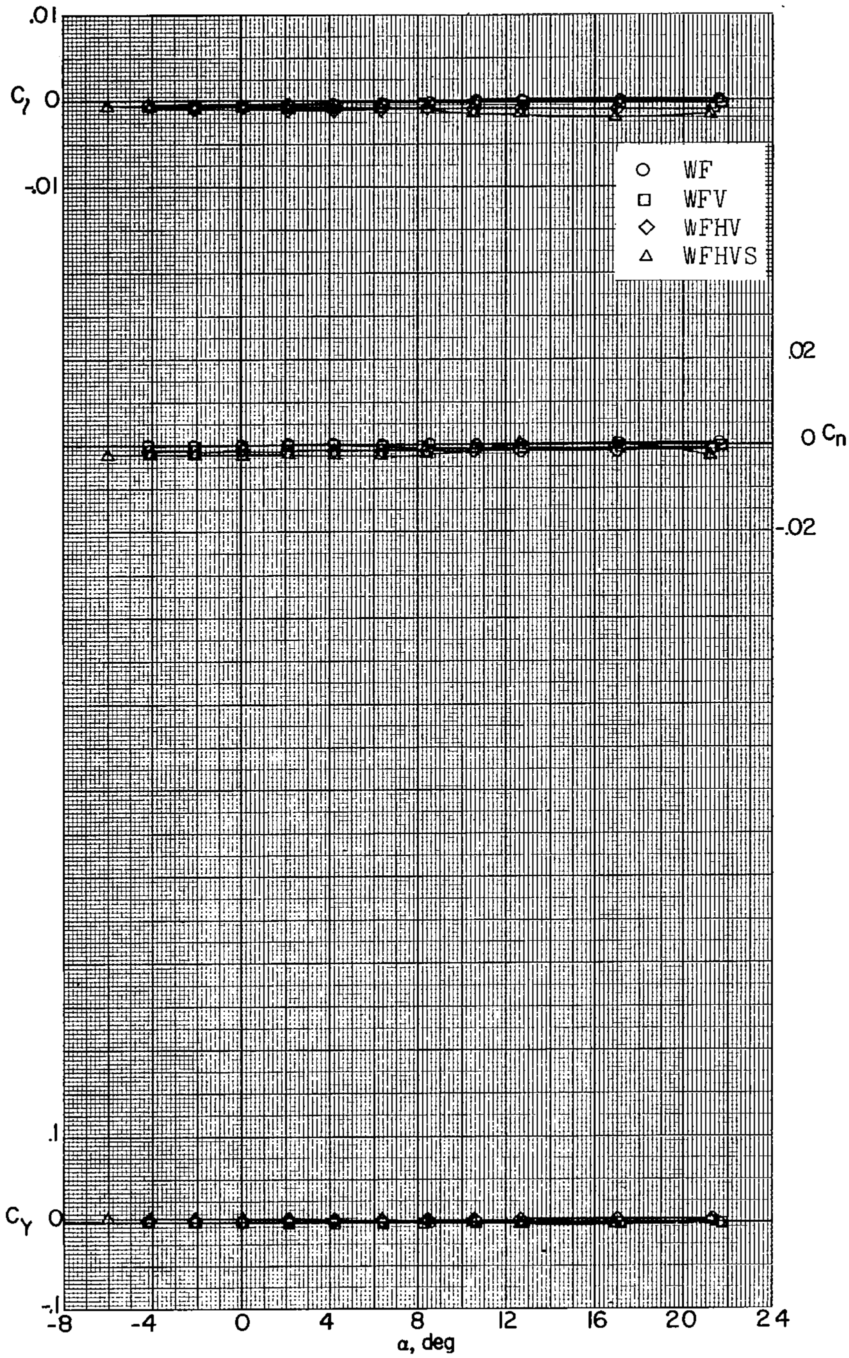

(d) M = 2.98; β = 0°.

Figure 21.- Continued.

L-229

[redacted]

[redacted]

L-229

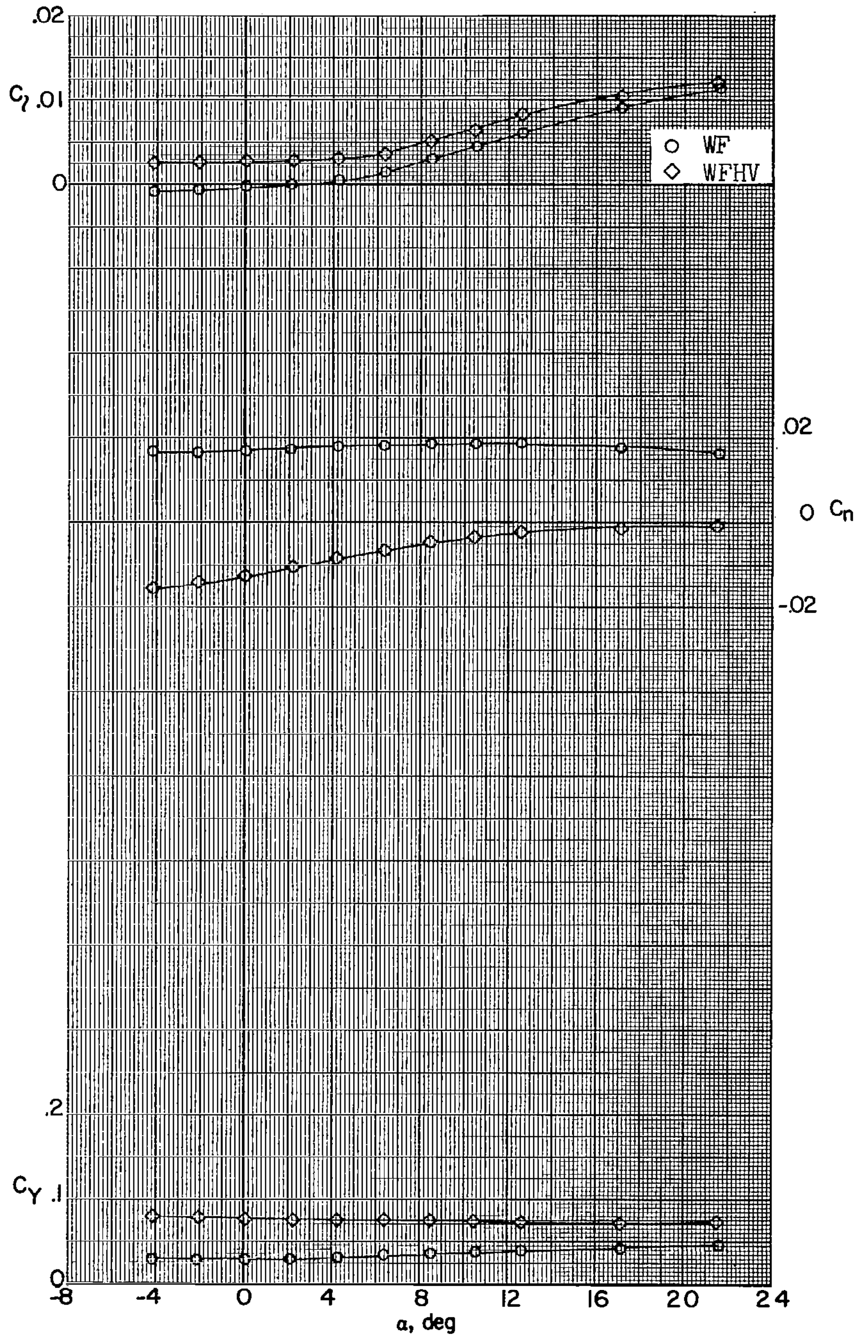

(e) M = 2.98; β = -5.2°.

Figure 21.- Continued.

[redacted]

[redacted]

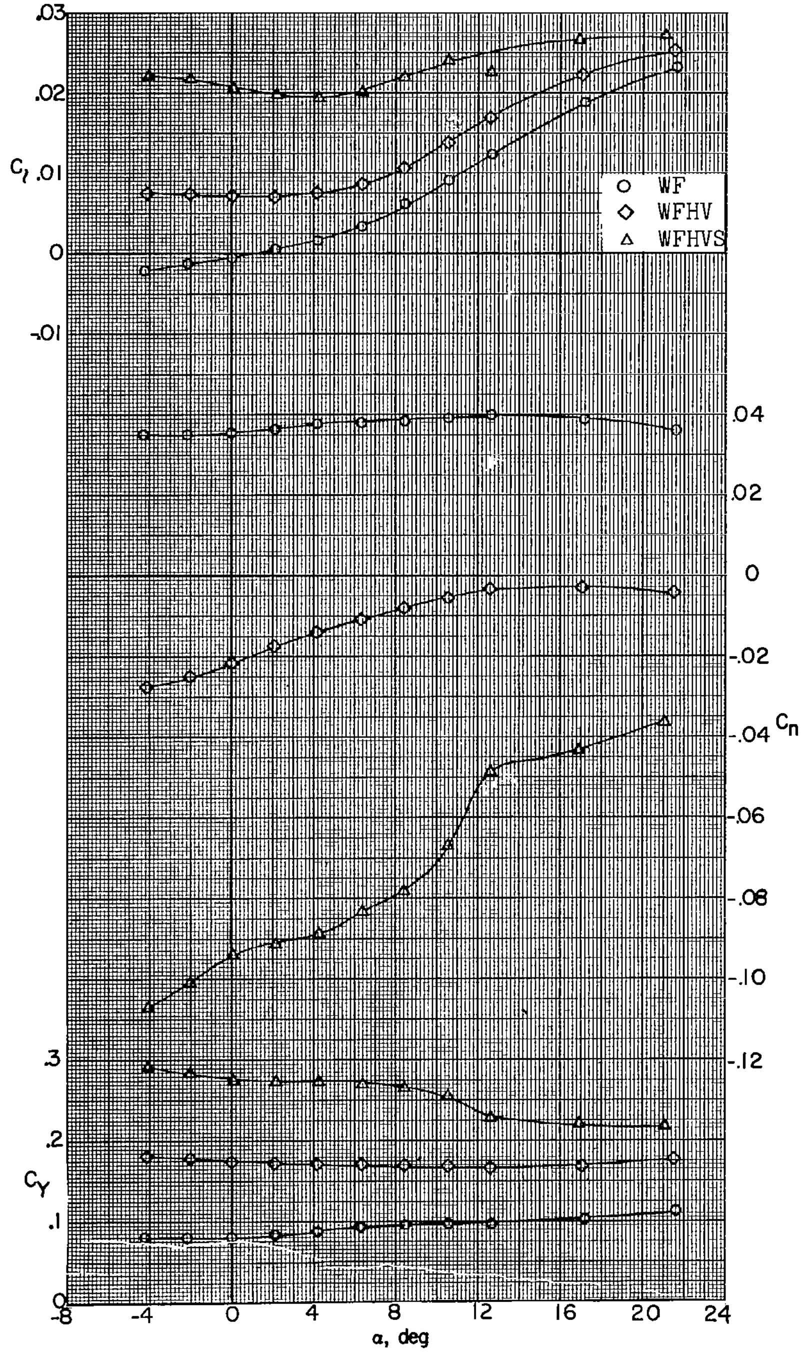

(f) M = 2.98; β = -10.6°.

Figure 21.- Continued.

L-229

[redacted]

L-229

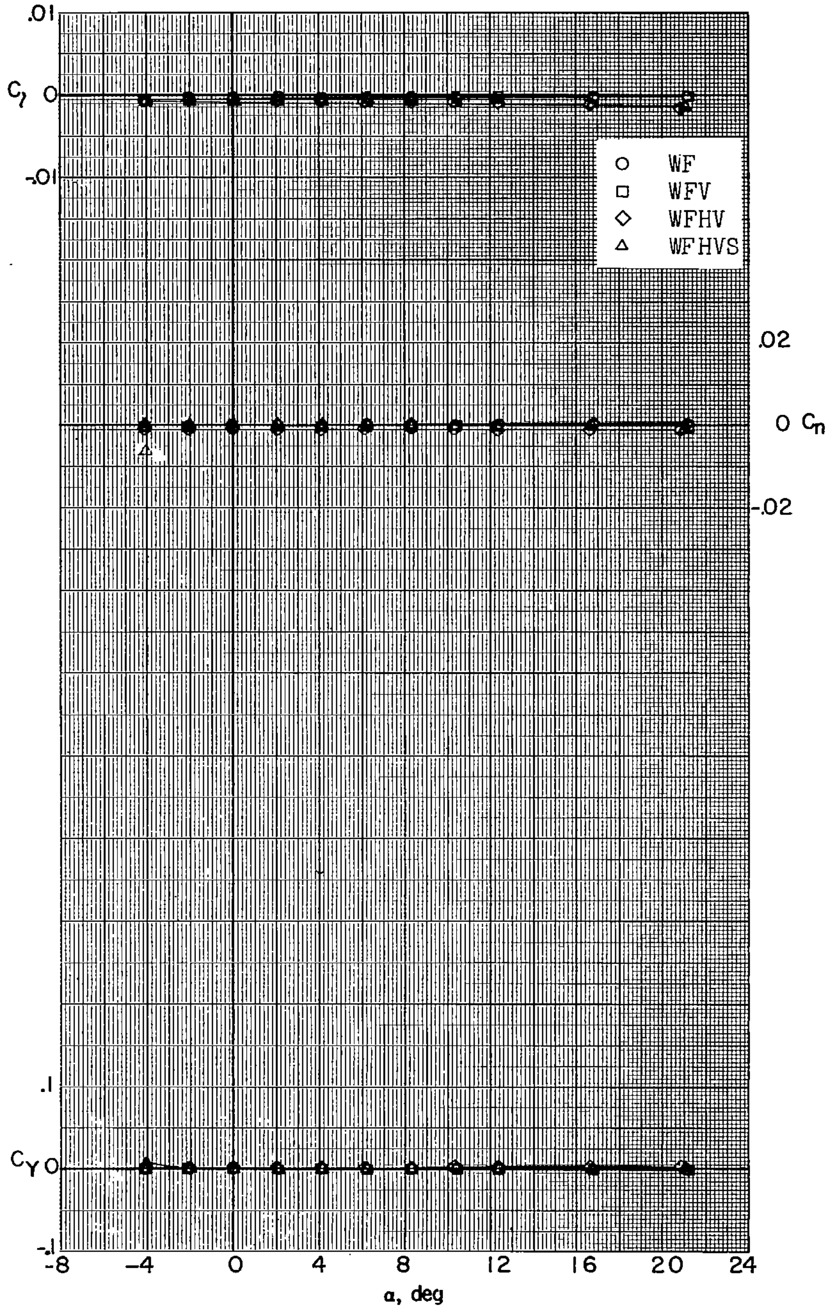

(g) $M = 3.96$; $\beta = 0^{\circ}$.

Figure 21.- Continued.

[redacted]

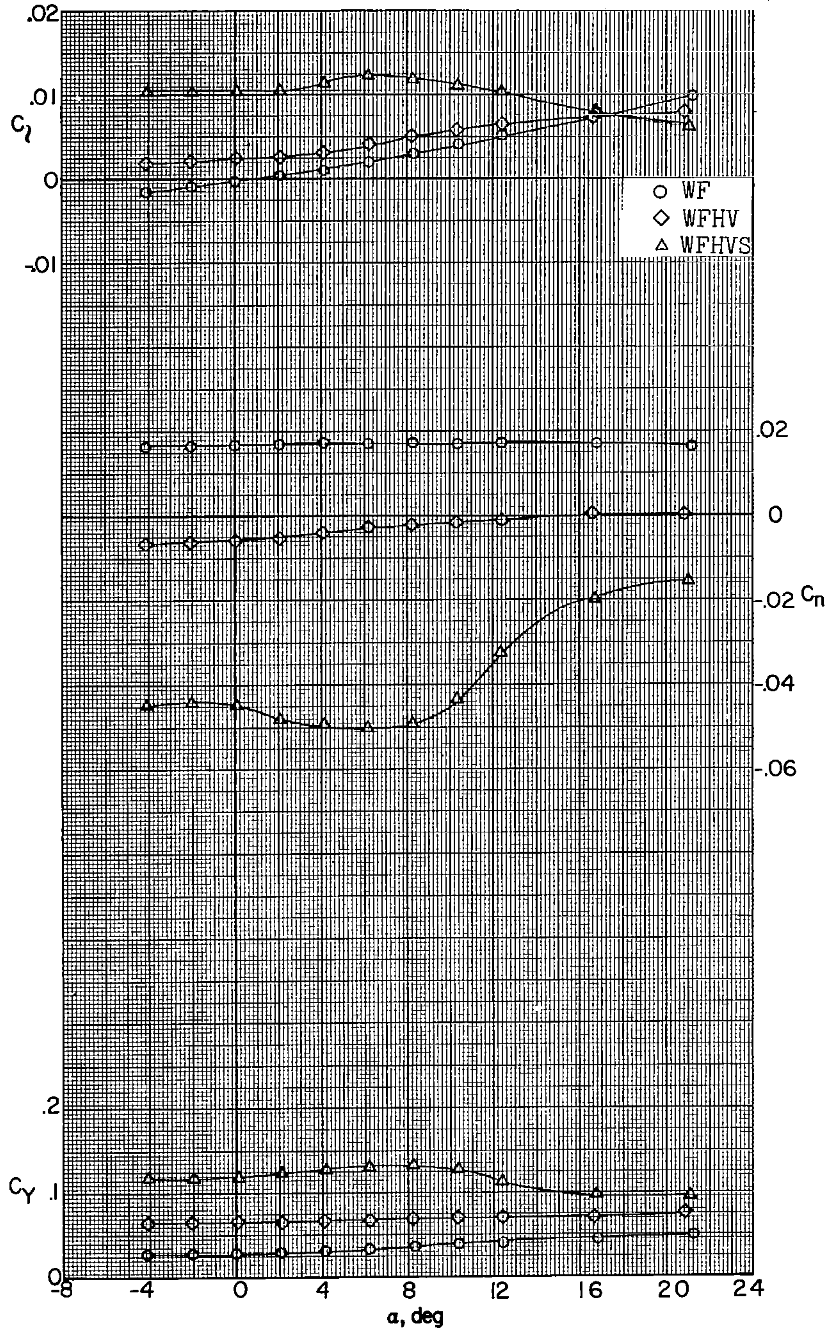

(h) M = 3.96; β = -5.1°.

Figure 21.- Continued.

L-229

[redacted]

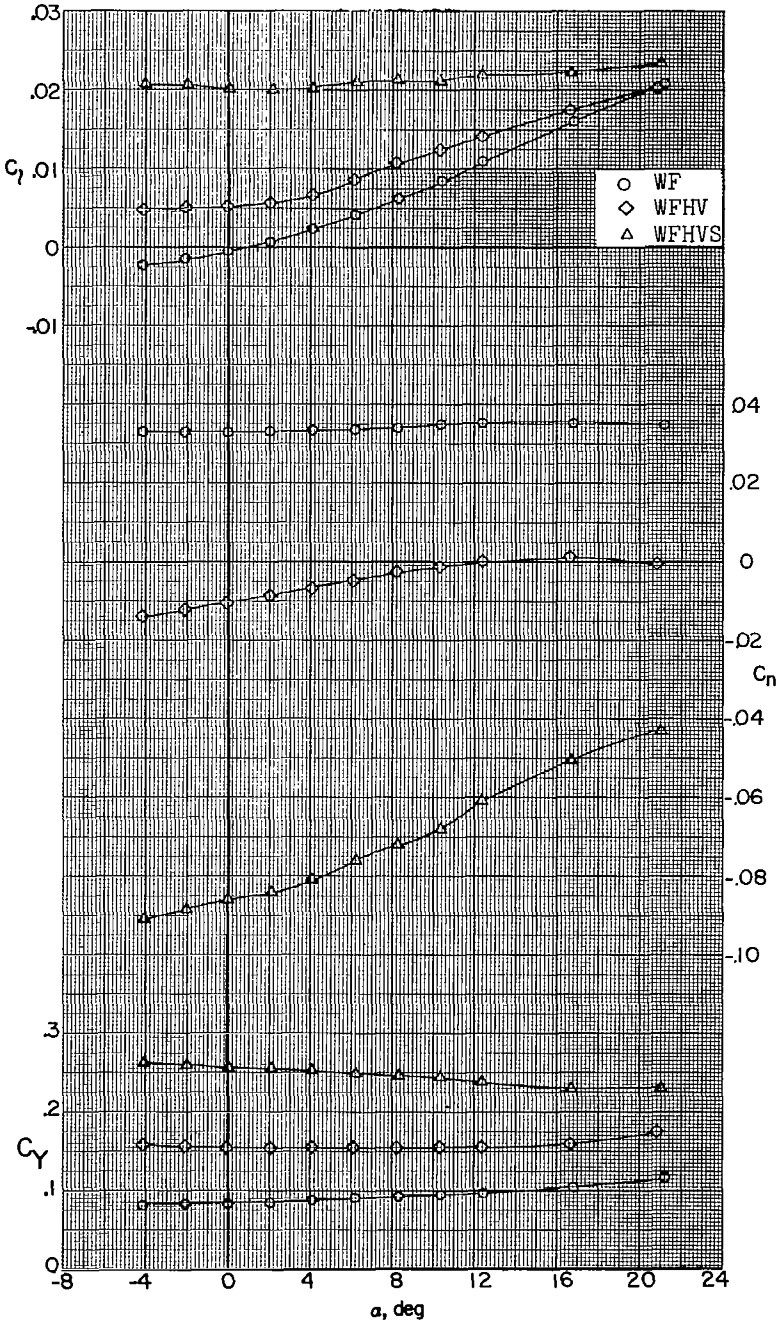

(i) M = 3.96; β = -10.6°.

Figure 21.- Continued.

[redacted]

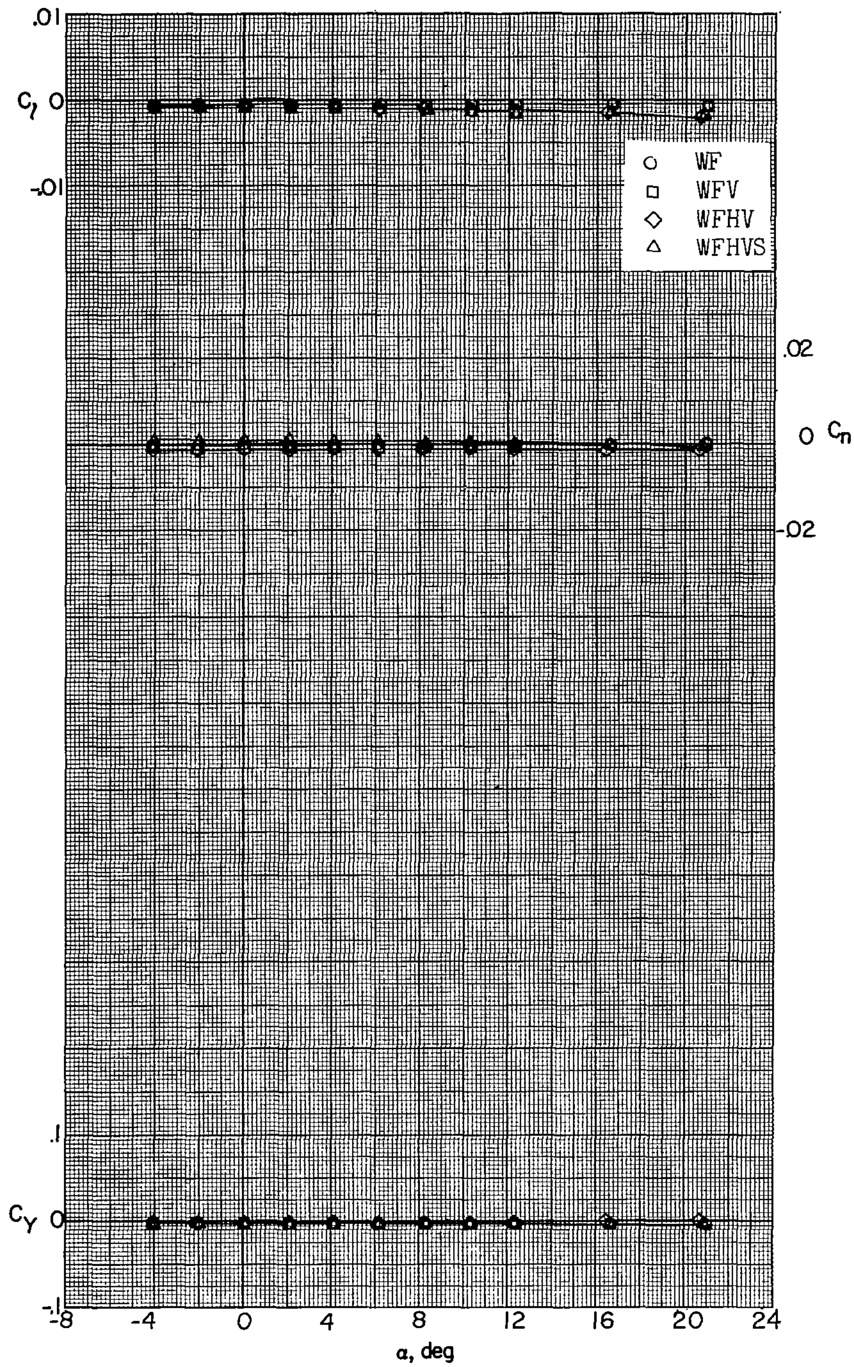

(j) M = 4.65; β = 0°.

Figure 21.- Continued.

[redacted]

[redacted]

L-229

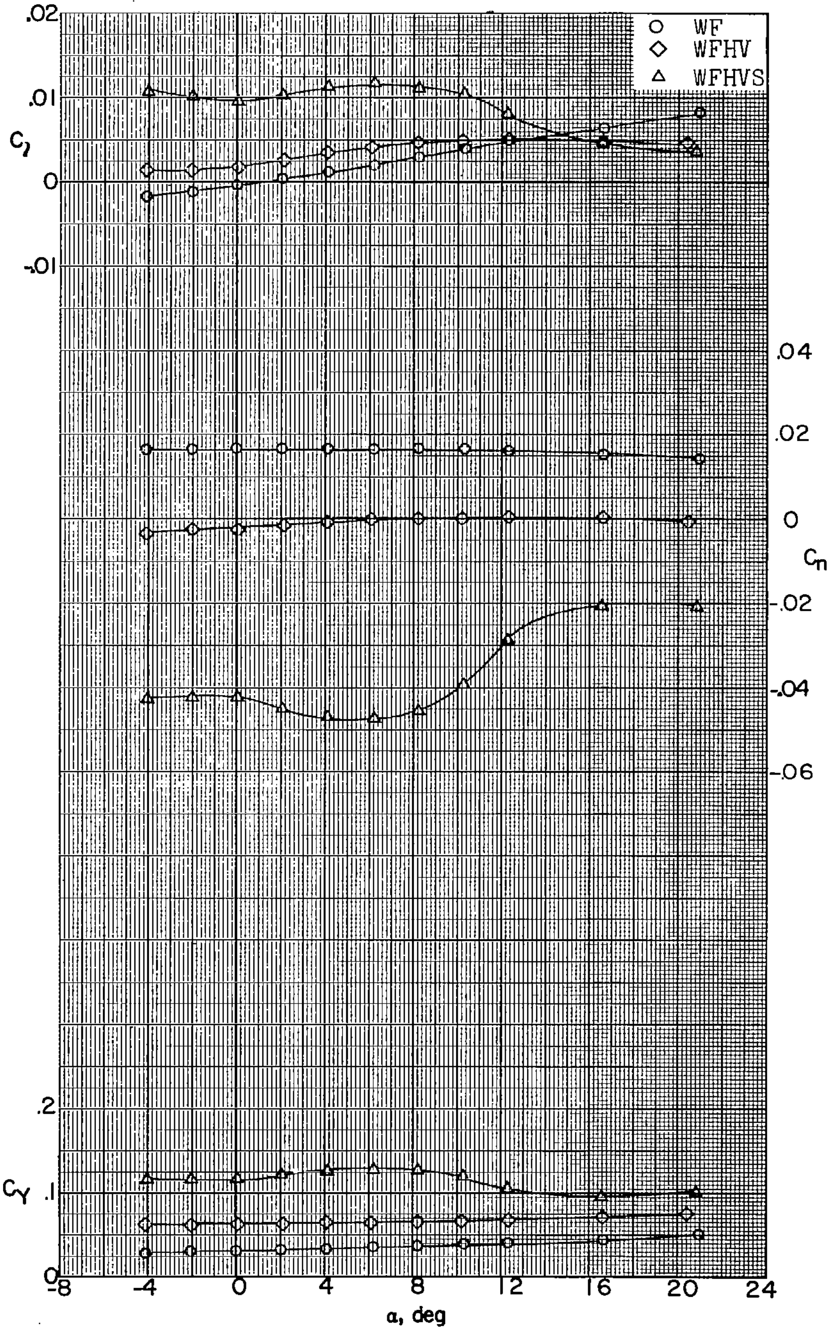

(k) $M = 4.65$; $\beta = -5.1^{\circ}$.

Figure 21.- Continued.

[redacted]

[redacted]

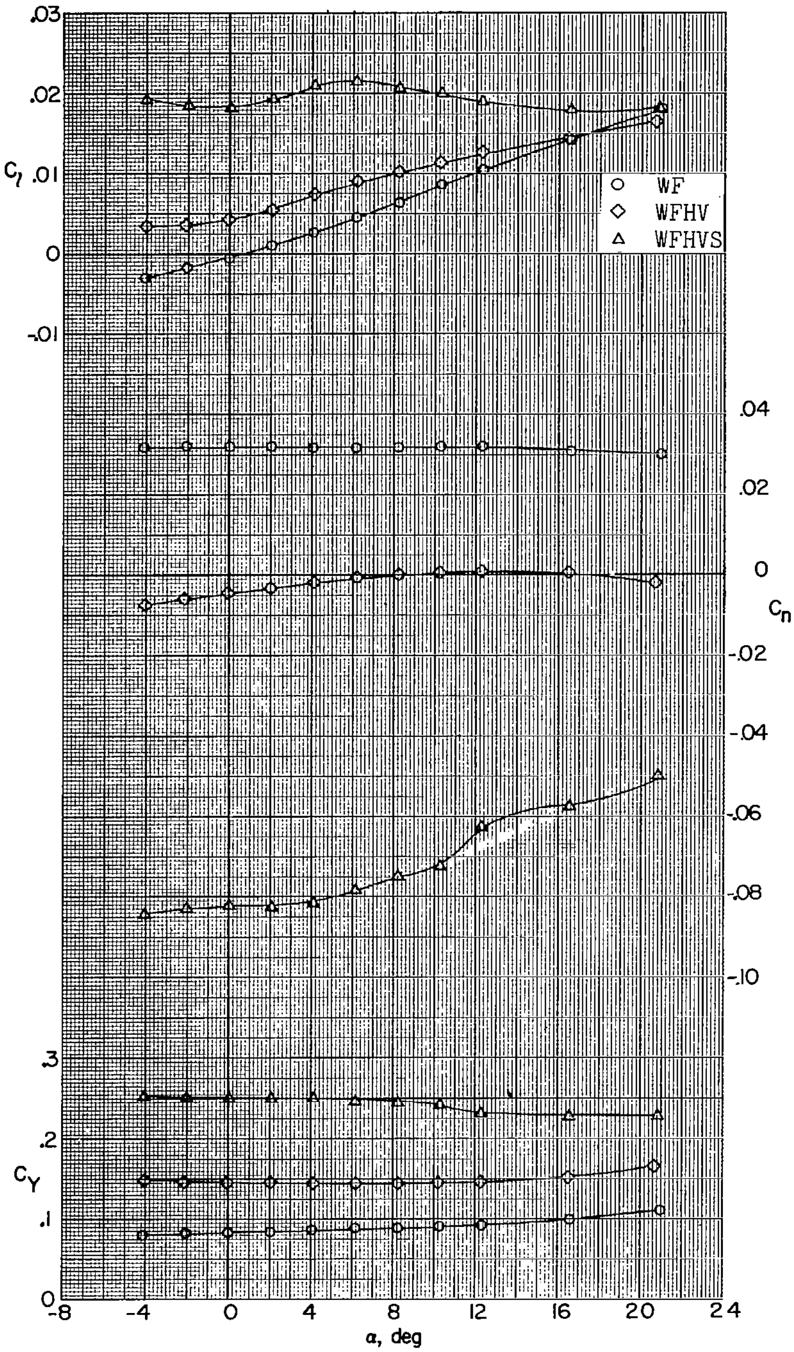

(l) $M = 4.65$; $\beta = -10.6^{\circ}$.

Figure 21.- Concluded.

[redacted]

L-229

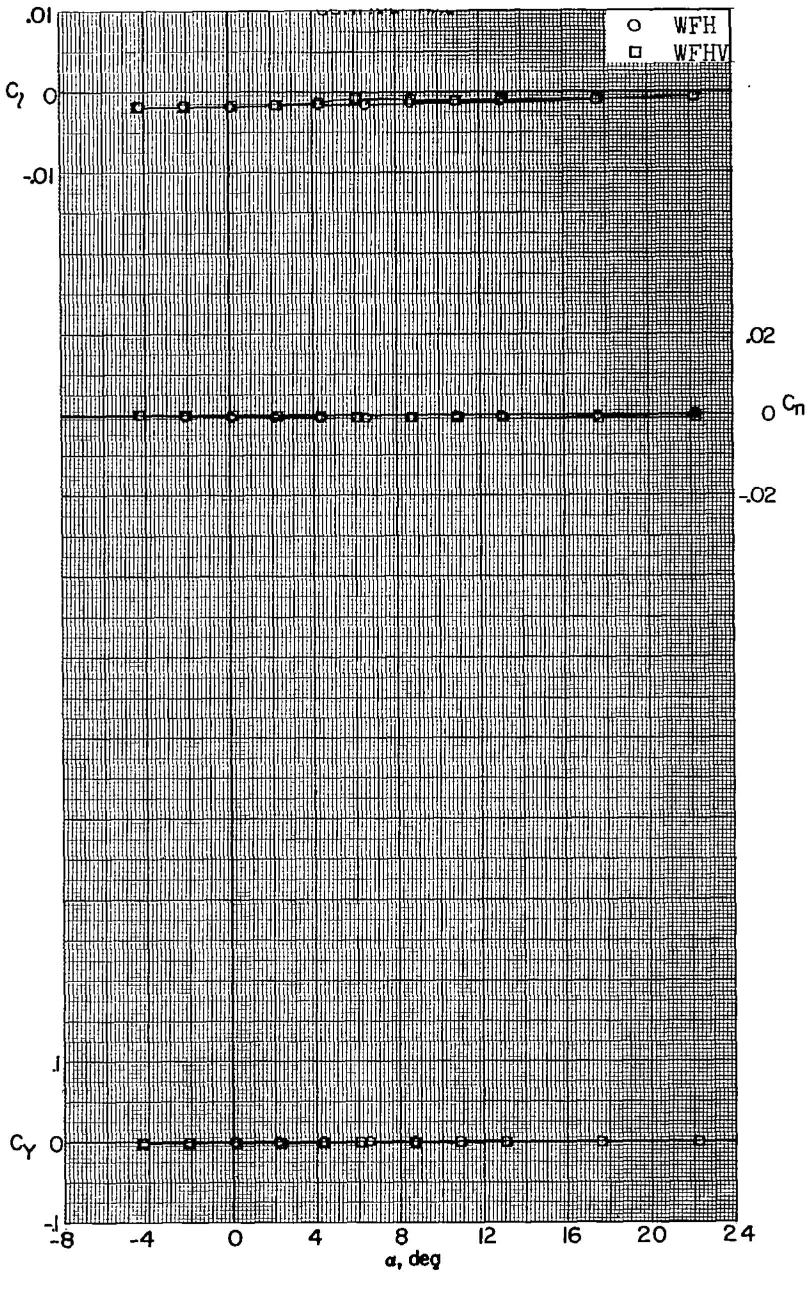

(a) $M = 2.29$; $\beta = 0^{\circ}$.

Figure 22.- Lateral stability characteristics of a 0.067-scale model of the X-15 airplane with and without the vertical tail.

[redacted]

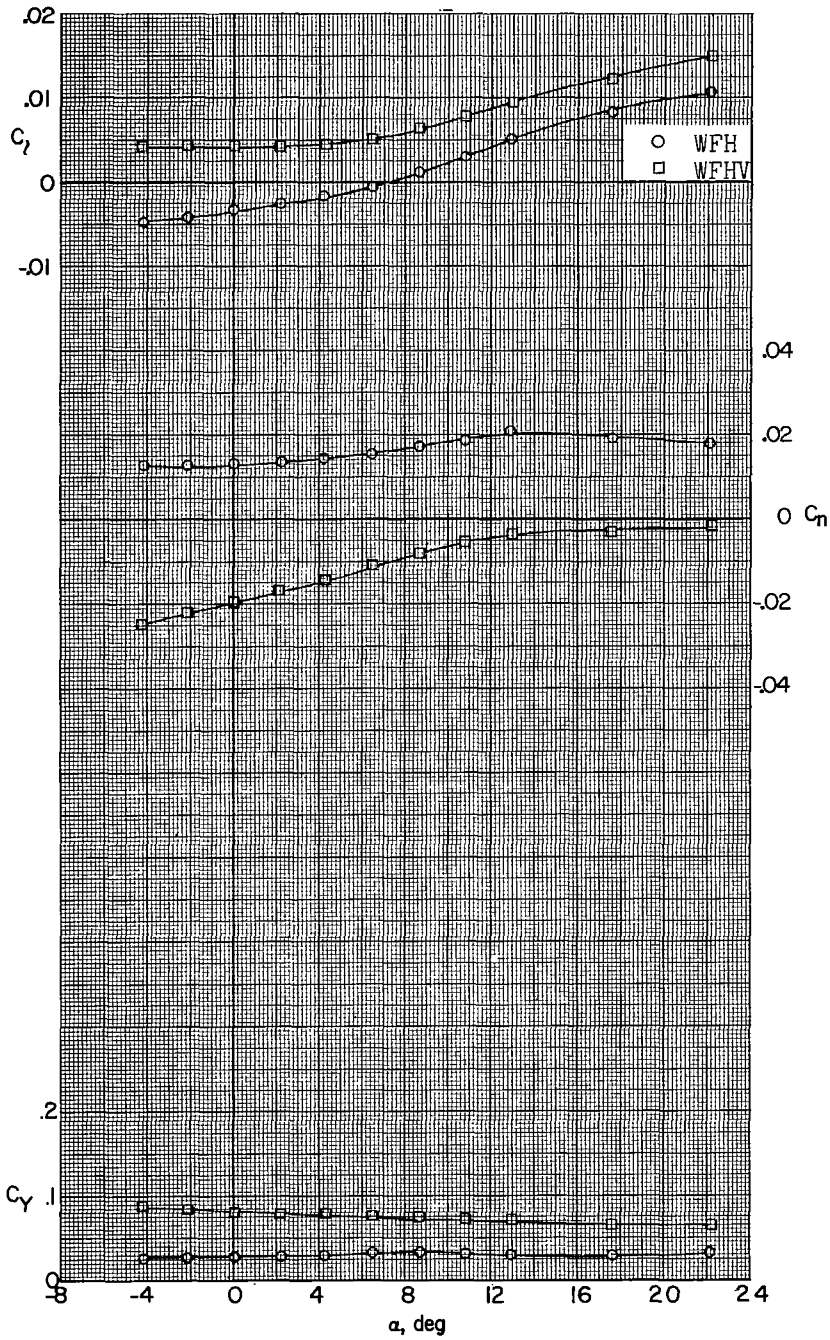

(b) M = 2.29; β = -5.2°.

Figure 22.- Continued.

L-229

[redacted]

L-229

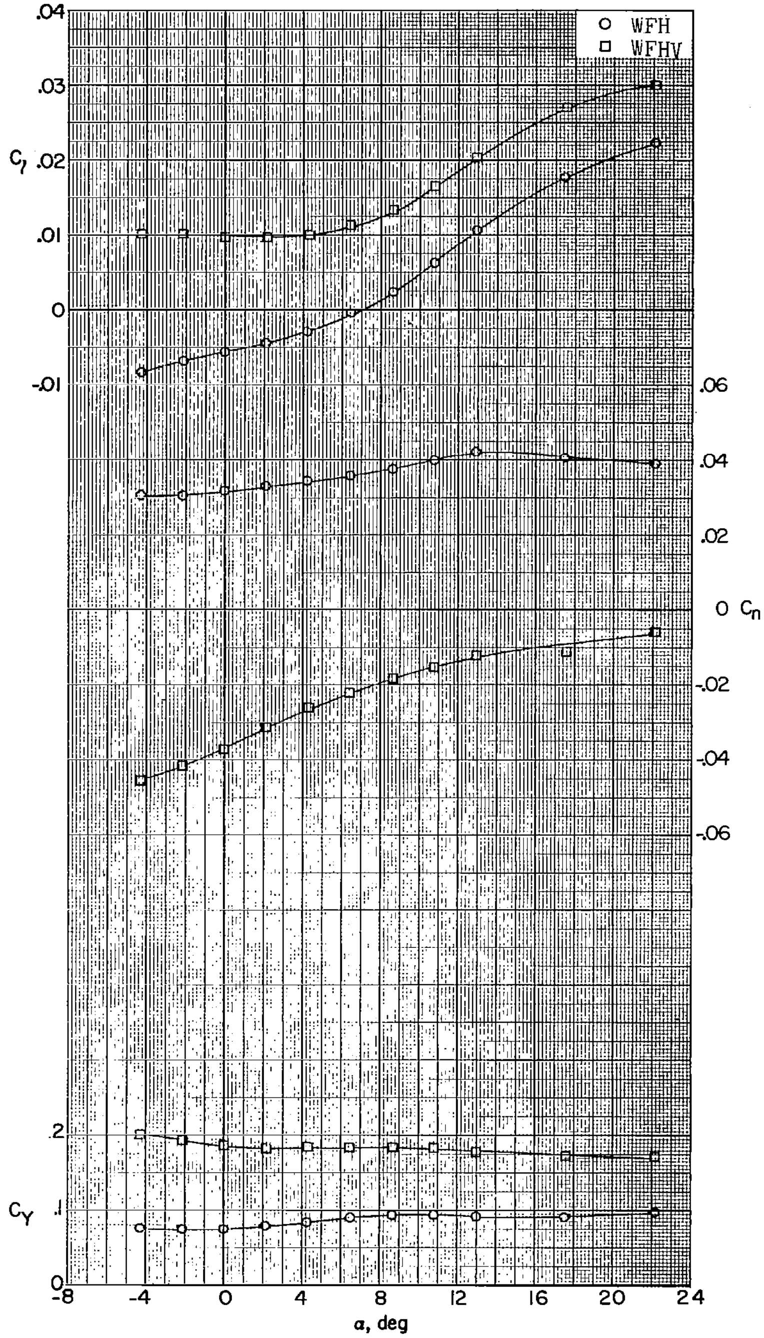

(c) M = 2.29; β = -10.7°.

Figure 22.- Continued.

[redacted]

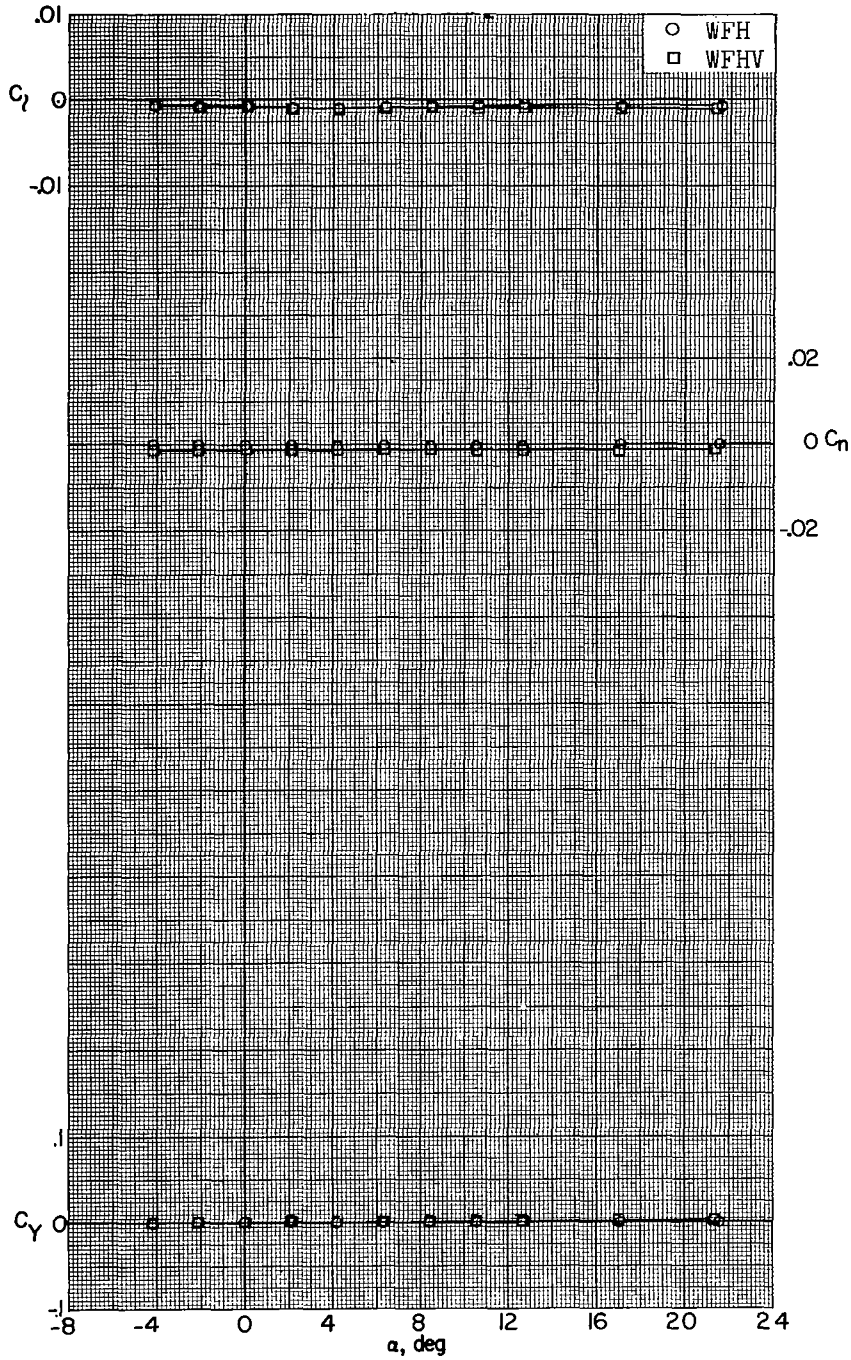

(d) M = 2.98; β = 0°.

Figure 22.- Continued.

L-229

[redacted]

L-229

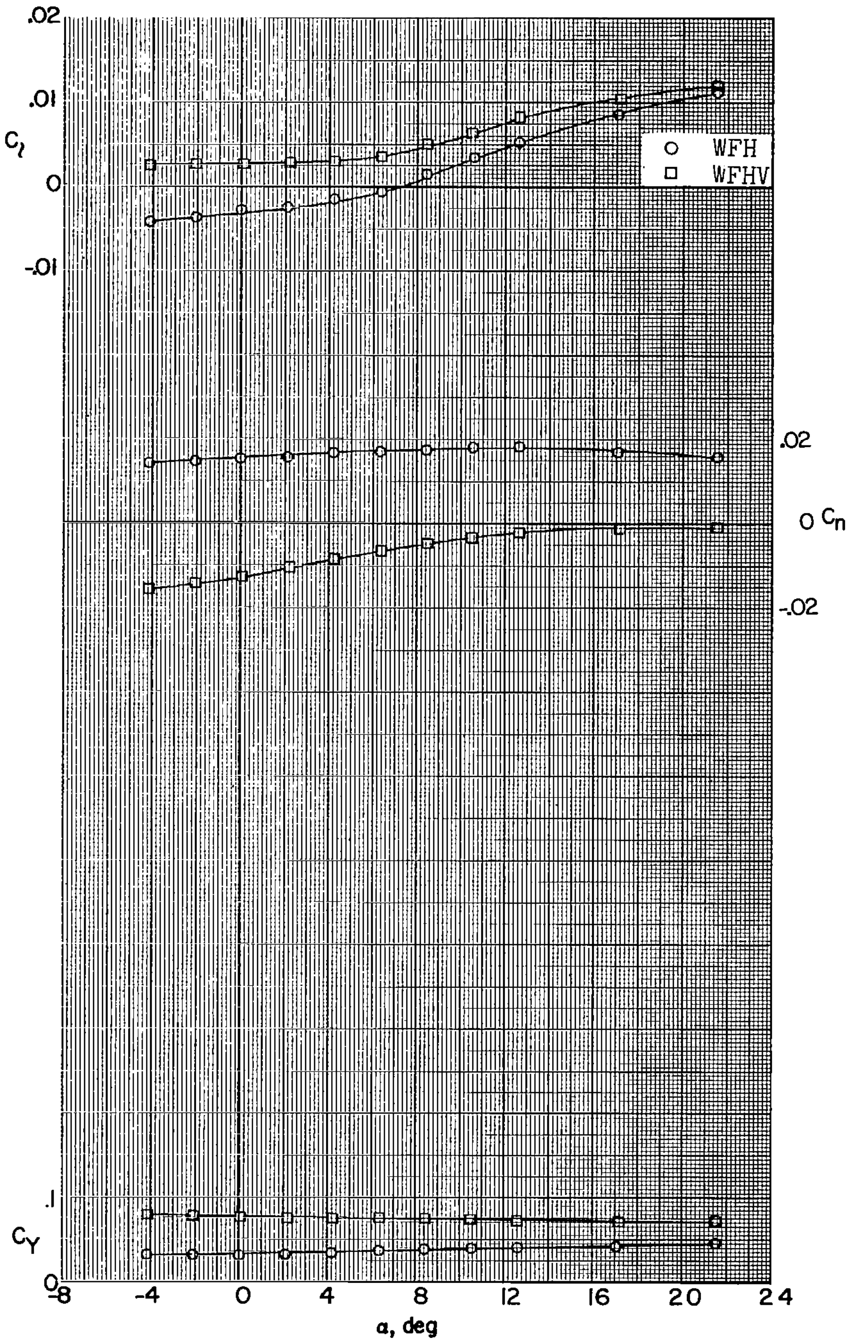

(e) M = 2.98; β = -5.2°.

Figure 22.- Continued.

[redacted]

L-229

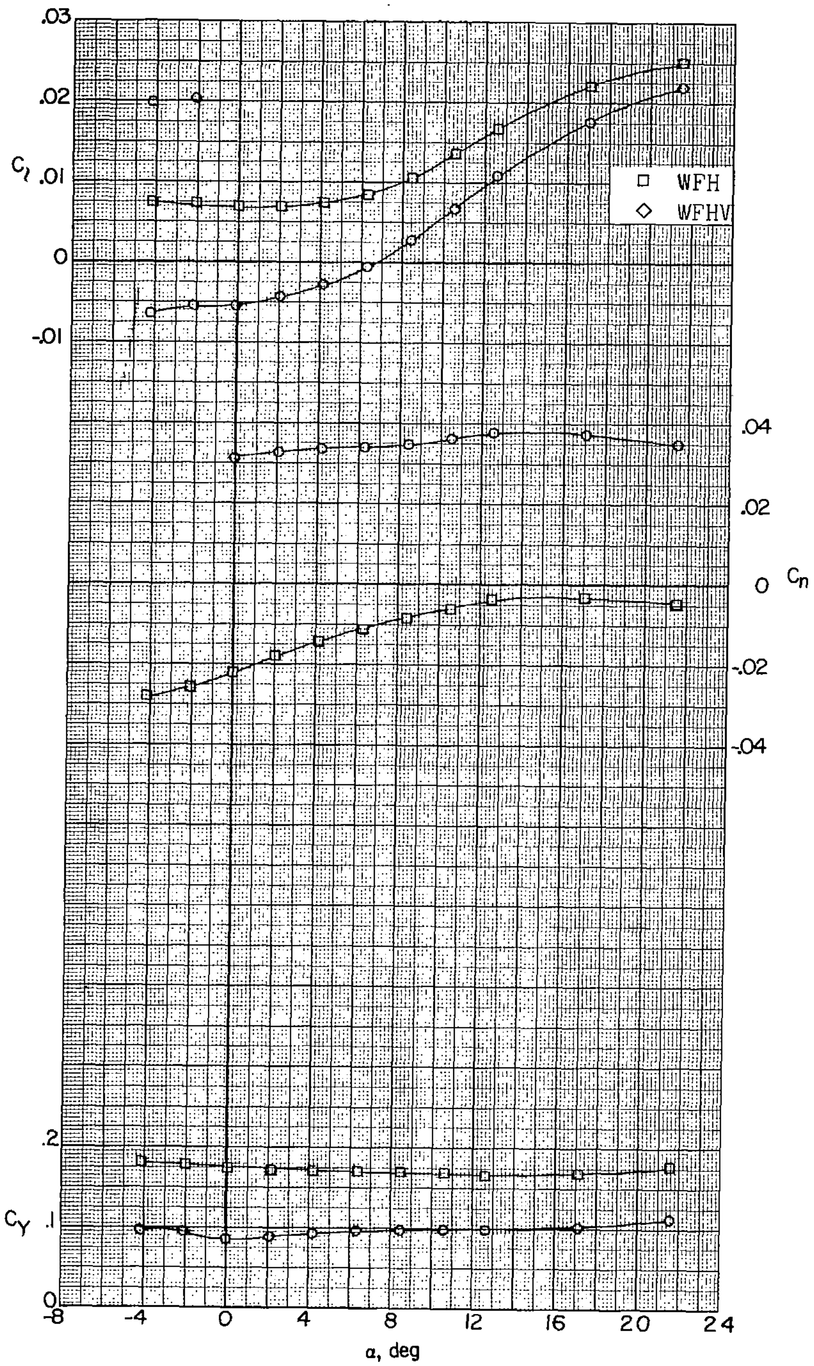

(f) M = 2.98; β = -10.7°.

Figure 22.- Continued.

[redacted]

[redacted]

L-229

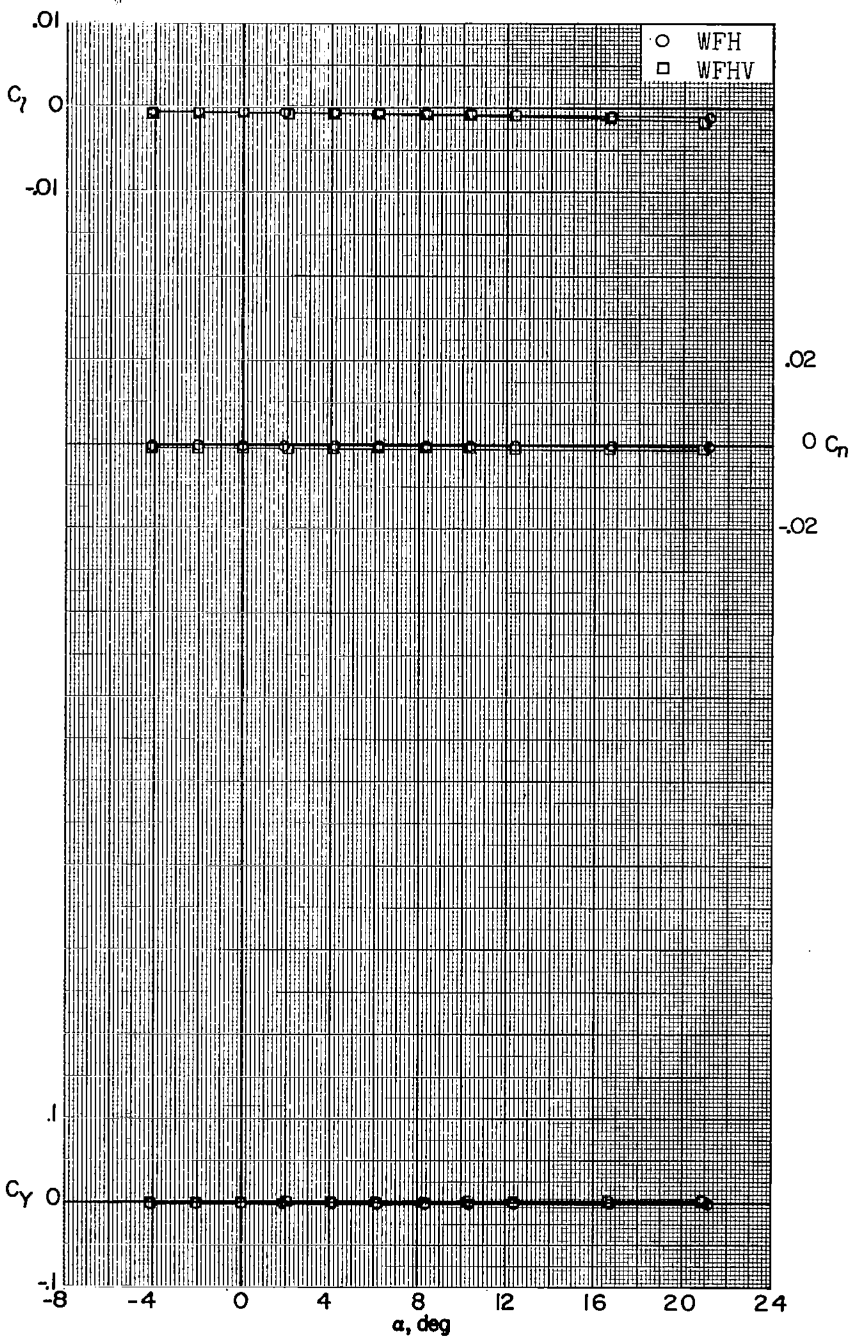

(g) $M = 3.96$; $\beta = 0^{\circ}$.

Figure 22.- Continued.

[redacted]

[redacted]

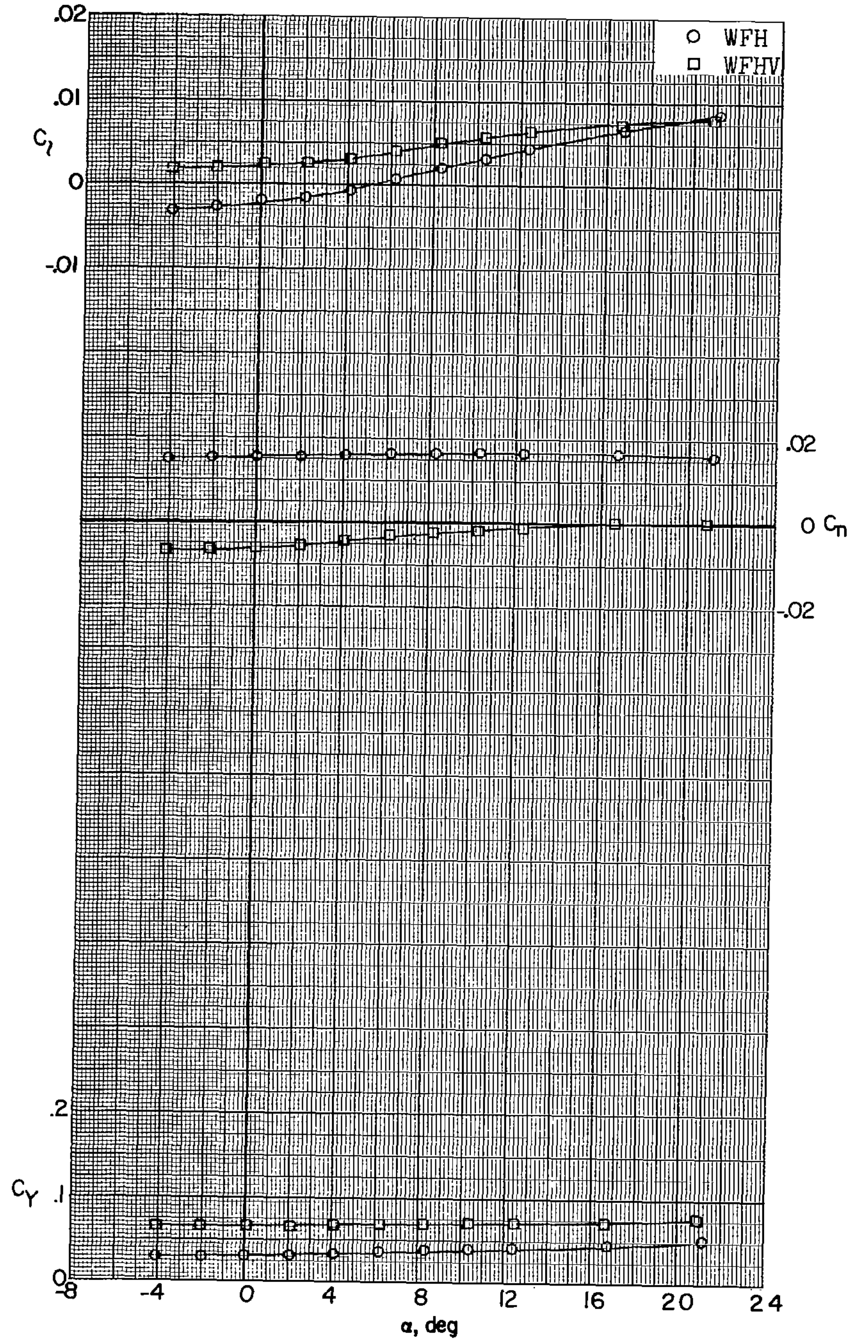

(h) M = 3.96; β = -5.1°.

Figure 22.- Continued.

L-229

[redacted]

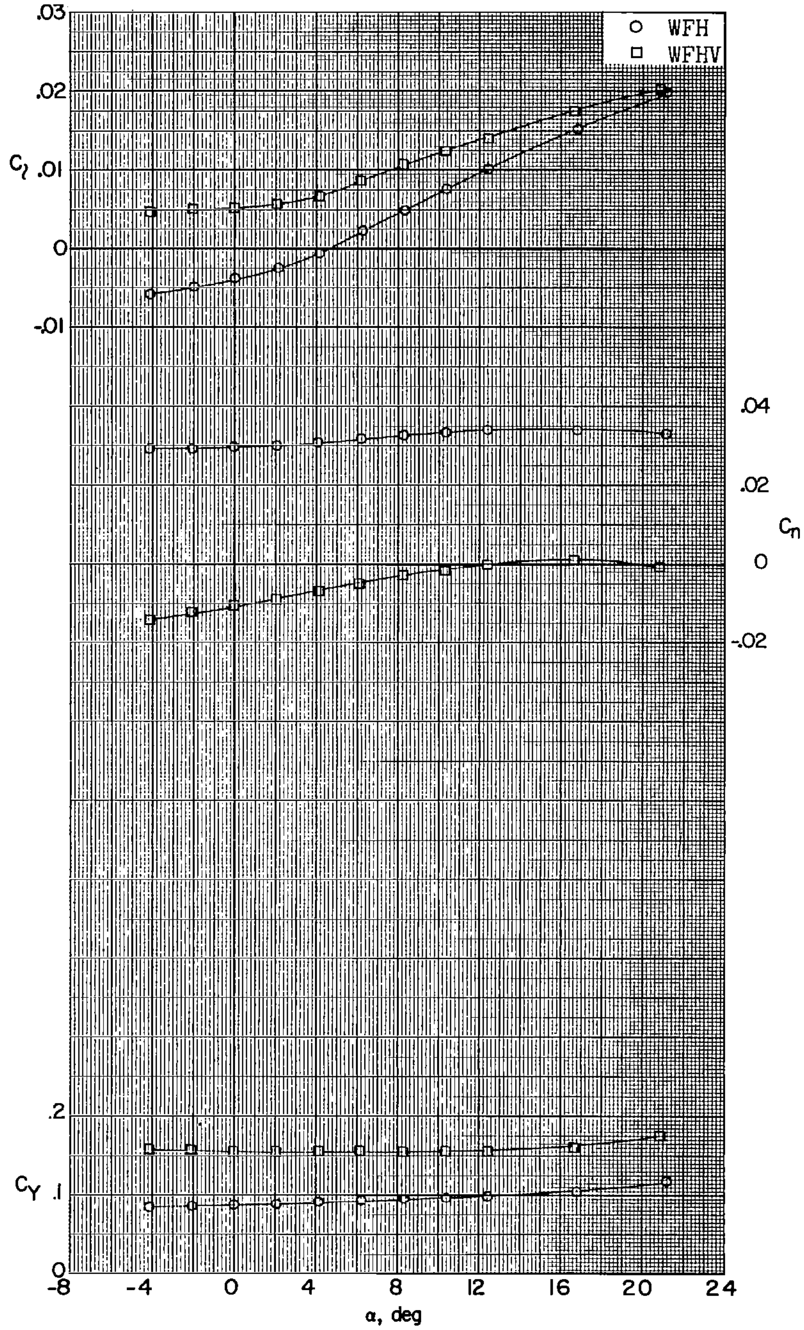

(i) M = 3.96; β = -10.6°.

Figure 22.- Continued.

[redacted]

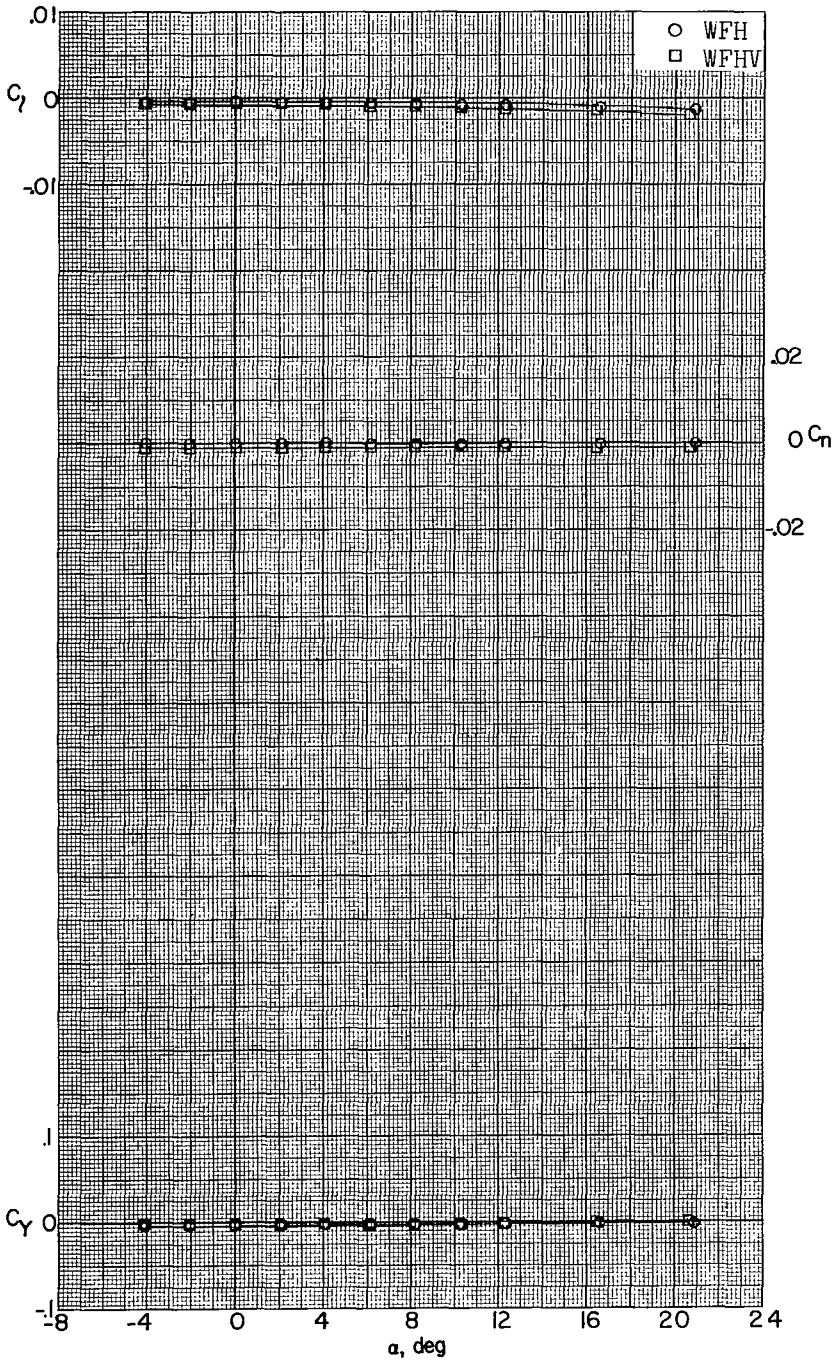

(j) M = 4.65; β = 0°.

Figure 22.- Continued.

L-229

[redacted]

[redacted]

L-229

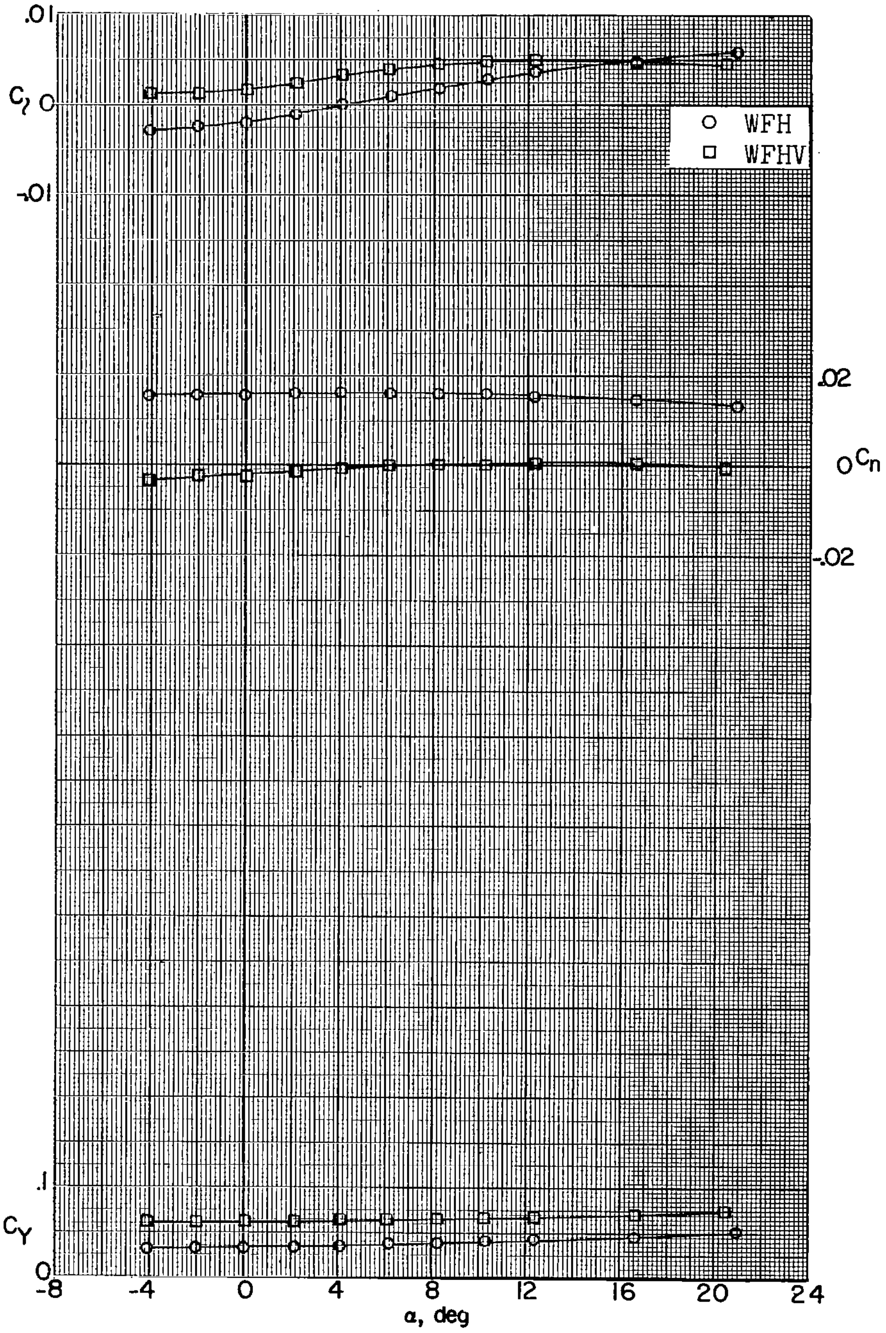

(k) $M = 4.65$; $\beta = -5.1^{\circ}$.

Figure 22.- Continued.

[redacted]

[redacted]

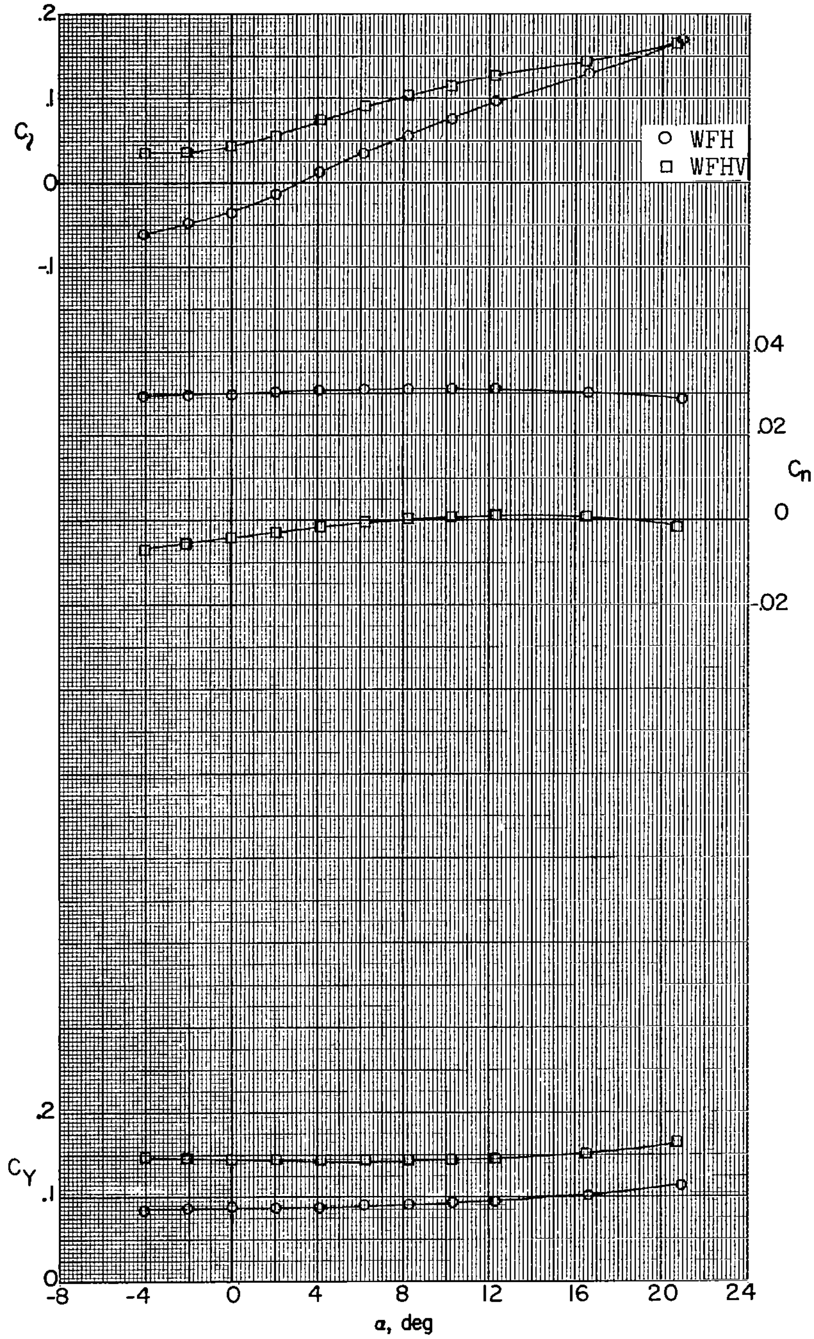

(*l*) M = 4.65; β = -10.6°.

Figure 22.- Concluded.

[redacted]

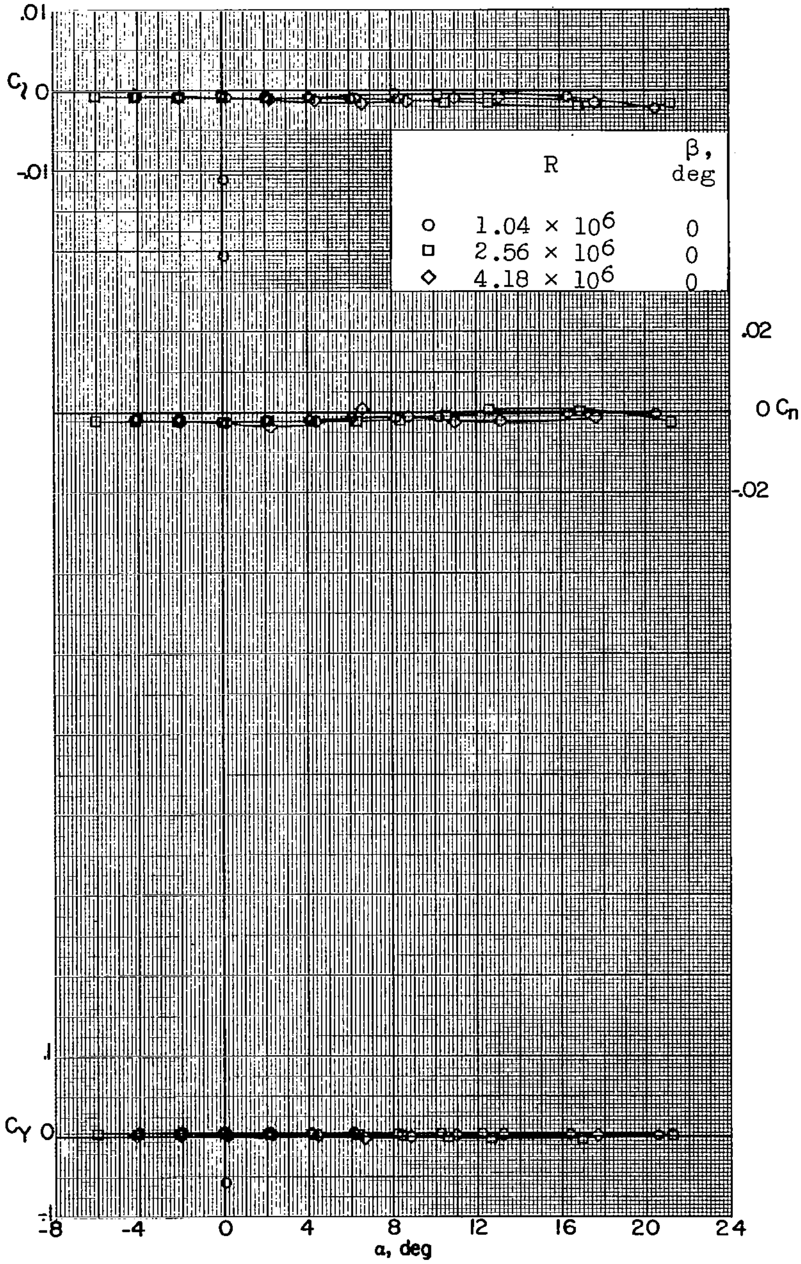

(a) M = 2.98.

Figure 23.- Lateral stability characteristics of a 0.067-scale model of the X-15 airplane at various Reynolds numbers. Speed brakes open 45°; $\delta_v = 0°$.

[redacted]

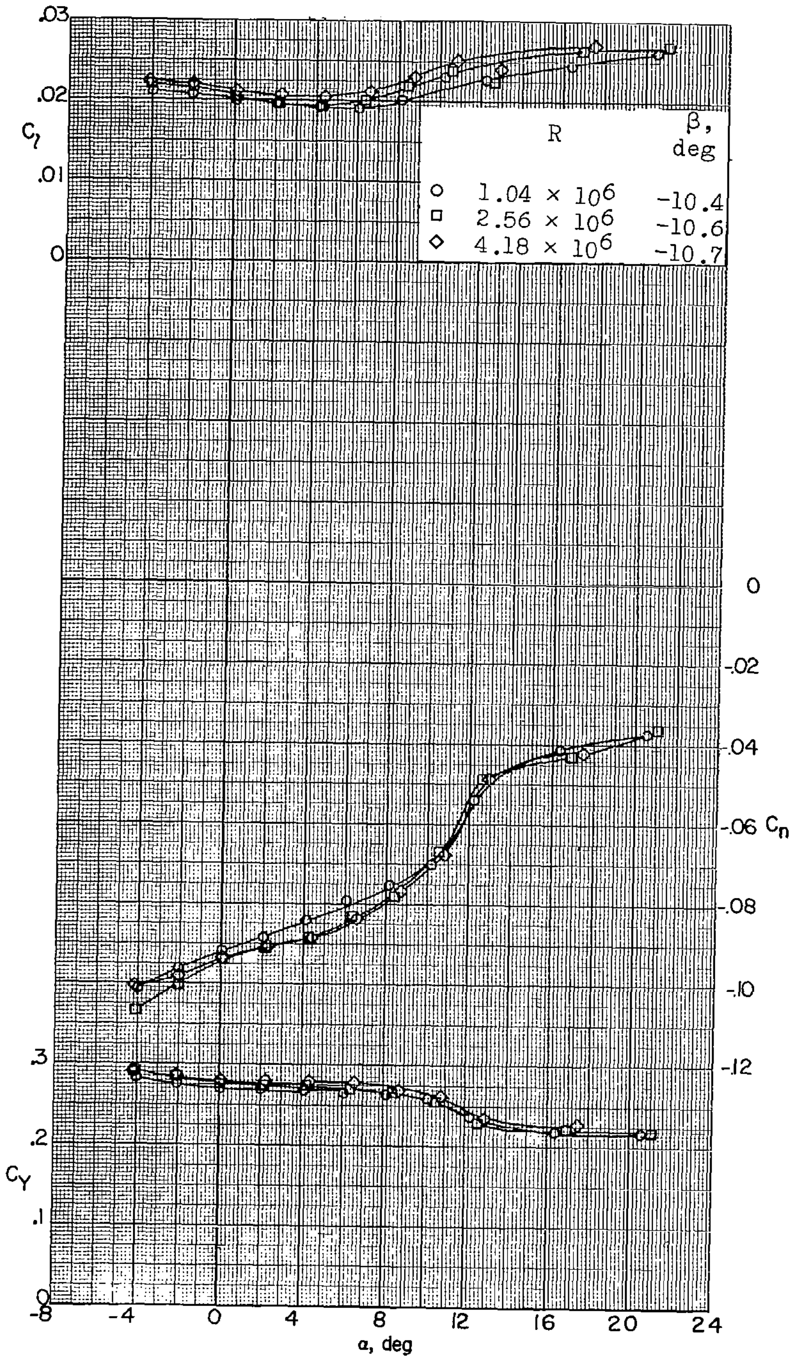

(a) Concluded.

Figure 23.- Continued.

L-229

[redacted]

[redacted]

L-229

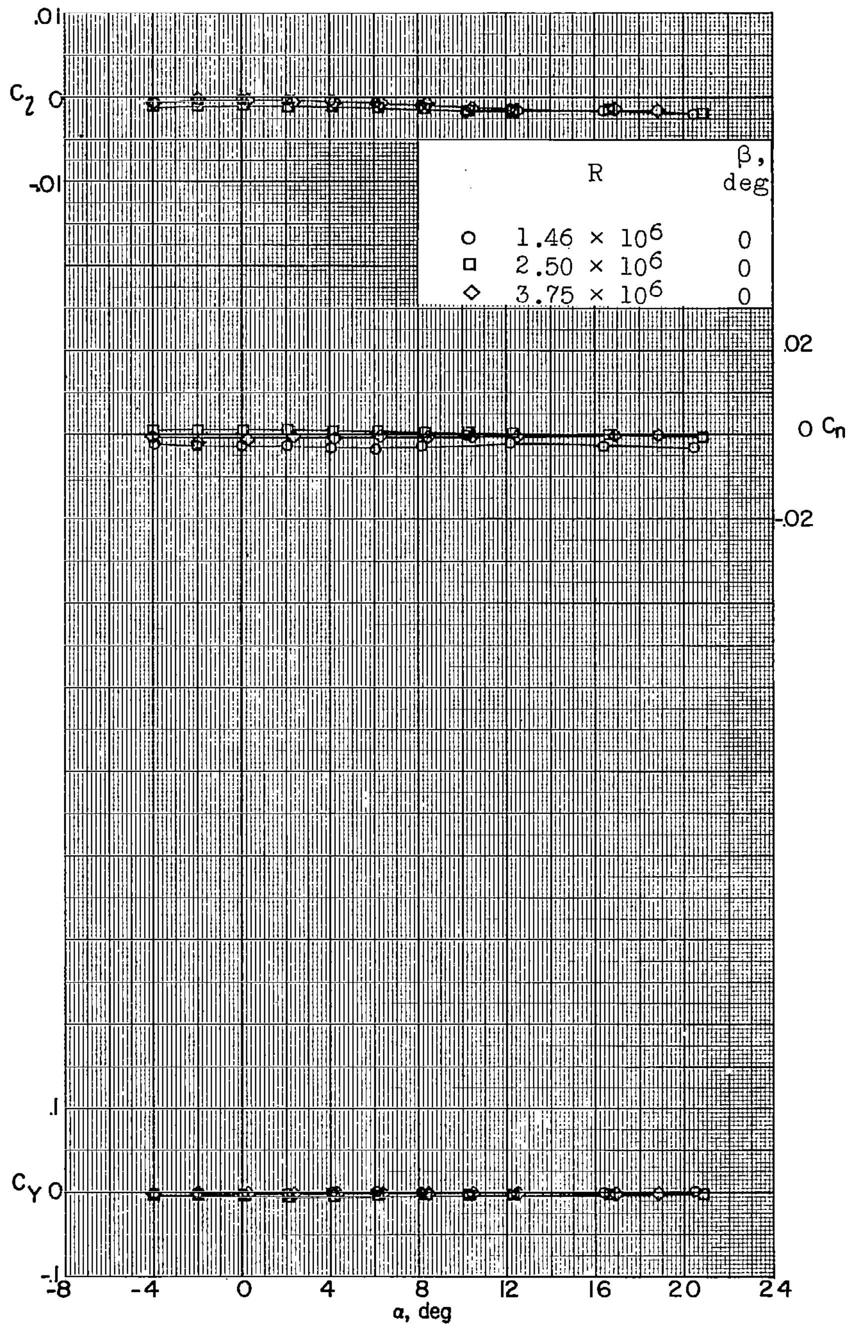

(b) M = 4.65.

Figure 23.- Continued.

[redacted]

[redacted]

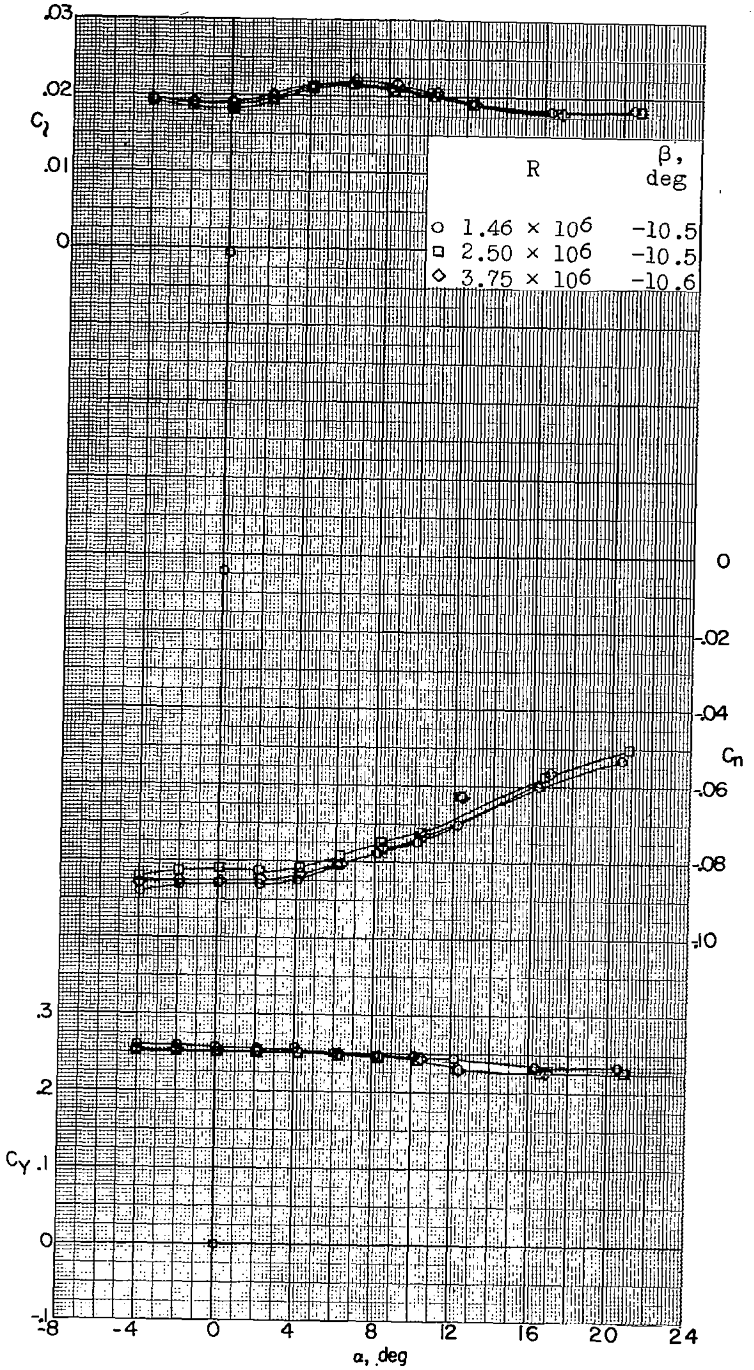

(b) Concluded.

Figure 23.- Concluded.

[redacted]

[redacted]

L-229

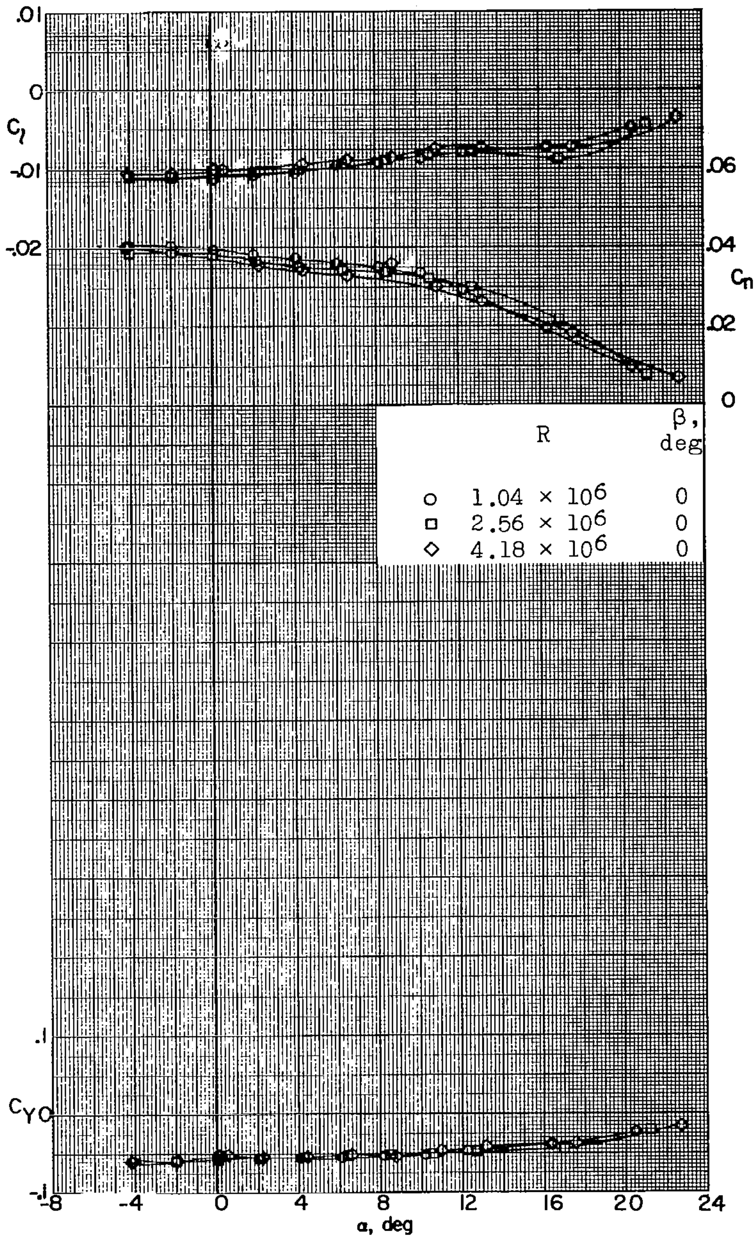

(a) M = 2.98.

Figure 24.- Lateral stability characteristics of a 0.067-scale model of the X-15 airplane at various Reynolds numbers. Speed brakes open 45°; $\delta_v = -6^{\circ}$.

[redacted]

[redacted]

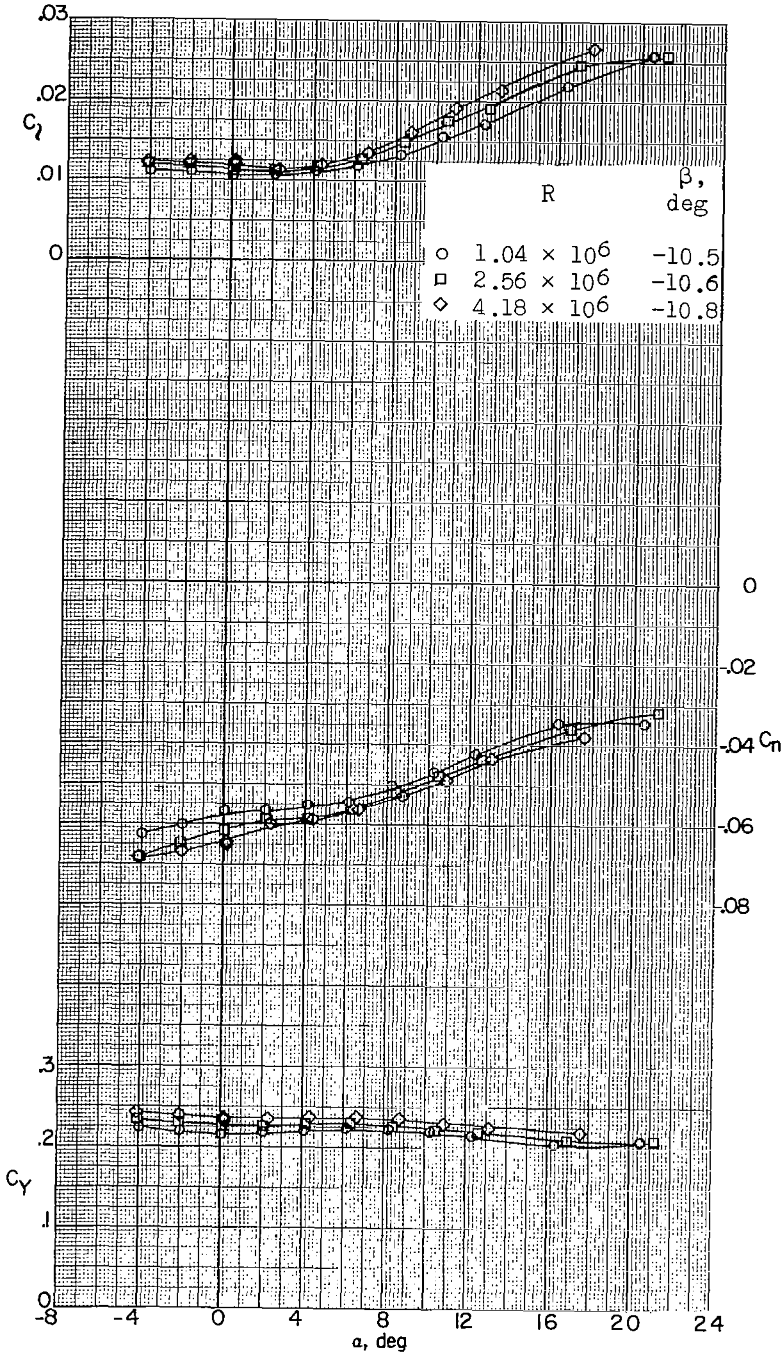

(a) Concluded.

Figure 24.- Continued.

L-229

[redacted]

[redacted]

L-229

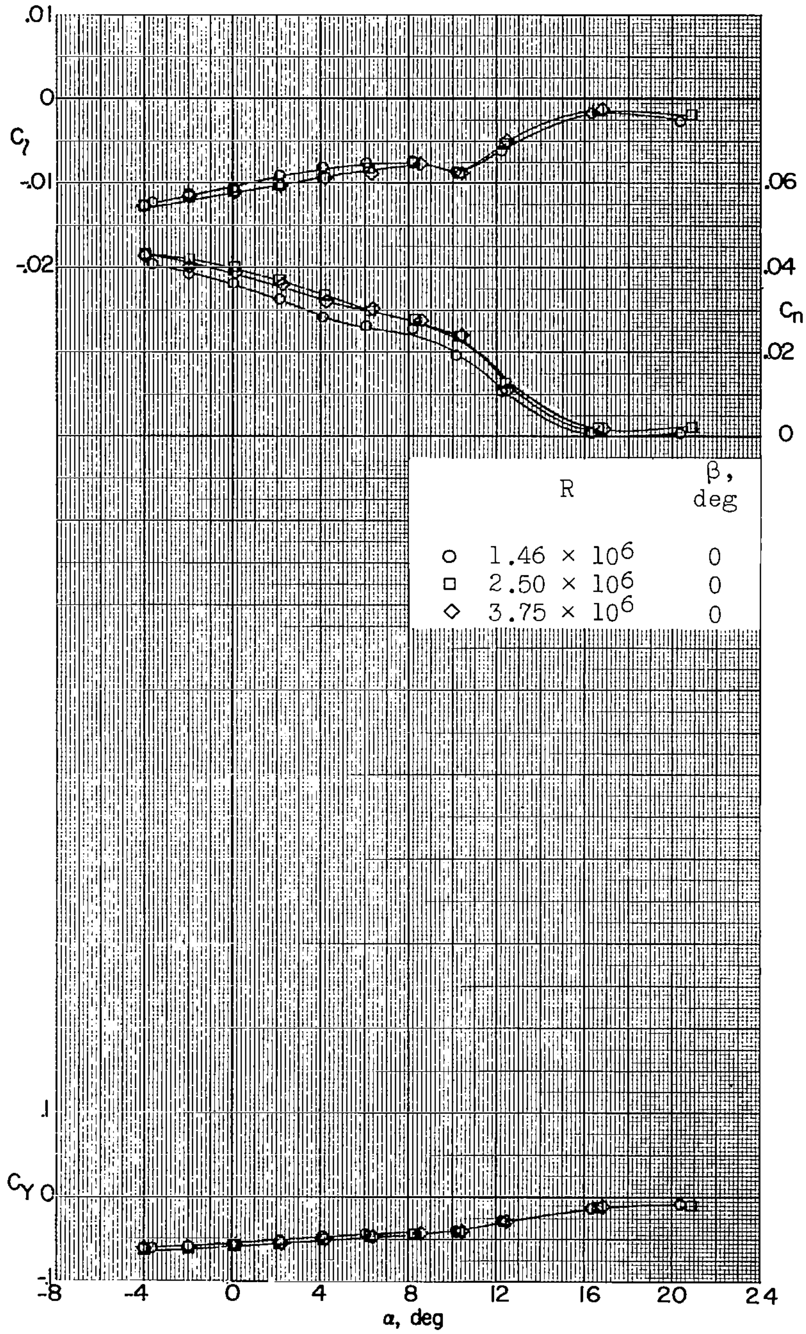

(b) M = 4.65.

Figure 24.- Continued.

[redacted]

[redacted]

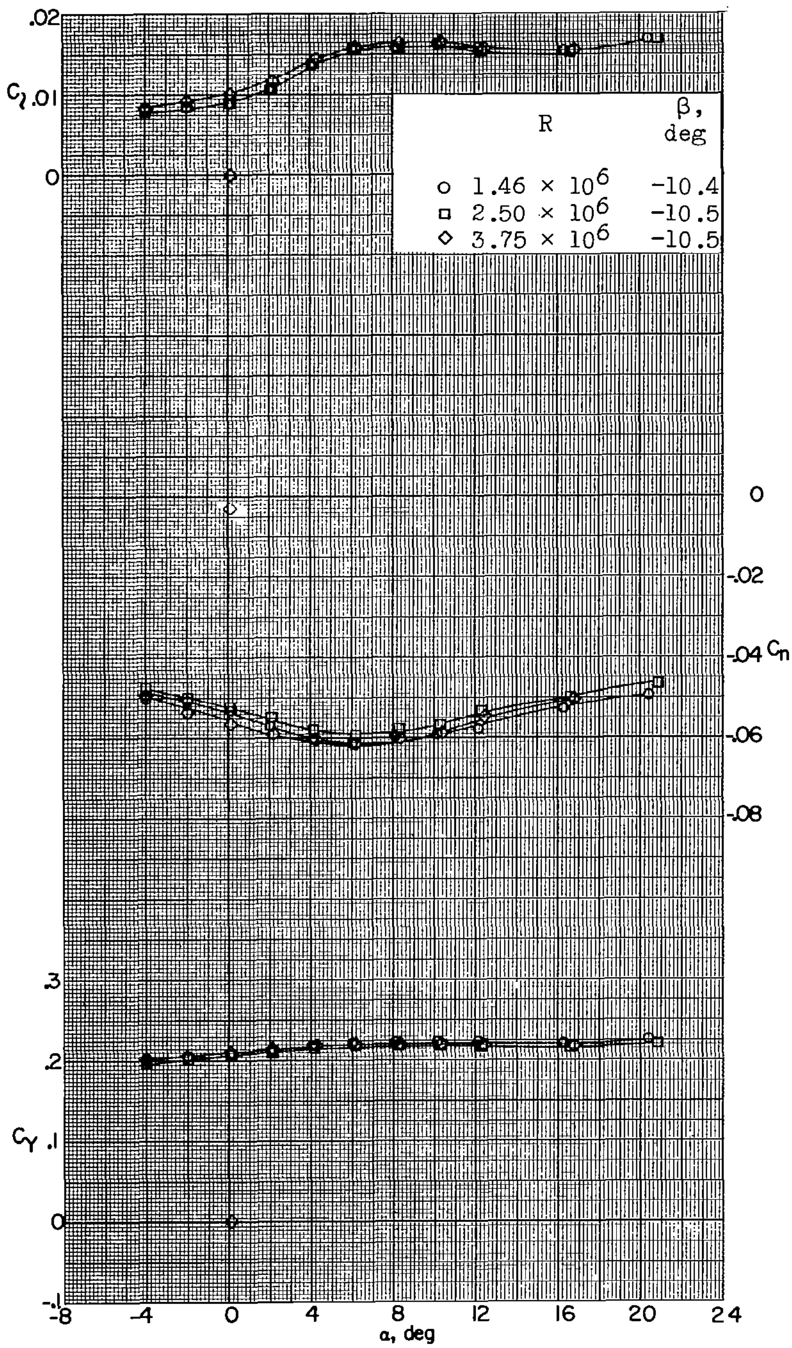

(b) Concluded.

Figure 24.- Concluded.

L-229

[redacted]

[redacted]

16E

L-229

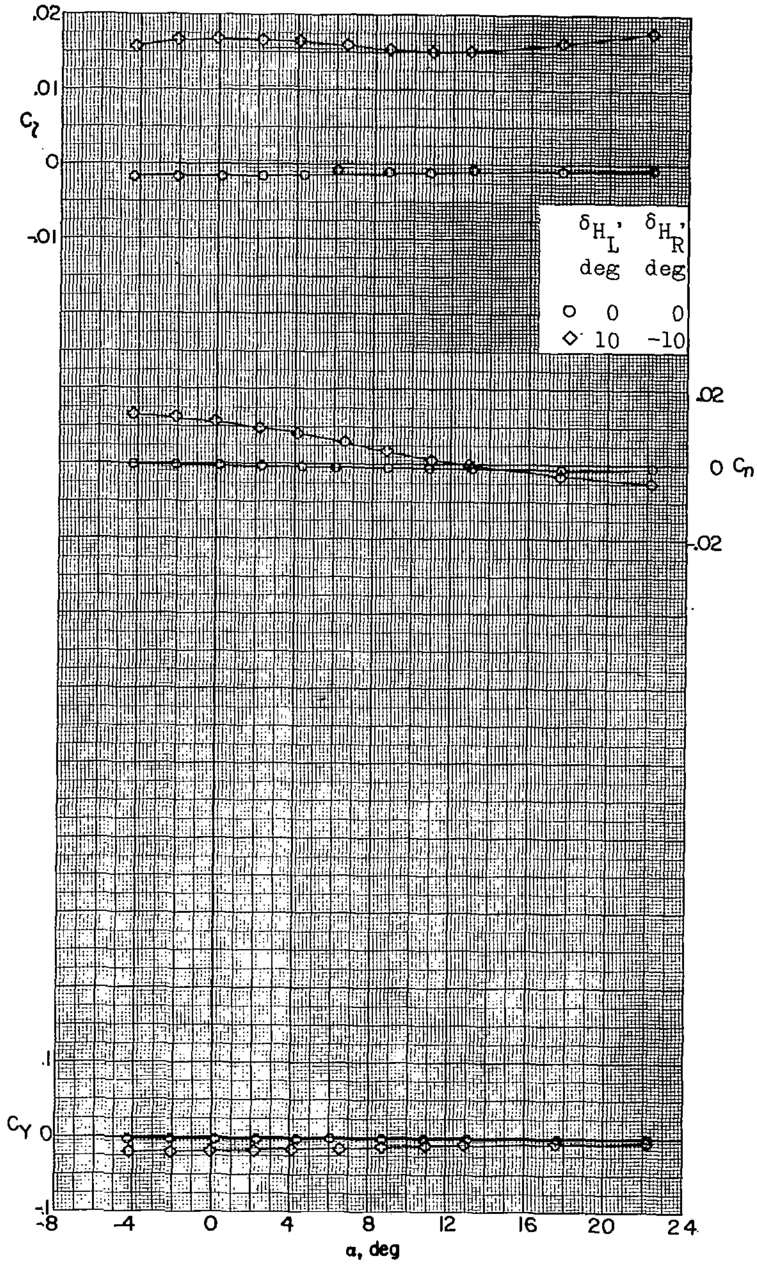

(a) $M = 2.29$; $\beta = 0^{\circ}$.

Figure 25.- Lateral stability characteristics of a 0.067-scale model of the X-15 airplane with various pitch-control deflections of the horizontal tail. Speed brakes closed.

[redacted]

[redacted]

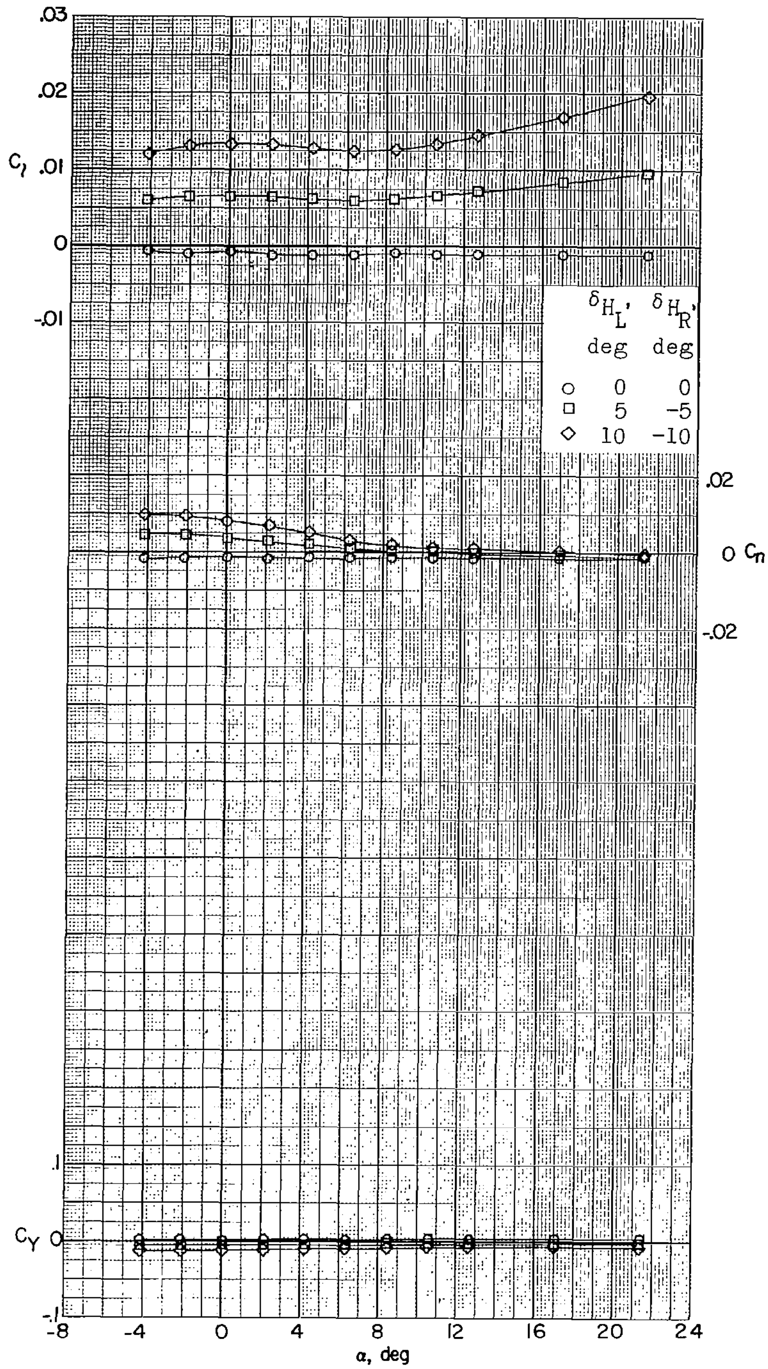

(b) M = 2.98; β = 0°.

Figure 25.- Continued.

L-229

[redacted]

L-229

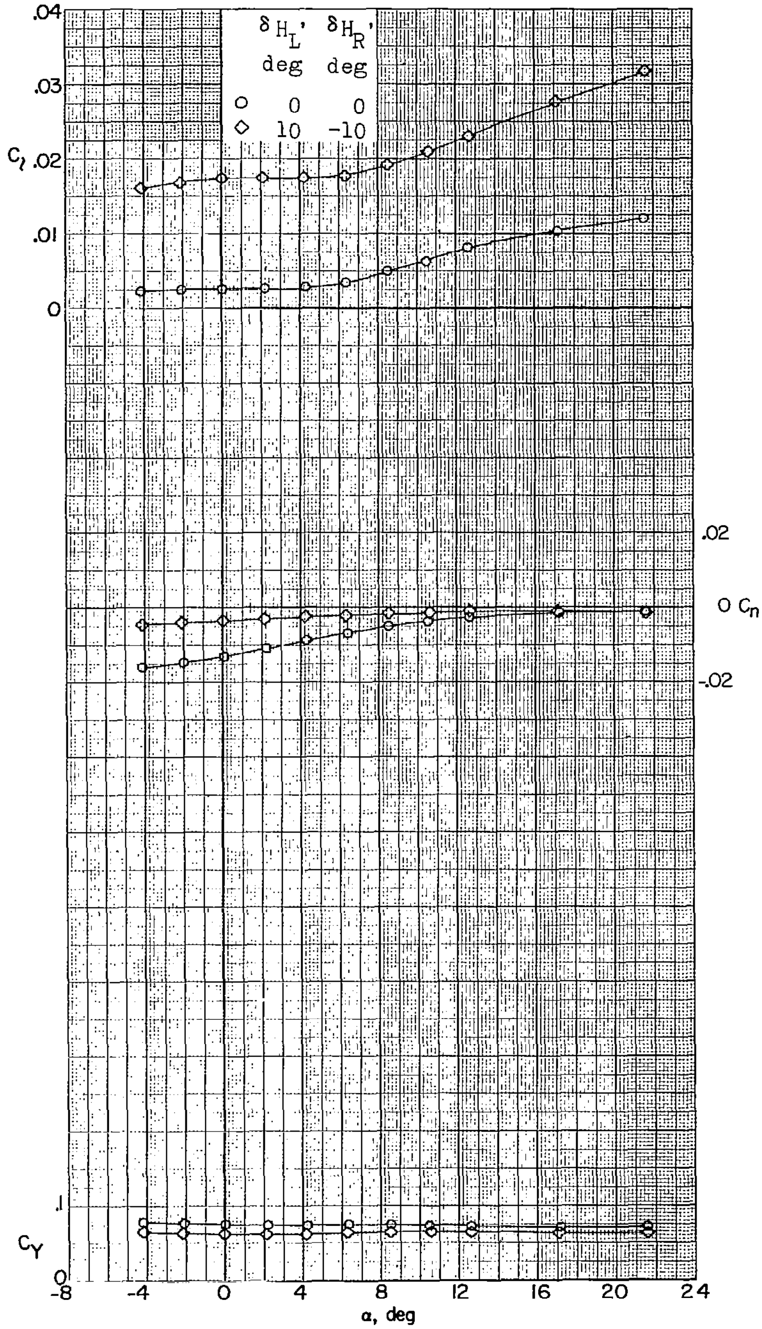

(c) M = 2.98; β = -5.1°.

Figure 25.- Continued.

[redacted]

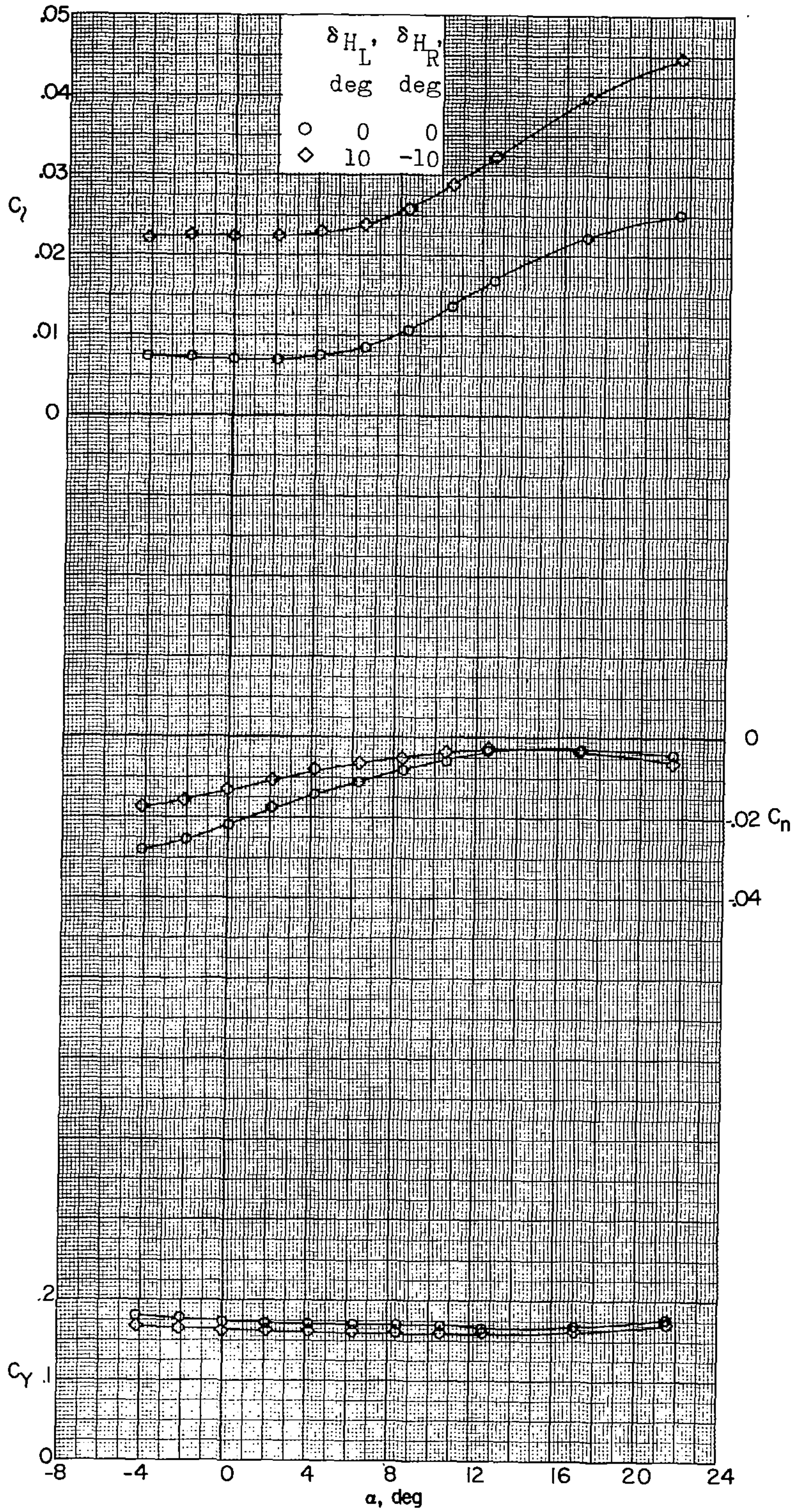

(d) M = 2.98; β = -9.7°.

Figure 25.- Continued.

[redacted]

L-229

L-229

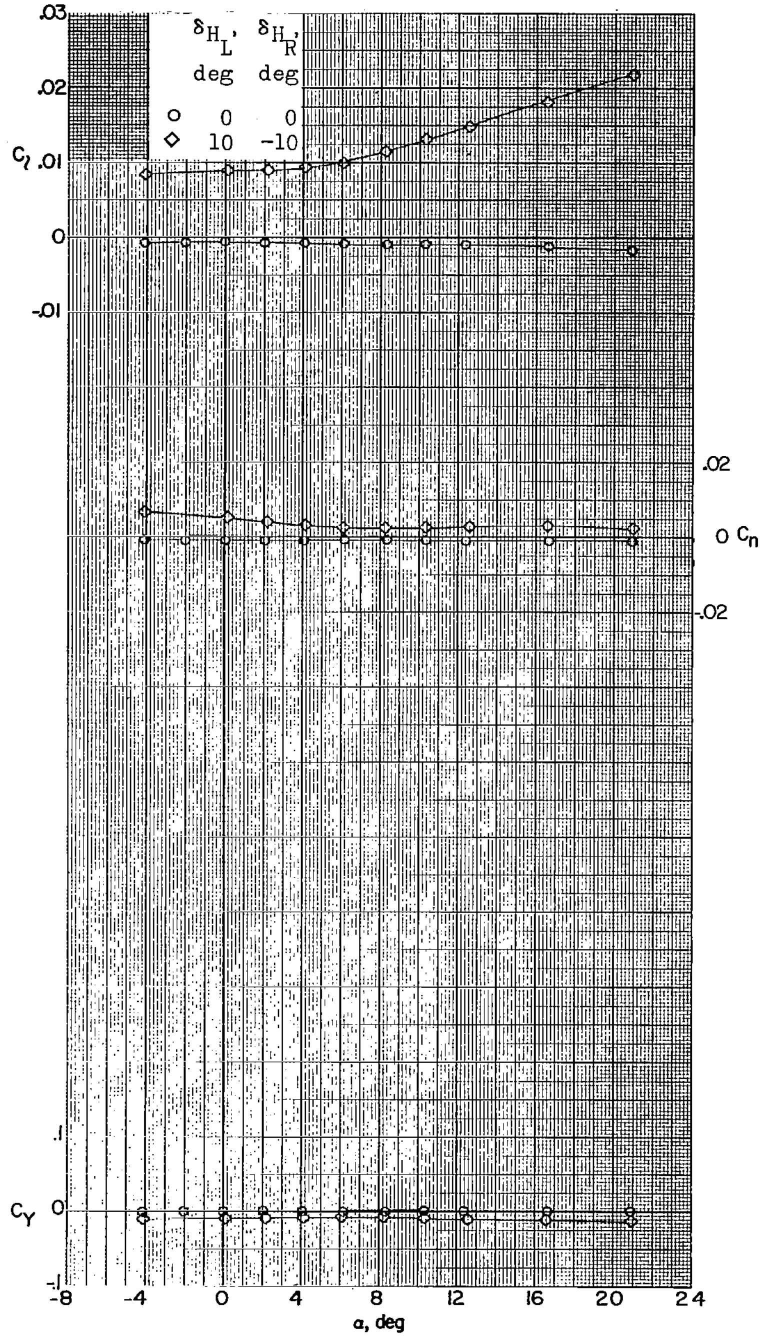

(e) $M = 3.96$; $\beta = 0^{\circ}$.

Figure 25.- Continued.

[redacted]

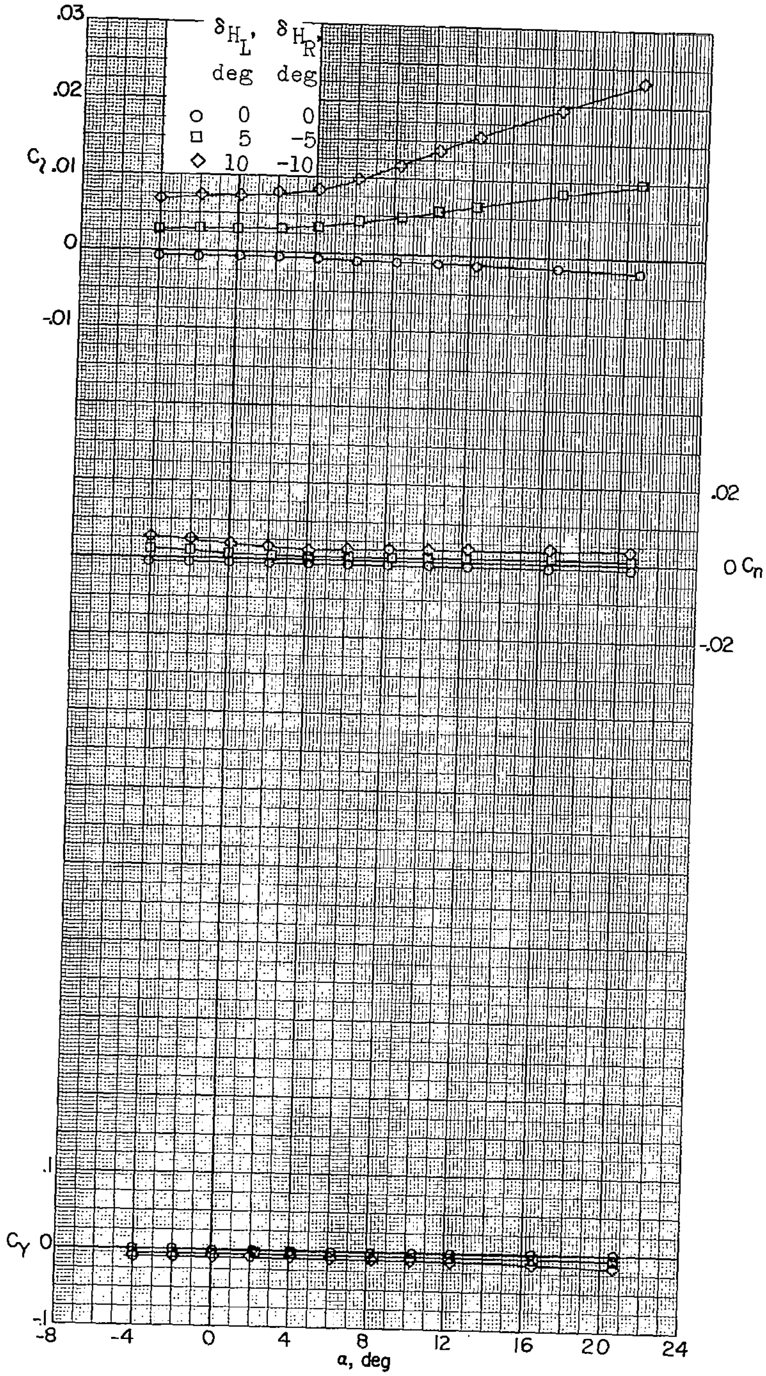

(f) M = 4.65; β = 0.1°.

Figure 25.- Continued.

[redacted]

[redacted]

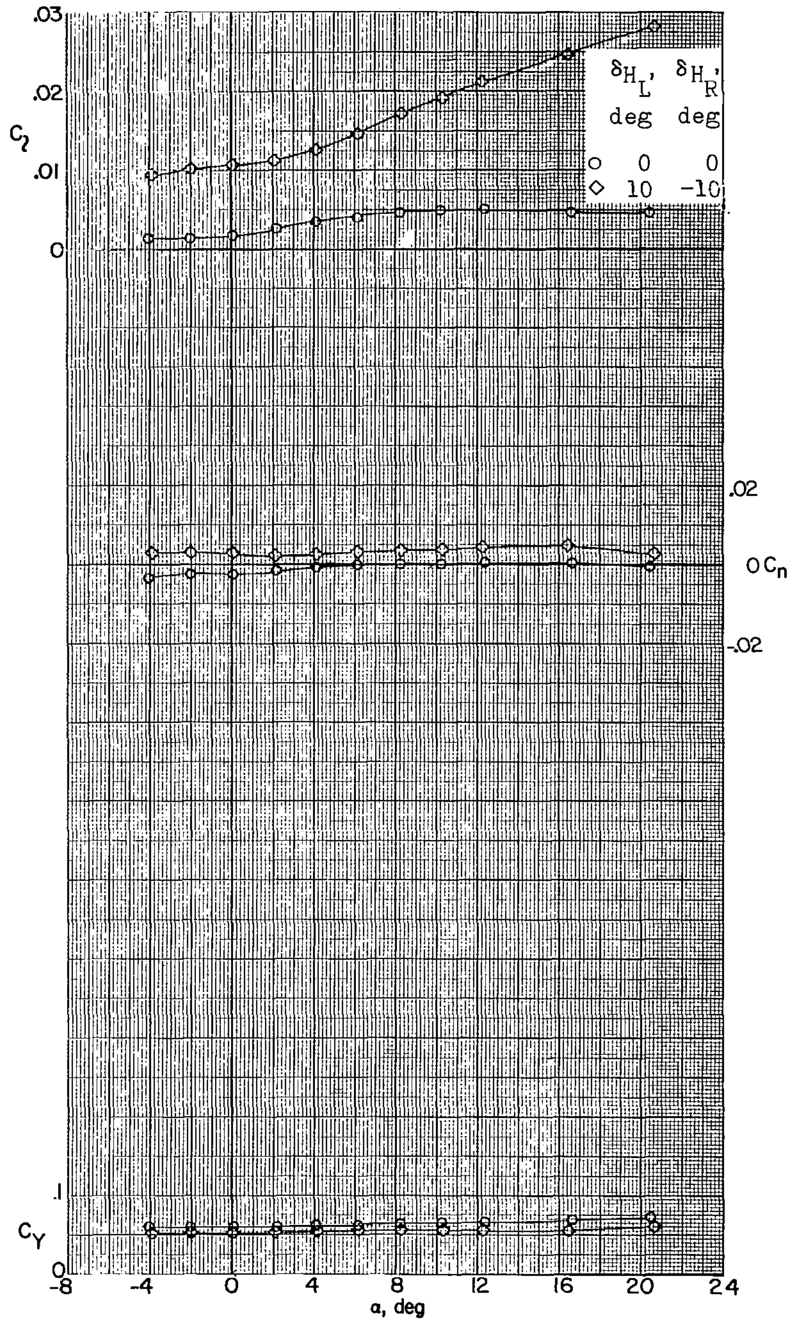

(g) M = 4.65; β = -5.1°.

Figure 25.- Continued.

[redacted]

[redacted]

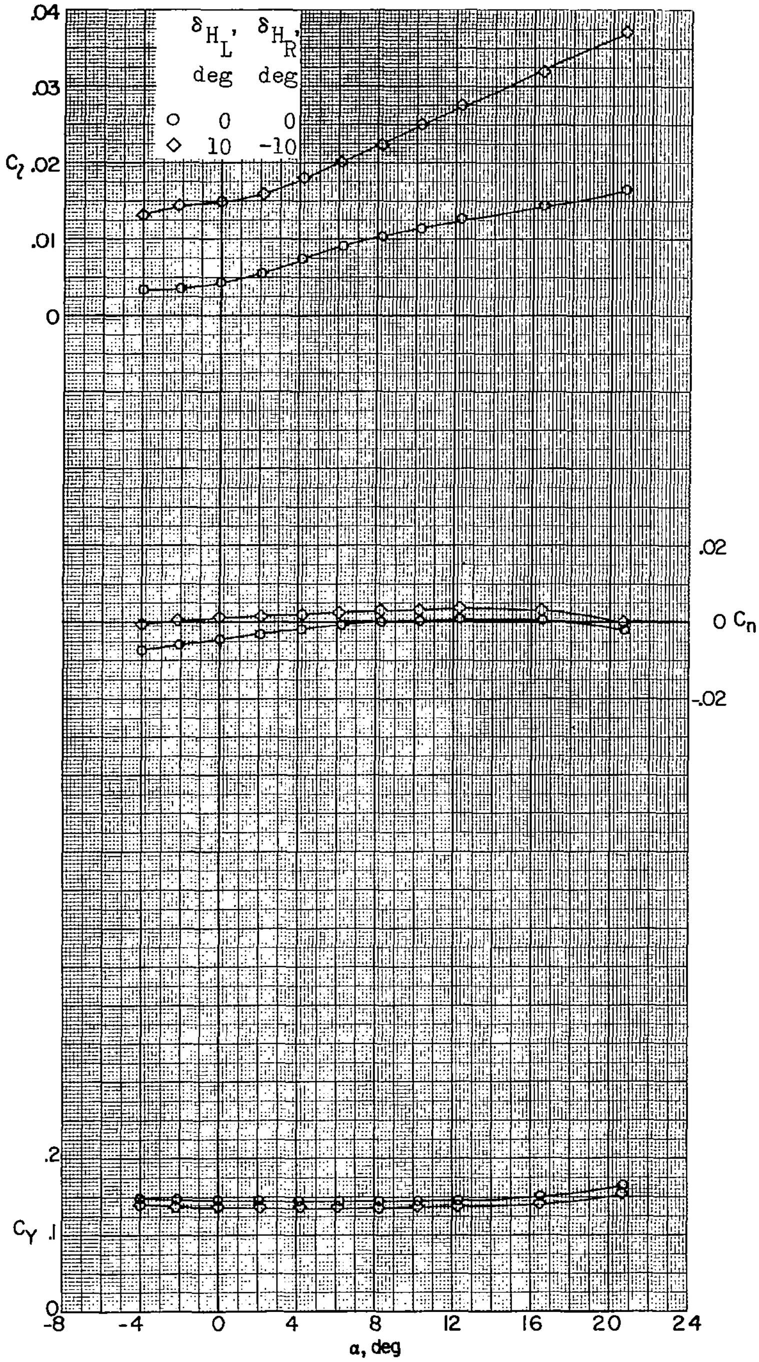

(h) M = 4.65; β = -10.6°.

Figure 25.- Concluded.

L-229

[redacted]

[redacted]

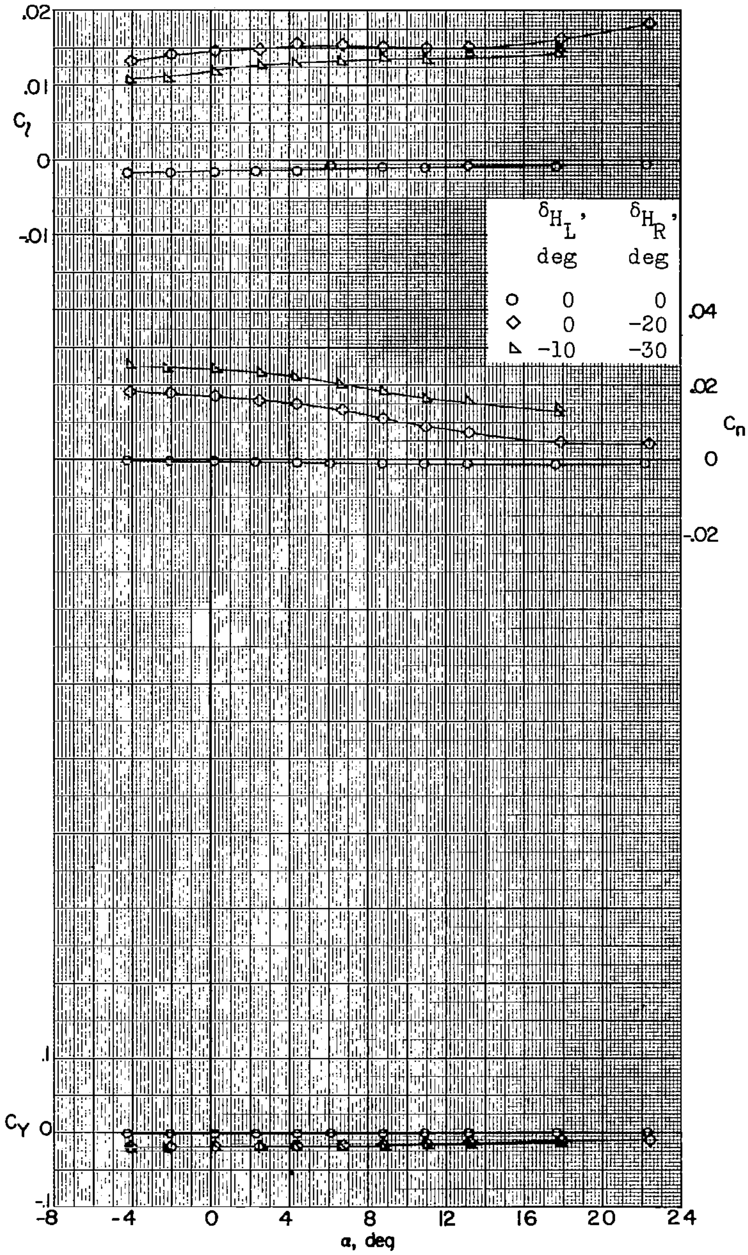

(a) M = 2.29.

Figure 26.- Lateral stability characteristics of a 0.067-scale model of the X-15 airplane with various roll-control deflections of the left and right panels of the horizontal tail. Speed brakes closed.

[redacted]

[redacted]

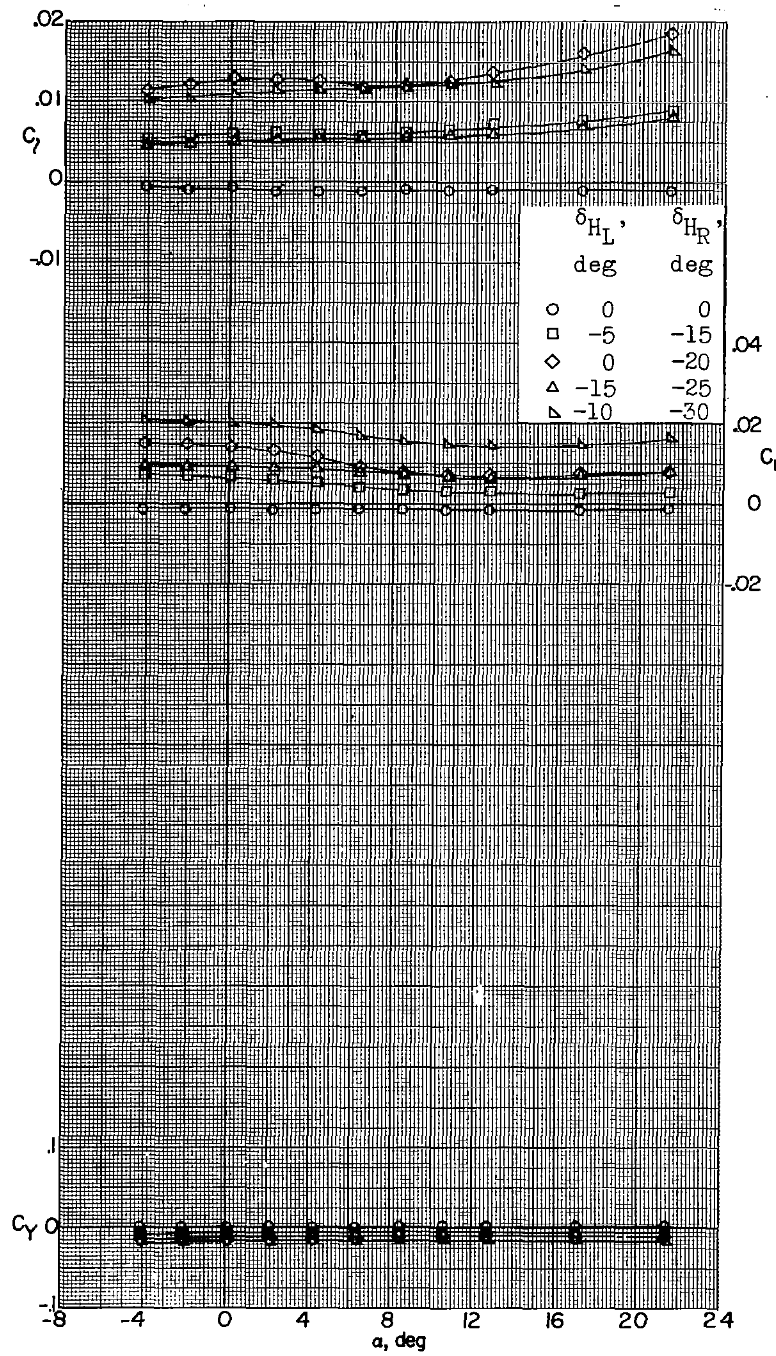

(b) M = 2.98.

Figure 26.- Continued.

L-229

[redacted]

L-229

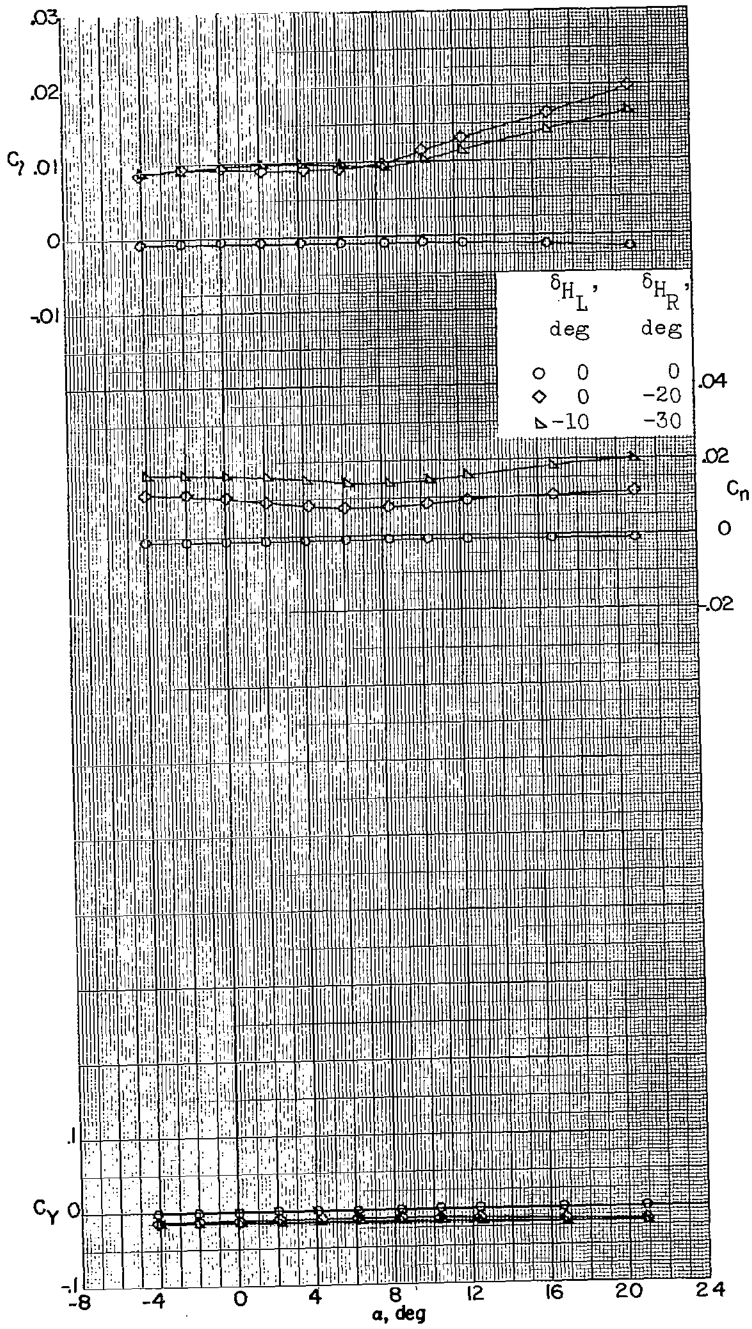

(c) M = 3.96.

Figure 26.- Continued.

[redacted]

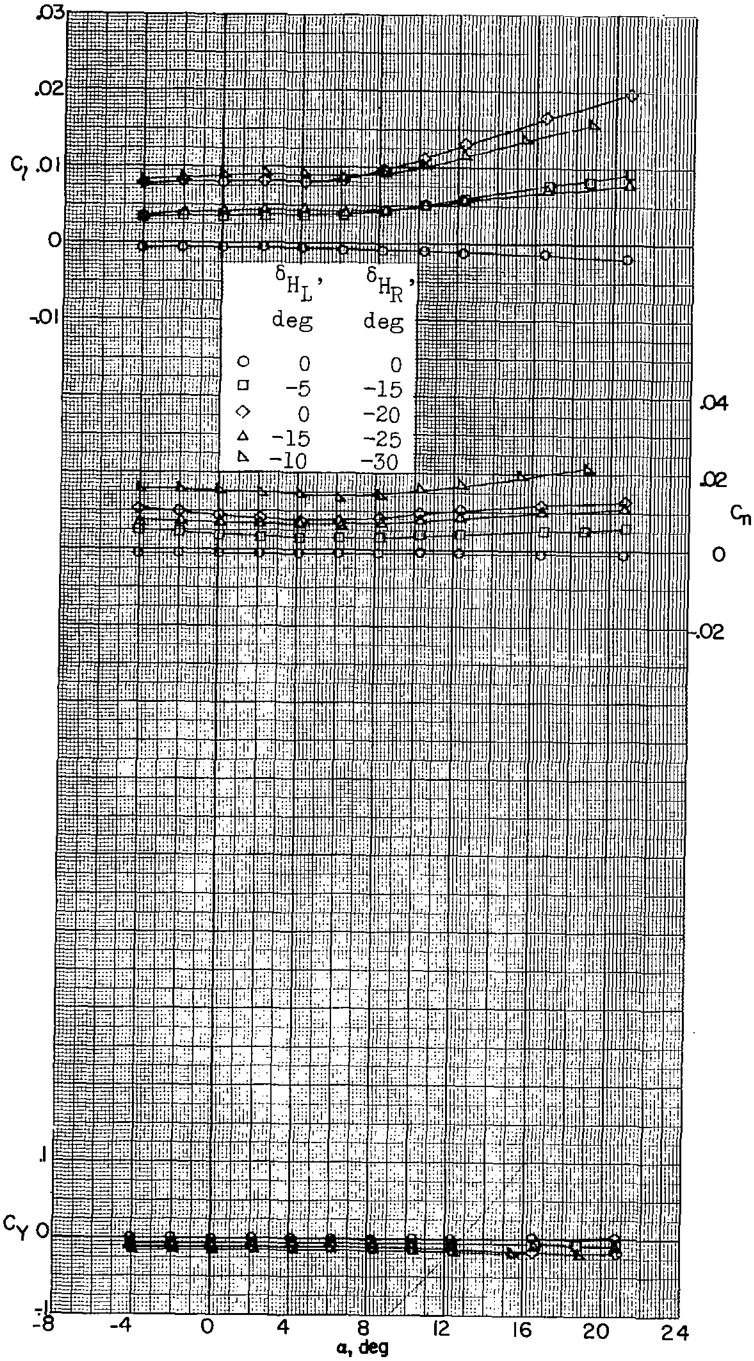

(d) M = 4.65.

Figure 26.- Concluded.

[redacted]

L-229

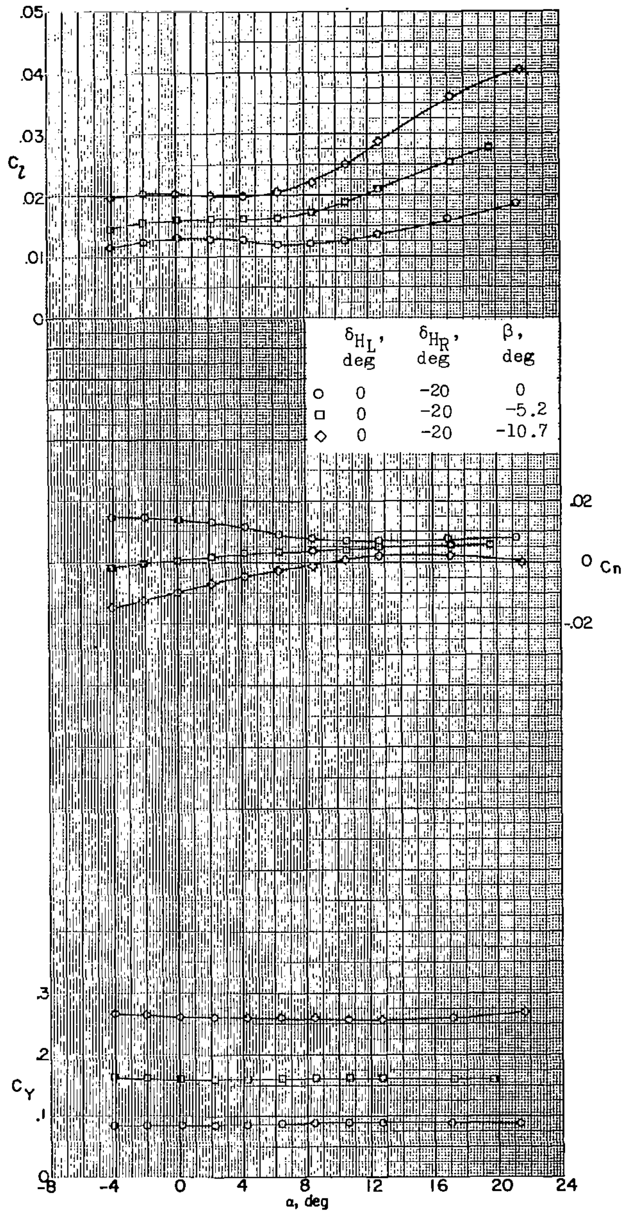

(a) M = 2.98.

Figure 27.- Lateral stability characteristics of a 0.067-scale model of the X-15 airplane with a roll-control deflection of the left and right panels of the horizontal tail at different angles of sideslip. Speed brakes closed.

[redacted]

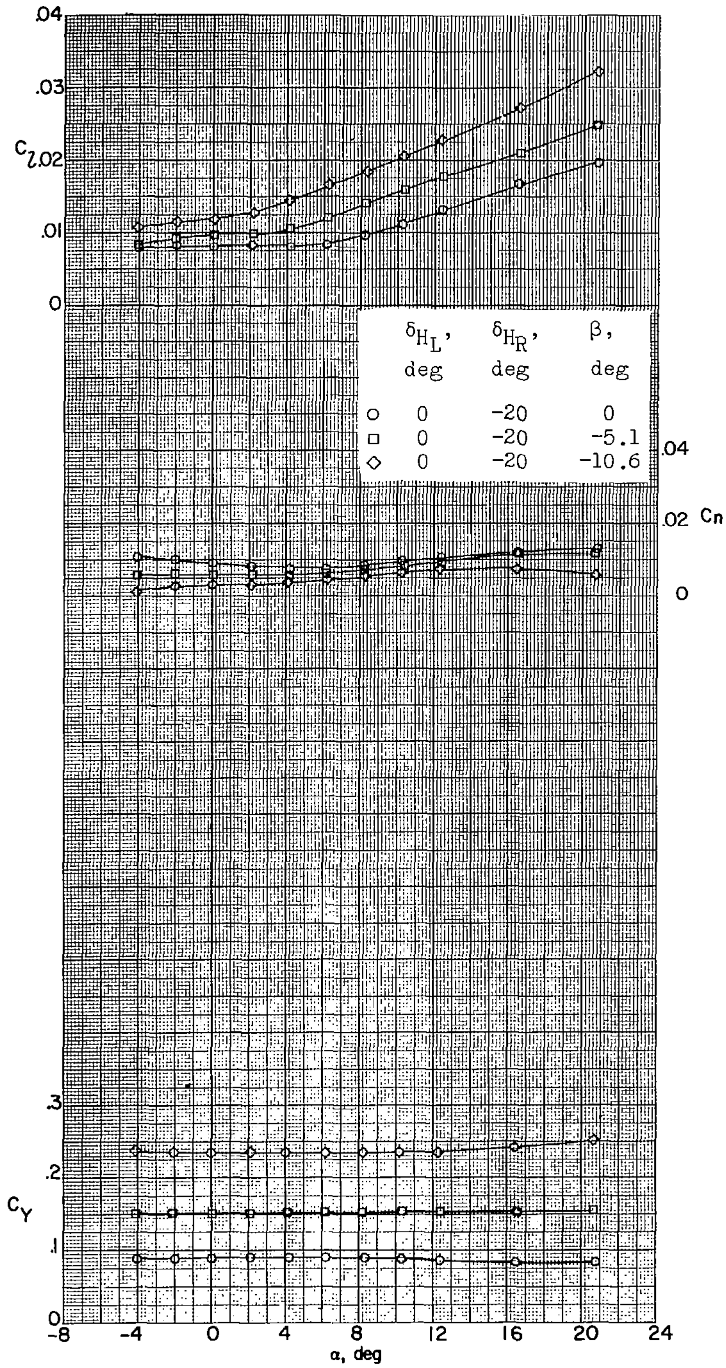

(b) M = 4.65.

Figure 27.- Concluded.

L-229

[redacted]

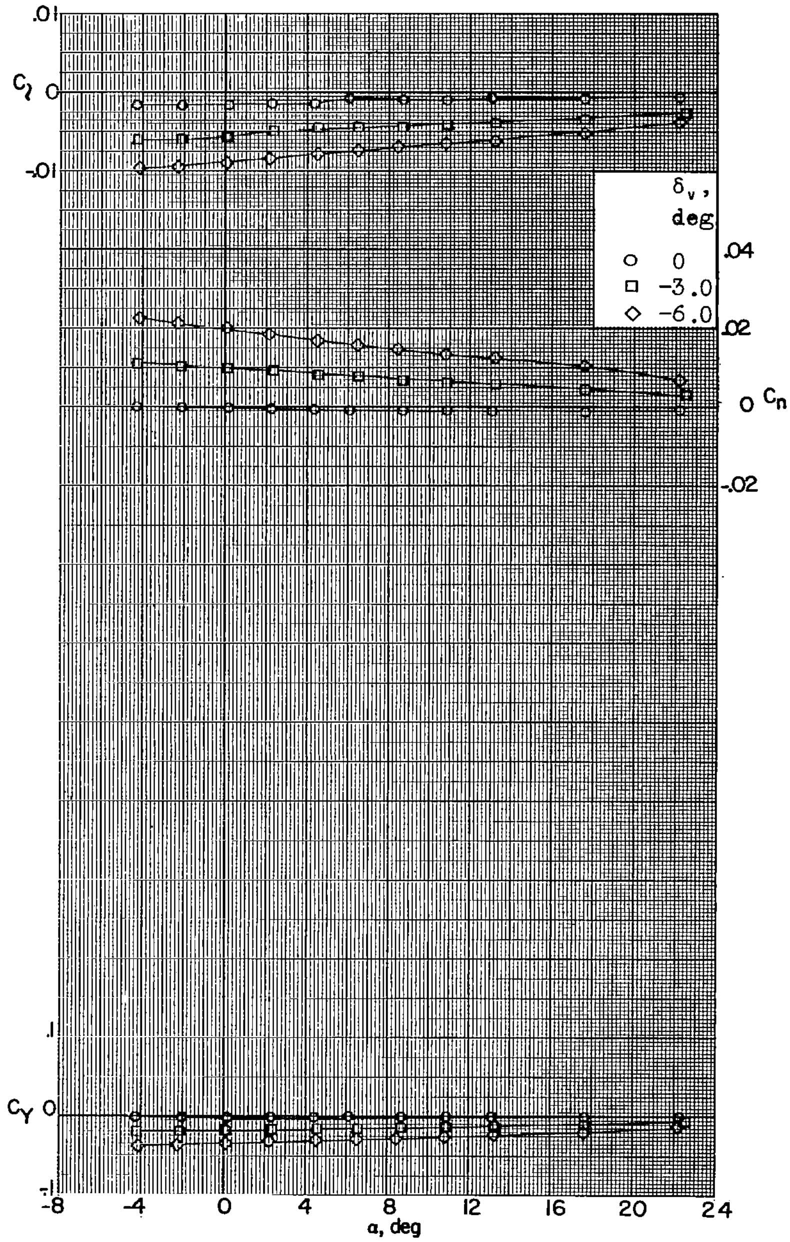

(a) M = 2.29; β = 0°.

Figure 28.- Lateral stability characteristics of a 0.067-scale model of the X-15 airplane with various deflections of the vertical tail. Speed brakes closed.

[redacted]

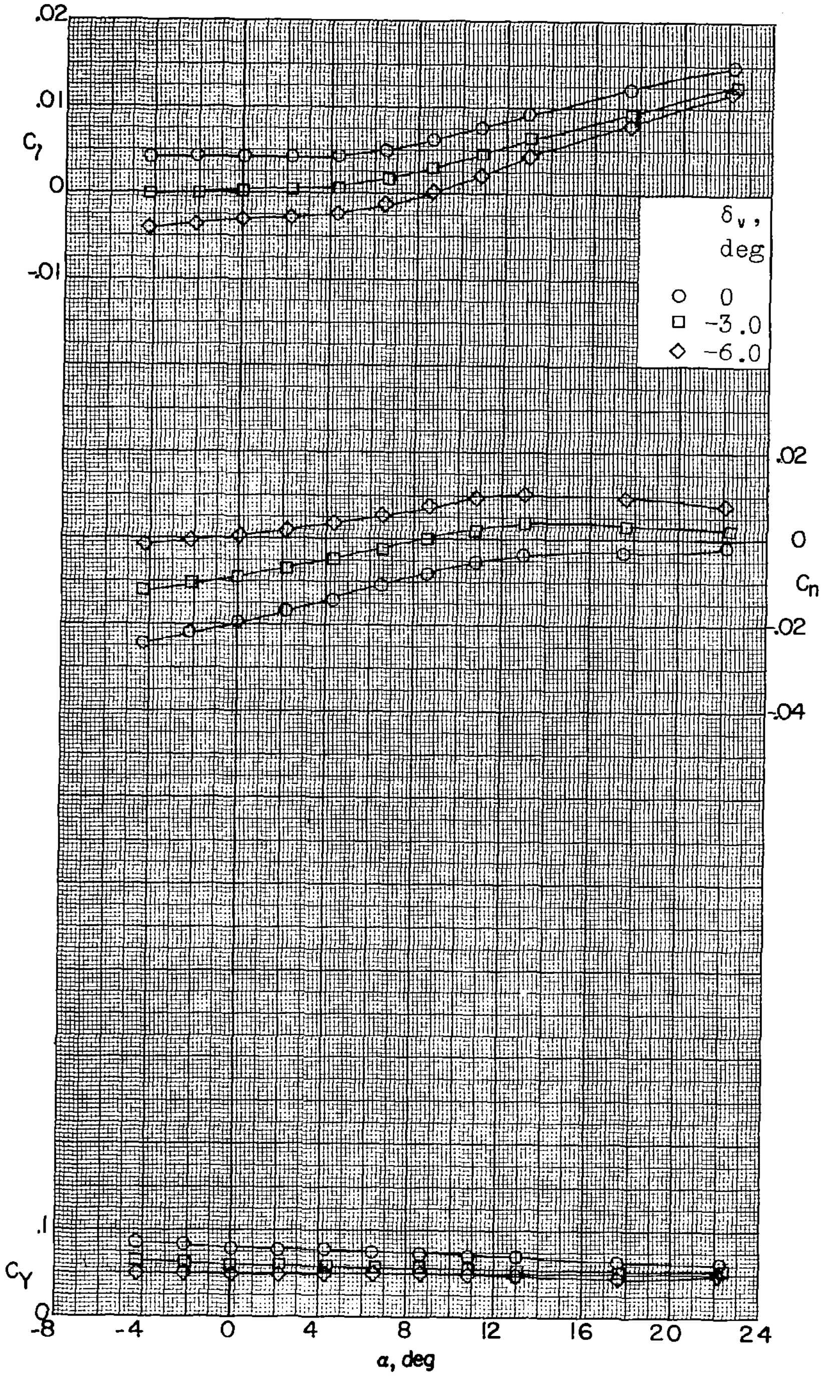

(b) $M = 2.29$; $\beta = -5.2^{\circ}$.

Figure 28.- Continued.

L-229

[redacted]

L-229

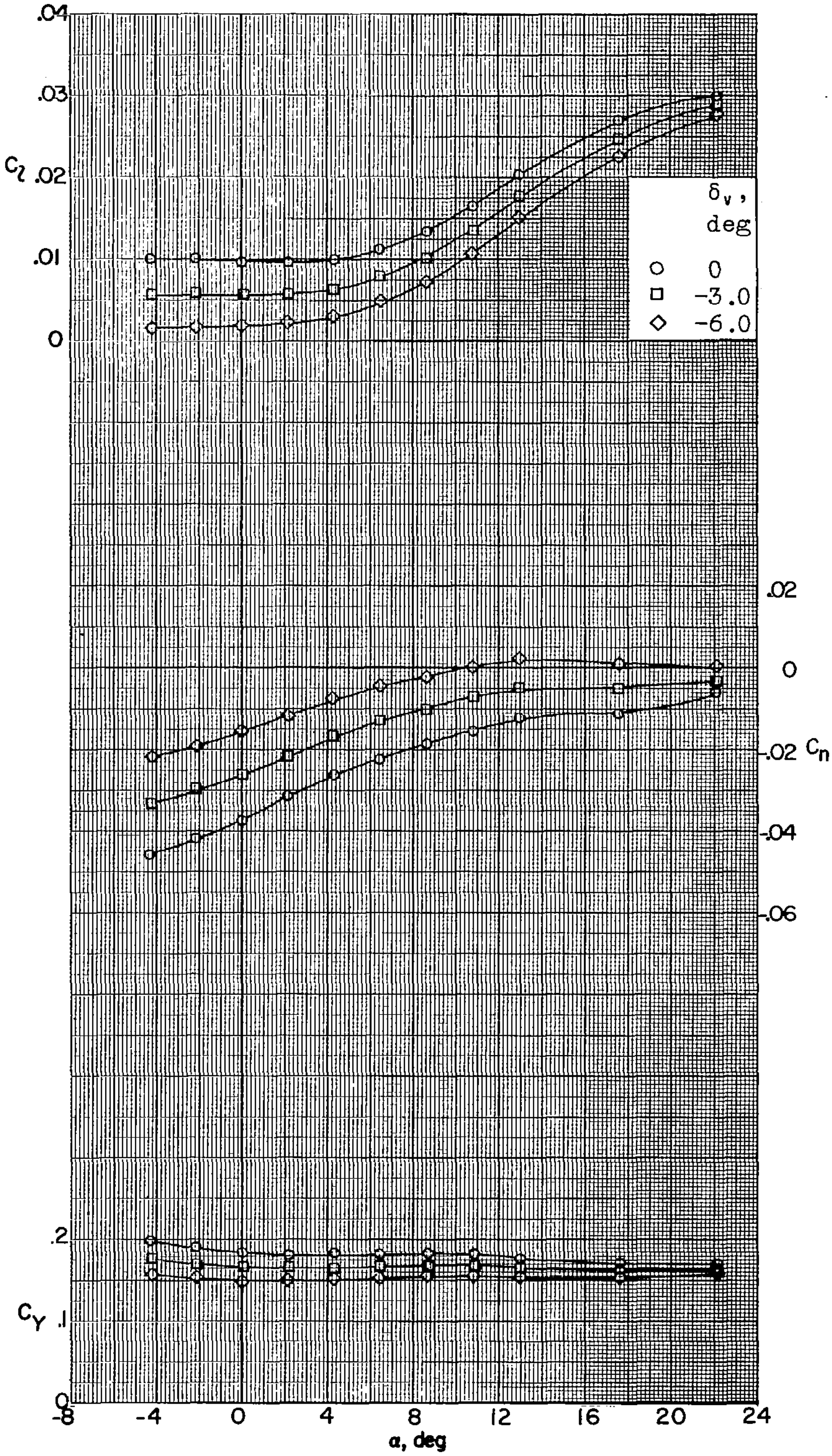

(c) M = 2.29; β = -10.7°.

Figure 28.- Continued.

[redacted]

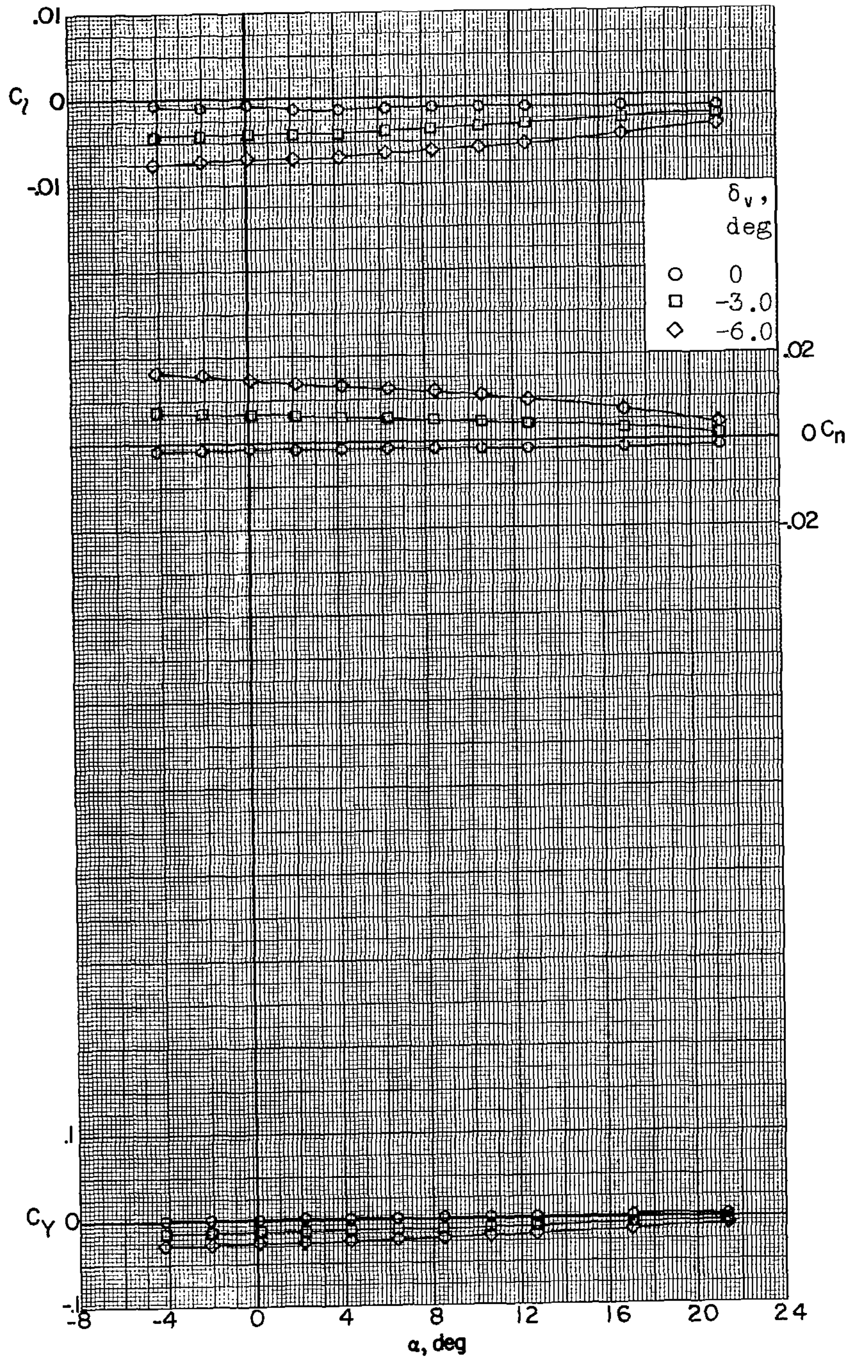

(d) M = 2.98; β = 0°.

Figure 28.- Continued.

L-229

[redacted]

[redacted]

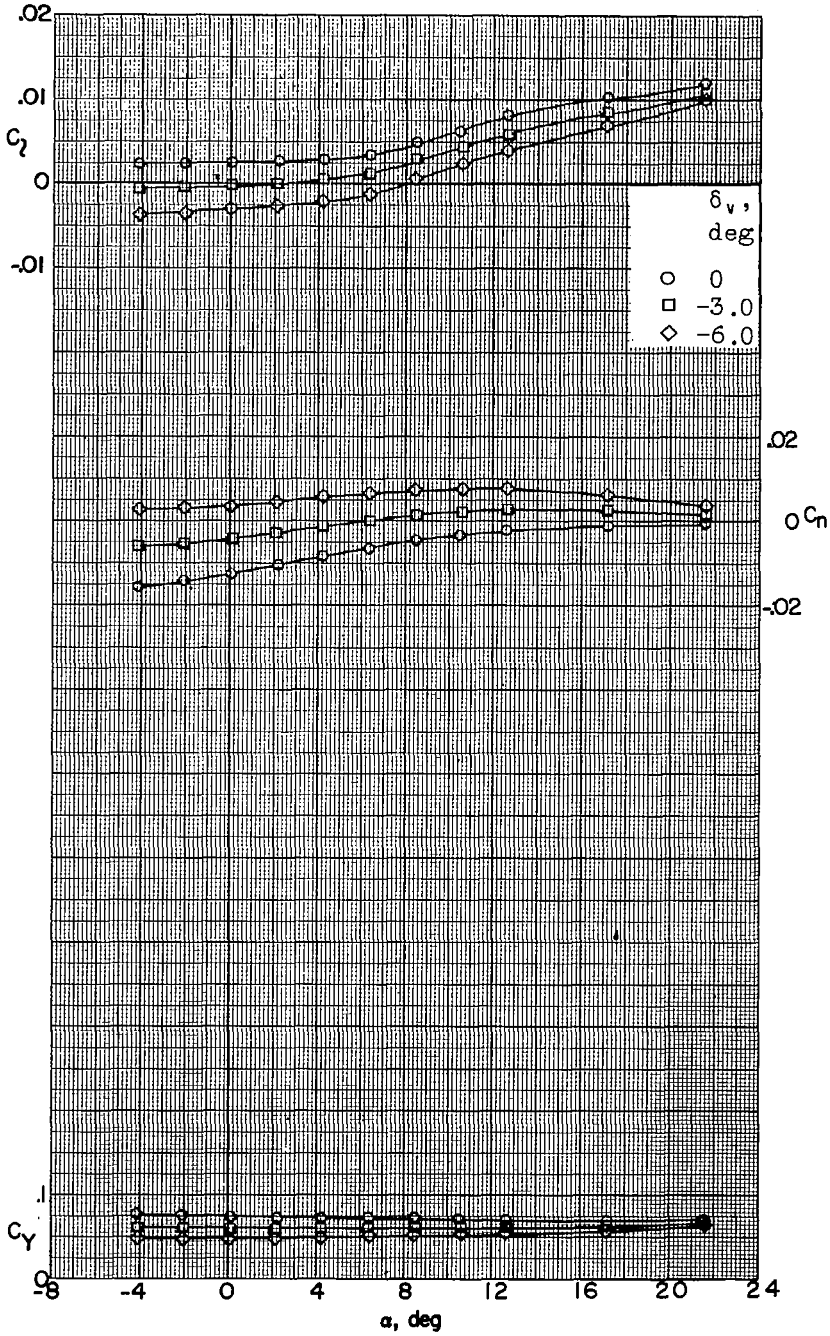

(e) M = 2.98; β = -5.2°.

Figure 28.- Continued.

L-229

[redacted]

[redacted]

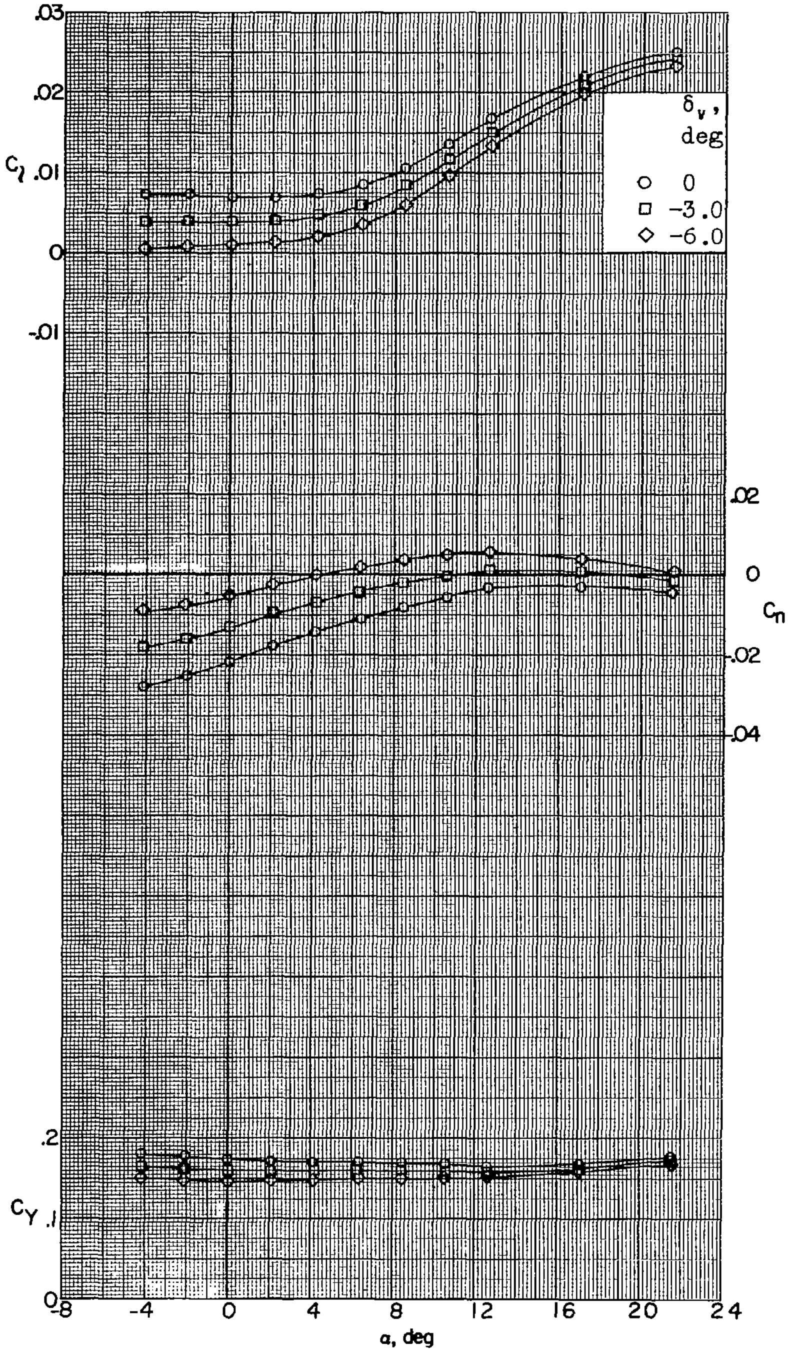

(f) M = 2.98; β = -10.6°.

Figure 28.- Continued.

[redacted]

L-229

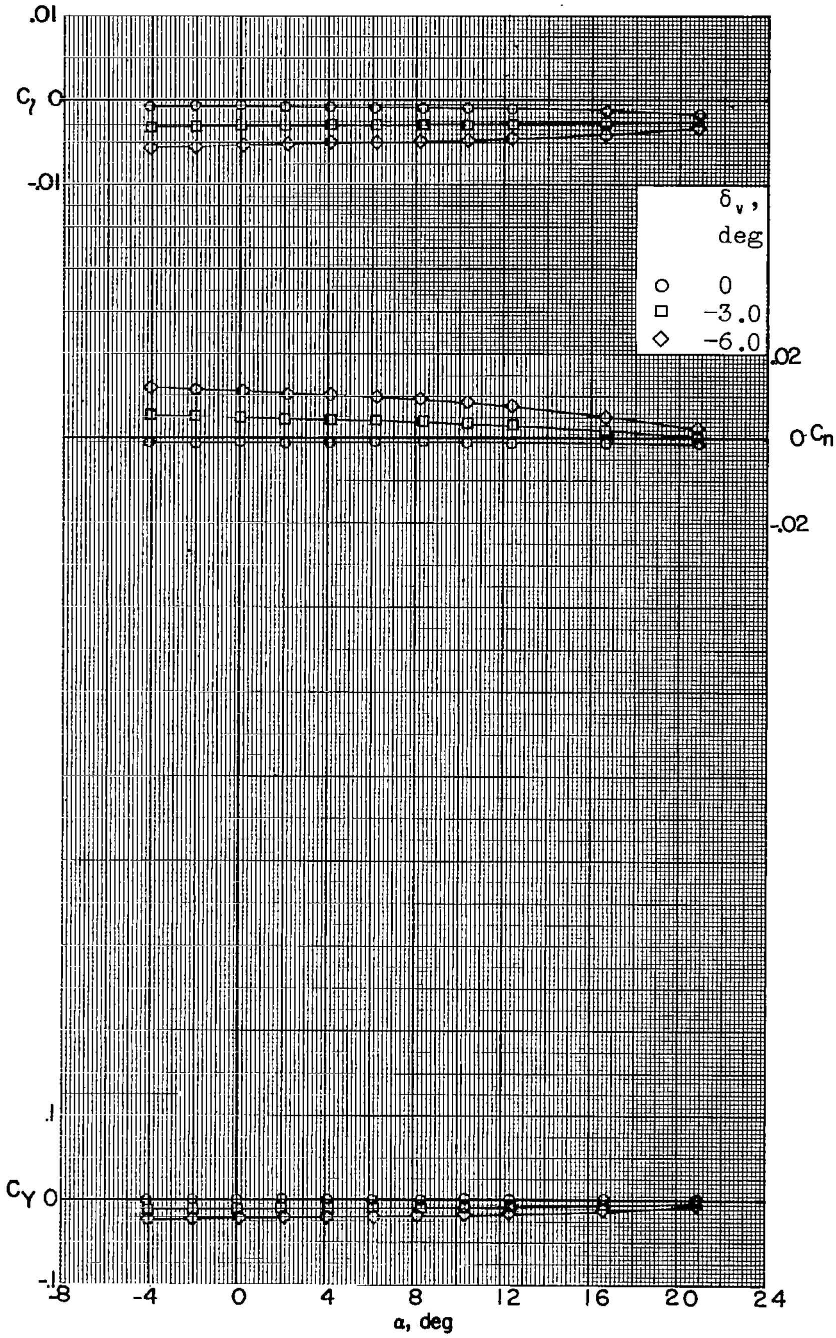

(g) $M = 3.96$; $\beta = 0^{\circ}$.

Figure 28.- Continued.

[redacted]

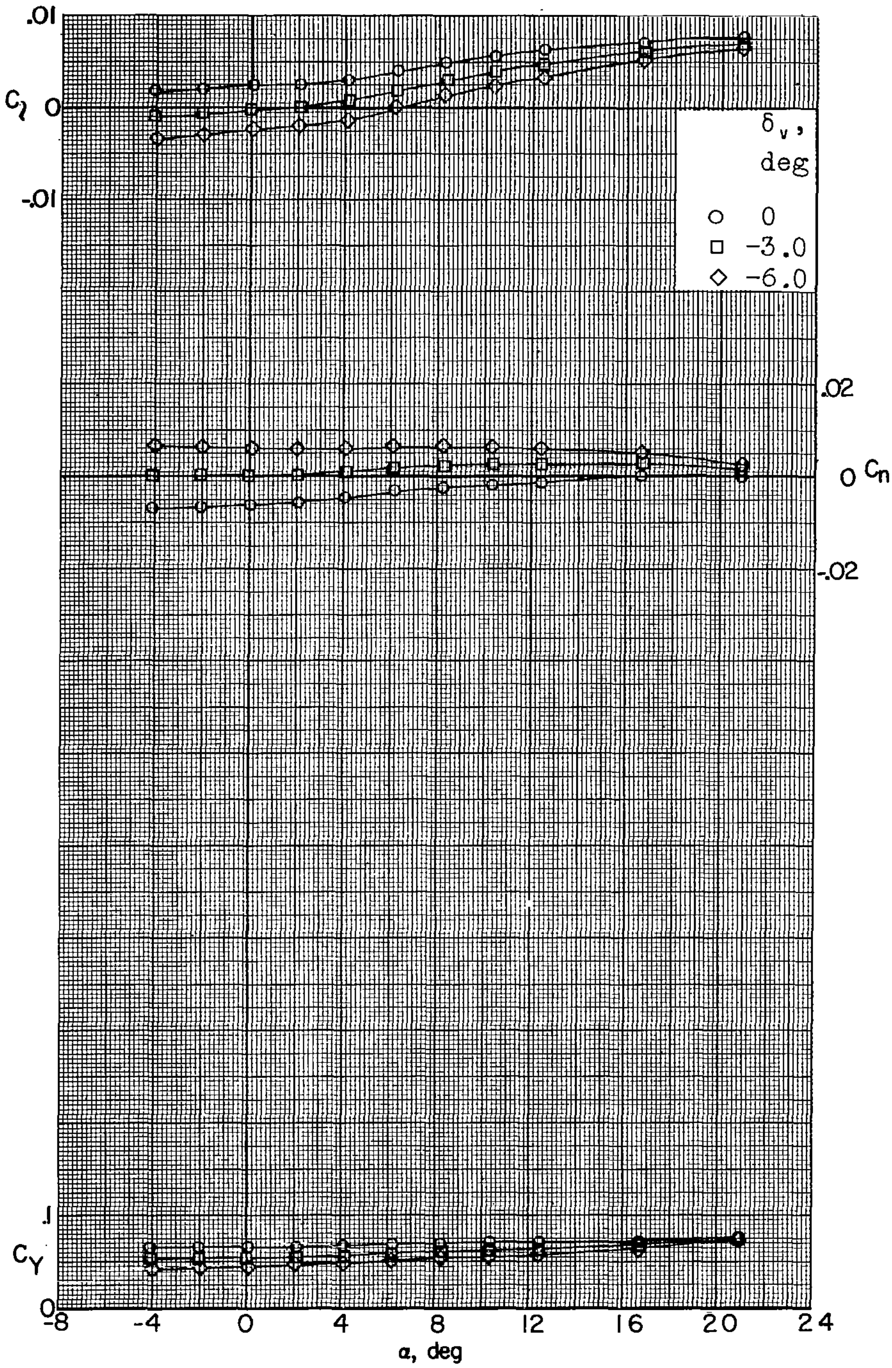

(h) $M = 3.96$; $\beta = -5.1^{\circ}$.

Figure 28.- Continued.

L-229

[redacted]

[redacted]

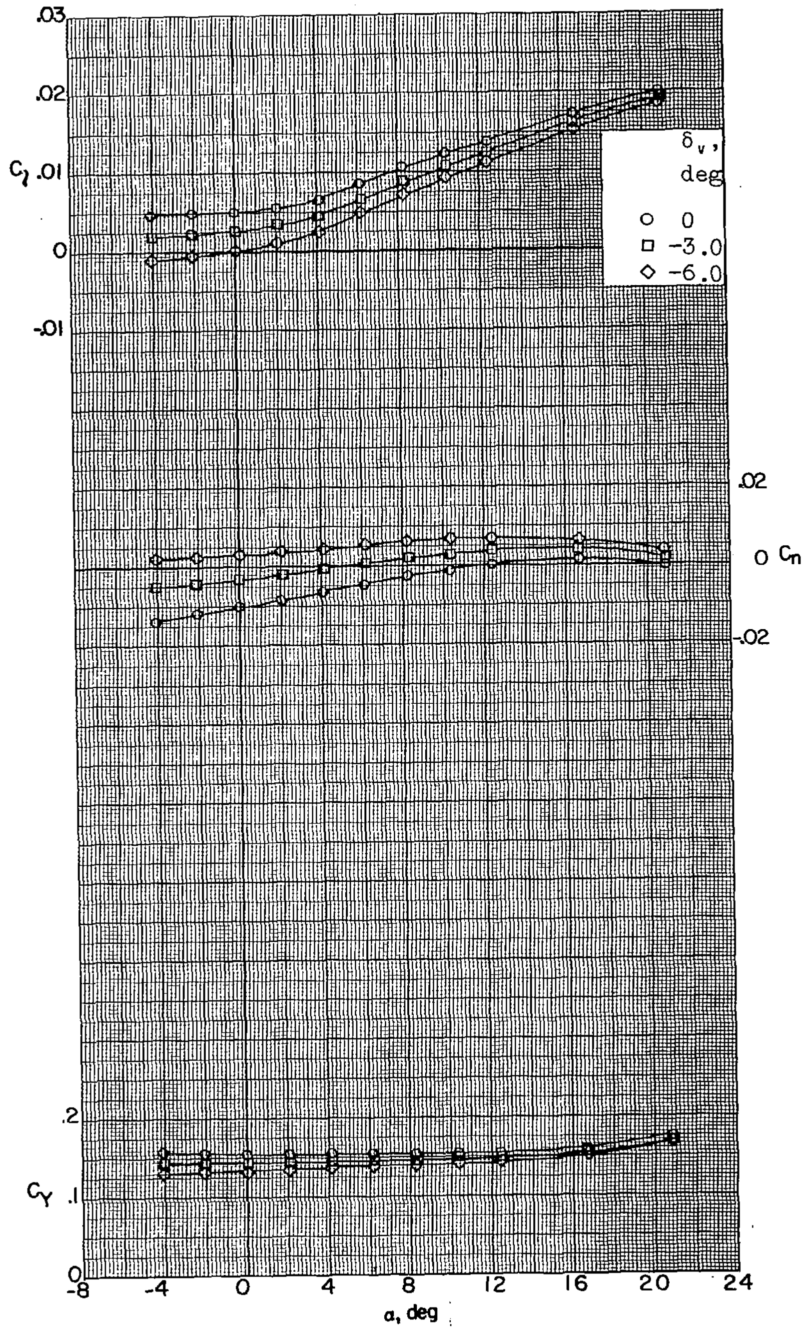

(i) $M = 3.96$; $\beta = -10.6^{\circ}$.

Figure 28.- Continued.

[redacted]

[redacted]

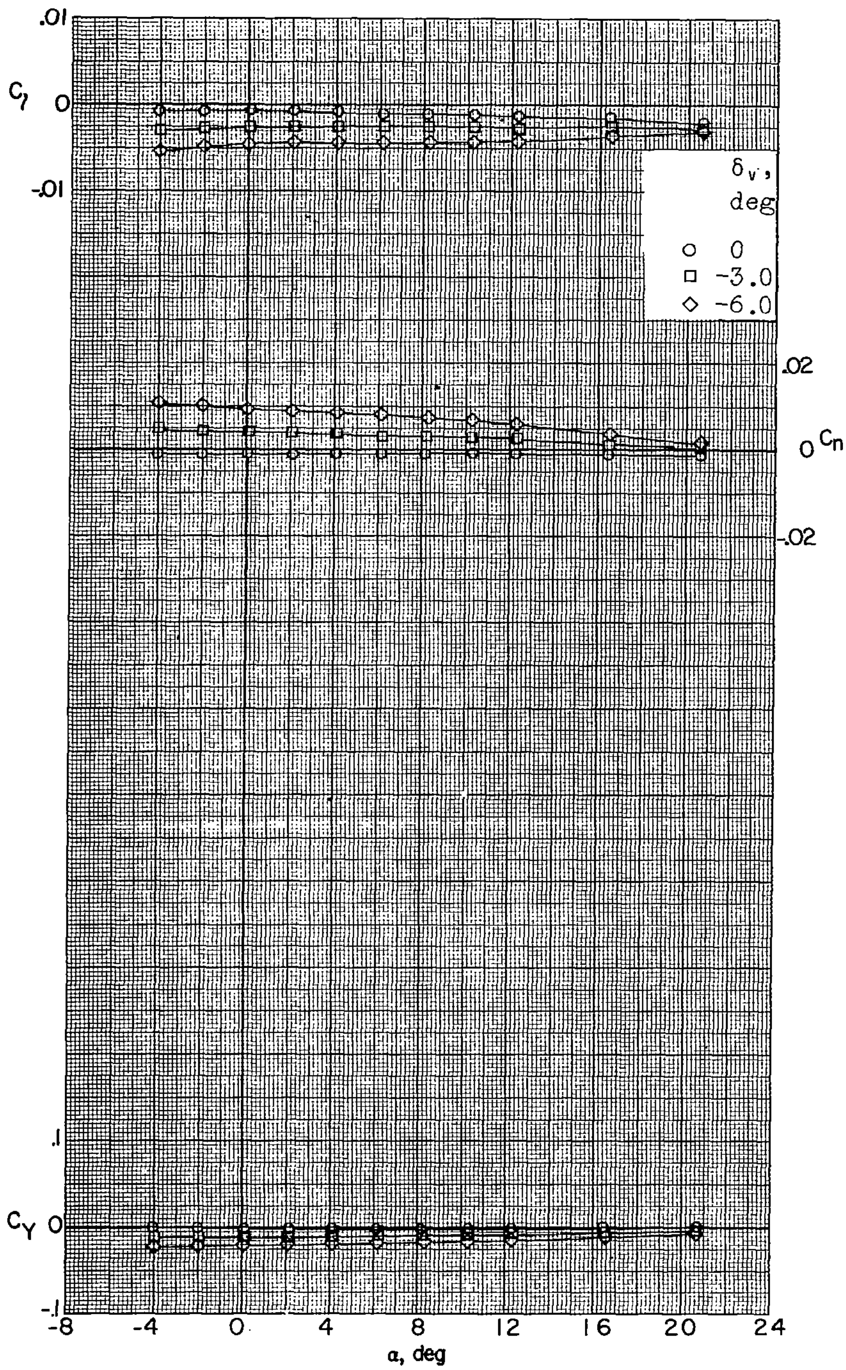

(j) M = 4.65; β = 0.1°.

Figure 28.- Continued.

L-229

[redacted]

L-229

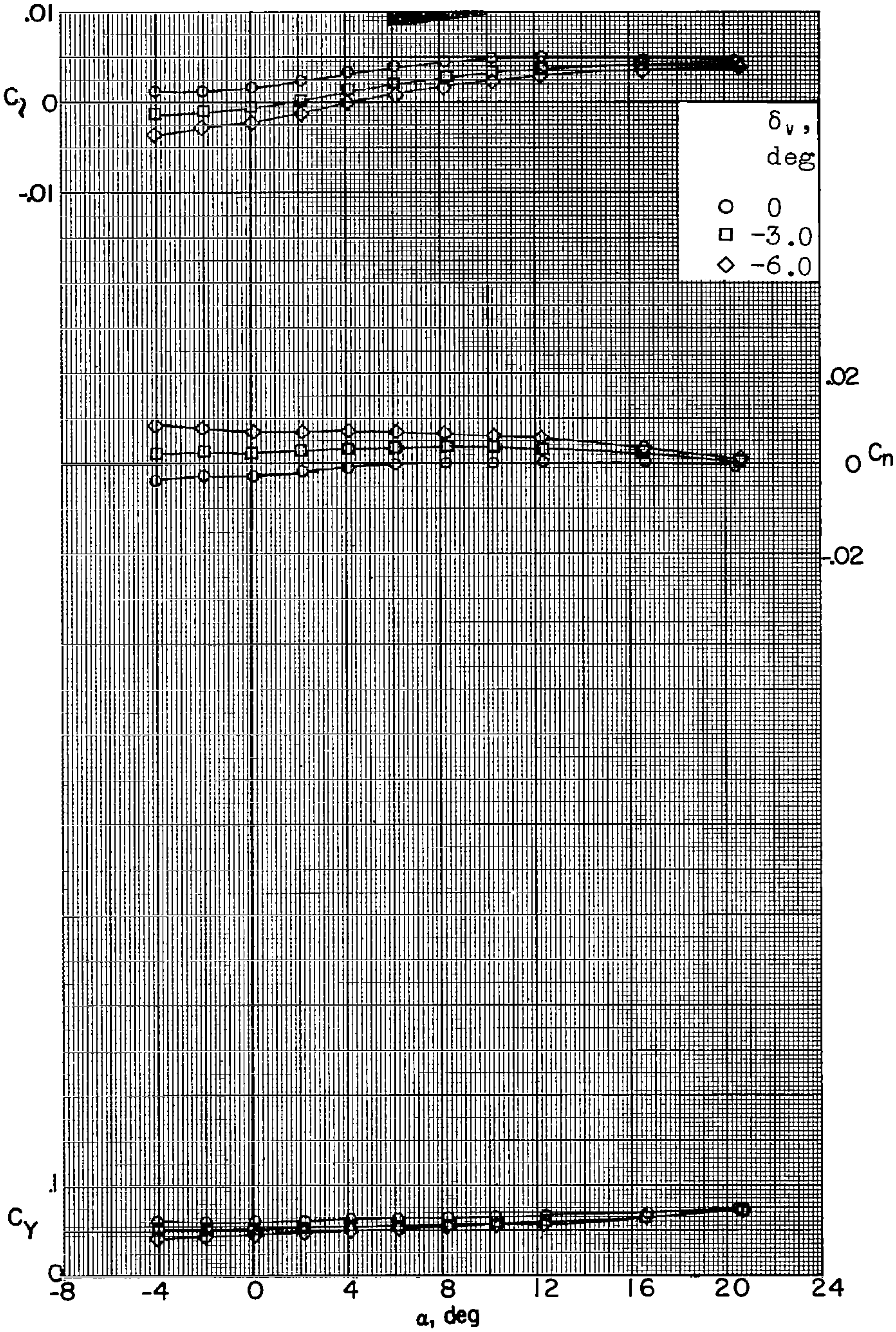

(k) M = 4.65; β = -5.1°.

Figure 28.- Continued.

[redacted]

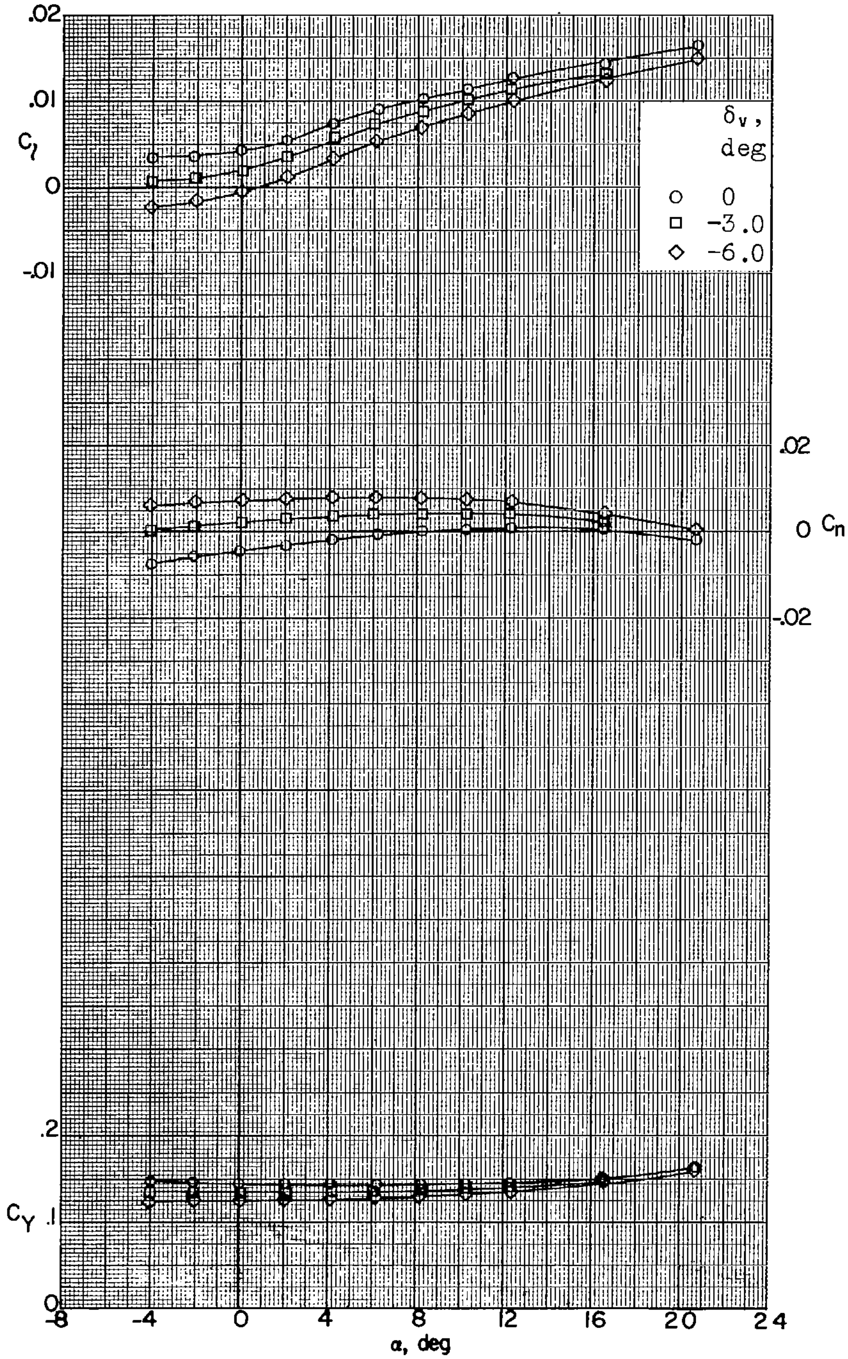

(l) M = 4.65; β = -10.5°.

Figure 28.- Concluded.

L-229

[redacted]

L-229

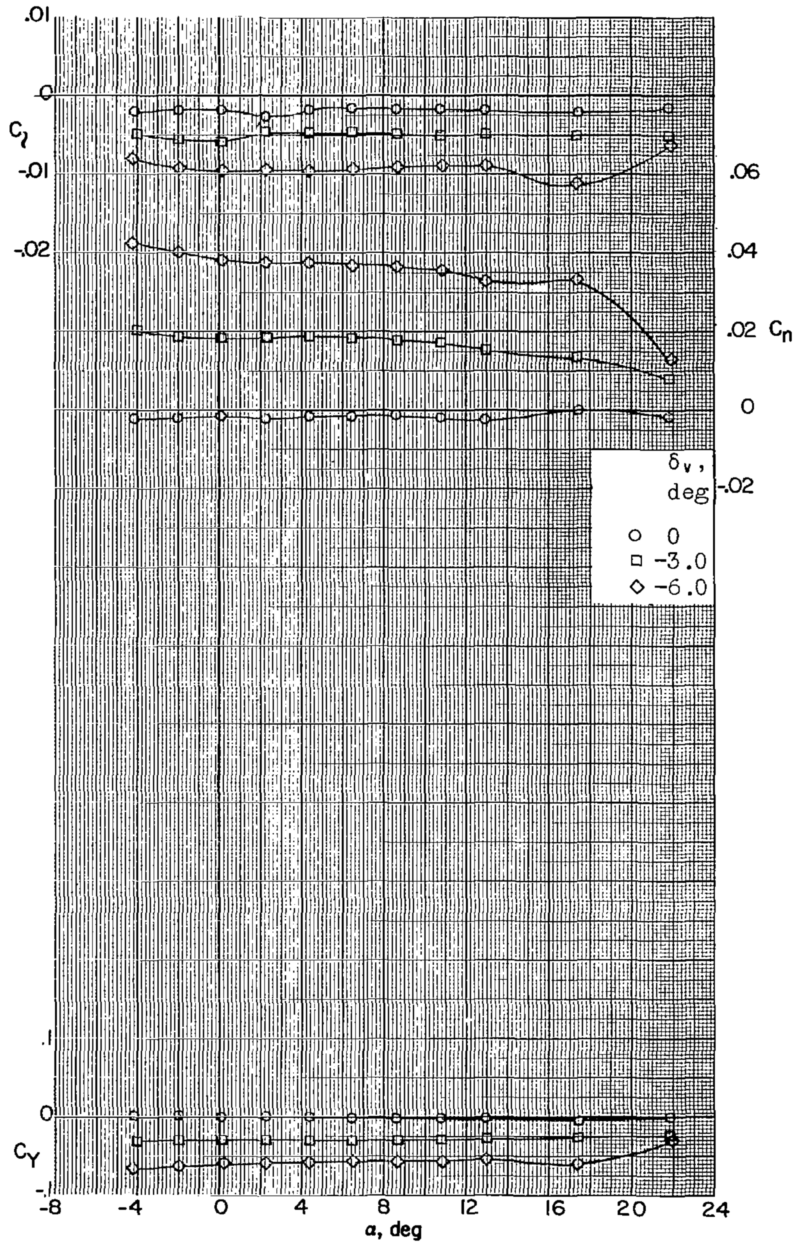

(a) M = 2.29; β = -0.1°.

Figure 29.- Lateral stability characteristics of a 0.067-scale model of the X-15 airplane with various deflections of the vertical tail. Speed brakes open 45°.

[redacted]

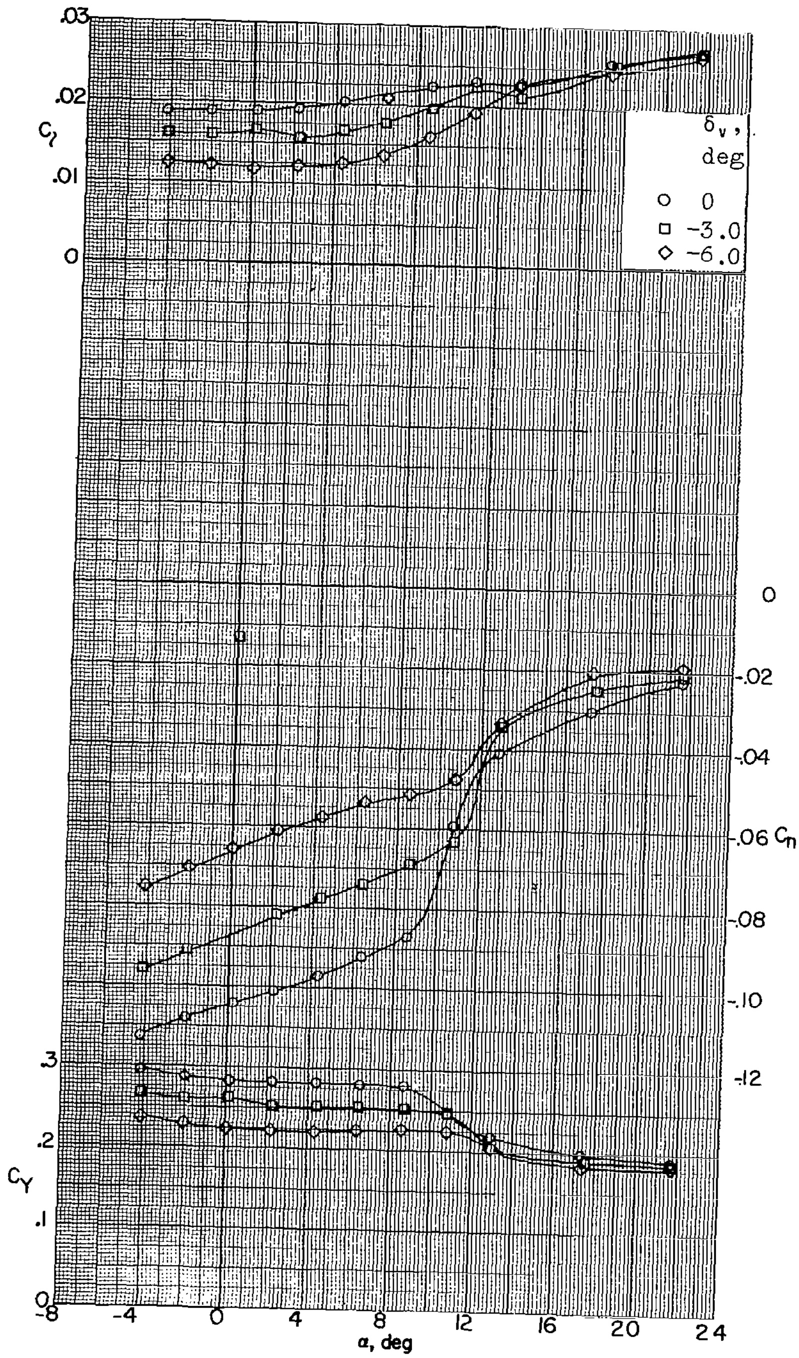

(b) M = 2.29; β = -10.6°

Figure 29.- Continued.

[redacted]

L-229

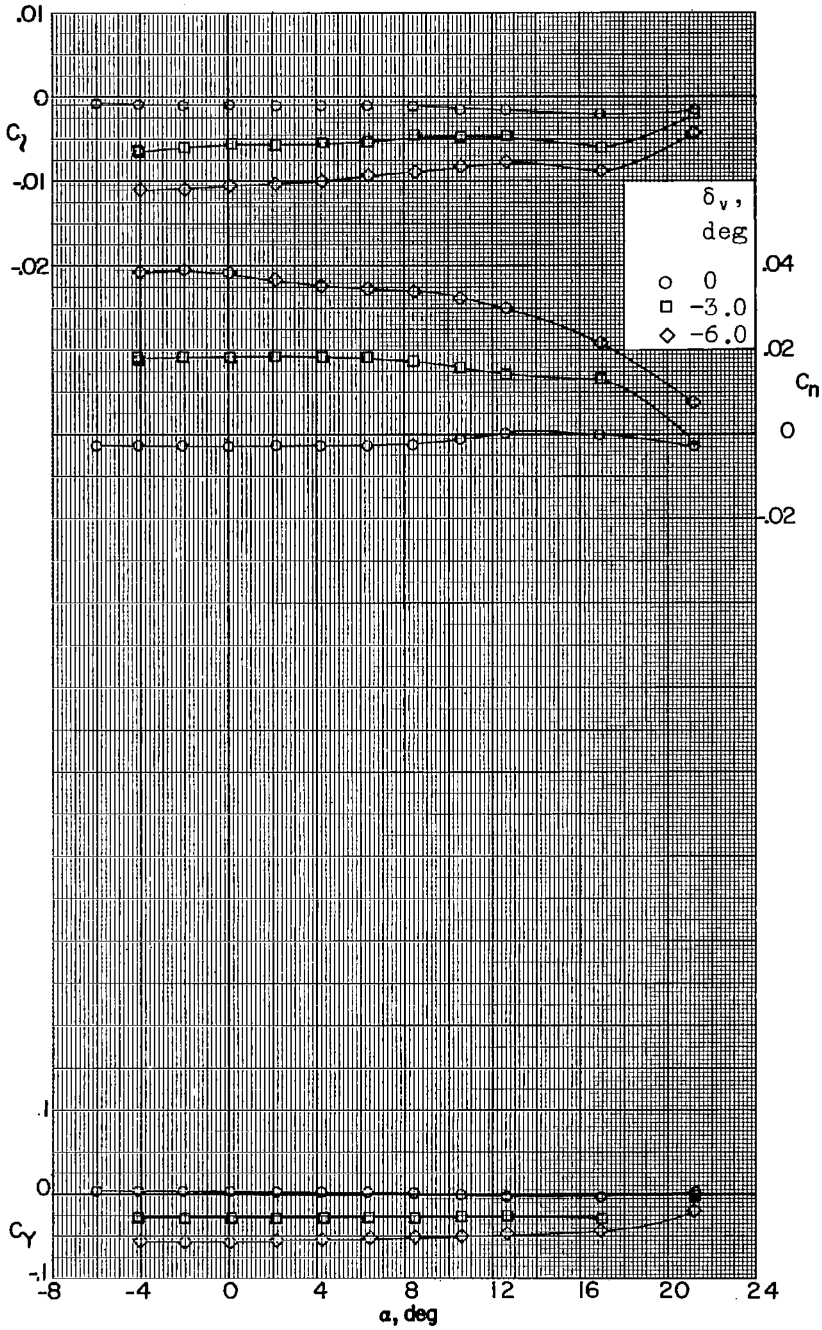

(c) M = 2.98; β = 0°.

Figure 29.- Continued.

[redacted]

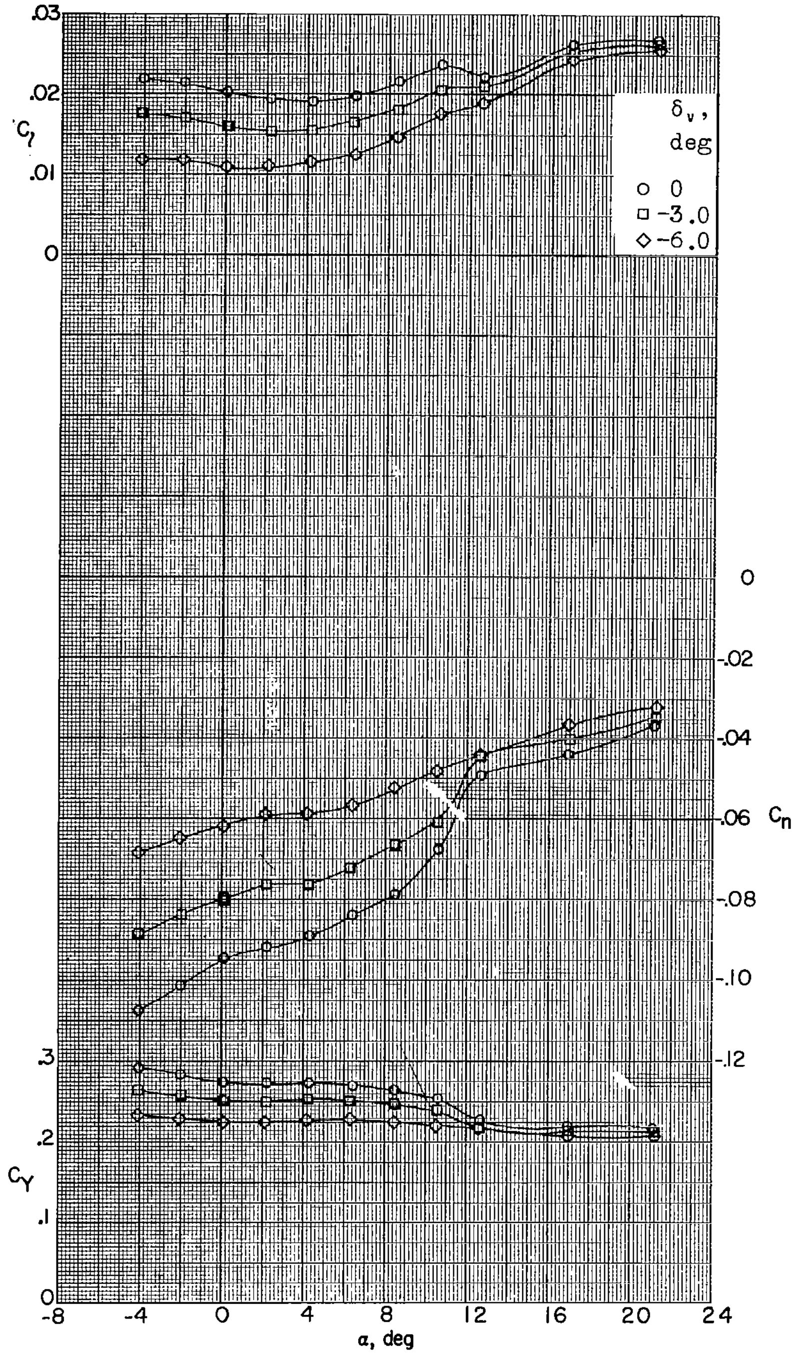

(d) $M = 2.98$; $\beta = -10.6^{\circ}$.

Figure 29.- Continued.

[redacted]

[redacted]

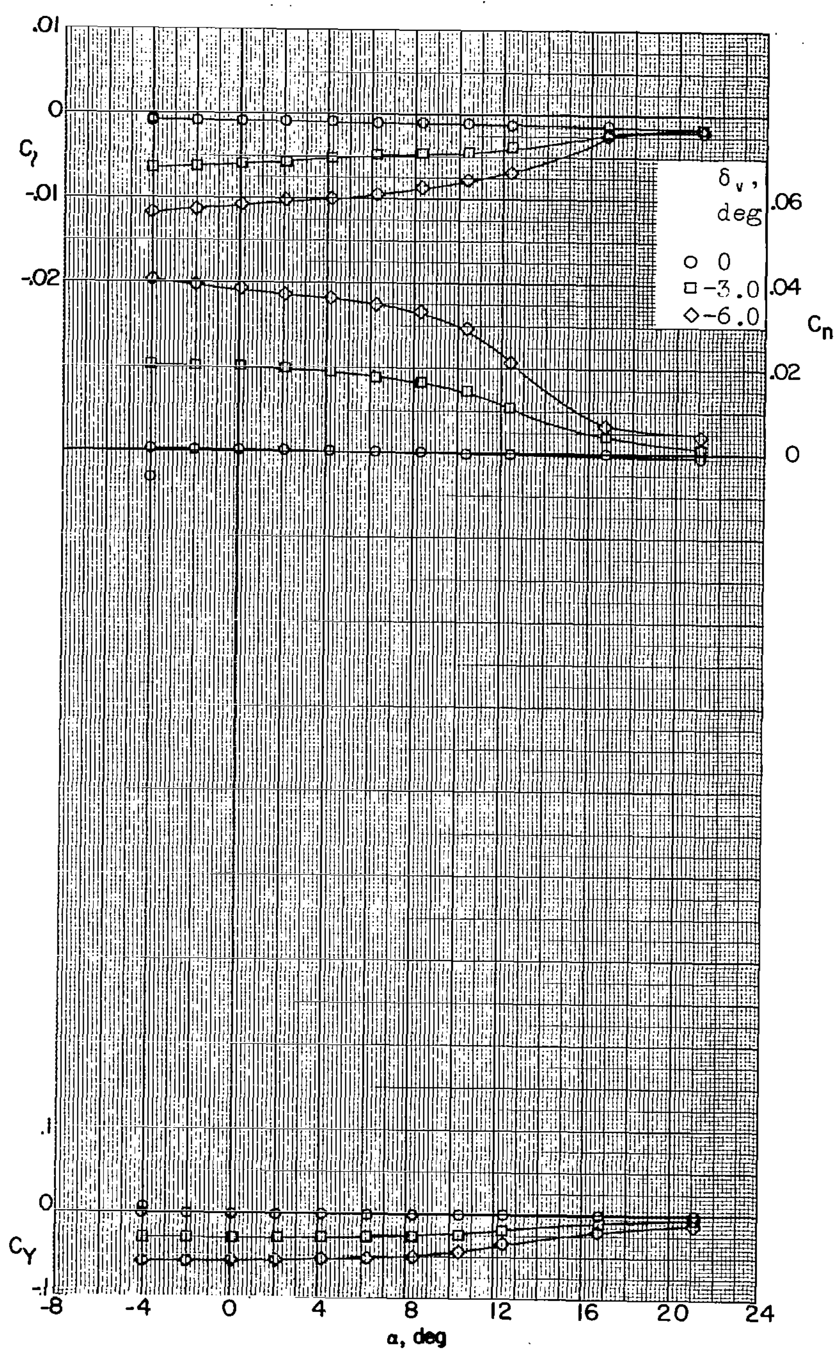

(e) $M = 3.96$; $\beta = -0.1^{\circ}$.

Figure 29.- Continued.

[redacted]

[redacted]

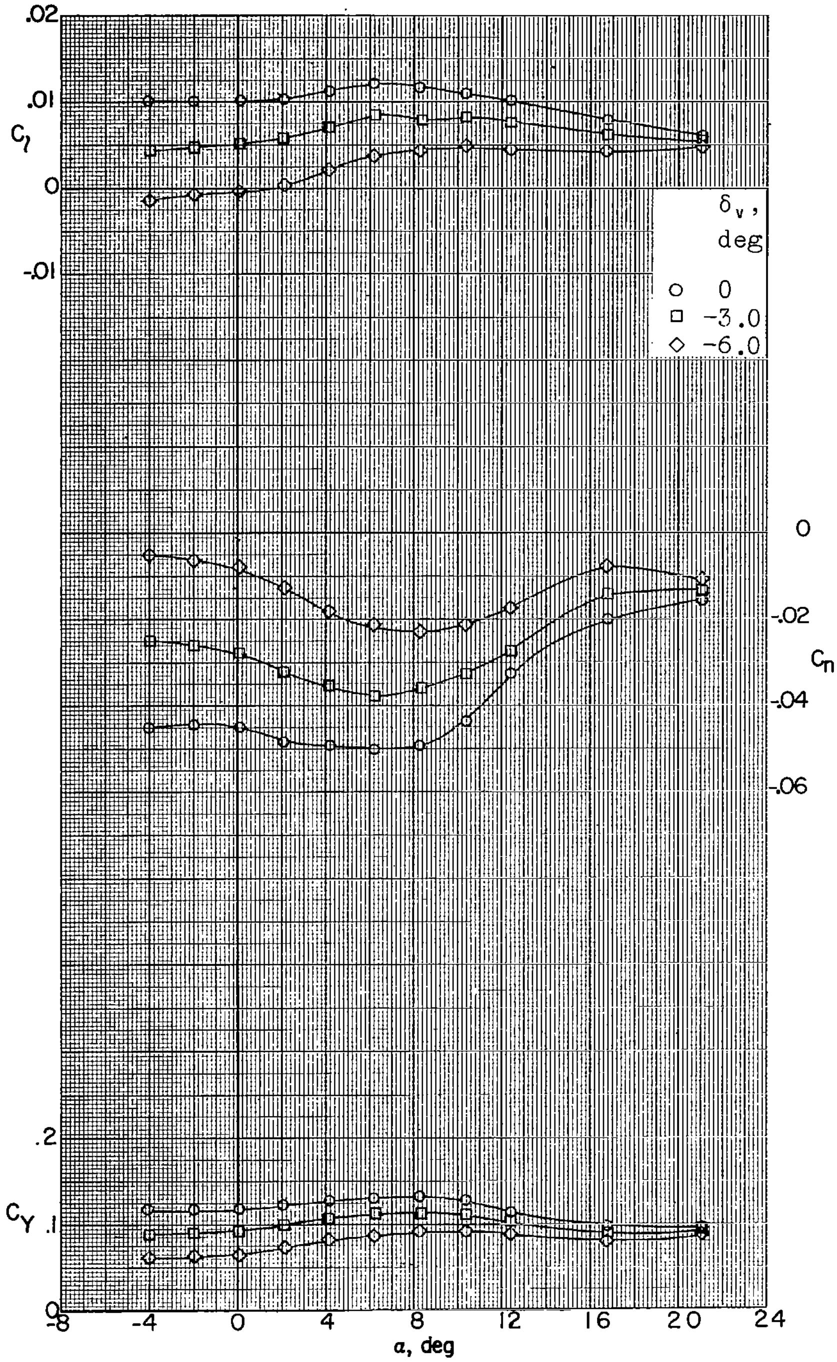

(f) $M = 3.96$; $\beta = -5.1^{\circ}$.

Figure 29.- Continued.

L-229

[redacted]

L-229

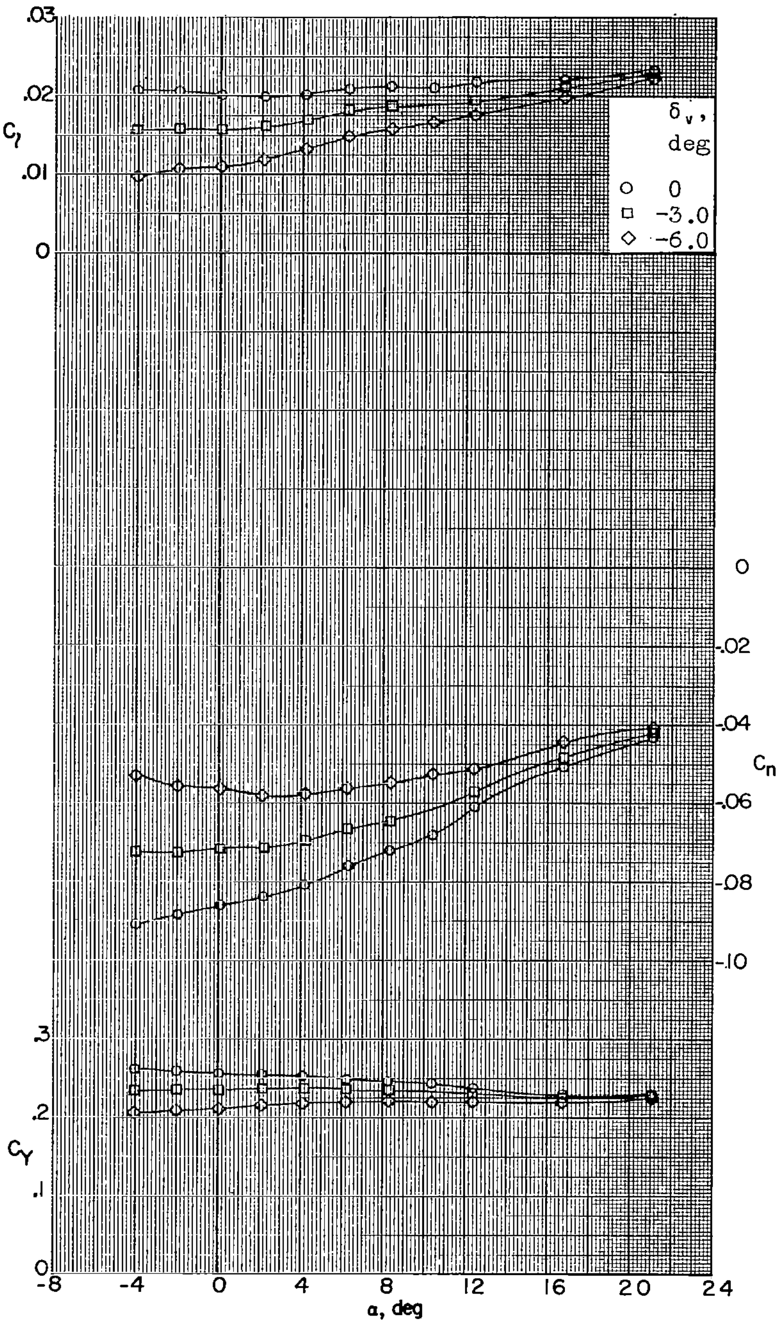

(g) M = 3.96; β = -10.5°.

Figure 29.- Continued.

[redacted]

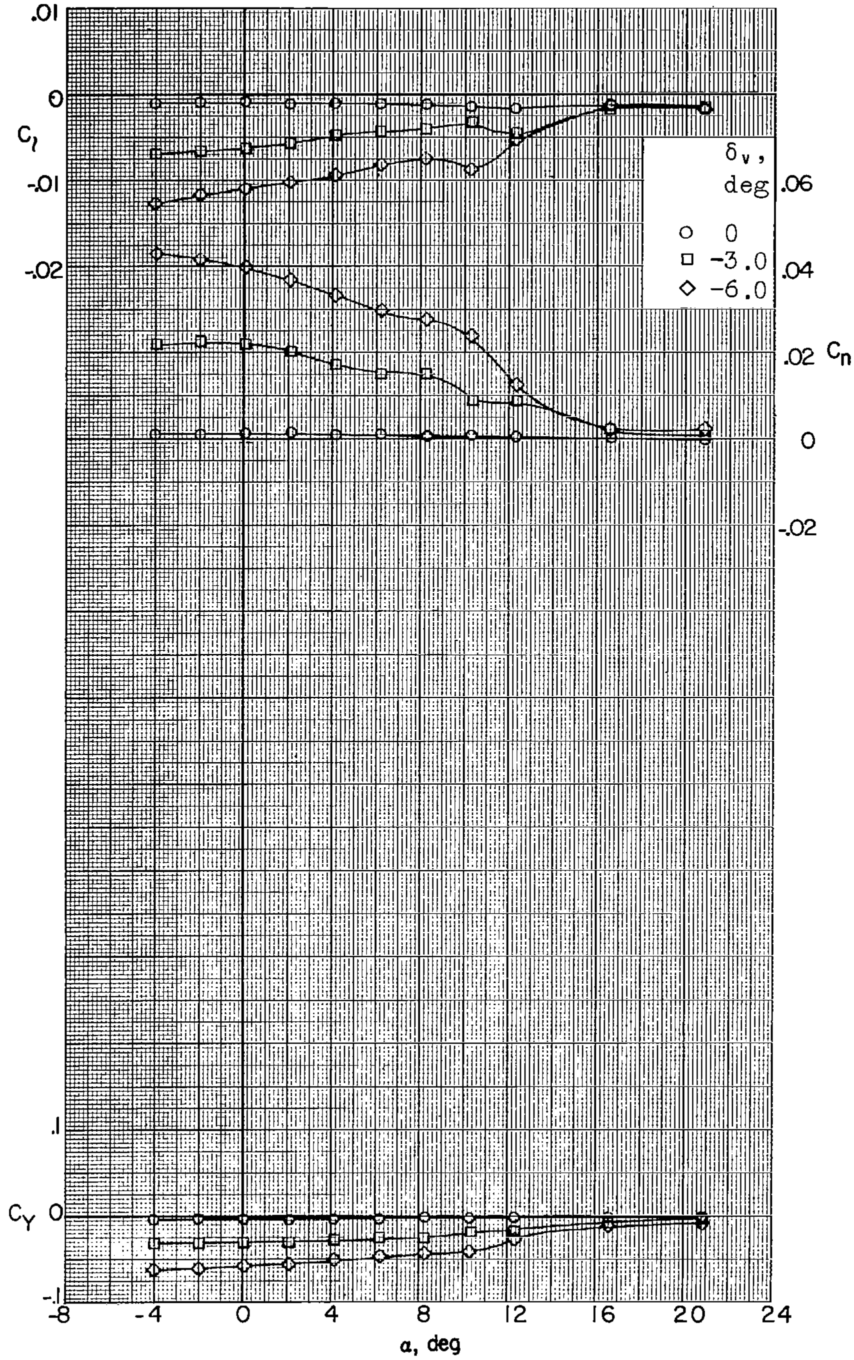

(h) M = 4.65; β = 0°.

Figure 29.- Continued.

L-229

[redacted]

[redacted]

L-229

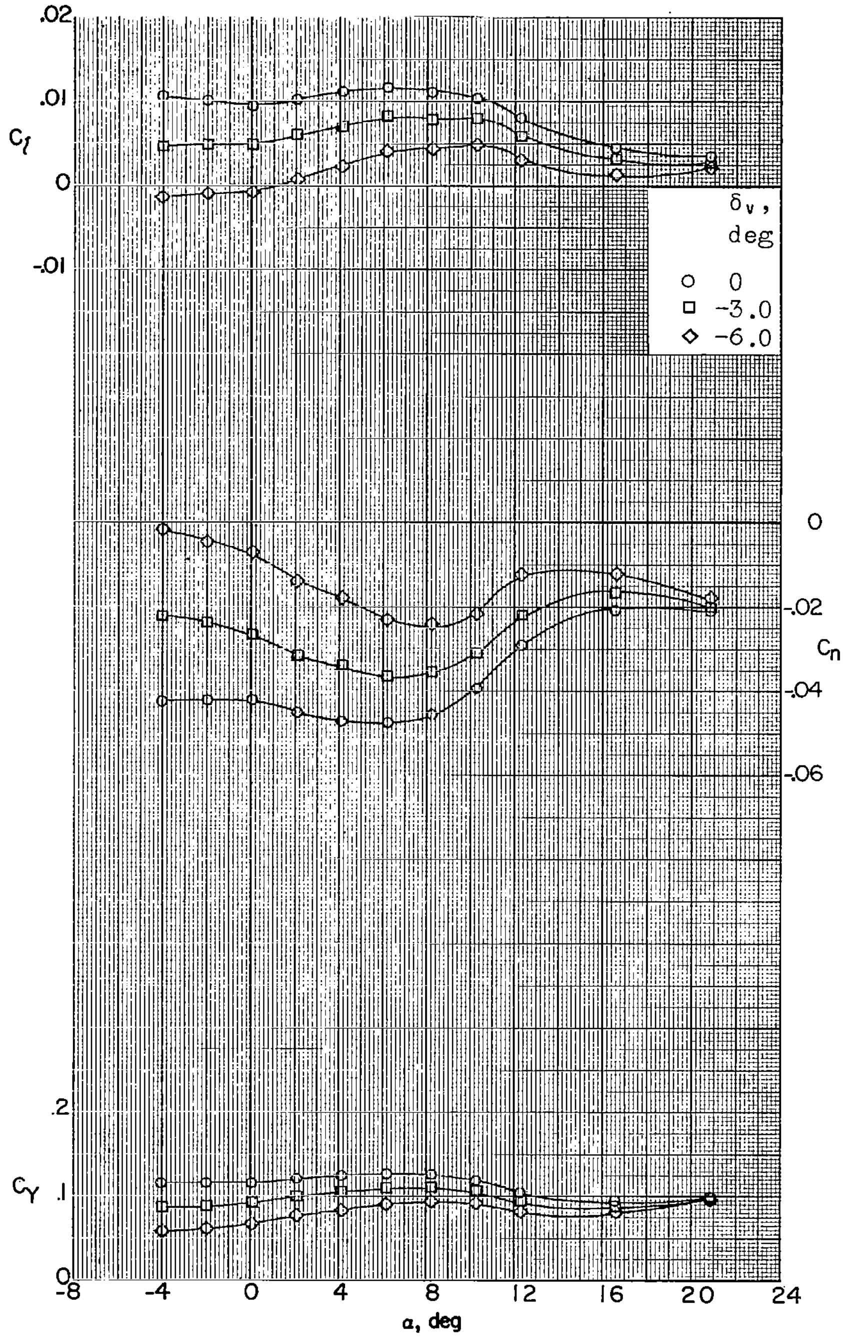

(i) M = 4.65; β = -5.1°.

Figure 29.- Continued.

[redacted]

[redacted]

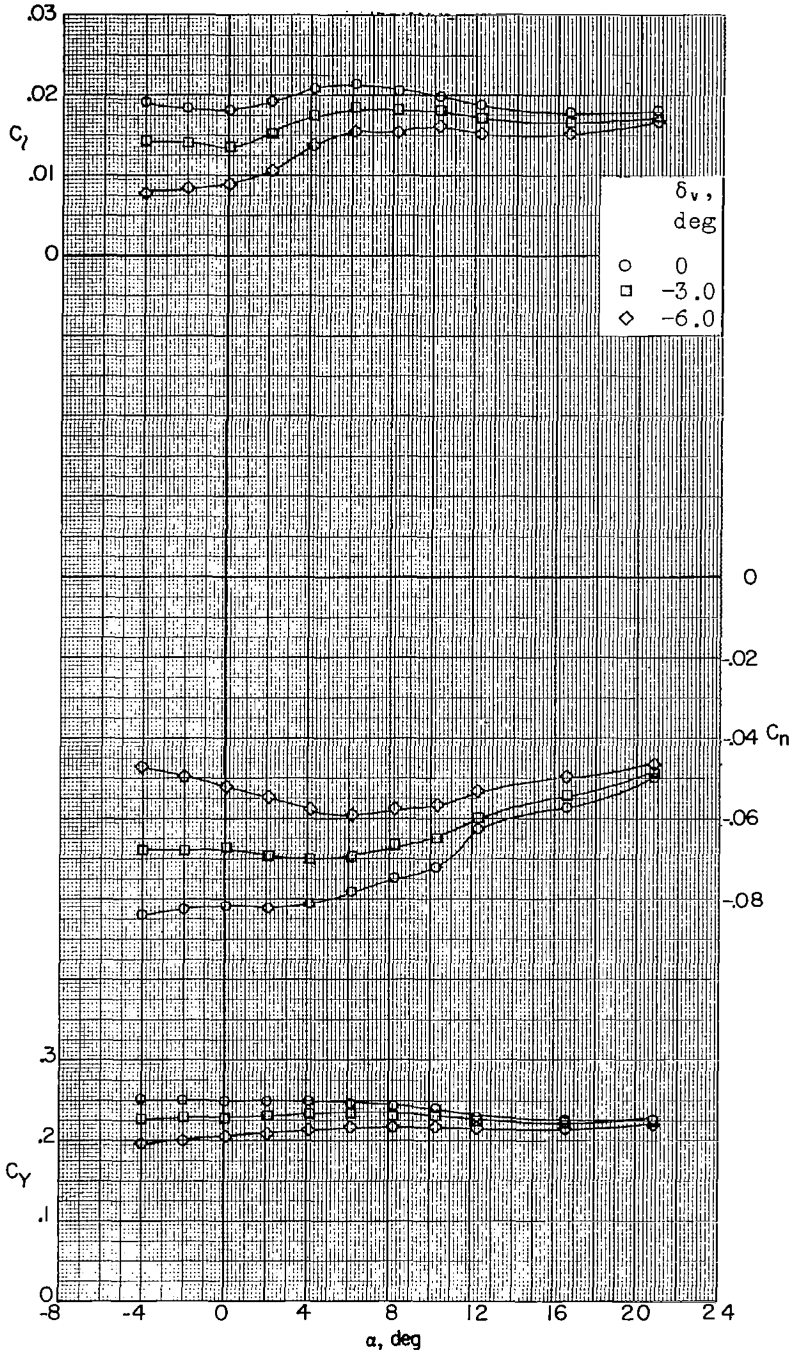

(j) M = 4.65; β = -10.5°.

Figure 29.- Concluded.

[redacted]

[redacted]

L-229

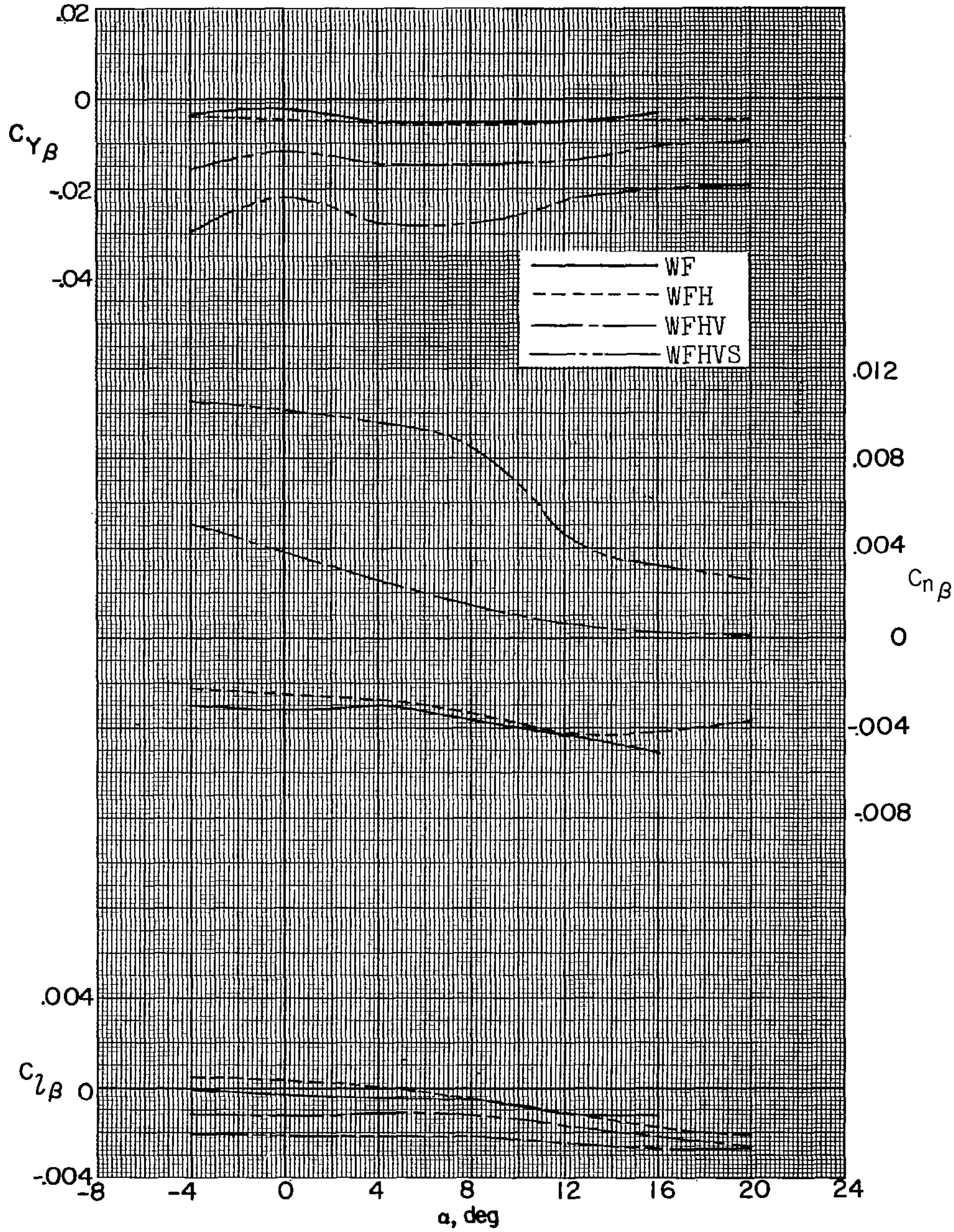

(a) M = 2.29.

Figure 30.- Summary of lateral stability characteristics of a 0.067-scale model of the X-15 airplane as affected by various model components.

[redacted]

[redacted]

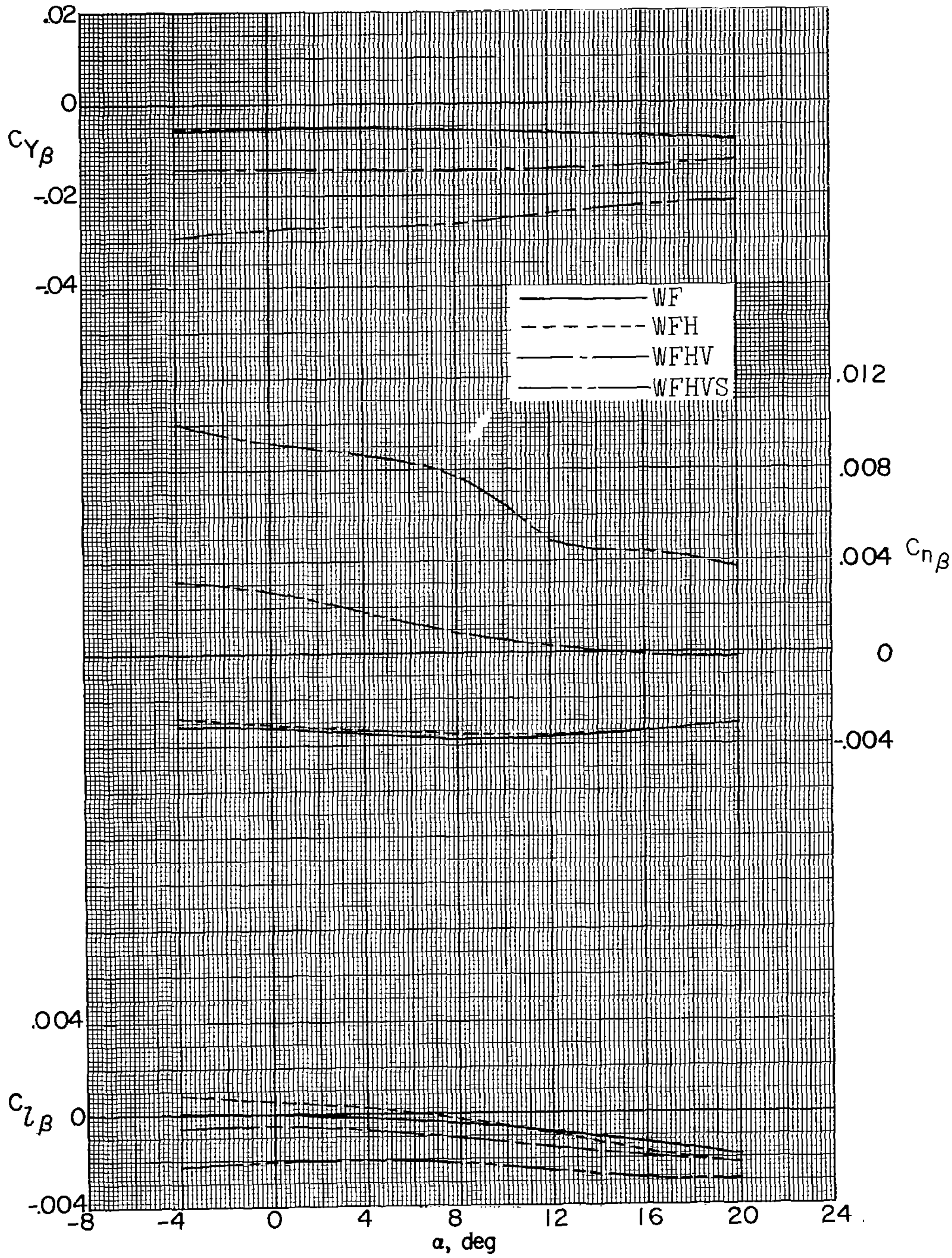

(b) M = 2.98.

Figure 30.- Continued.

L-229

[redacted]

[redacted]

L-229

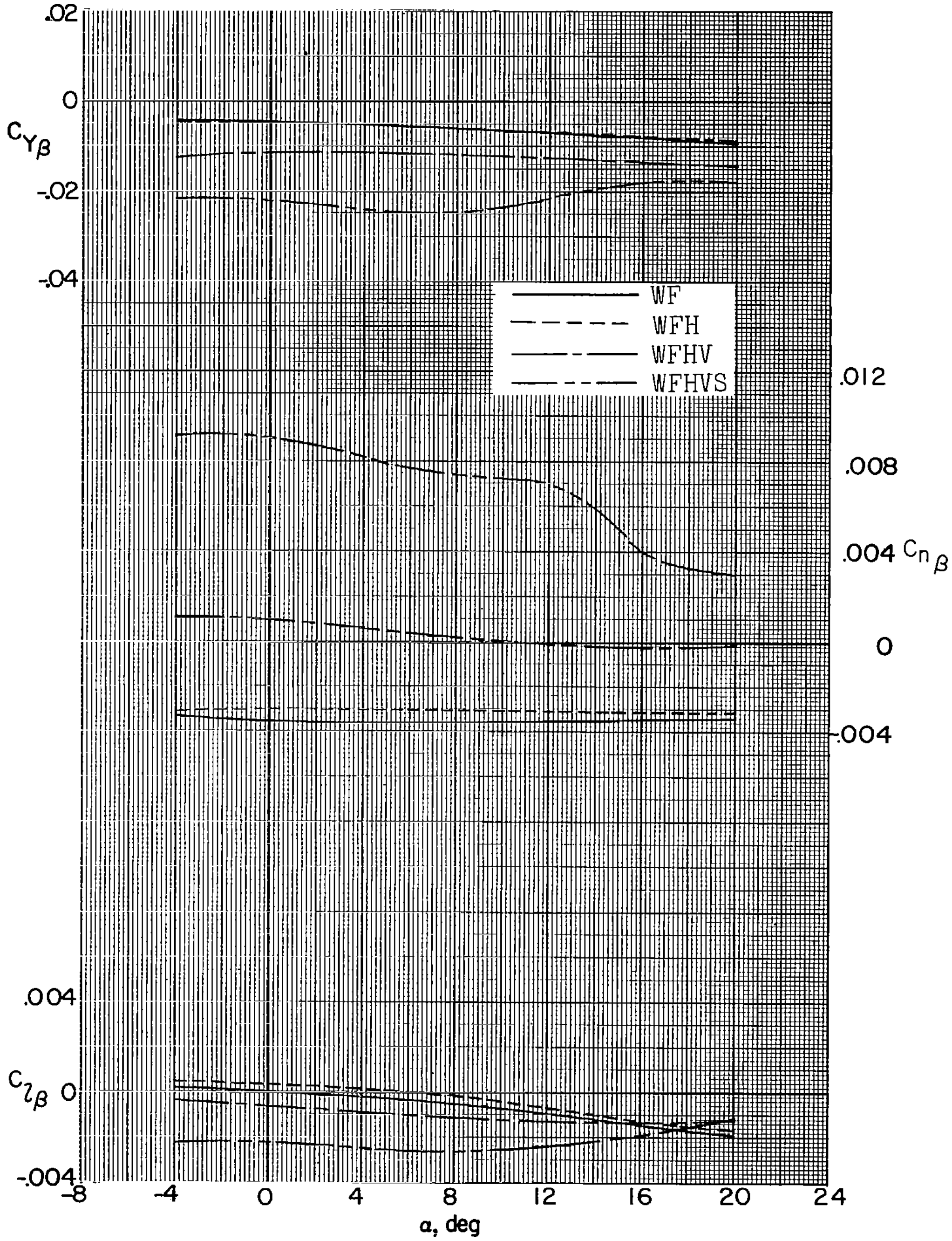

(c) M = 3.96.

Figure 30.- Continued.

[redacted]

[redacted]

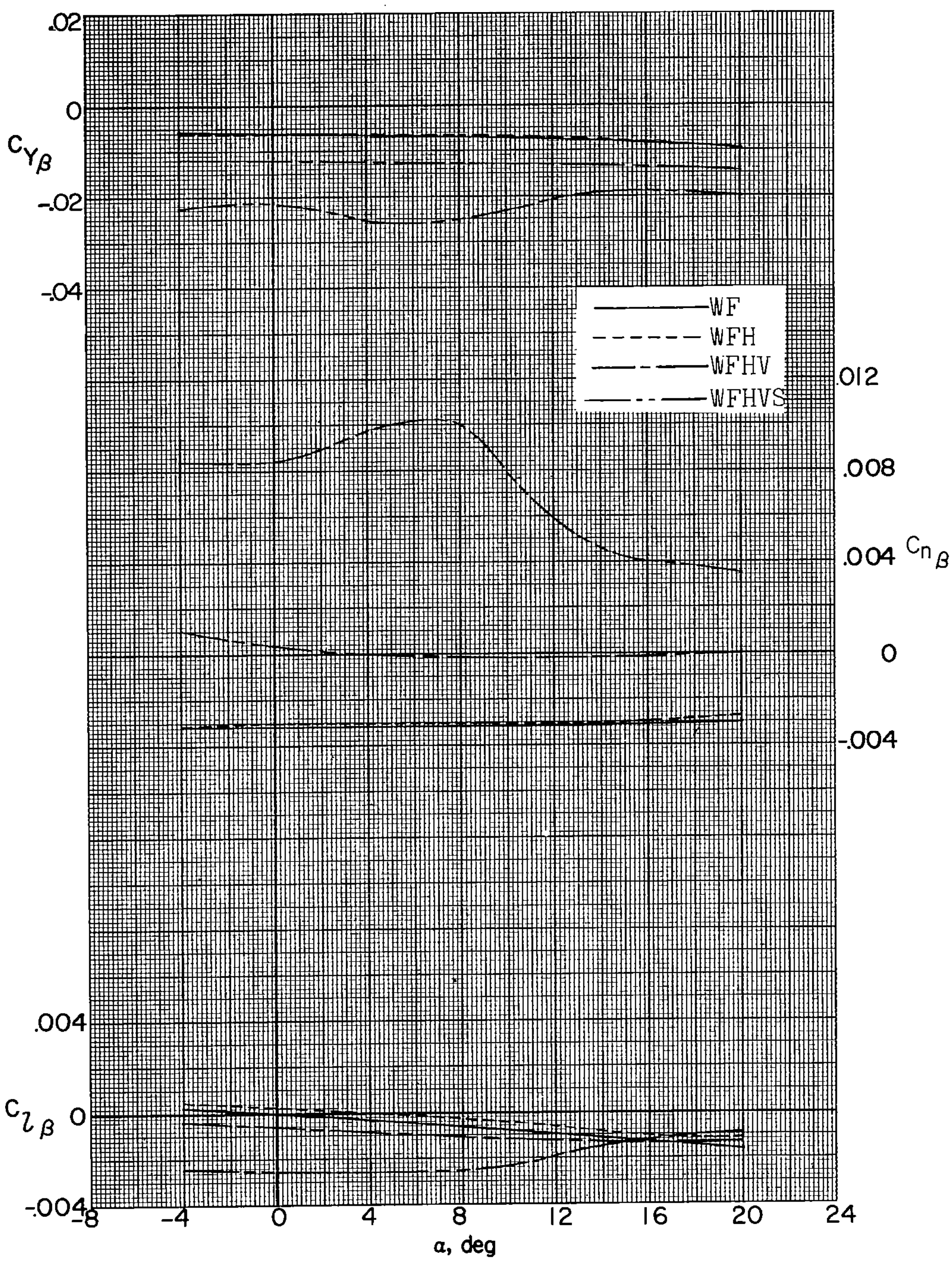

(d) M = 4.65.

Figure 30.- Concluded.

L-229

[redacted]

L-229

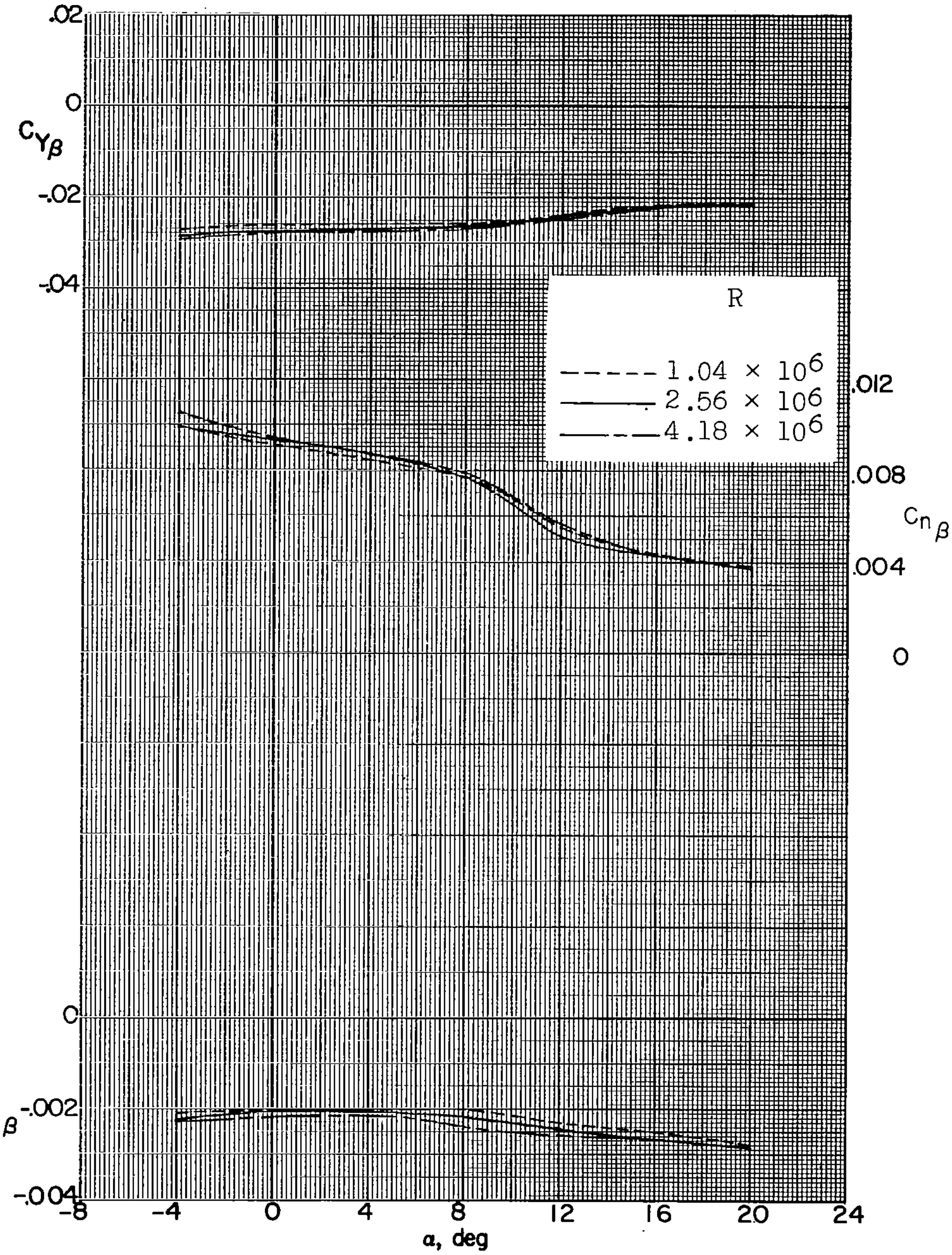

(a) M = 2.98.

Figure 31.- Summary of lateral stability characteristics of a 0.067-scale model of the X-15 airplane as affected by Reynolds numbers. Speed brakes open 45°.

[redacted]

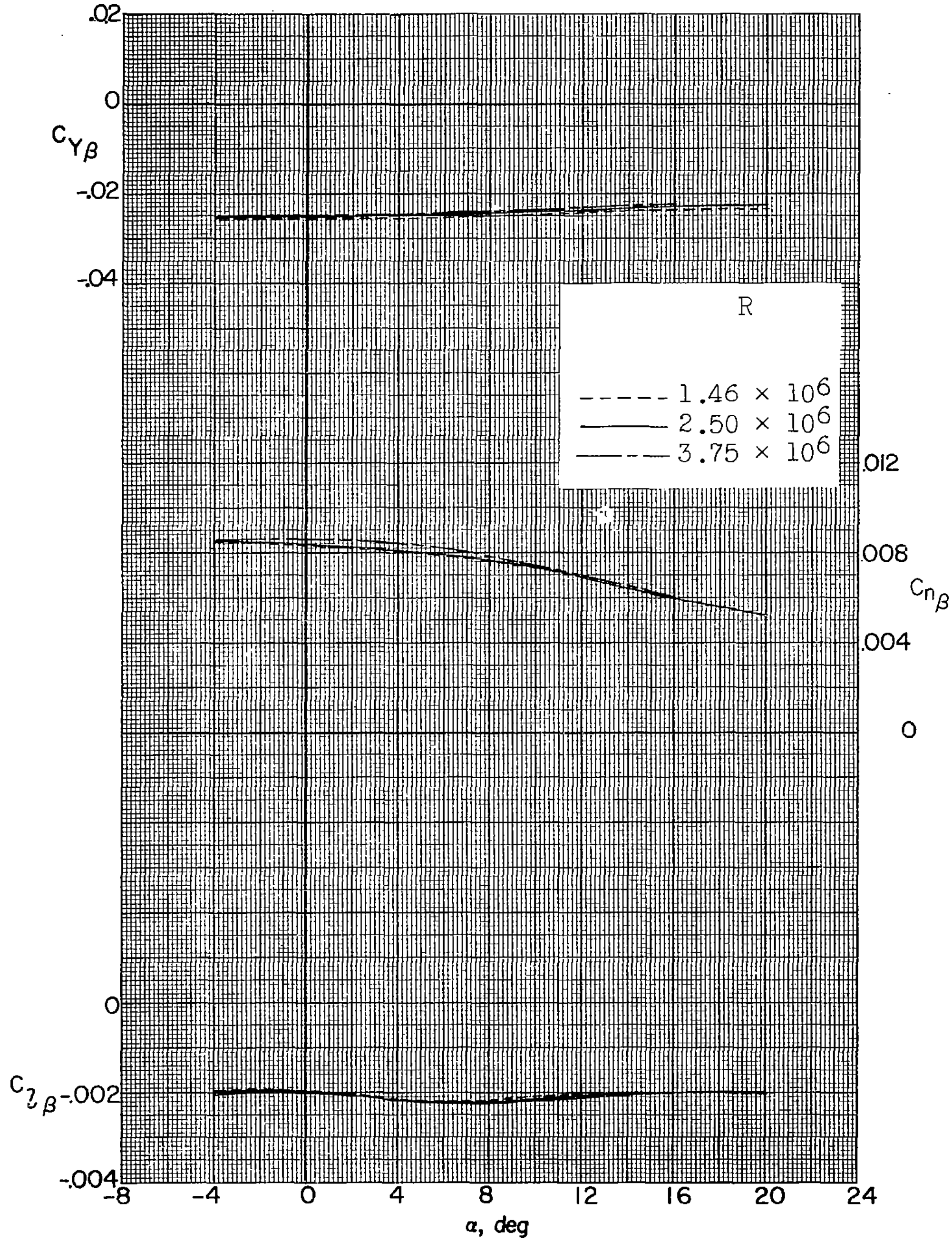

(b) M = 4.65.

Figure 31.- Concluded.

L-229

[redacted]

[redacted]

L-229

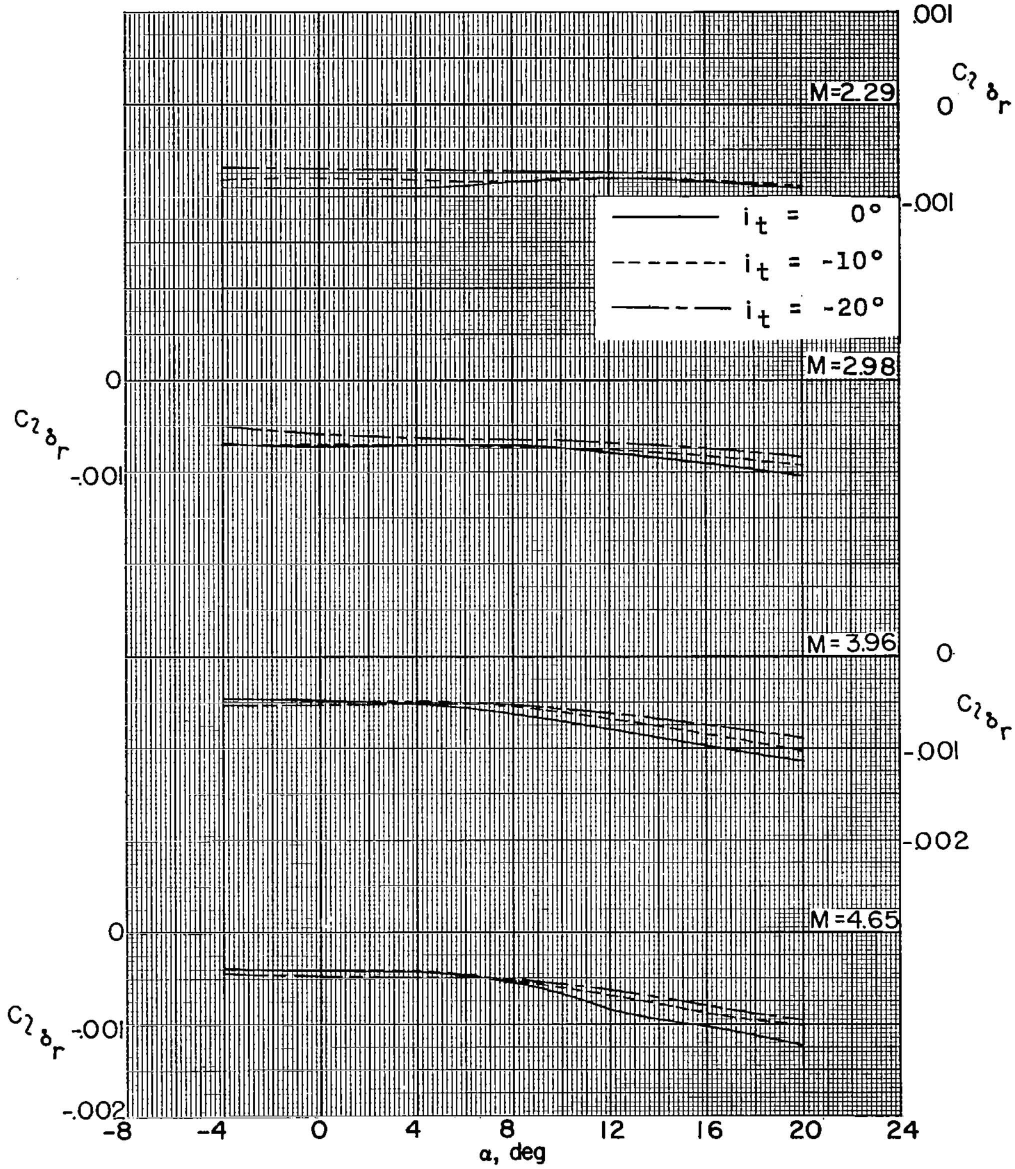

(a) Variation of $C_{l_{\delta_r}}$ with α.

Figure 32.- Summary of roll-control characteristics of a 0.067-scale model of the X-15 airplane as affected by various stabilizer deflections. $\beta = 0^{\circ}$; speed brakes closed.

[redacted]

[redacted]

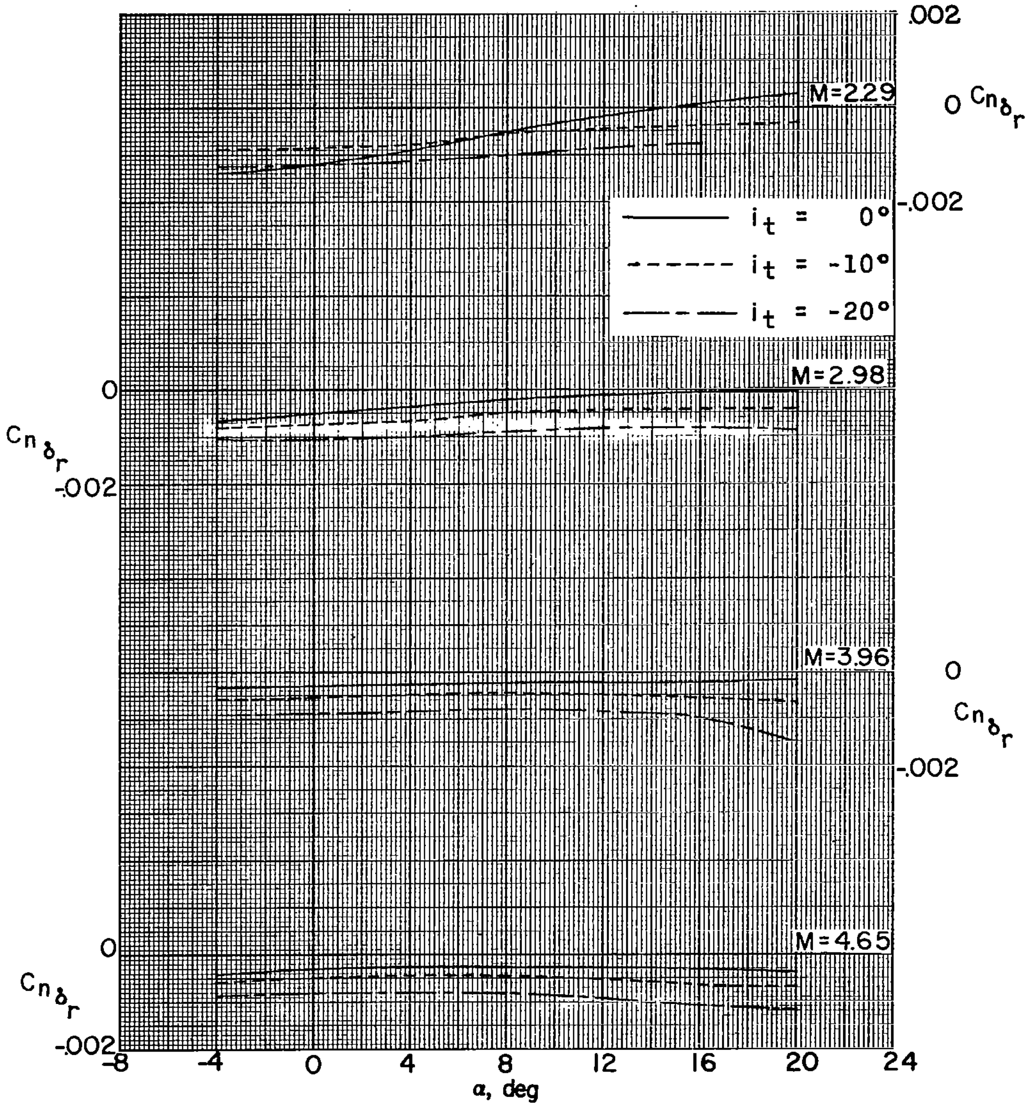

(b) Variation of $C_{n_{\delta_r}}$ with α.

Figure 32.- Concluded.

L-229

[redacted]

[redacted]

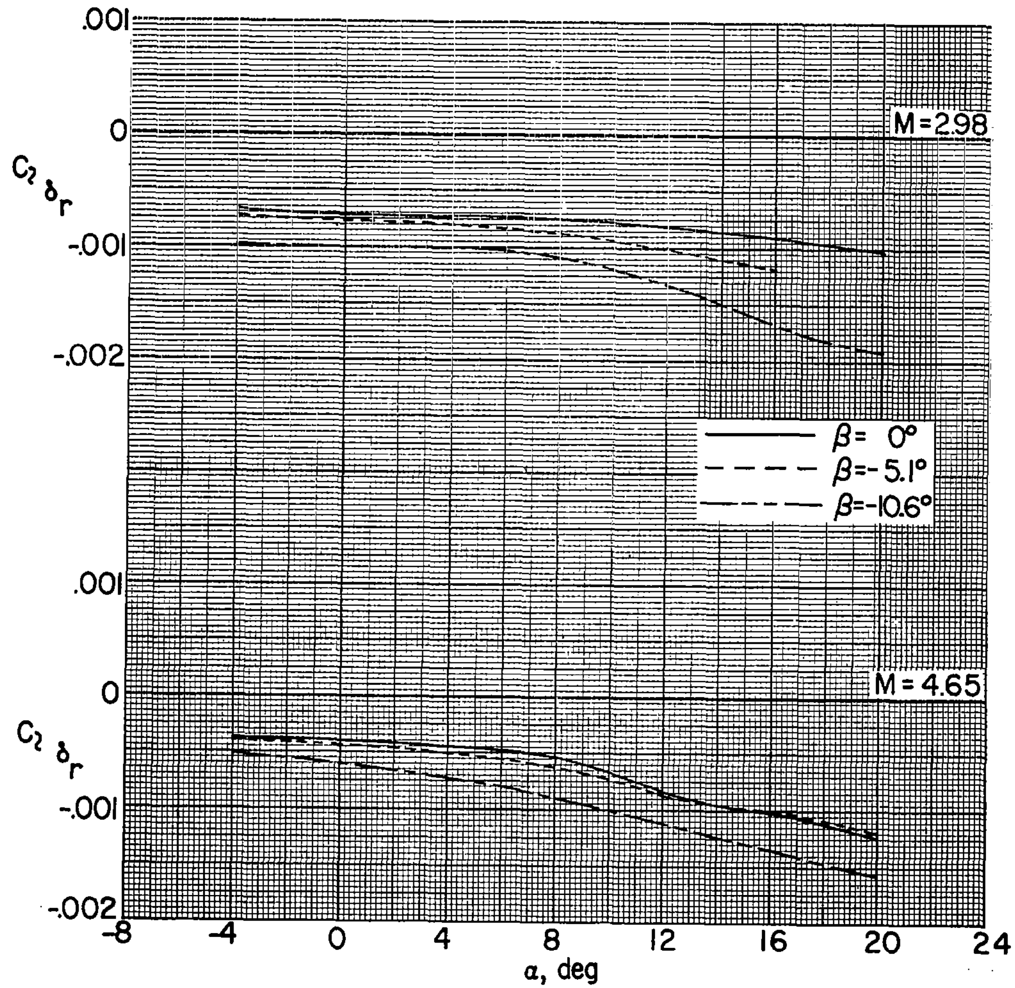

(a) Variation of $C_{l_{\delta_r}}$ with α.

Figure 33.- Summary of roll-control characteristics of a 0.067-scale model of the X-15 airplane as affected by various angles of sideslip.

[redacted]

[redacted]

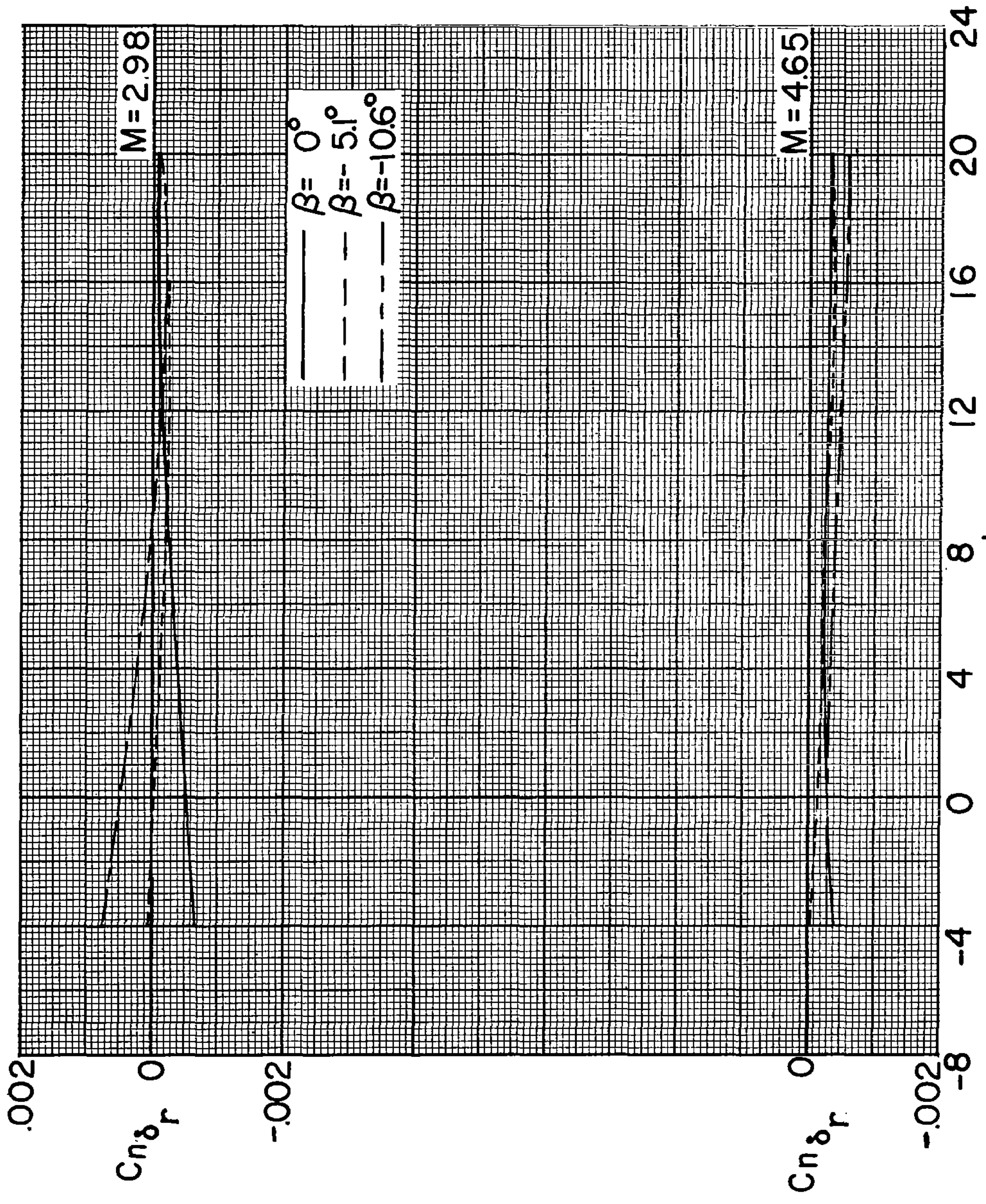

(b) Variation of $C_{n_{\delta_r}}$ with α.

Figure 33.- Concluded.

[redacted]

[redacted]

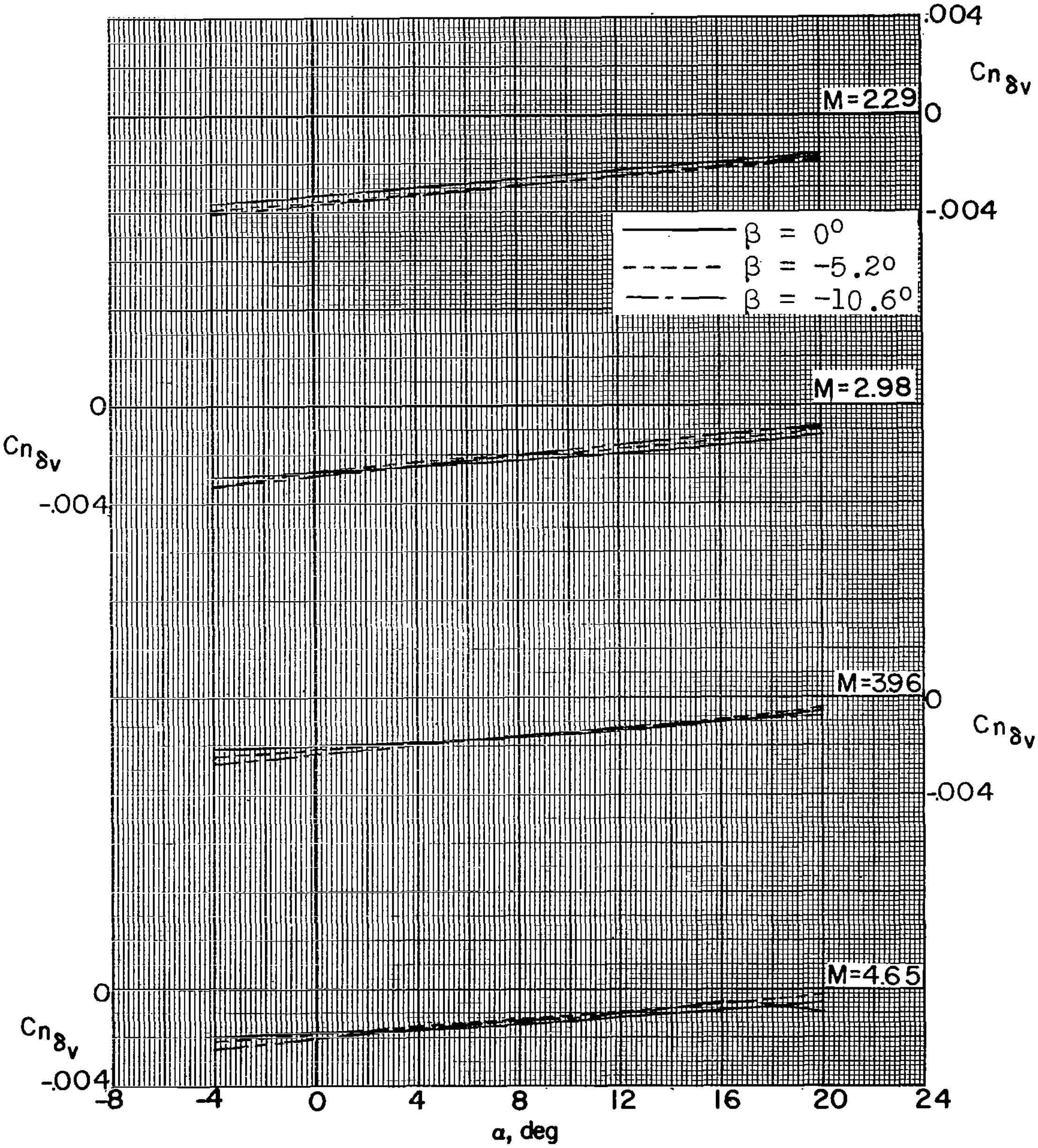

(a) Variation of $C_{n_{\delta_v}}$ with α.

Figure 34.- Summary of vertical-tail control characteristics of a 0.067-scale model of the X-15 airplane as affected by various angles of sideslip. Speed brakes closed.

[redacted]

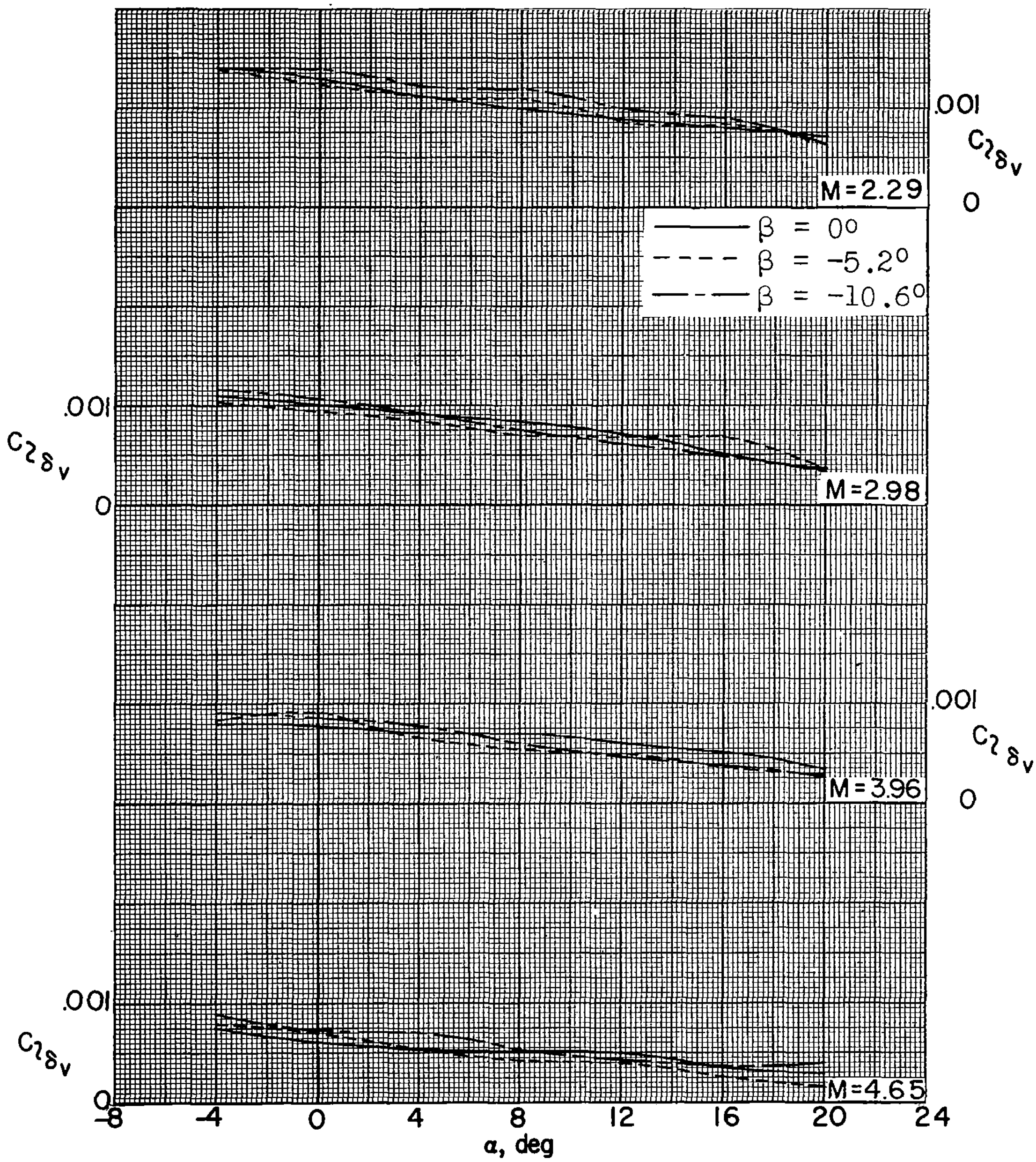

(b) Variation of $C_{l_{\delta_v}}$ with α.

Figure 34.- Concluded.

L-229

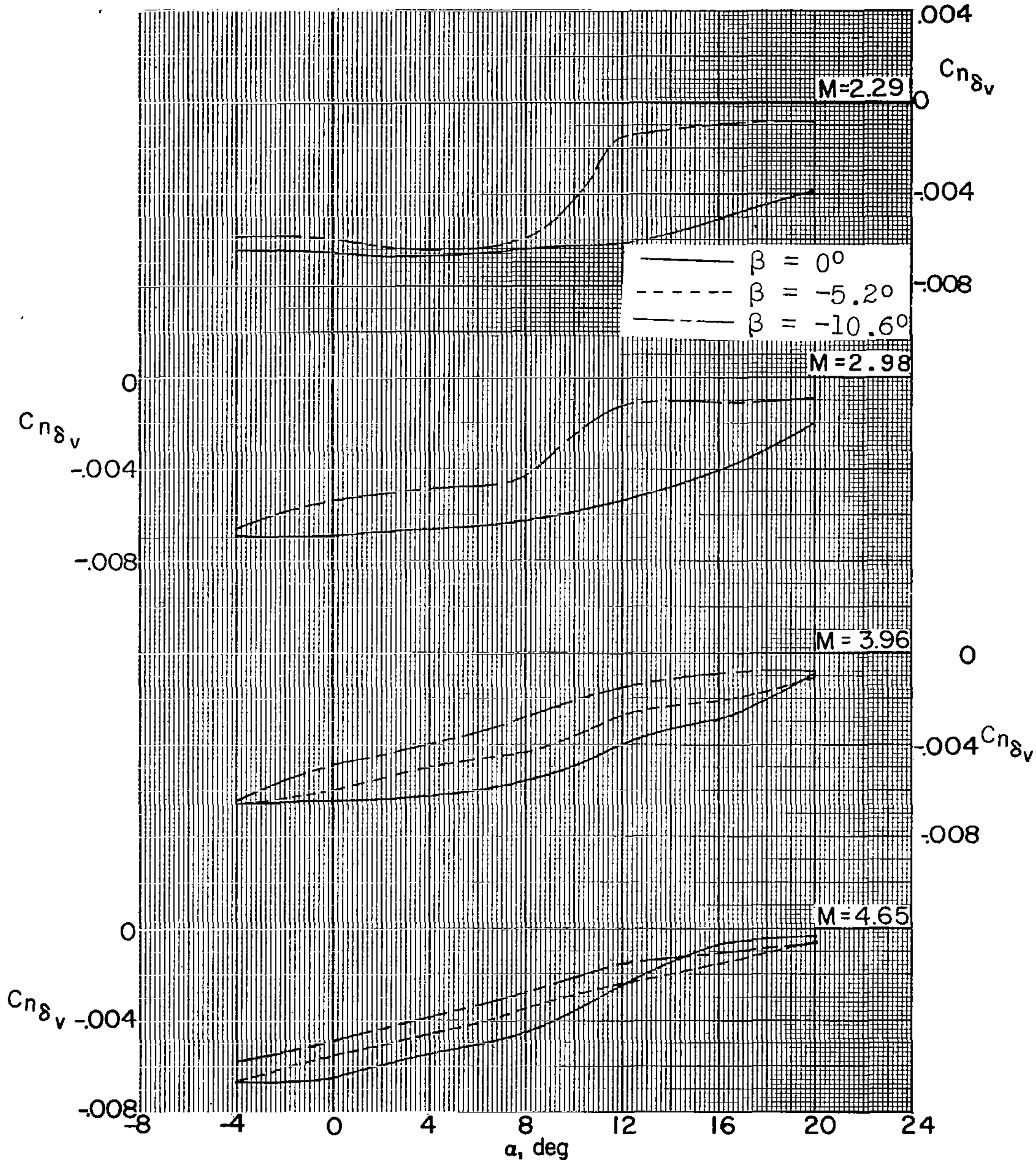

(a) Variation of $C_{n_{\delta_v}}$ with α.

Figure 35.- Summary of vertical-tail control characteristics of a 0.067-scale model of the X-15 airplane as affected by various angles of sideslip. Speed brakes open 45°.

[redacted]

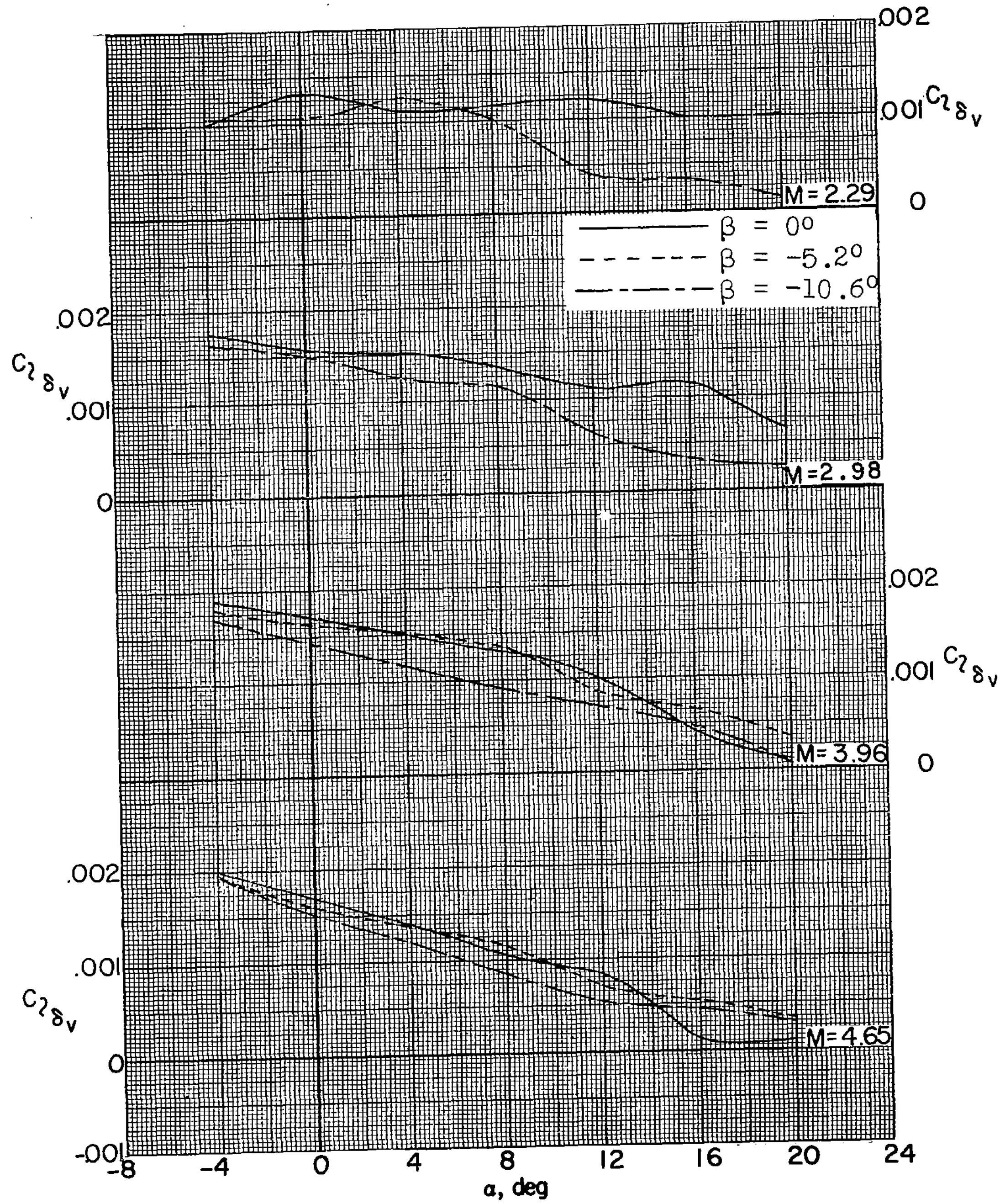

(b) Variation of $C_{l_{\delta_v}}$ with α.

Figure 35.- Concluded.

L-229

[redacted]

L-229

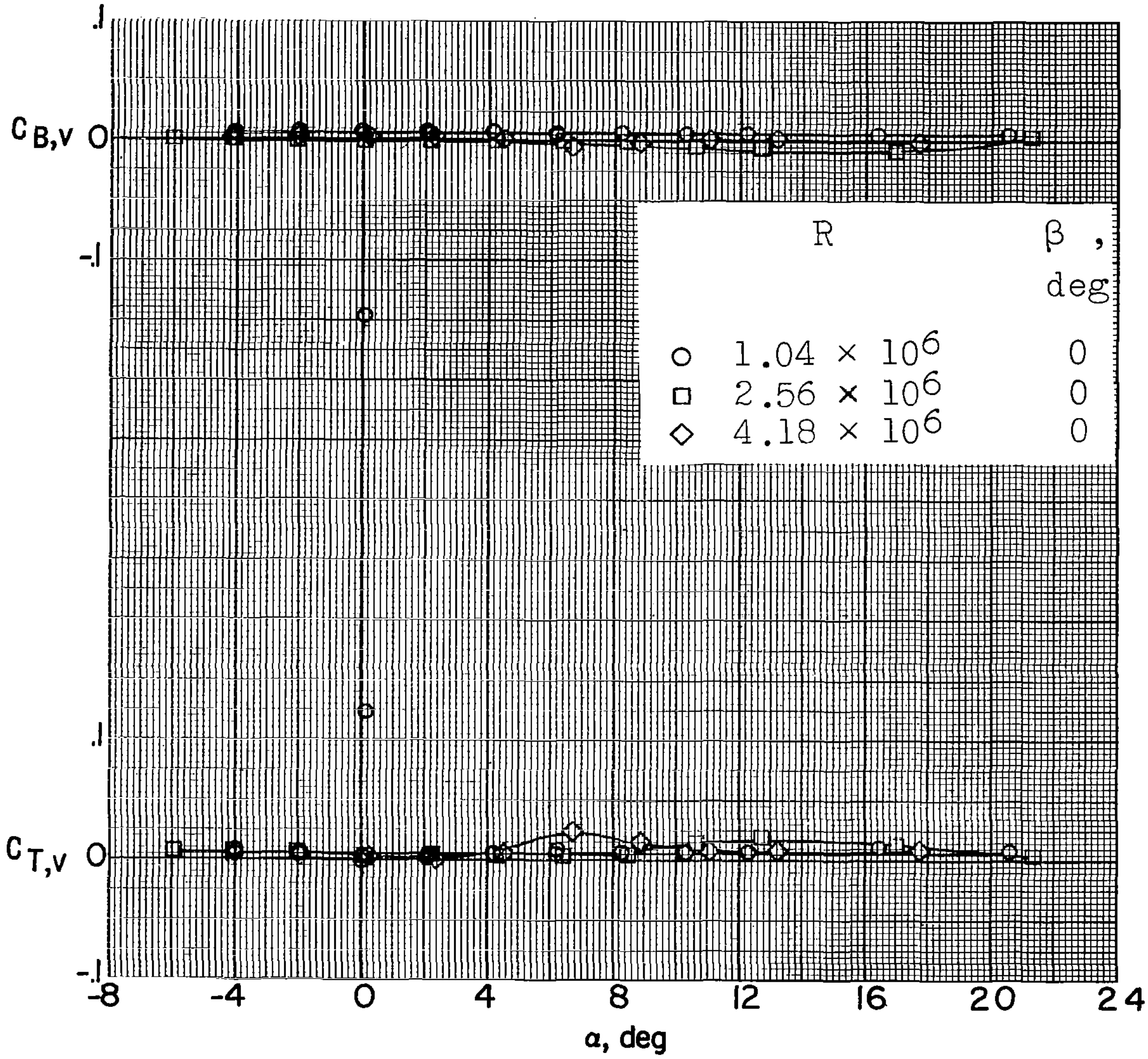

(a) M = 2.98.

Figure 36.- Bending- and torsion-moment characteristics of the vertical tail of a 0.067-scale model of the X-15 airplane at various Reynolds numbers. Speed brakes open 45°; $\delta_v = 0^\circ$.

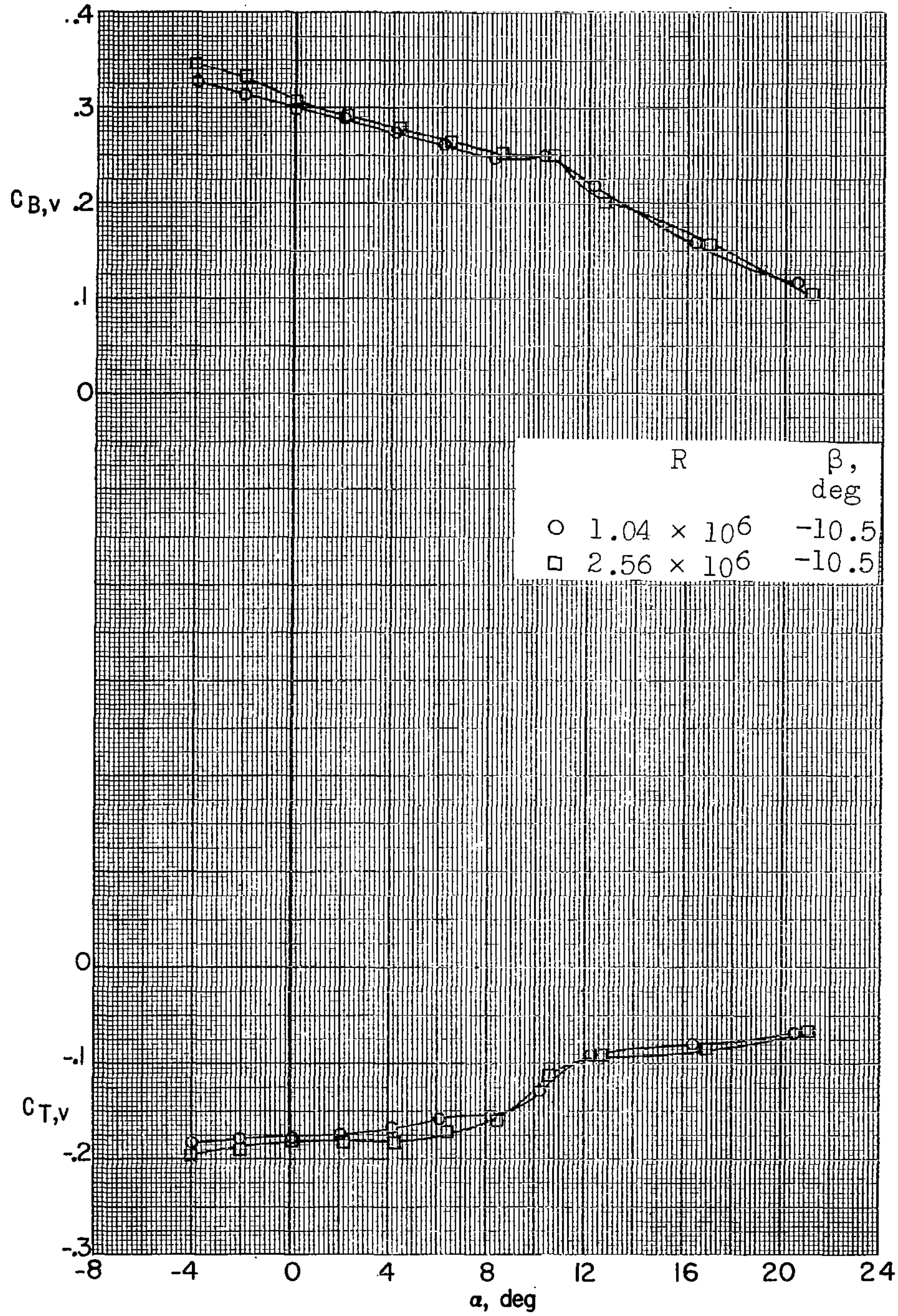

(a) Concluded.

Figure 36.- Continued.

L-229

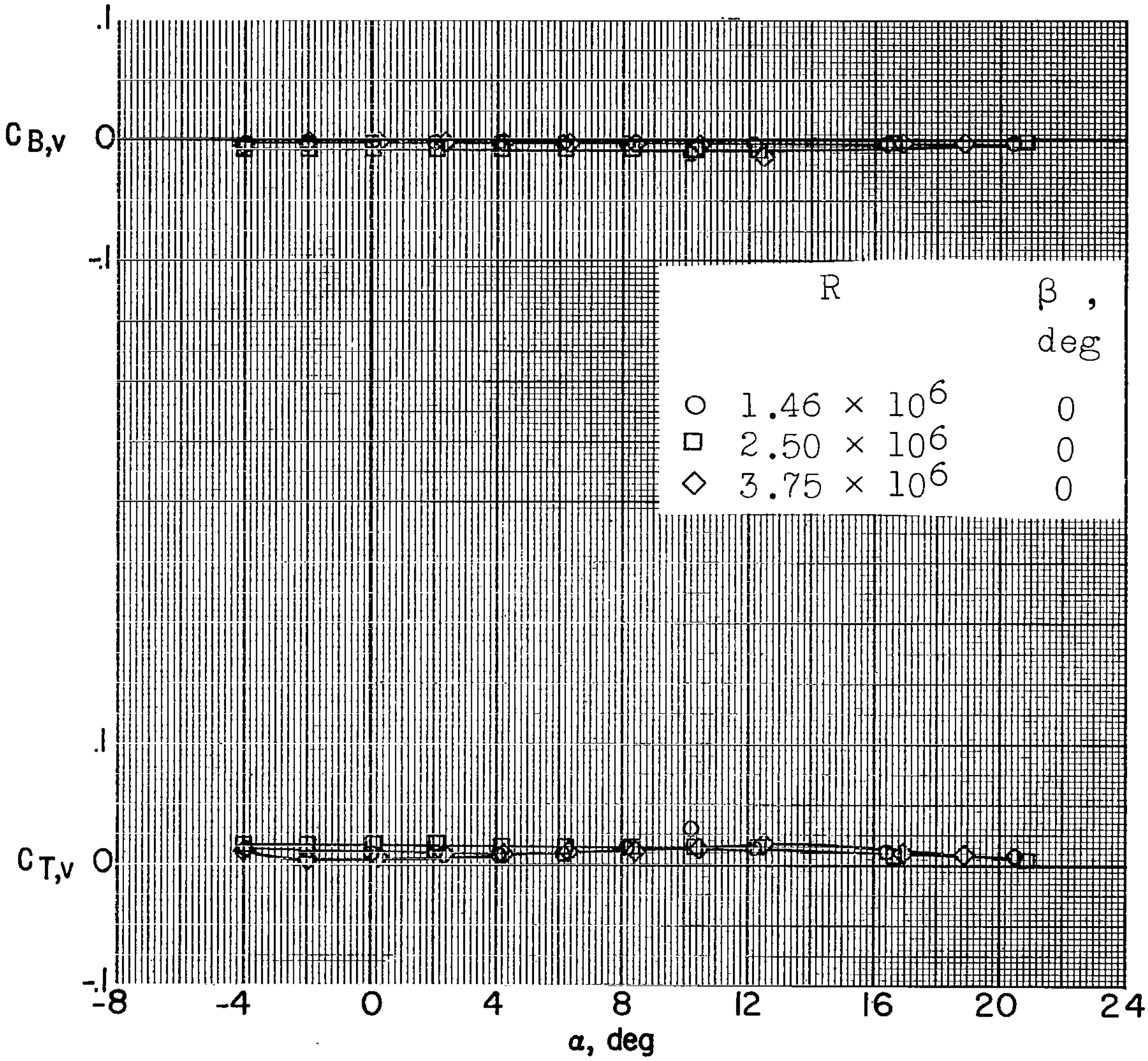

(b) M = 4.65.

Figure 36.- Continued.

[redacted]

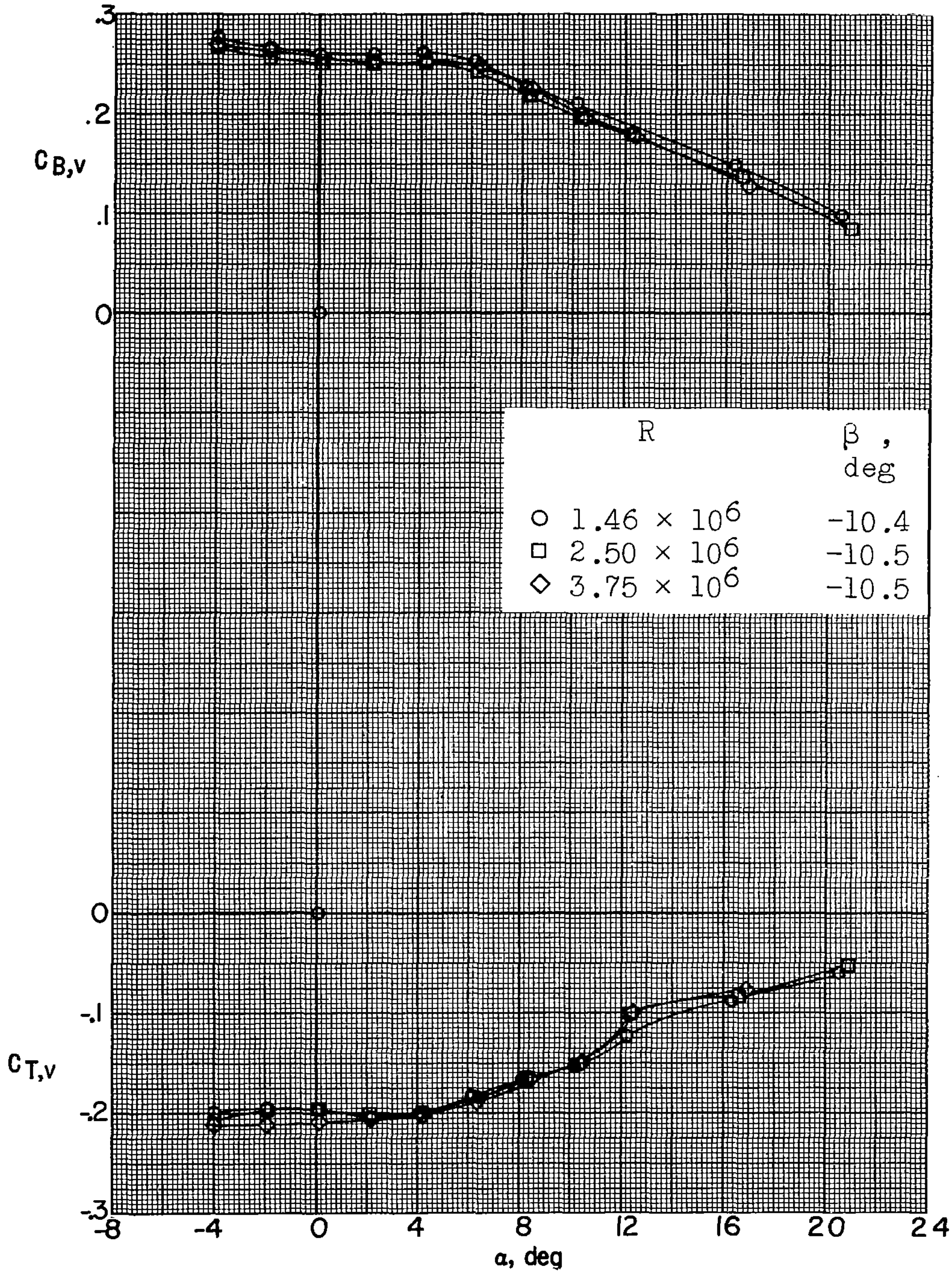

(b) Concluded.

Figure 36.- Concluded.

[redacted]

[redacted]

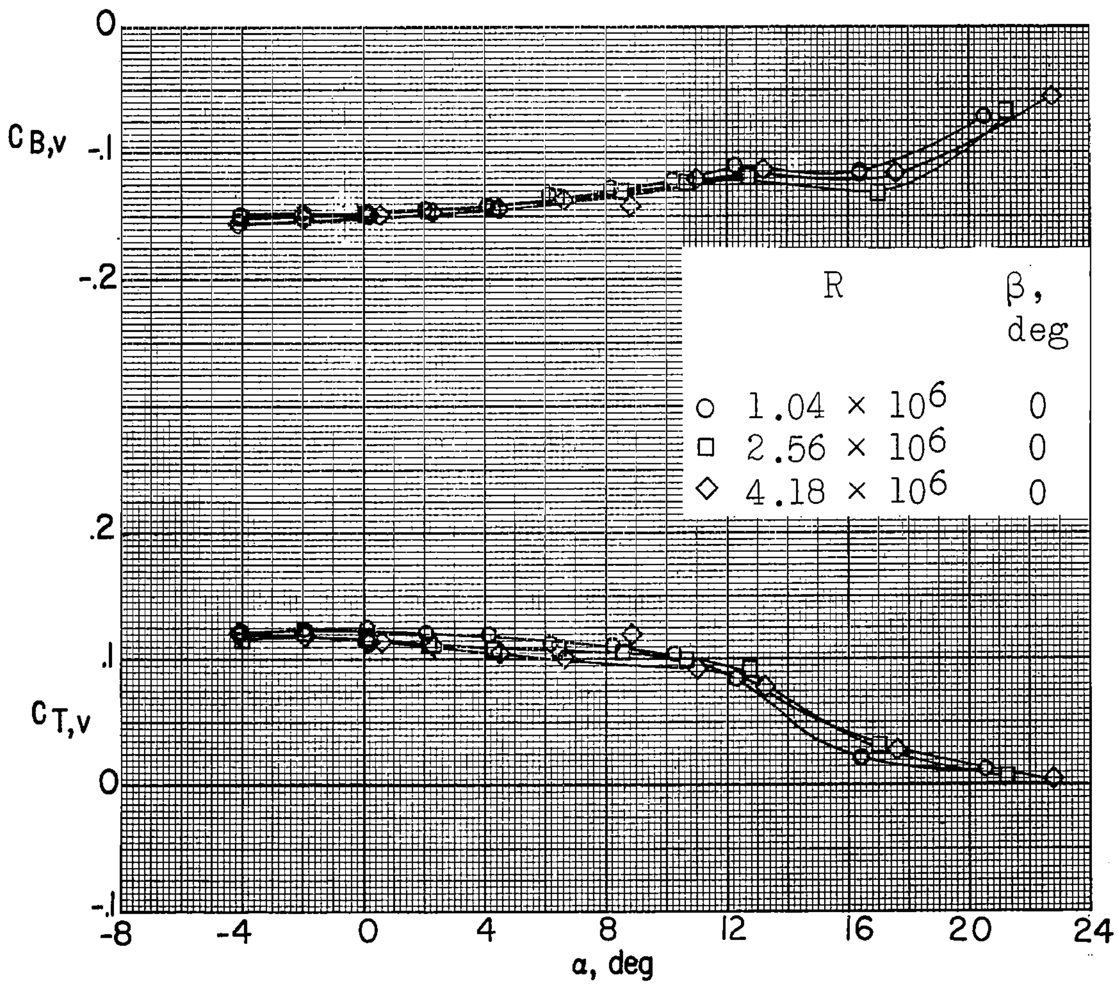

(a) M = 2.98.

Figure 37.- Bending- and torsion-moment characteristics of the vertical tail of a 0.067-scale model of the X-15 airplane at various Reynolds numbers. Speed brakes open 45°; $\delta_v = -6°$.

[redacted]

[redacted]

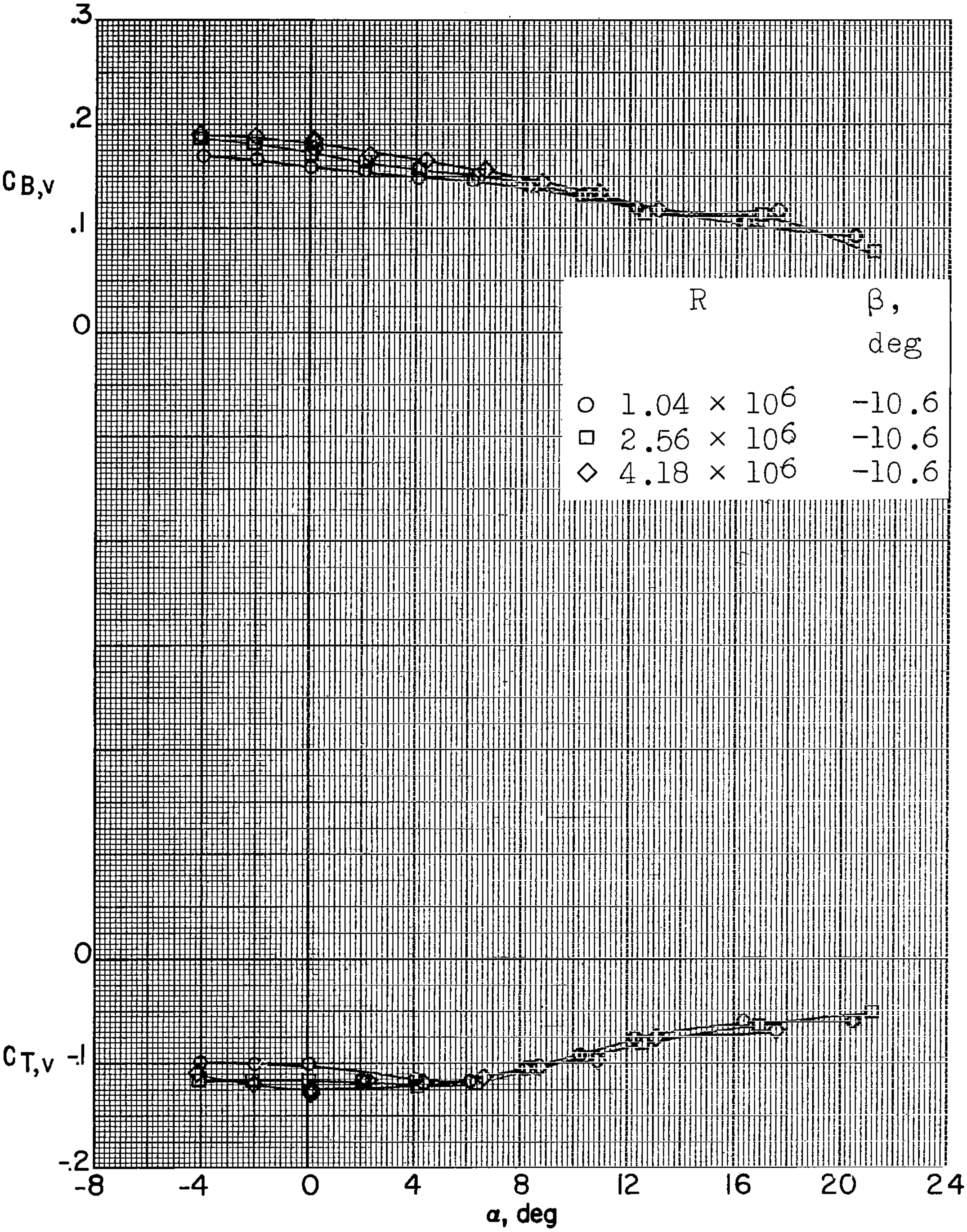

(a) Concluded.

Figure 37.- Continued.

[redacted]

L-229

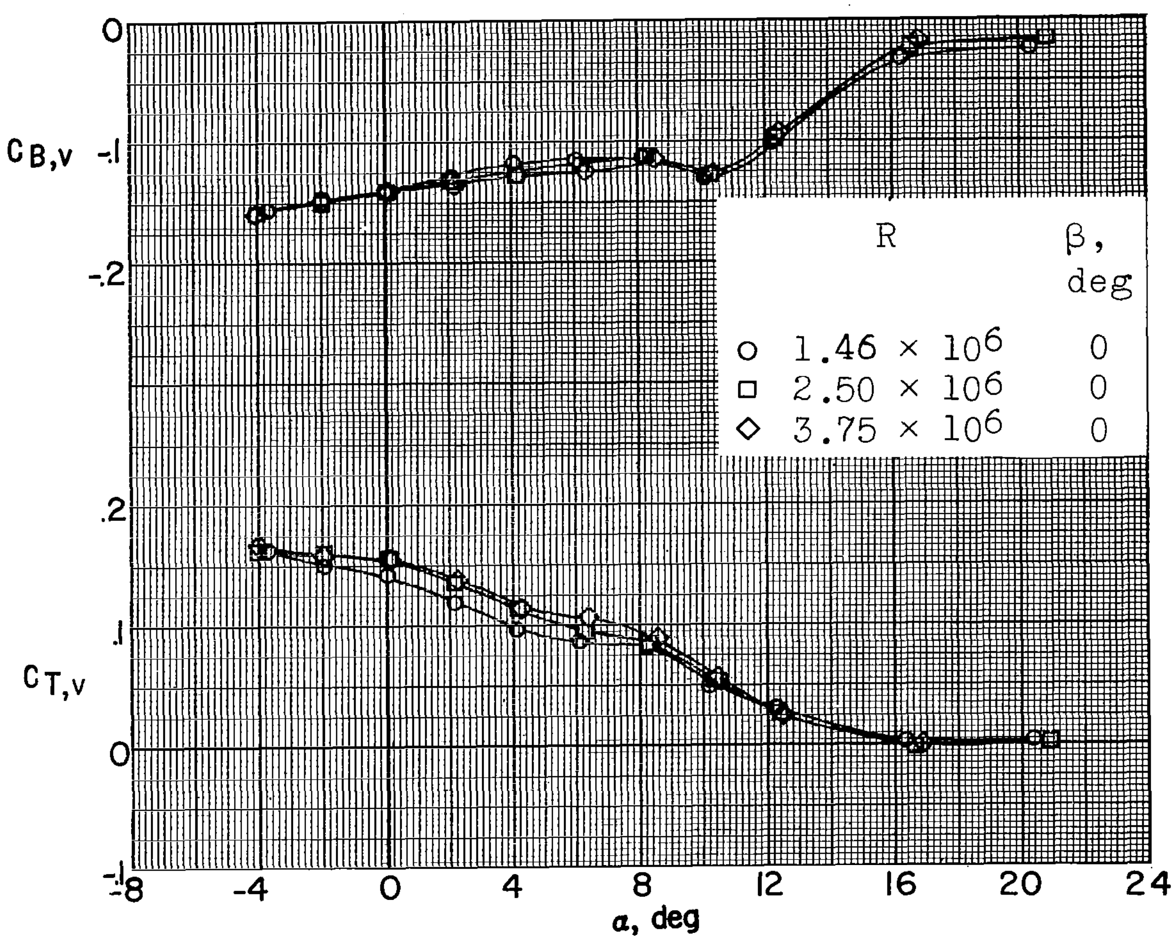

(b) M = 4.65.

Figure 37.- Continued.

[redacted]

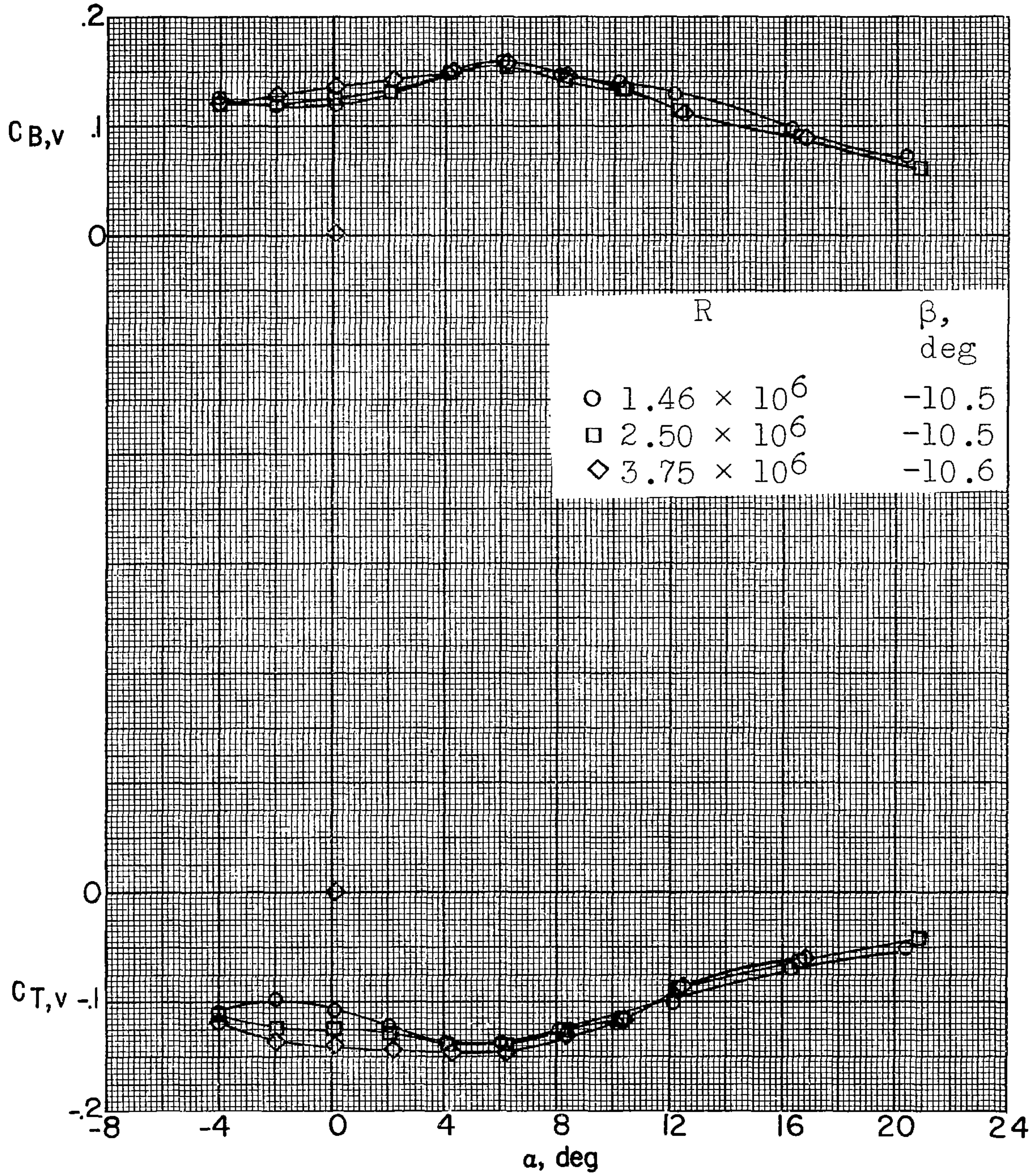

(b) Concluded.

Figure 37.- Concluded.

L-229

[redacted]

L-229

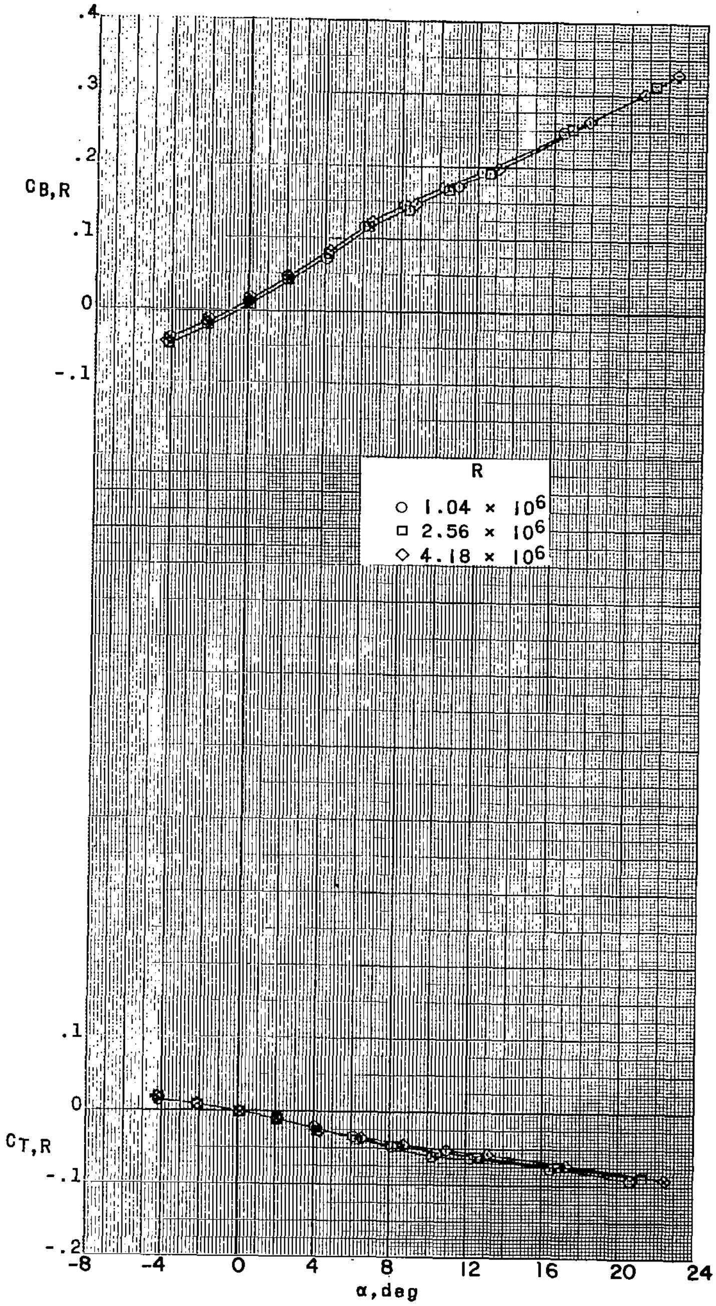

(a) M = 2.98.

Figure 38.- Bending- and torsion-moment characteristics of the right horizontal-tail panel of a 0.067-scale model of the X-15 airplane at various Reynolds numbers. Speed brakes closed.

[redacted]

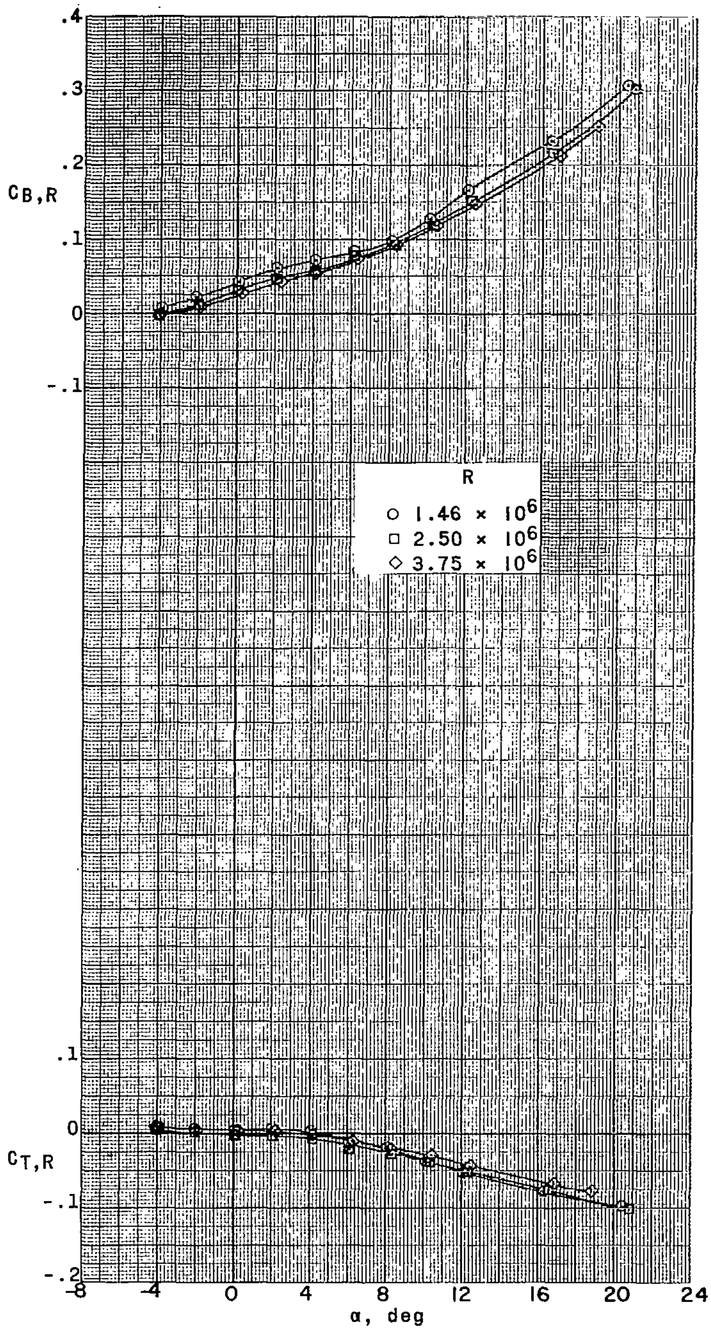

(b) M = 4.65.

Figure 38.- Concluded.

L-229

[redacted]

[redacted]

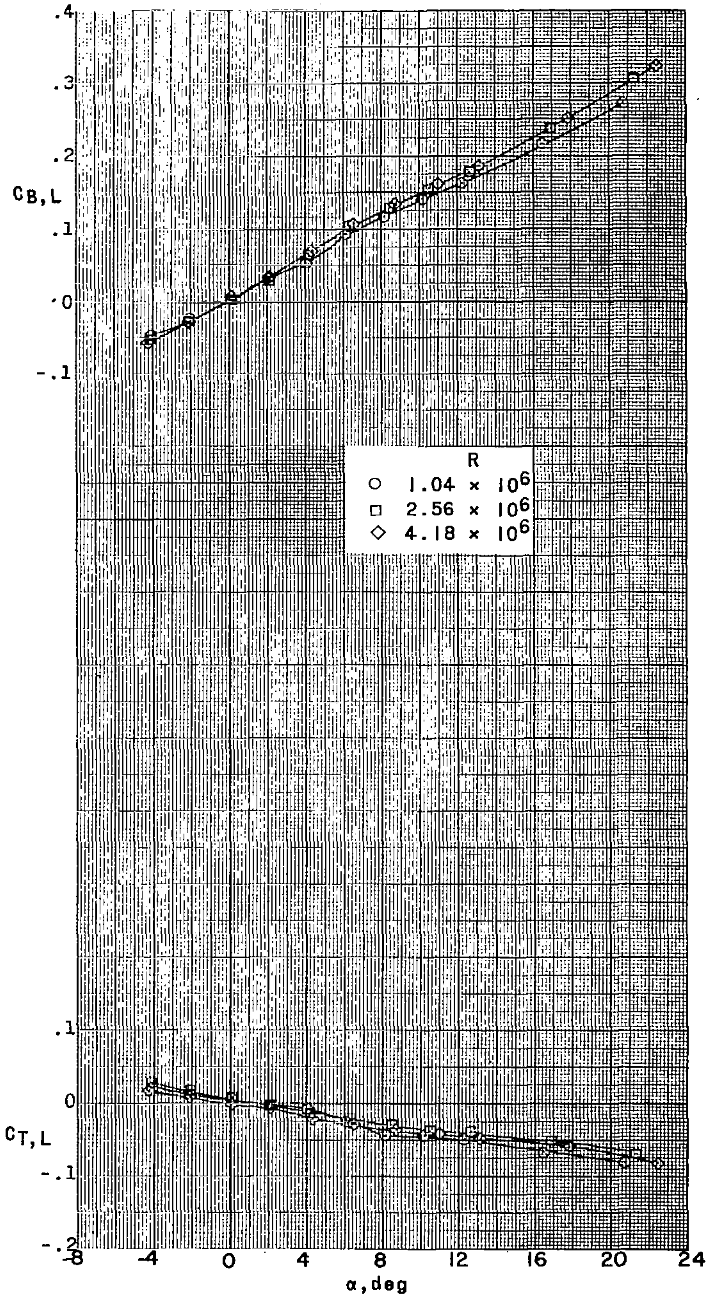

(a) M = 2.98.

Figure 39.- Bending- and torsion-moment characteristics of the left horizontal-tail panel of a 0.067-scale model of the X-15 airplane at various Reynolds numbers. Speed brakes closed.

L-229

[redacted]

[redacted]

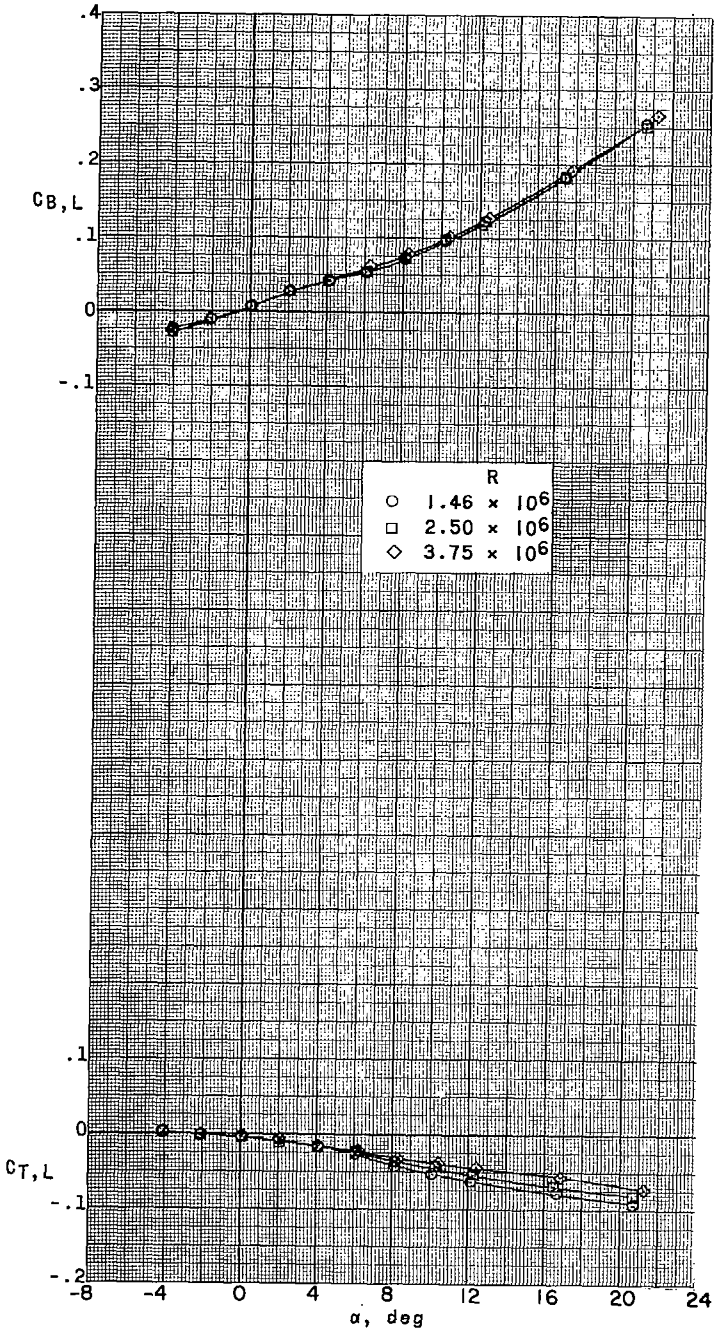

(b) M = 4.65.

Figure 39.- Concluded.

[redacted]

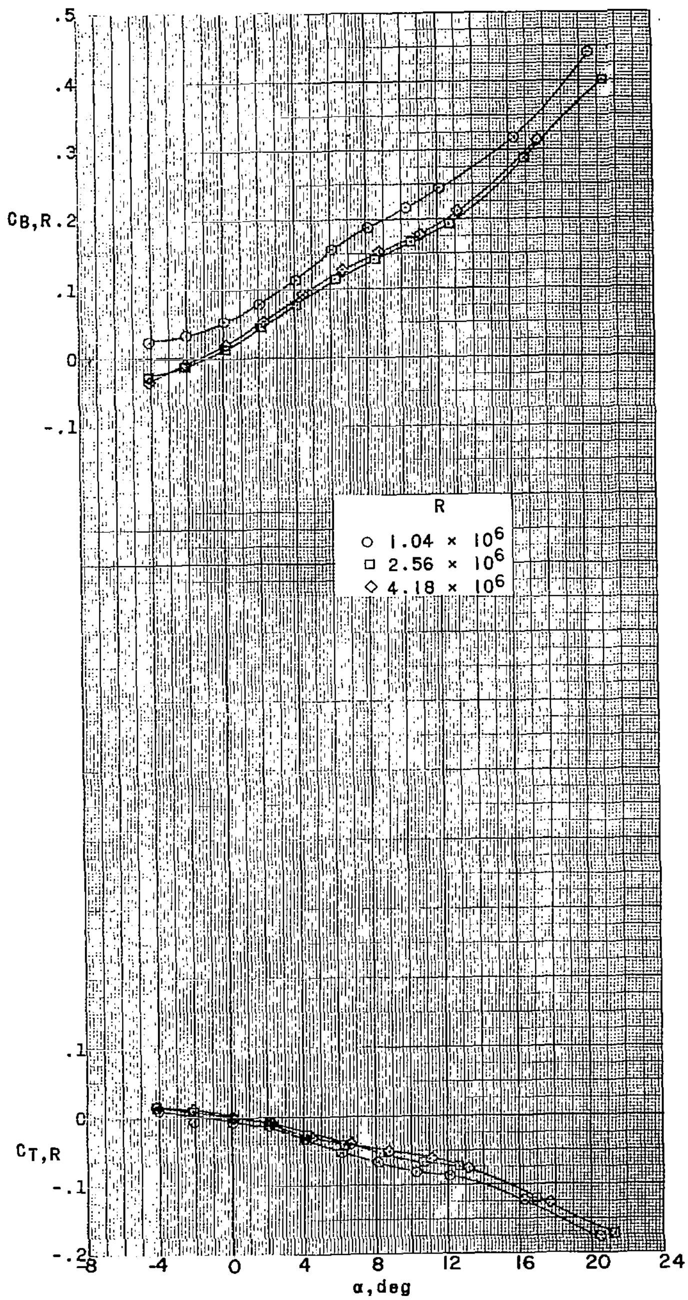

(a) M = 2.98.

Figure 40.- Bending- and torsion-moment characteristics of the right horizontal-tail panel of a 0.067-scale model of the X-15 airplane at various Reynolds numbers. Speed brakes open 45°.

[redacted]

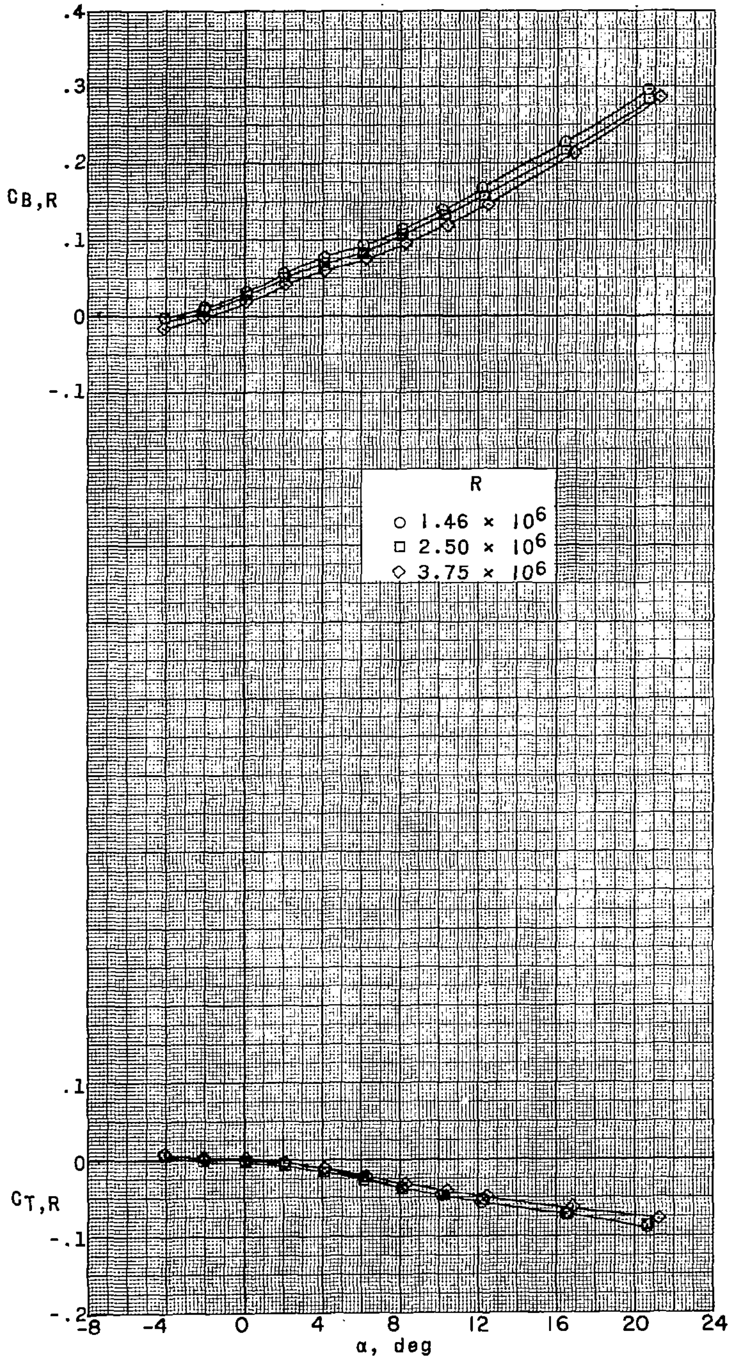

(b) M = 4.65.

Figure 40.- Concluded.

[redacted]

L-229

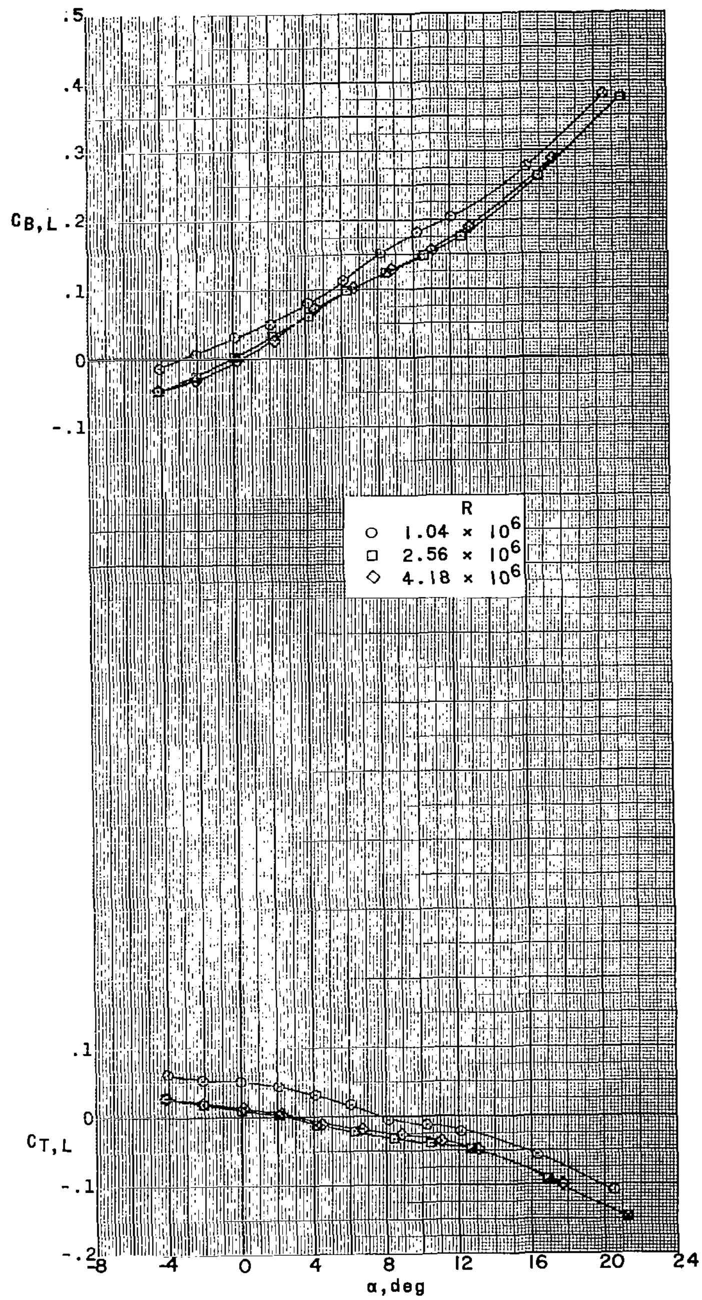

(a) M = 2.98.

Figure 41.- Bending- and torsion-moment characteristics of the left horizontal-tail panel of a 0.067-scale model of the X-15 airplane at various Reynolds numbers. Speed brakes open 45°.

[redacted]

L-229

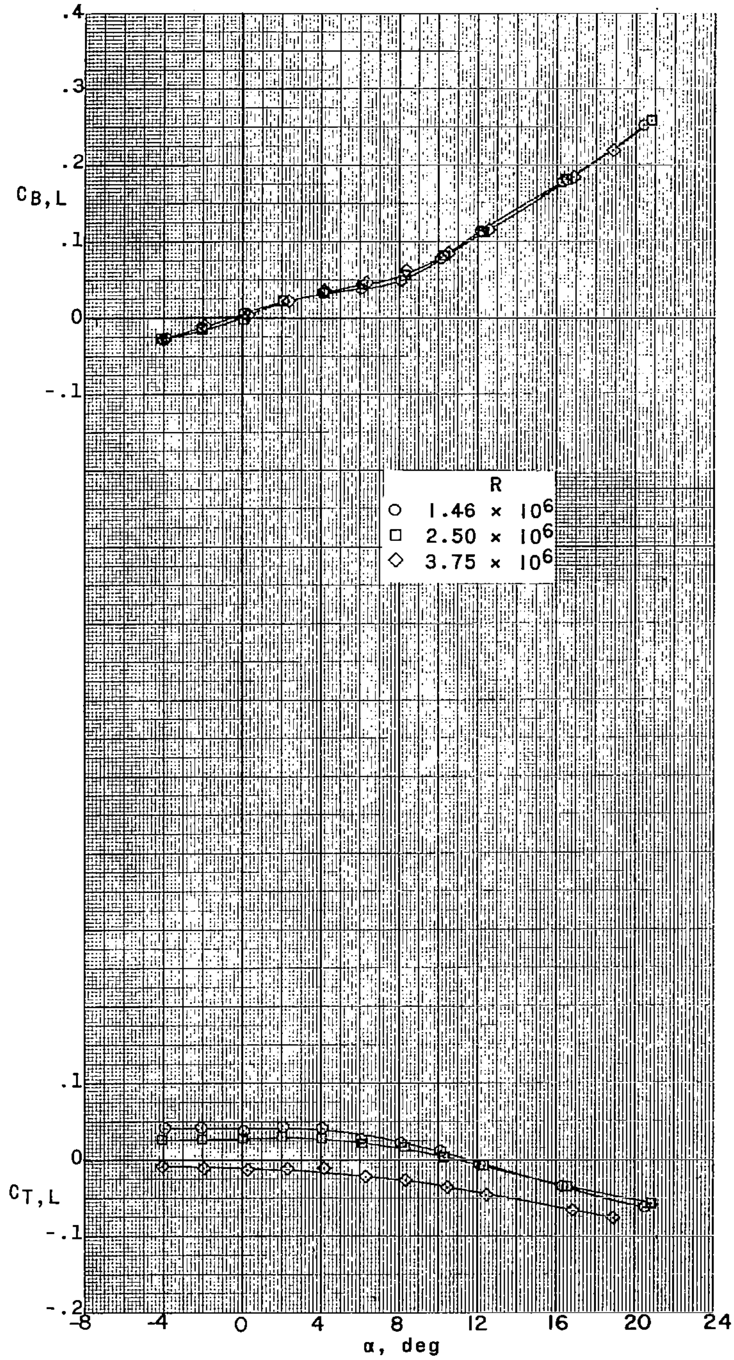

(b) M = 4.65.

Figure 41.- Concluded.

[redacted]

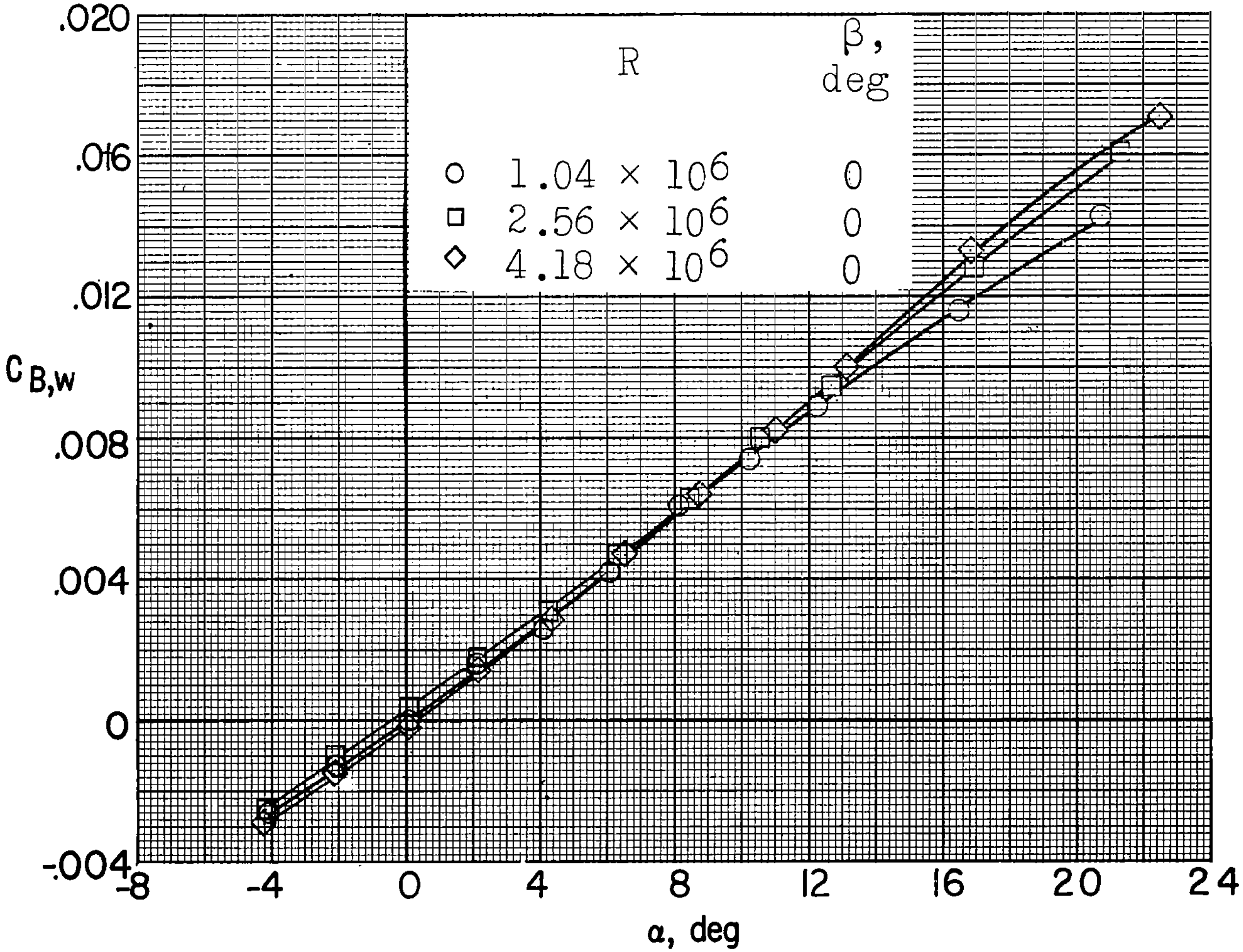

(a) M = 2.98.

Figure 42.- Bending-moment characteristics of the wing of a 0.067-scale model of the X-15 airplane at various Reynolds numbers. Speed brakes closed.

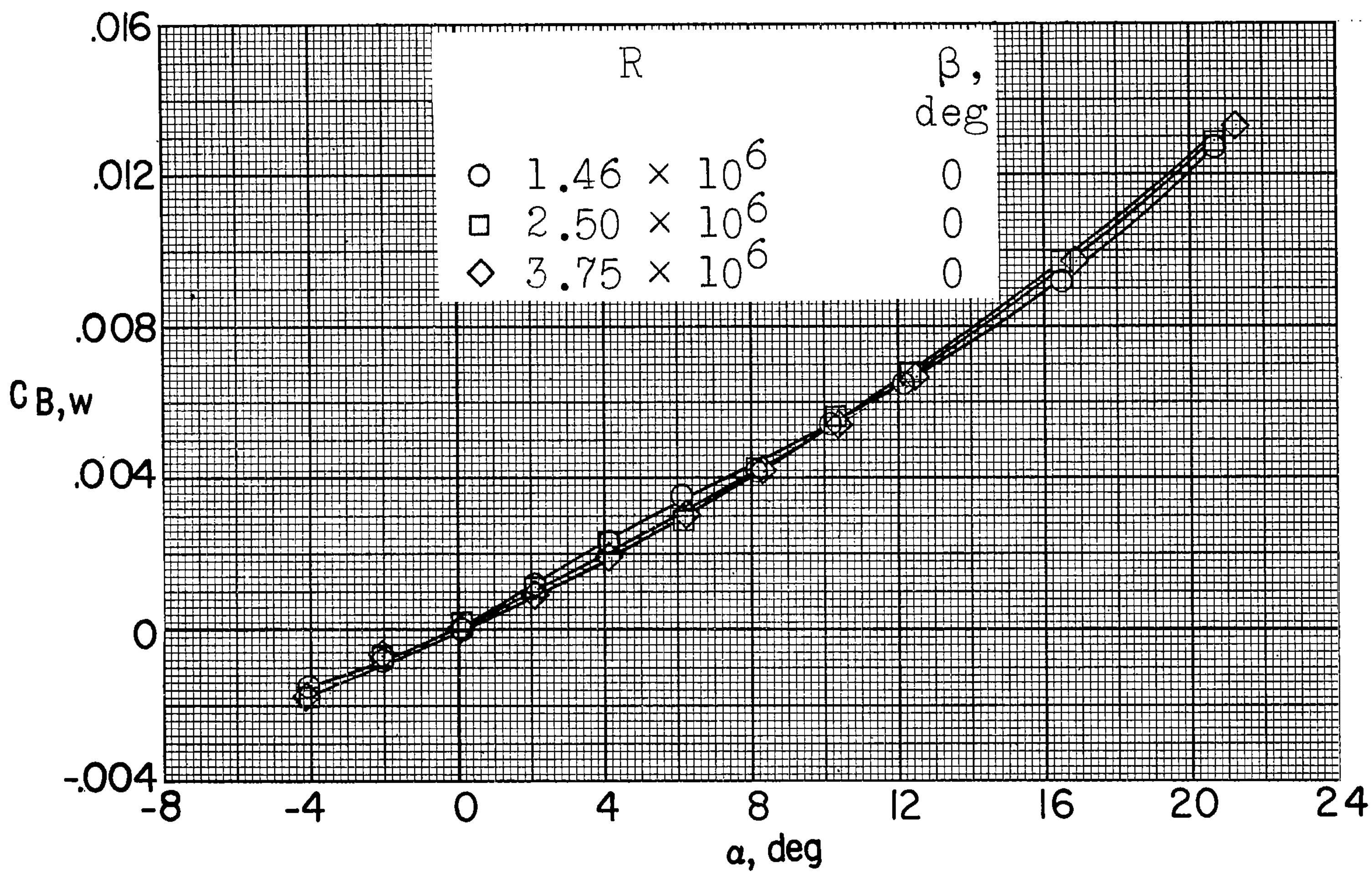

(b) M = 4.65.

Figure 42.- Concluded.

[redacted]

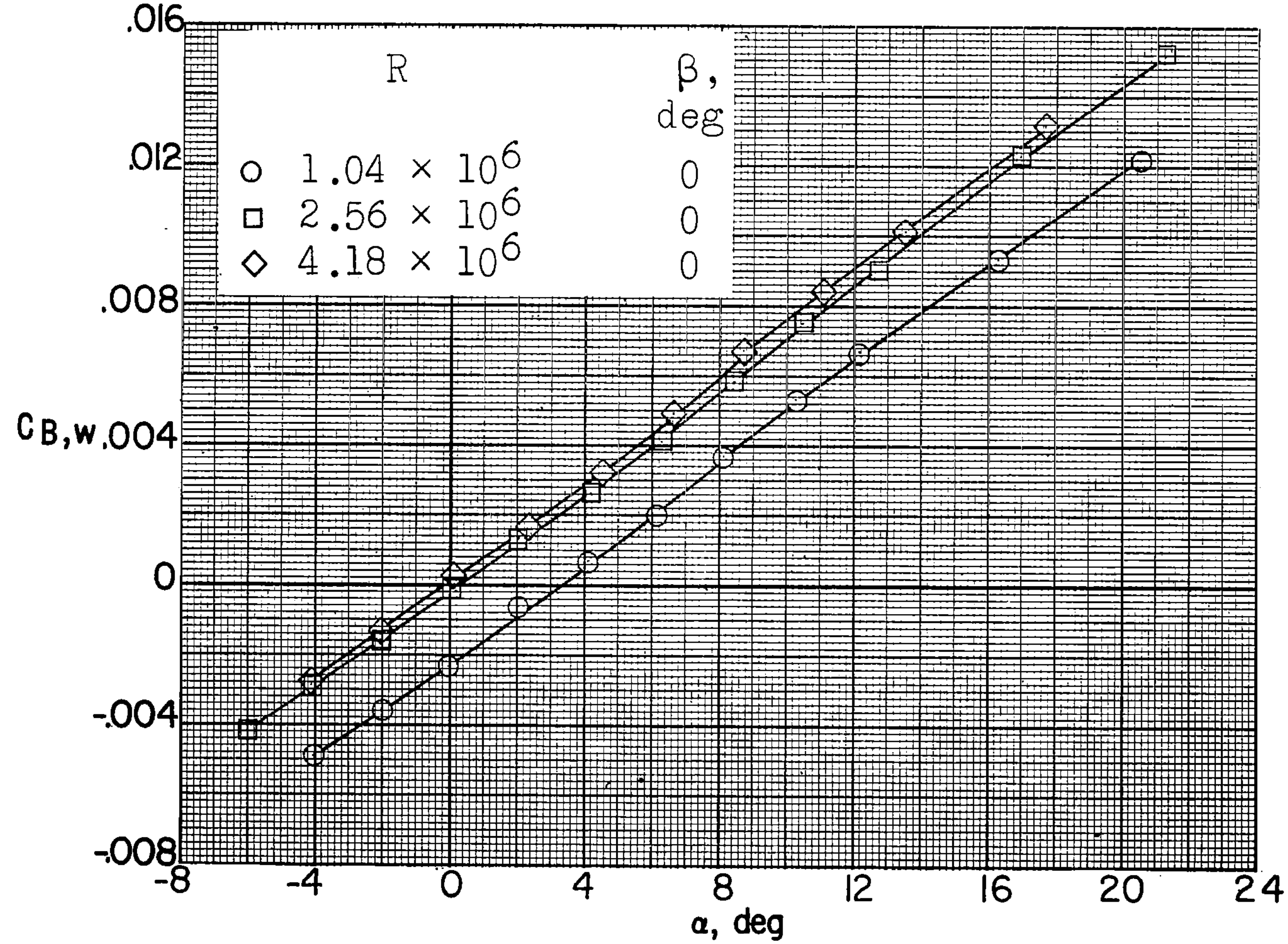

(a) M = 2.98.

Figure 43.- Bending-moment characteristics of the wing of a 0.067-scale model of the X-15 airplane at various Reynolds numbers. Speed brakes open 45°.

[redacted]

[redacted]

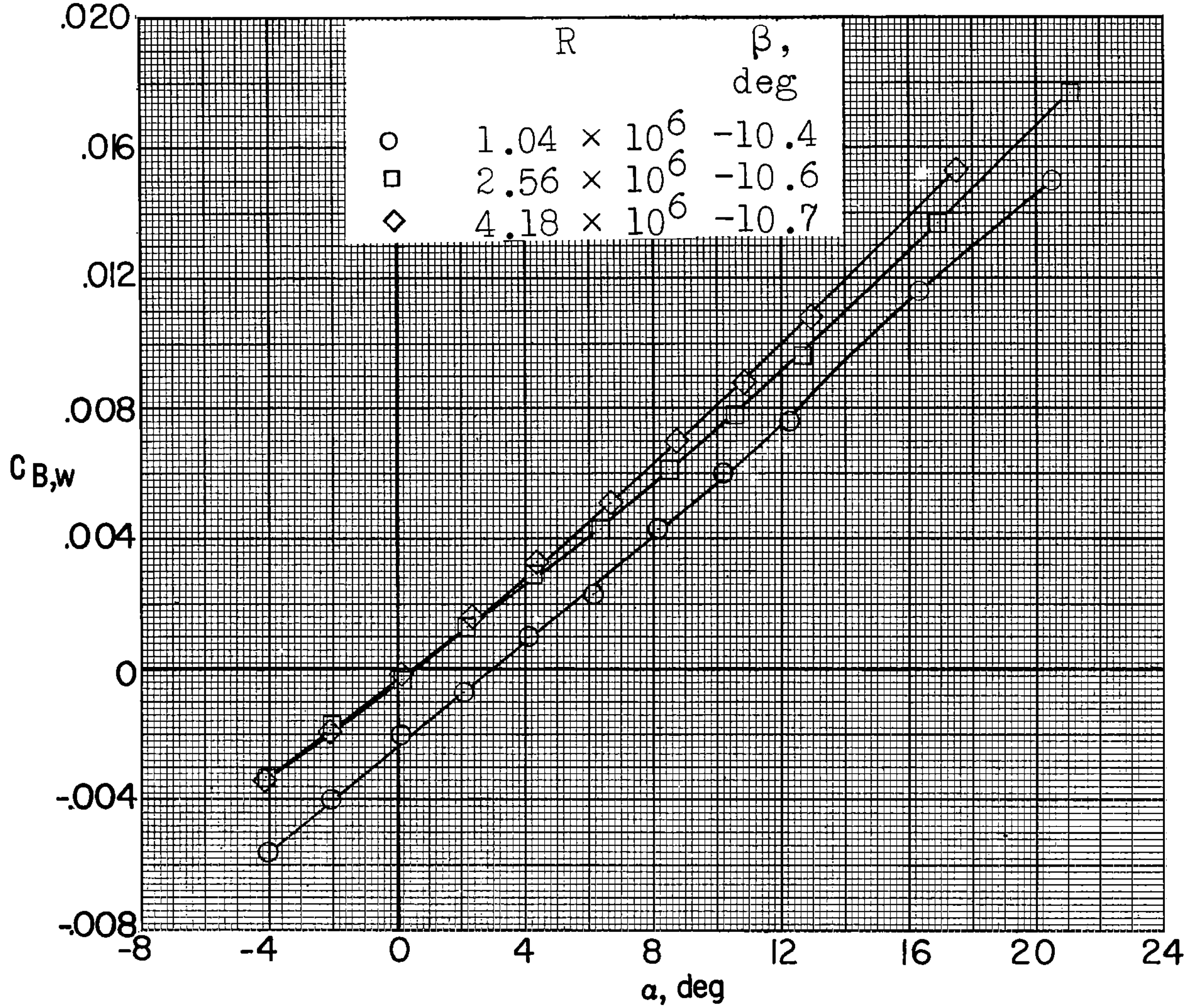

(a) Concluded.

Figure 43.- Continued.

[redacted]

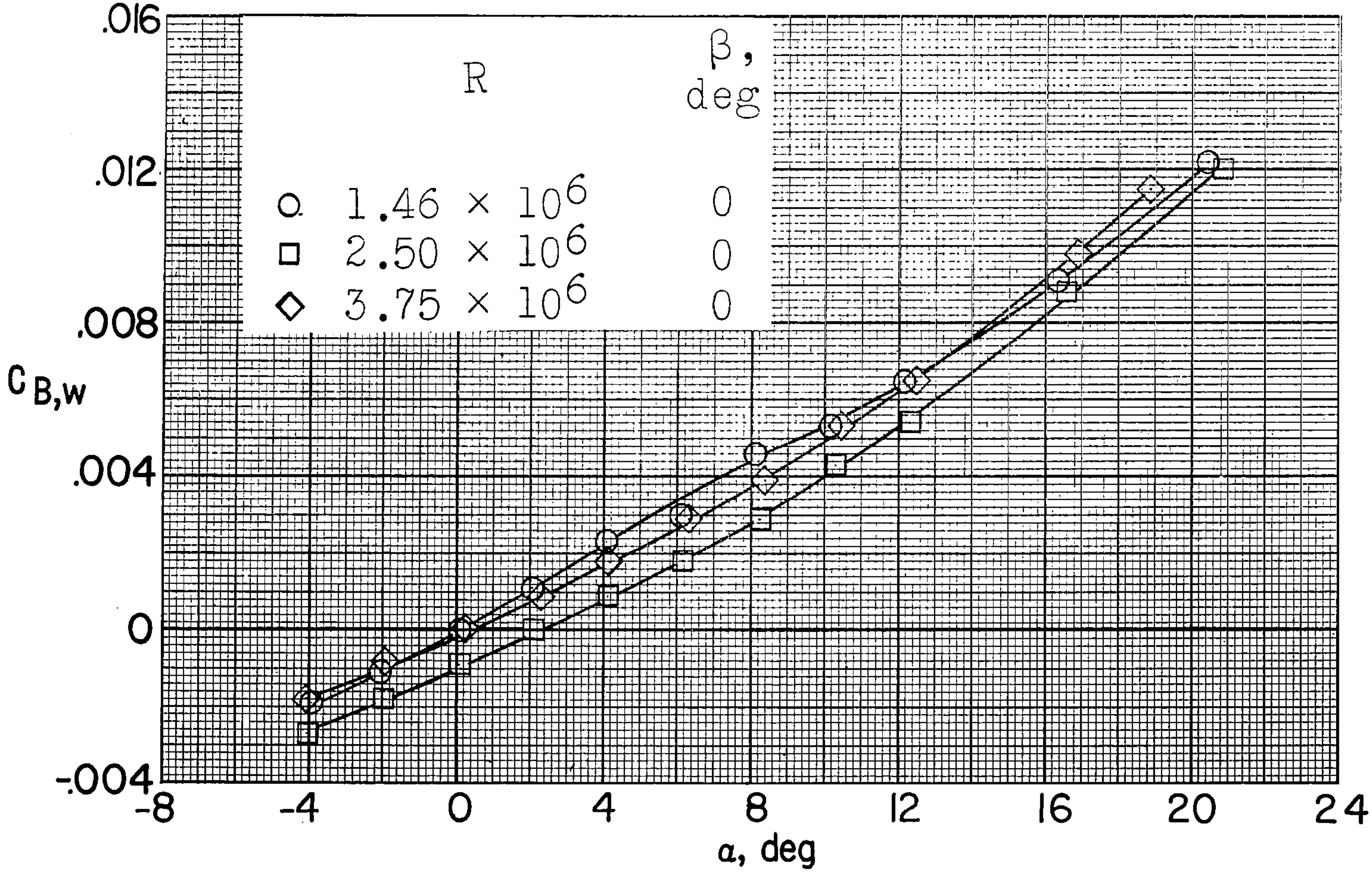

(b) $M = 4.65$.

Figure 43.- Continued.

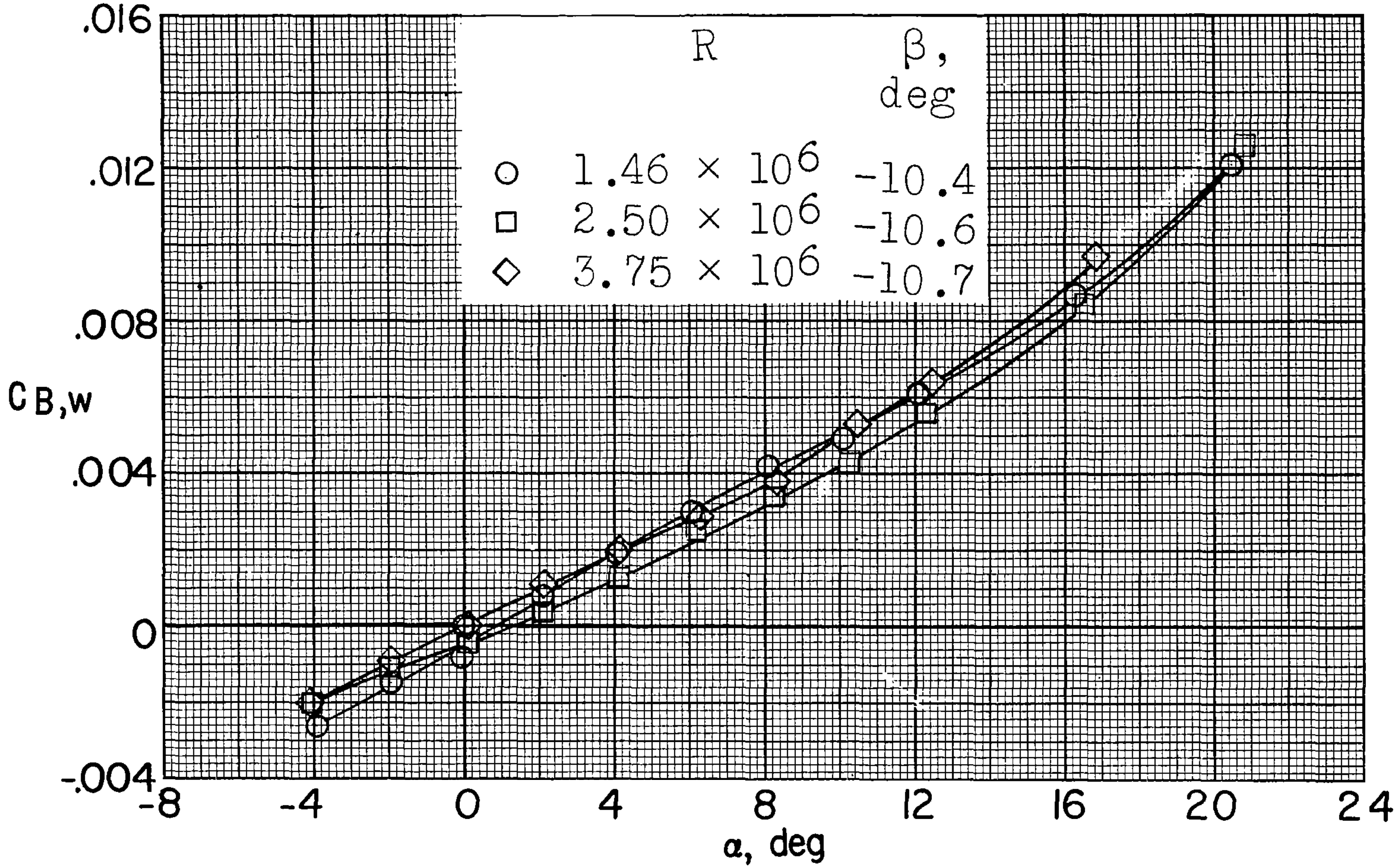

(b) Concluded.

Figure 43.- Concluded.

L-229

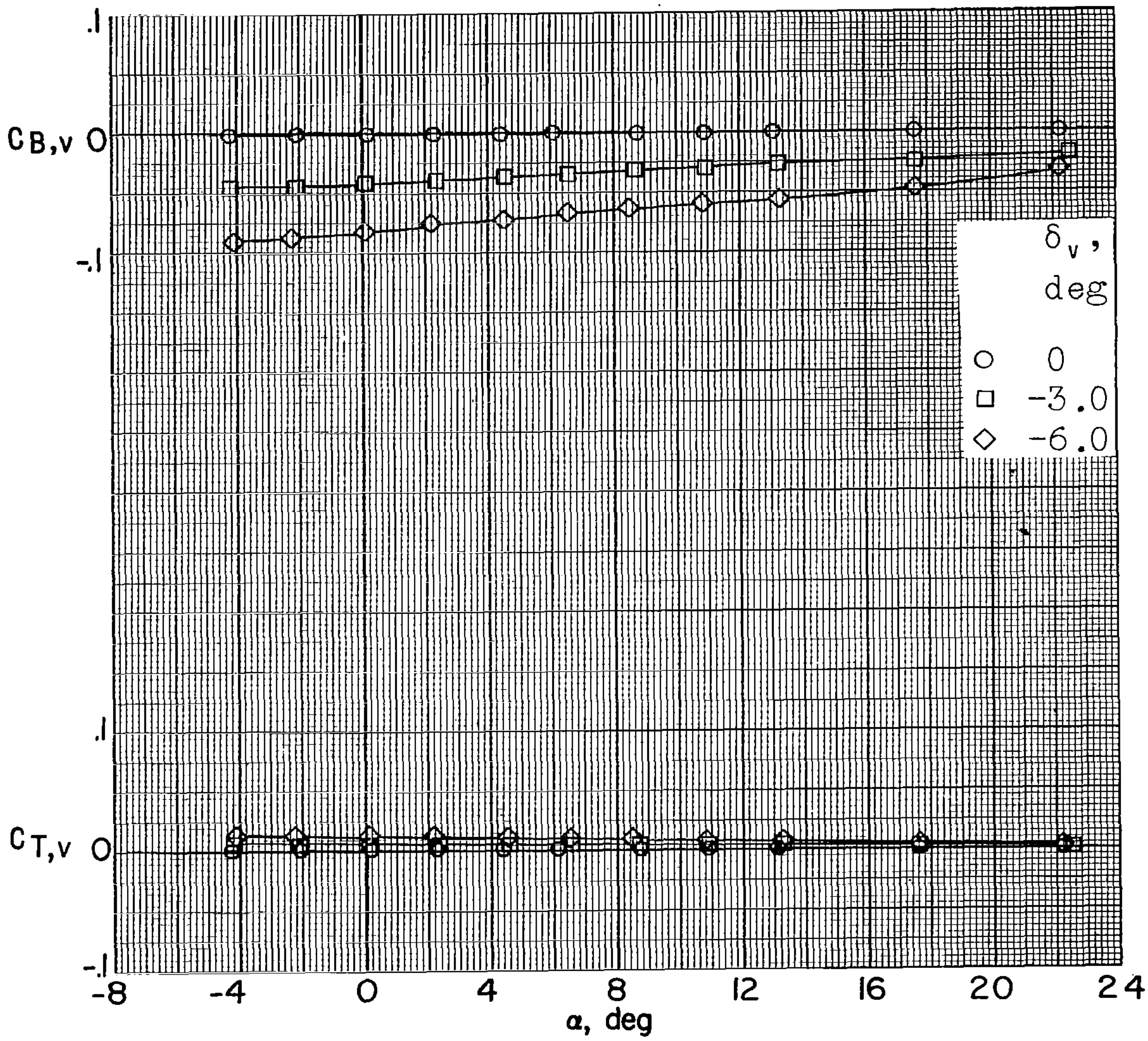

(a) M = 2.29; β = 0°.

Figure 44.- Bending- and torsion-moment characteristics of the vertical tail of a 0.067-scale model of the X-15 airplane with various deflections of the vertical tail. Speed brakes closed.

[redacted]

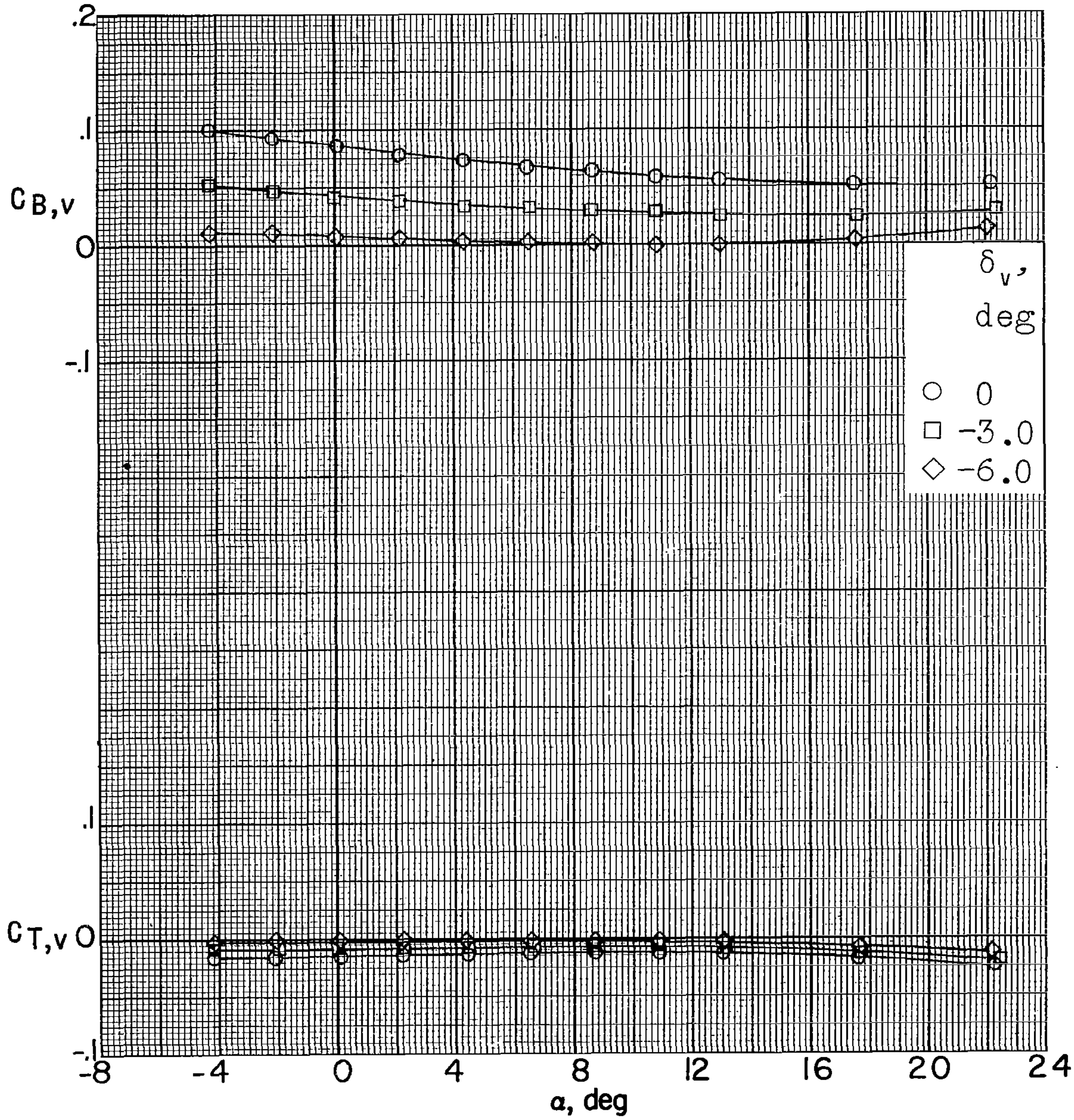

(b) M = 2.29; β = -5.2°.

Figure 44.- Continued.

L-229

[redacted]

[redacted]

L-229

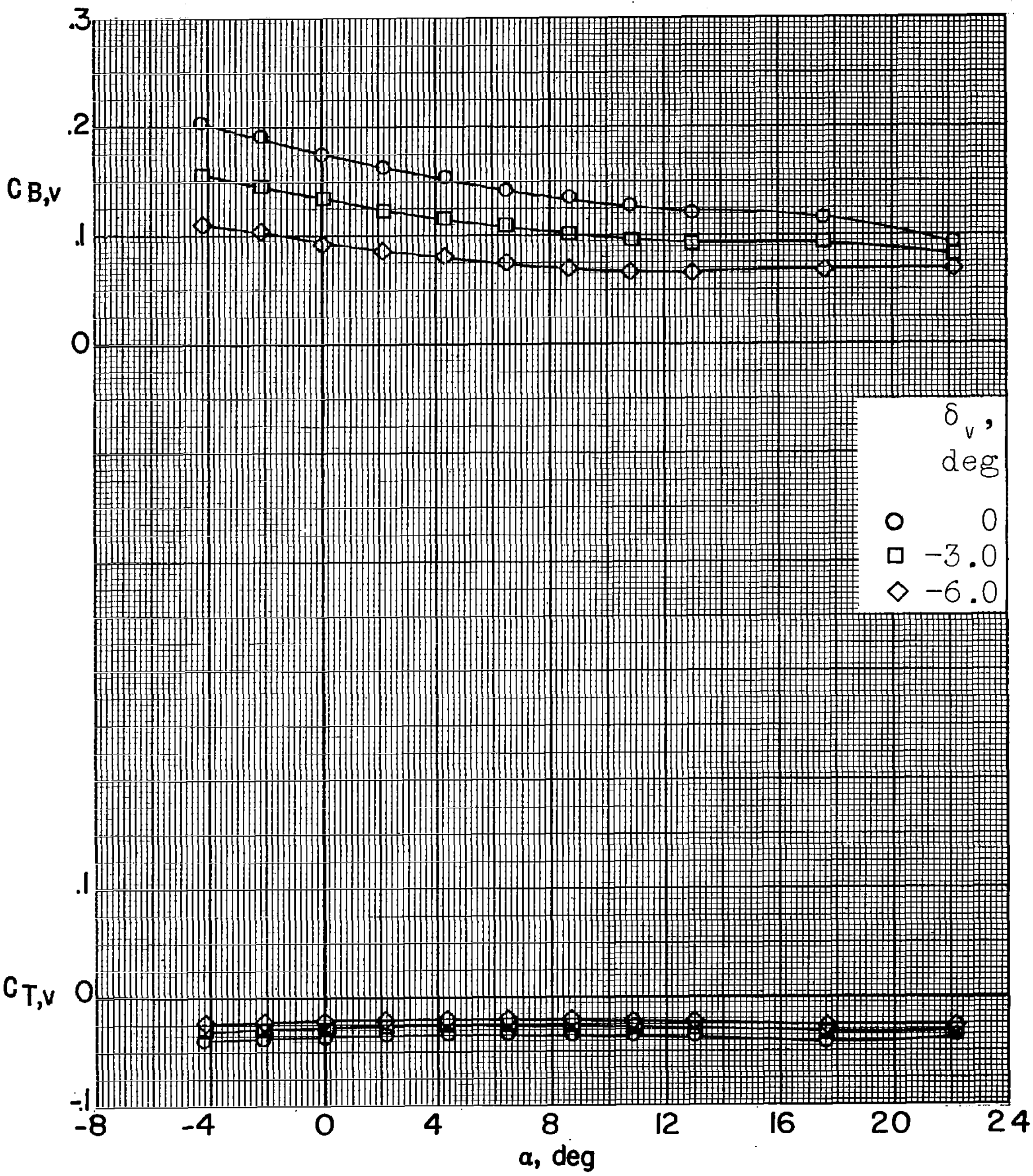

(c) M = 2.29; β = -10.7°.

Figure 44.- Continued.

[redacted]

[redacted]

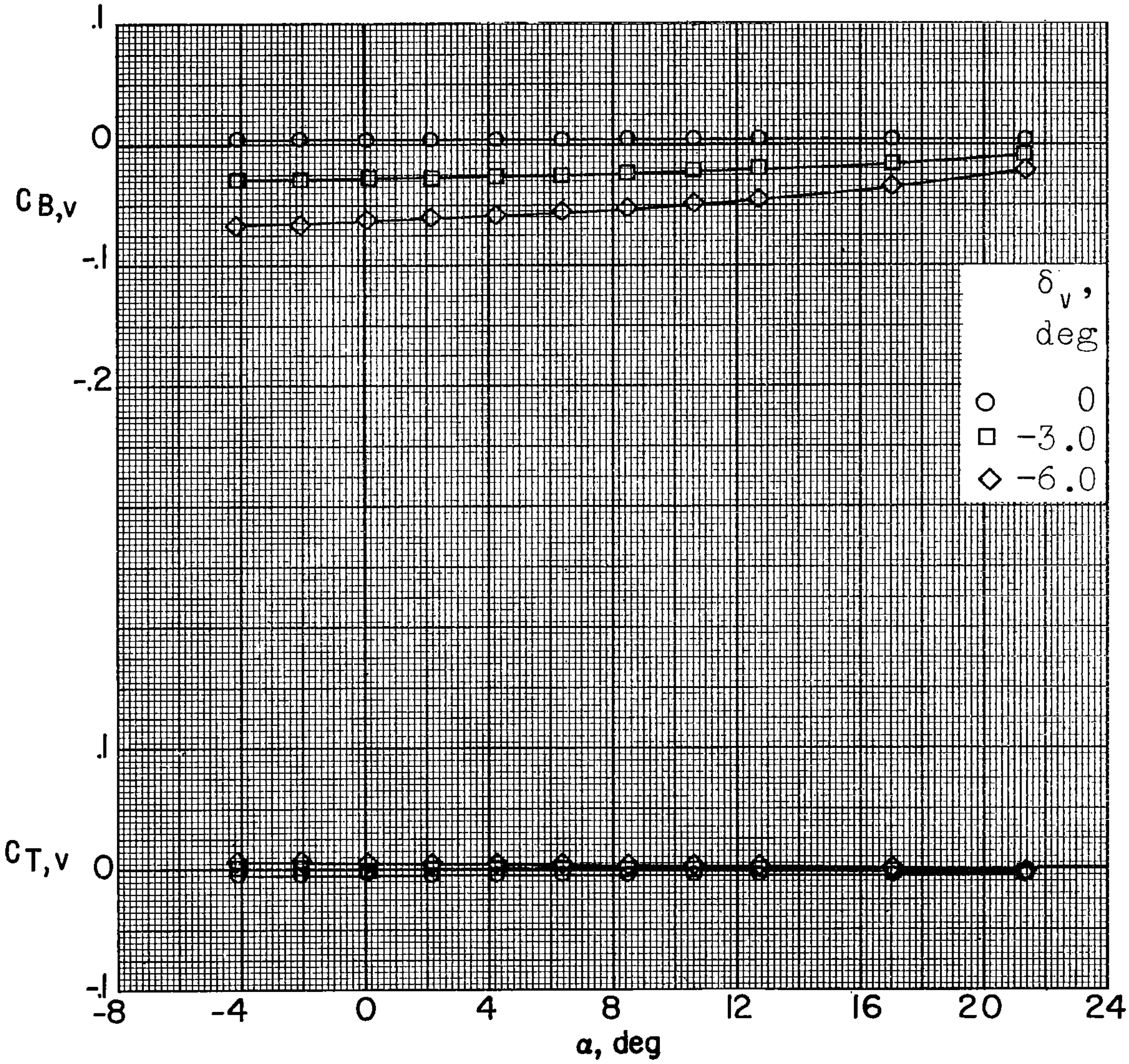

(d) M = 2.98; β = 0°.

Figure 44.- Continued.

L-229

[redacted]

L-229

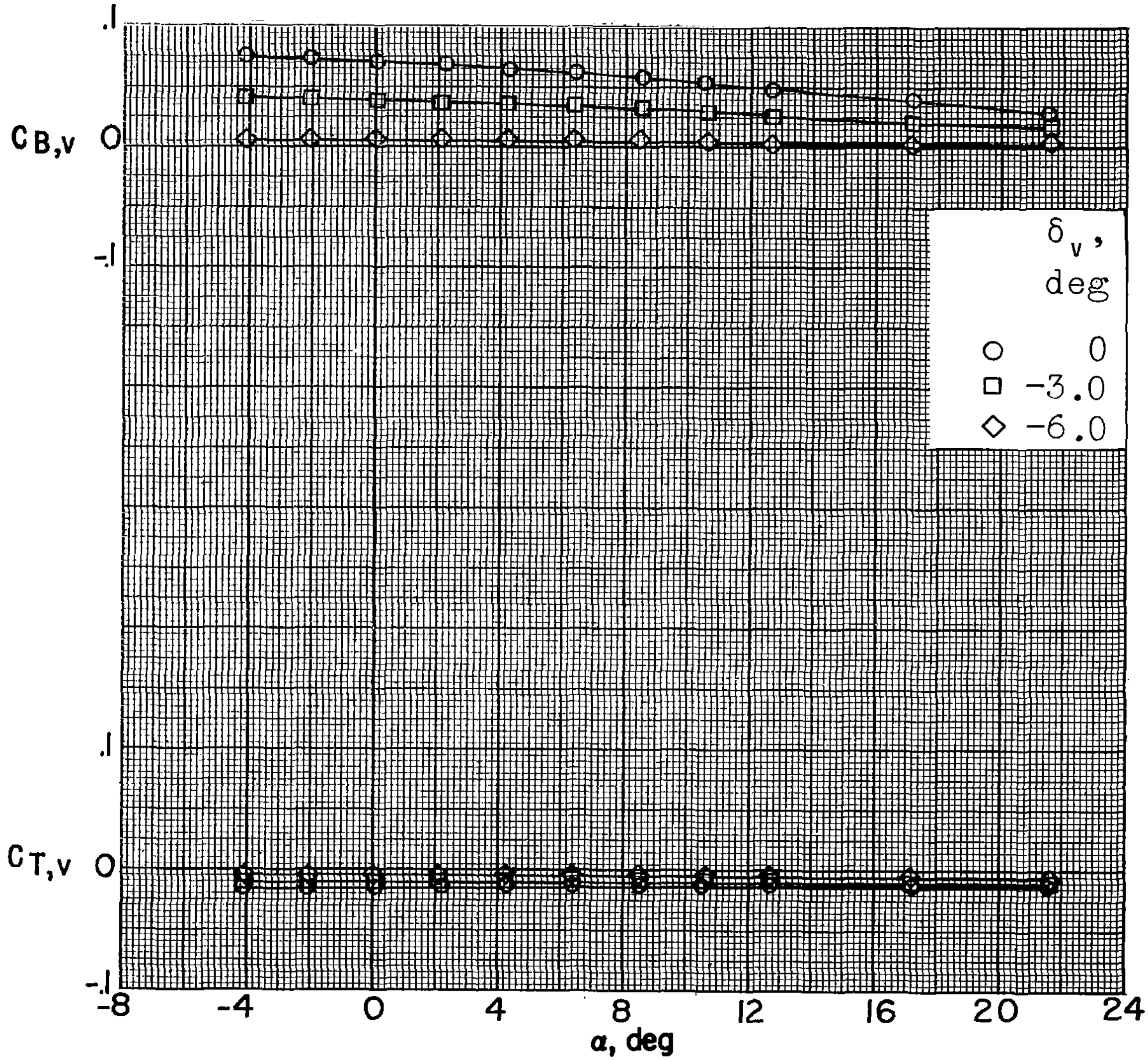

(e) M = 2.98; β = -5.2°.

Figure 44.- Continued.

[redacted]

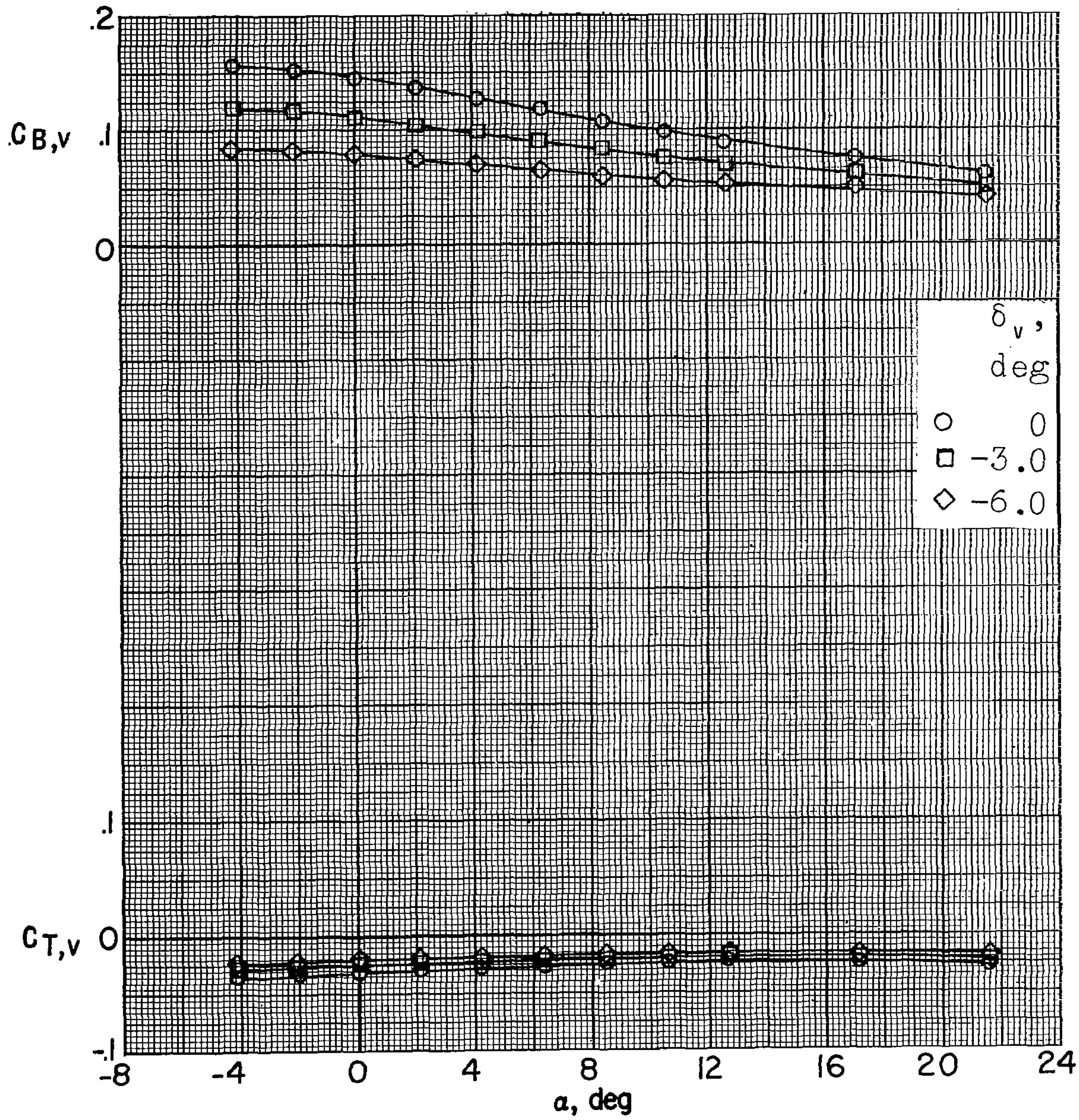

(f) M = 2.98; β = -10.6°.

Figure 44.- Continued.

[redacted]

[redacted]

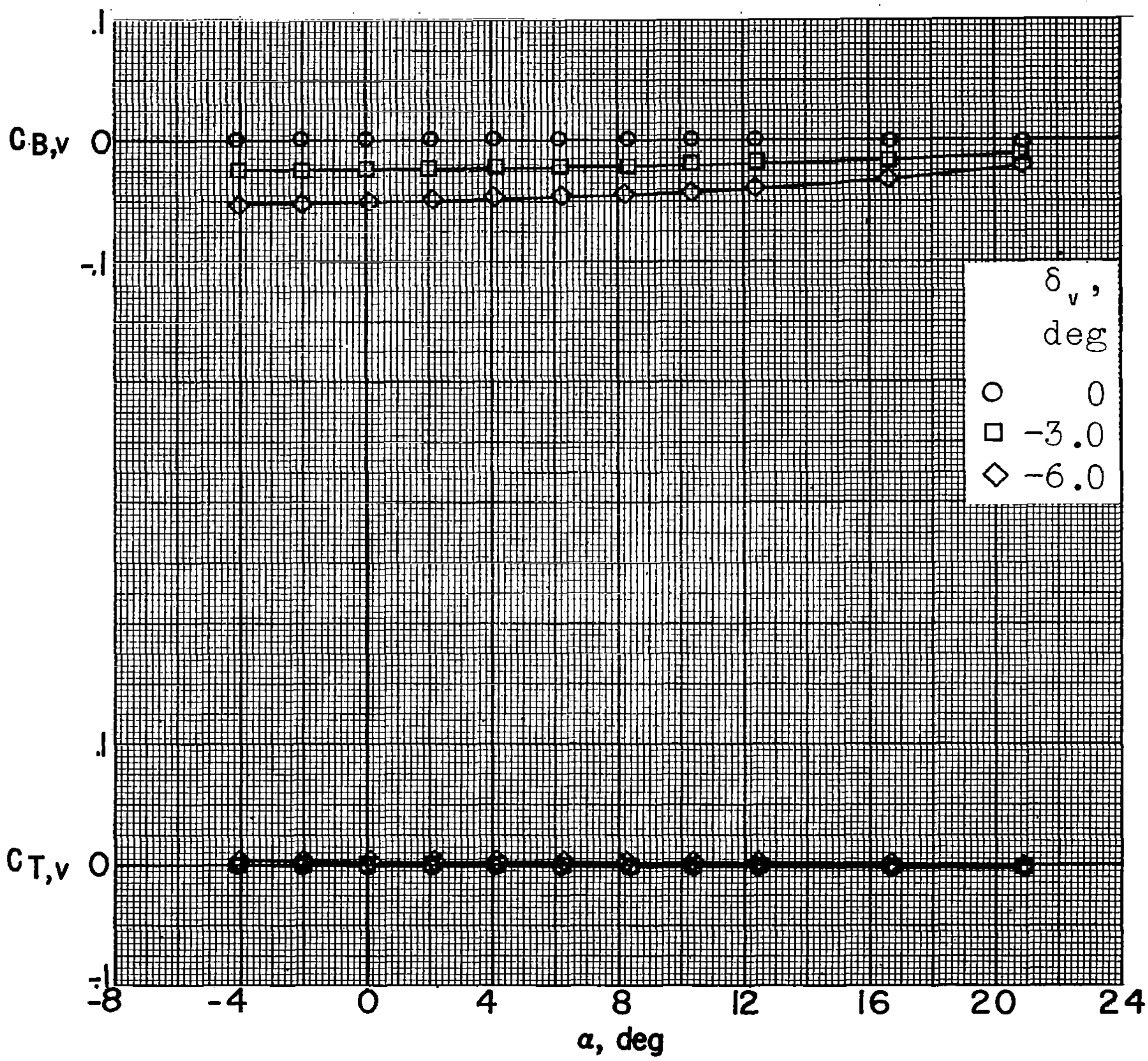

(g) M = 3.96; β = 0°.

Figure 44.- Continued.

[redacted]

[redacted]

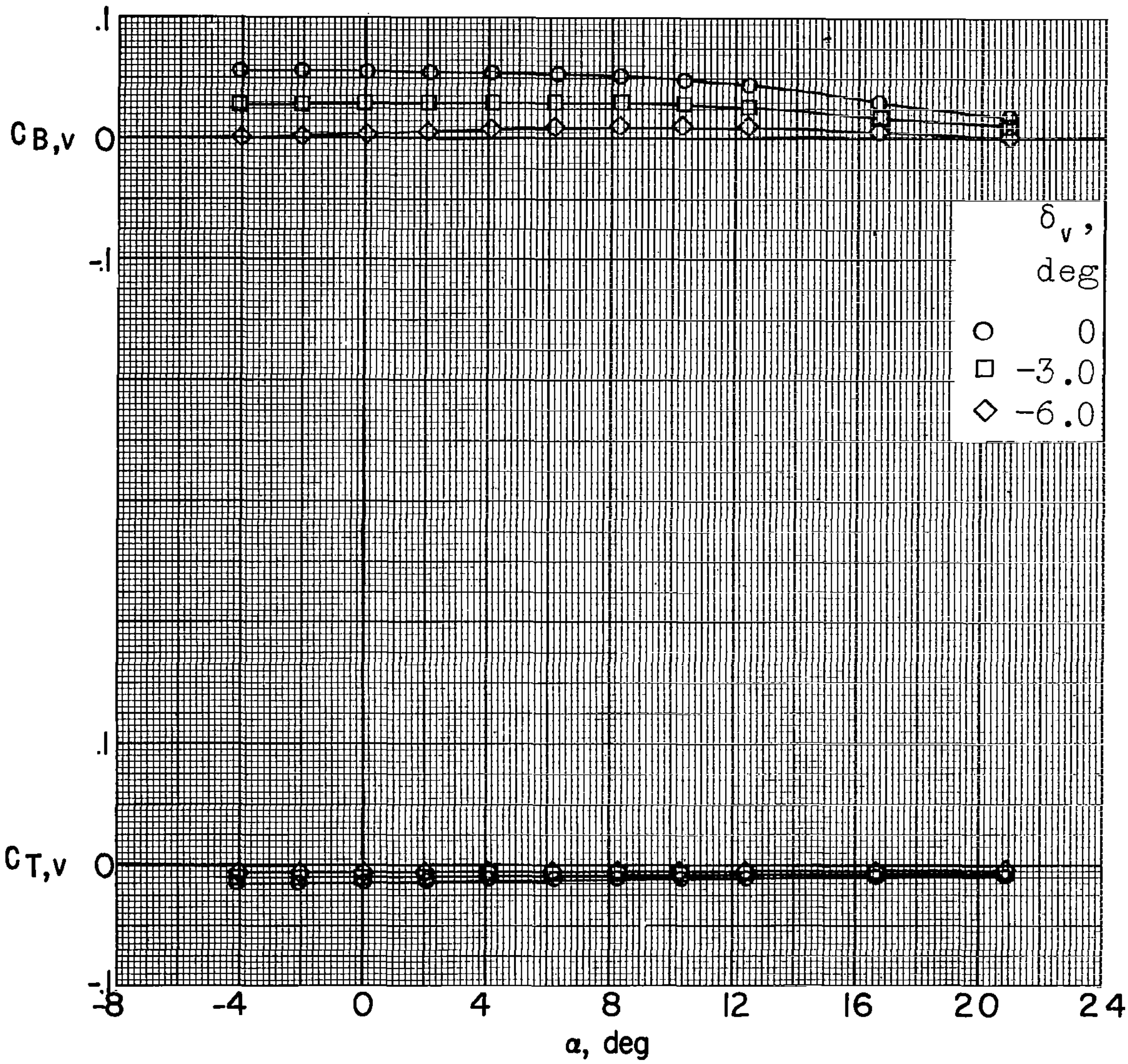

(h) $M = 3.96$; $\beta = -5.1^{\circ}$.

Figure 44.- Continued.

[redacted]

L-229

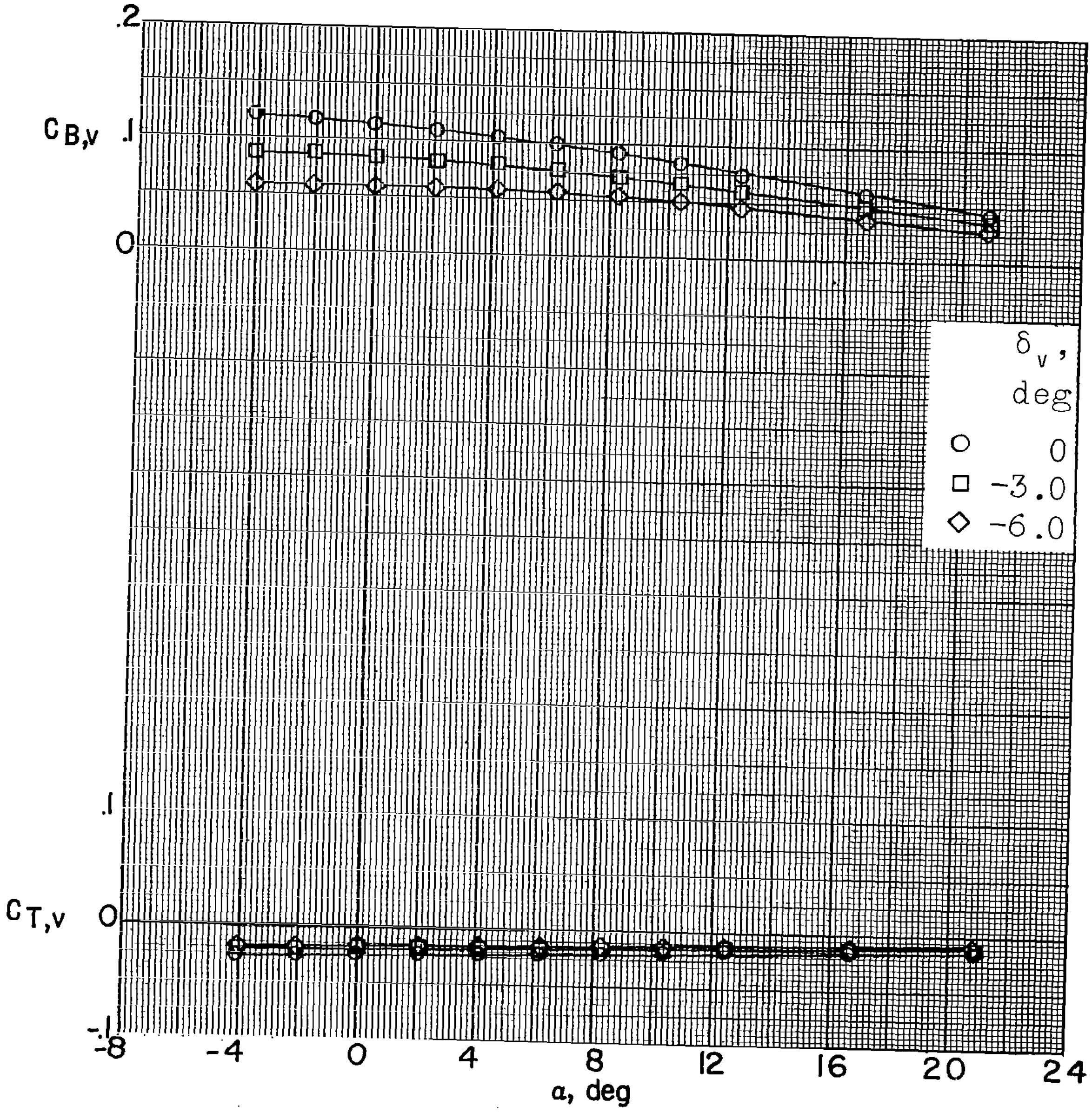

(i) $M = 3.96$; $\beta = -10.6^{\circ}$.

Figure 44.- Continued.

[redacted]

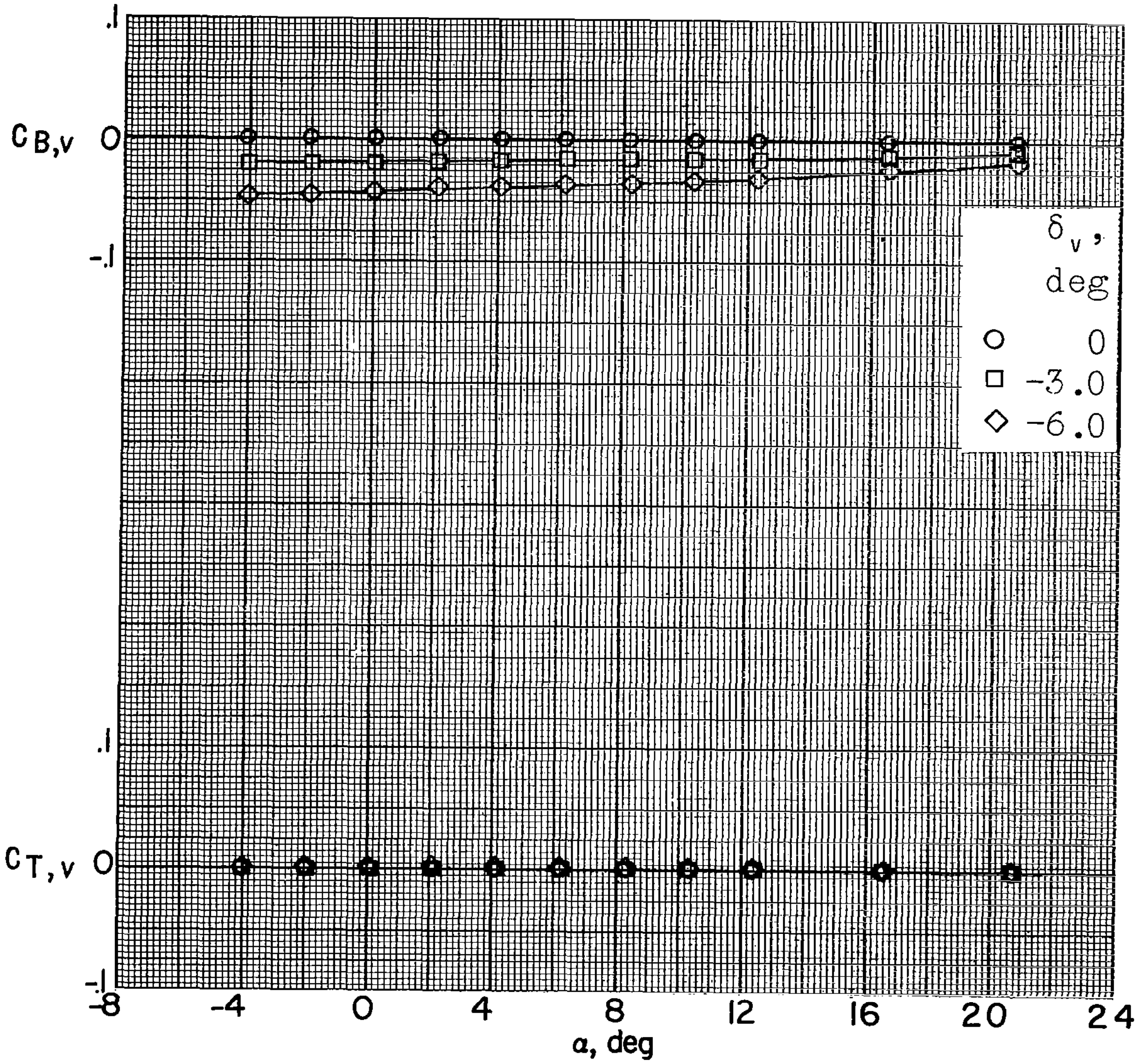

L-229

(j) M = 4.65; β = 0.1°.

Figure 44.- Continued.

[redacted]

[redacted]

L-229

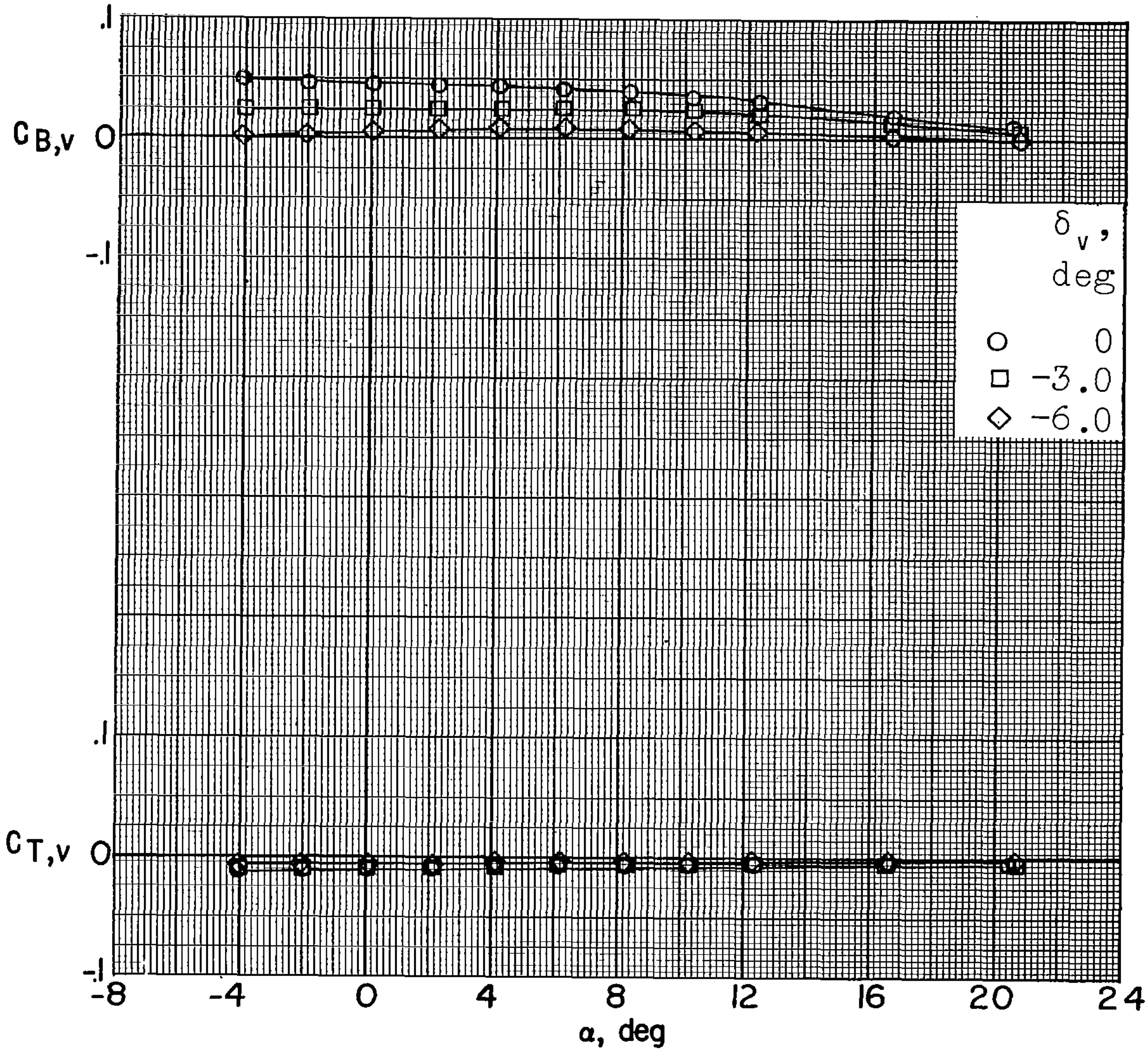

(k) $M = 4.65$; $\beta = -5.1^{\circ}$.

Figure 44.- Continued.

[redacted]

[redacted]

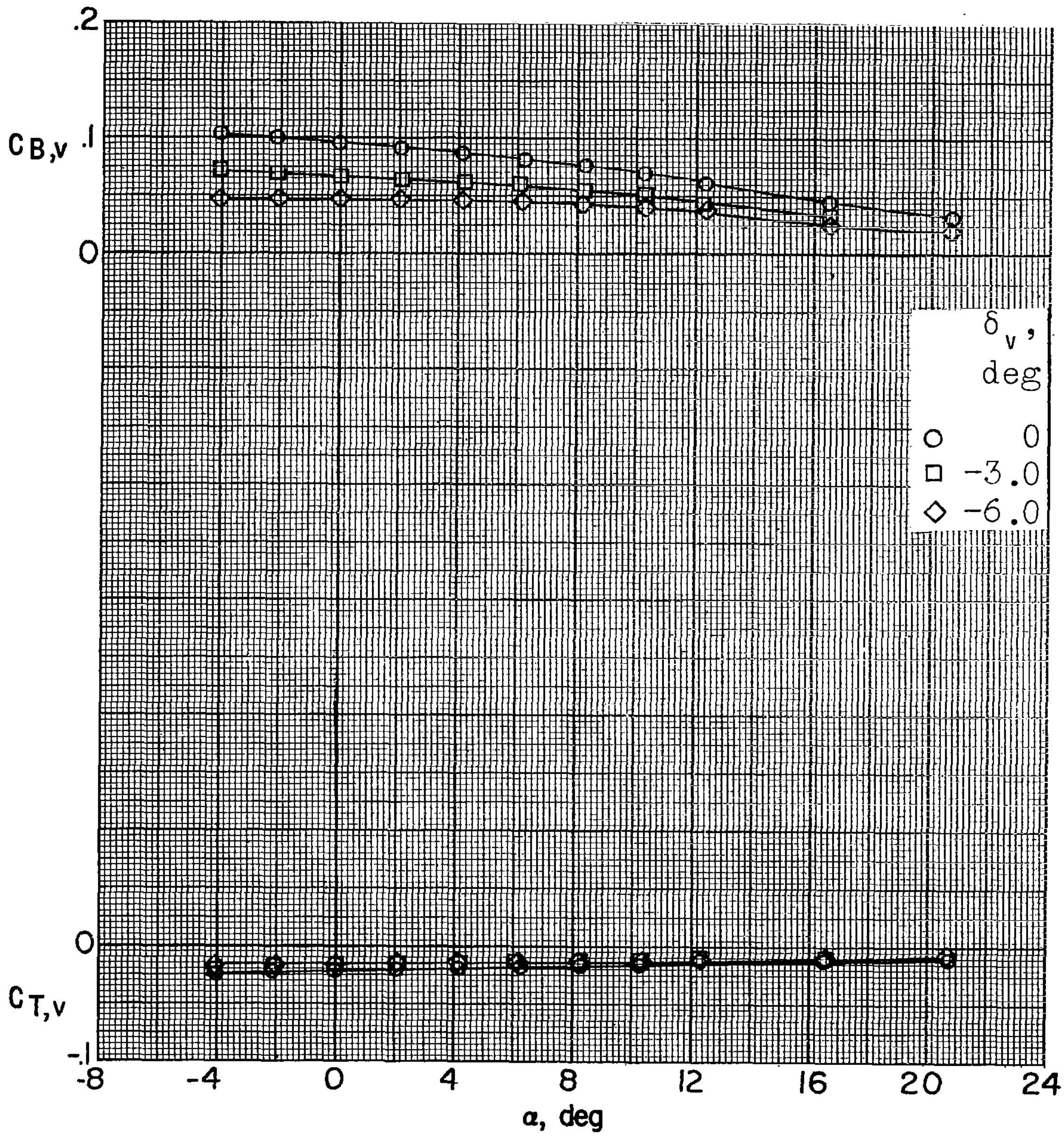

(l) M = 4.65; β = -10.5°.

Figure 44.- Concluded.

L-229

[redacted]

[redacted]

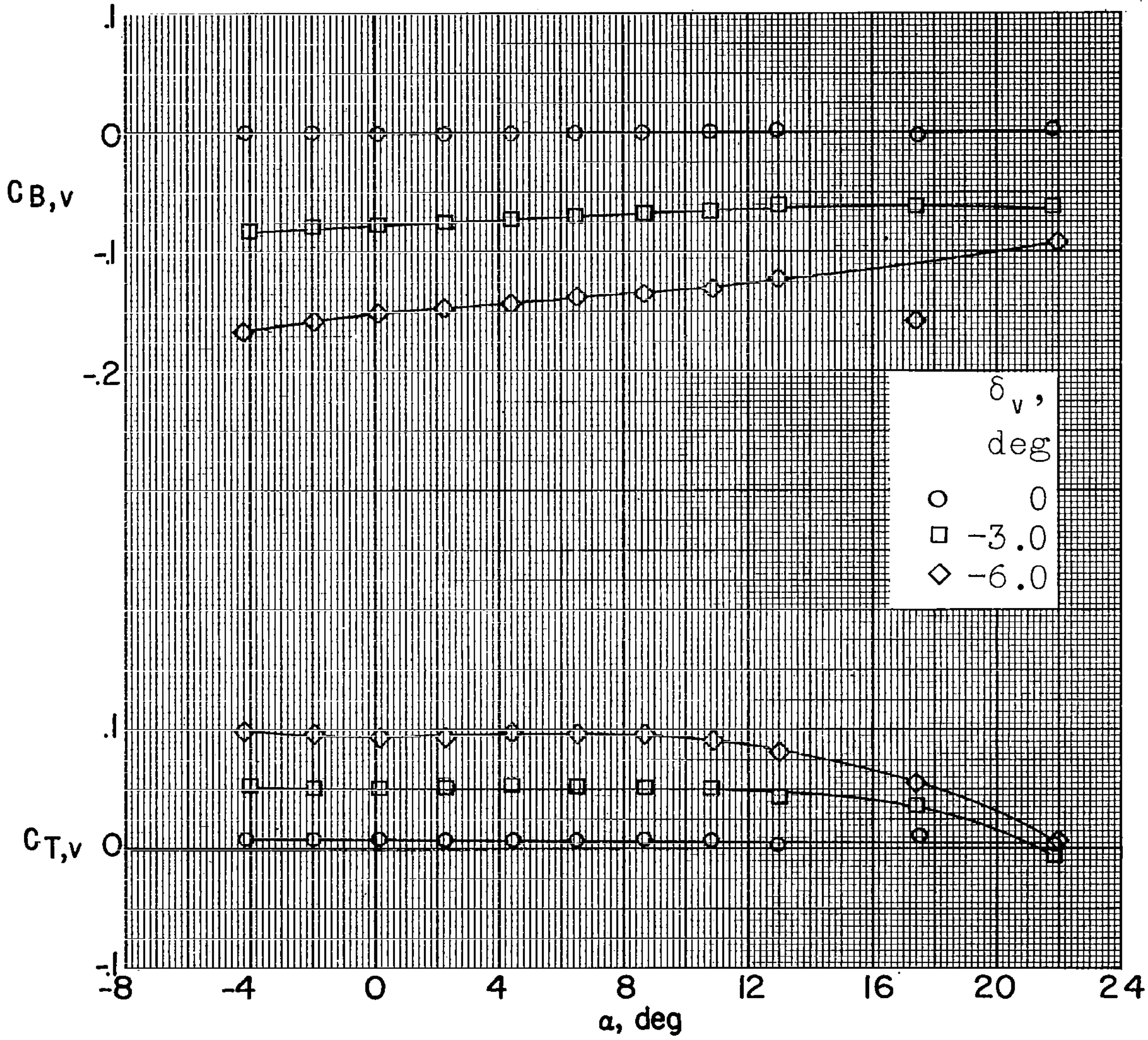

(a) M = 2.29; β = -0.1°.

Figure 45.- Bending- and torsion-moment characteristics of the vertical tail of a 0.067-scale model of the X-15 airplane with various deflections of the vertical tail. Speed brakes open 45°.

[redacted]

[redacted]

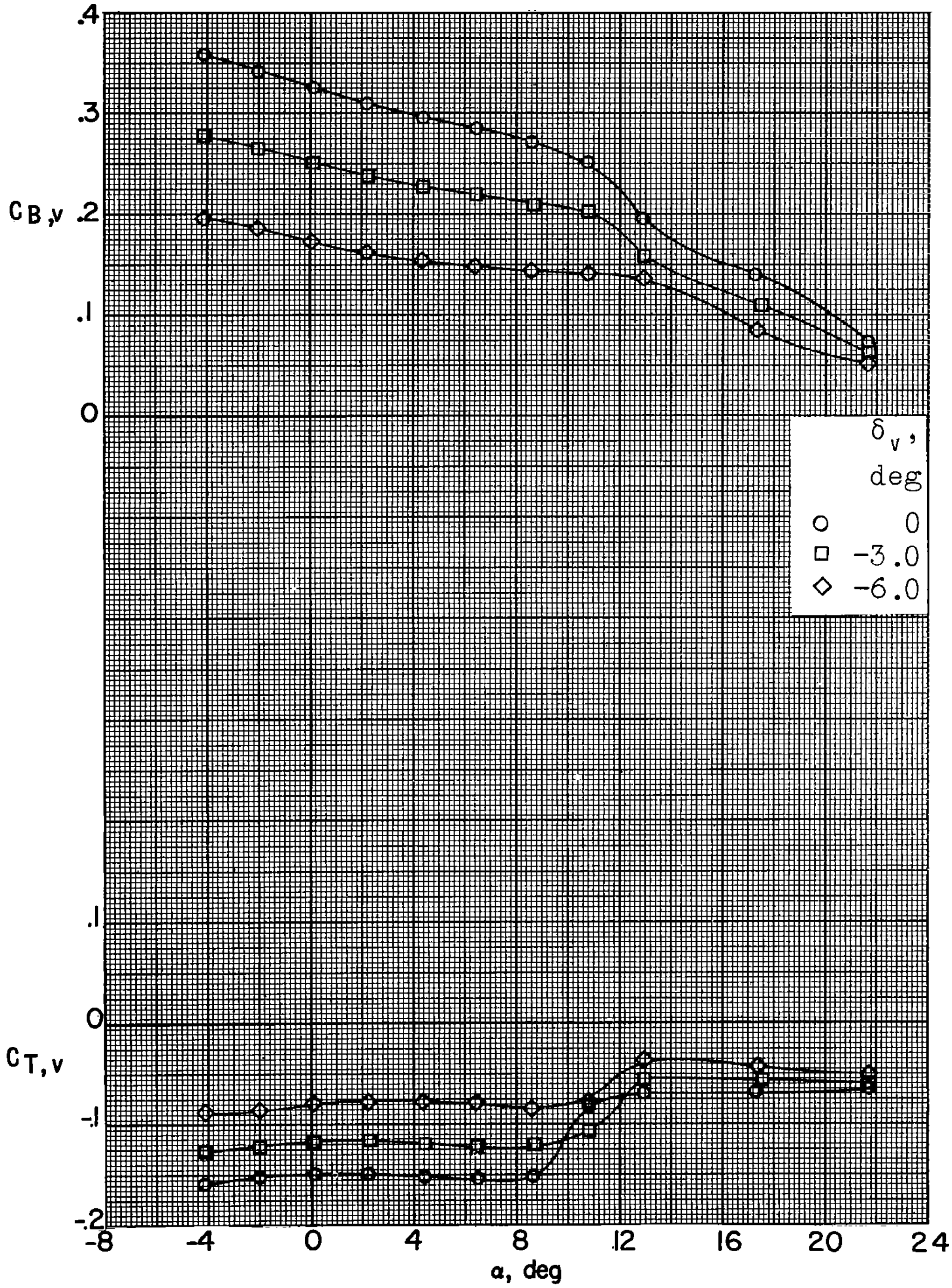

(b) M = 2.29; β = -10.6°.

Figure 45.- Continued.

[redacted]

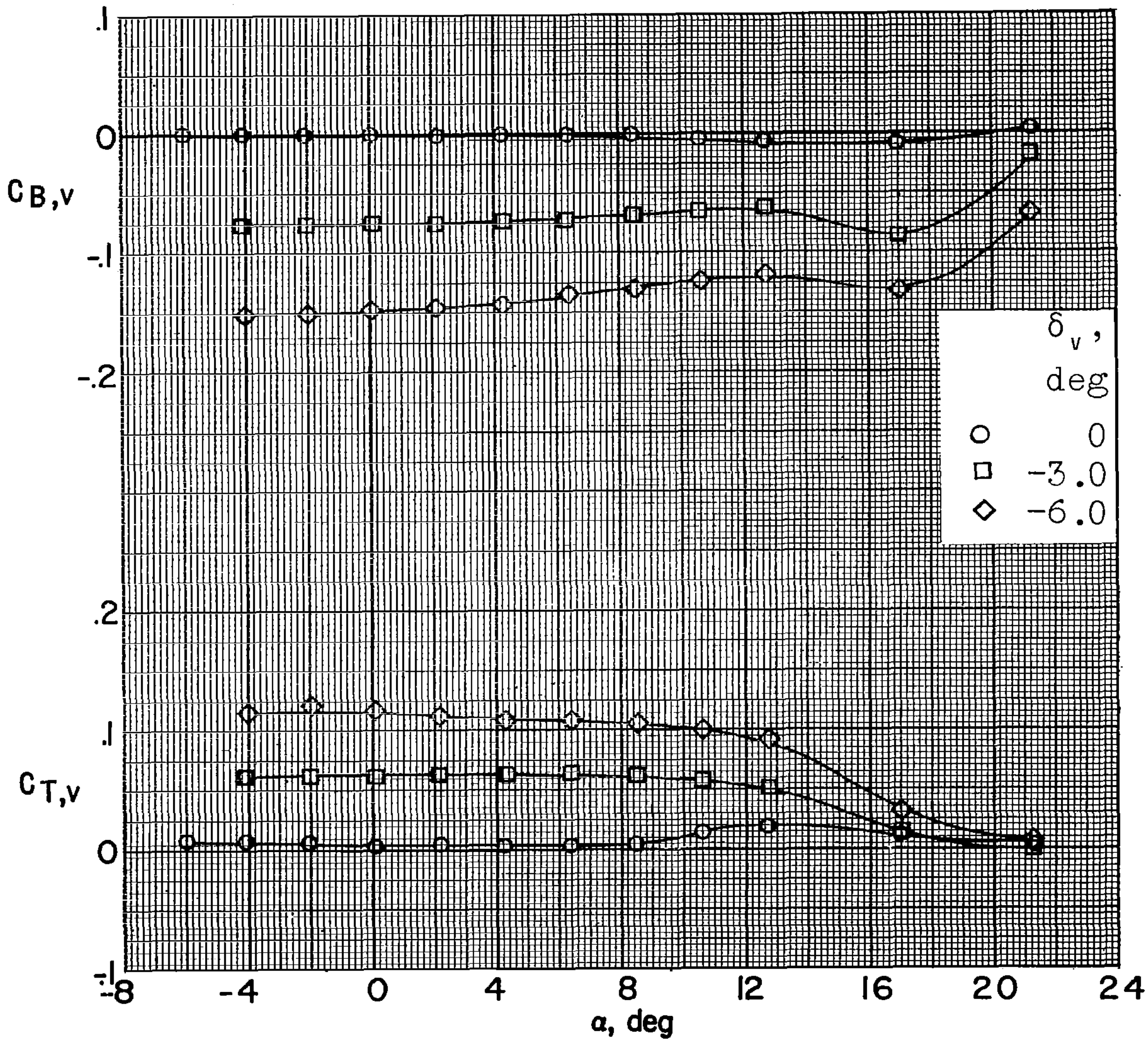

(c) M = 2.98; β = 0°.

Figure 45.- Continued.

[redacted]

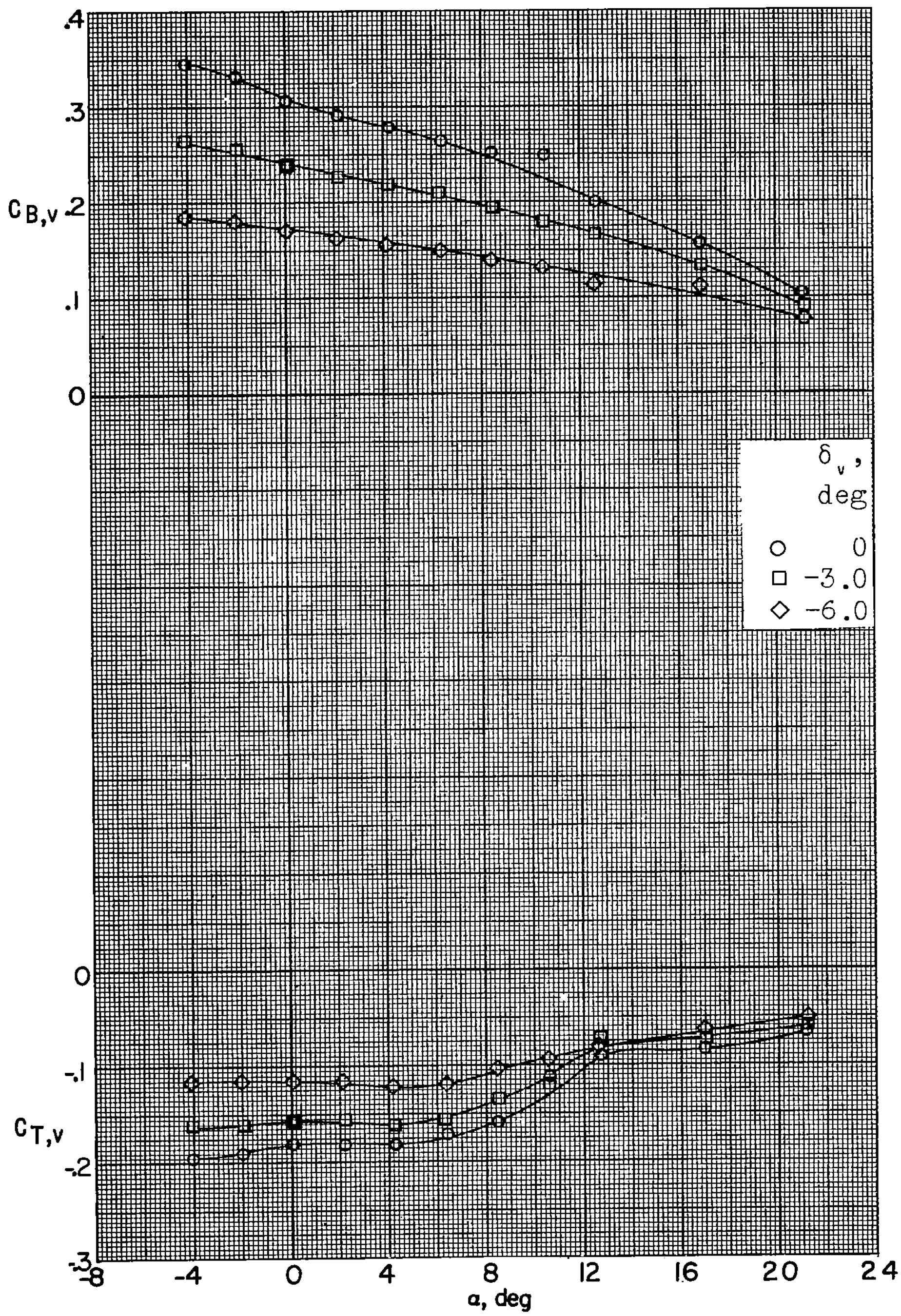

(d) M = 2.98; β = -10.6°.

Figure 45.- Continued.

[redacted]

[redacted]

L-229

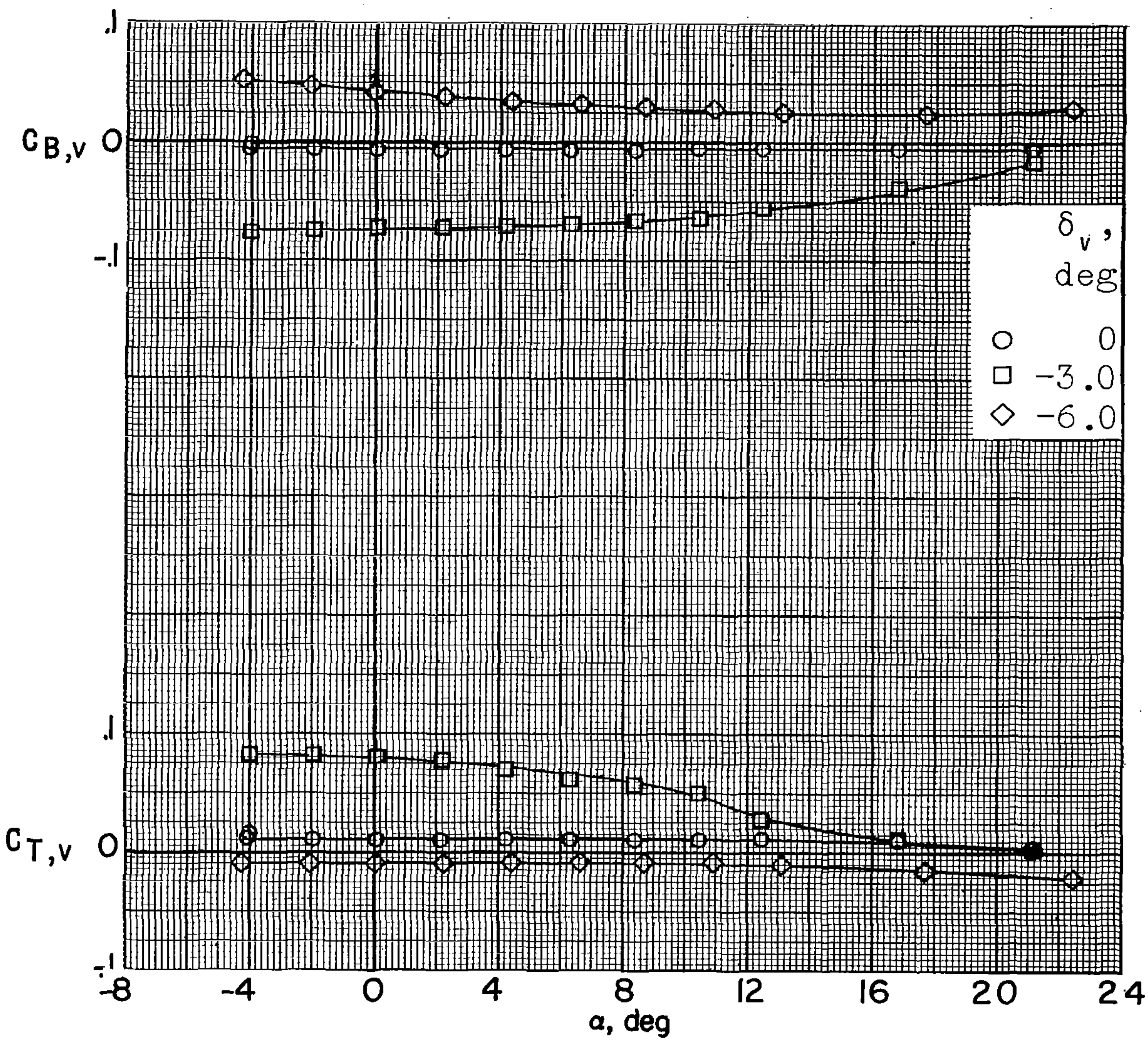

(e) M = 3.96; β = -0.1°.

Figure 45.- Continued.

[redacted]

[redacted]

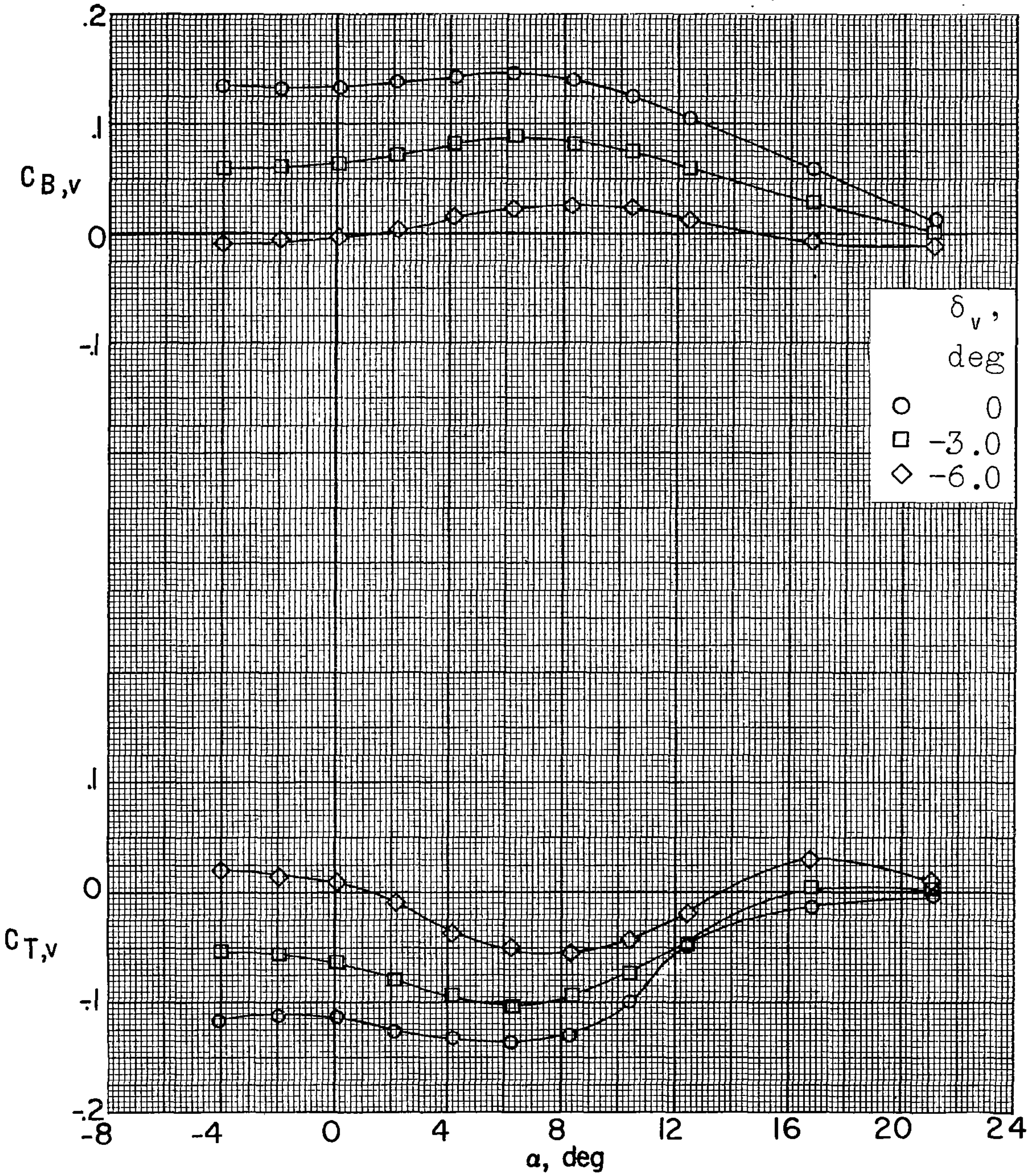

(f) $M = 3.96$; $\beta = -5.1^{\circ}$.

Figure 45.- Continued.

L-229

[redacted]

[redacted]

L-229

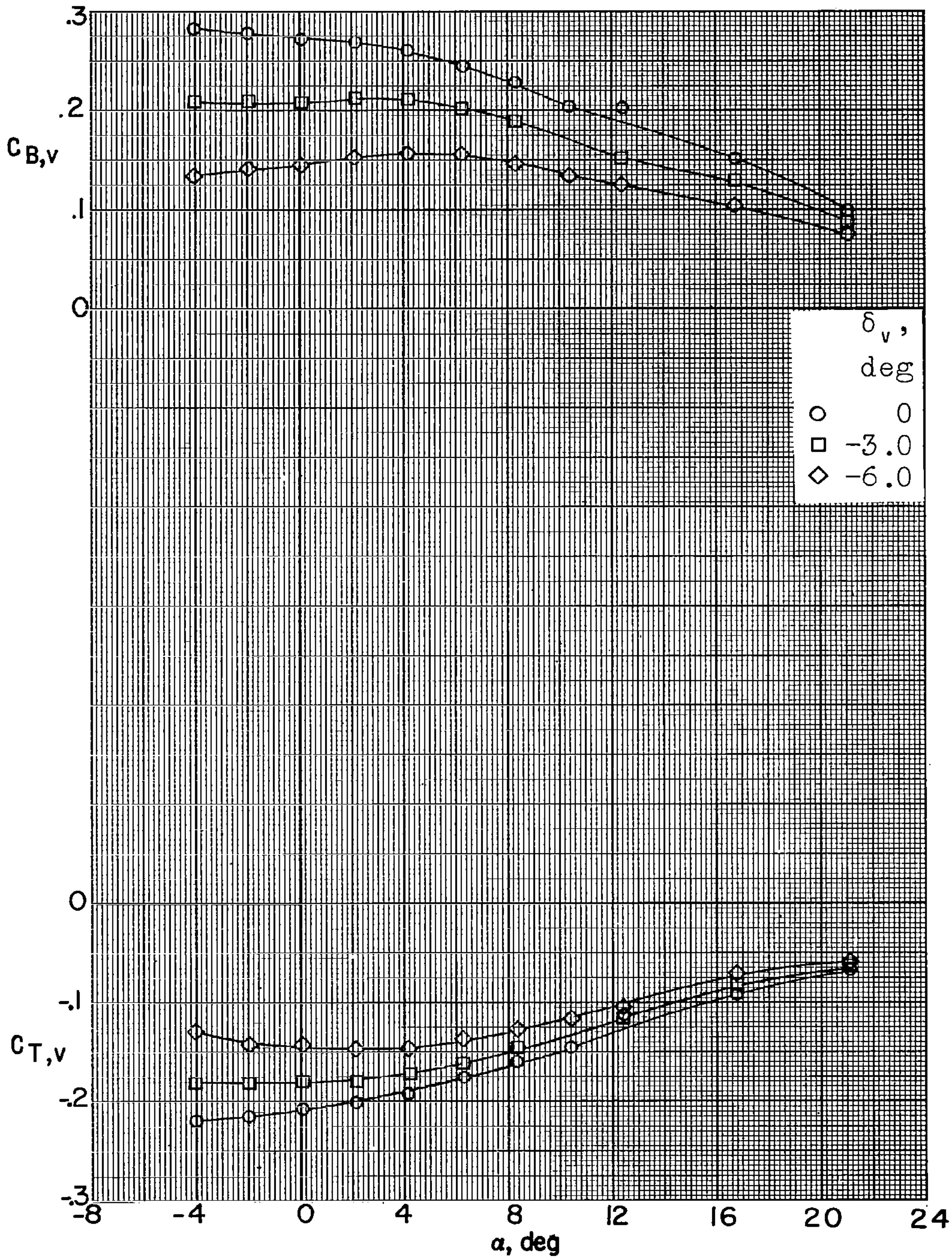

(g) $M = 3.96$; $\beta = -10.5^{\circ}$.

Figure 45.- Continued.

[redacted]

[redacted]

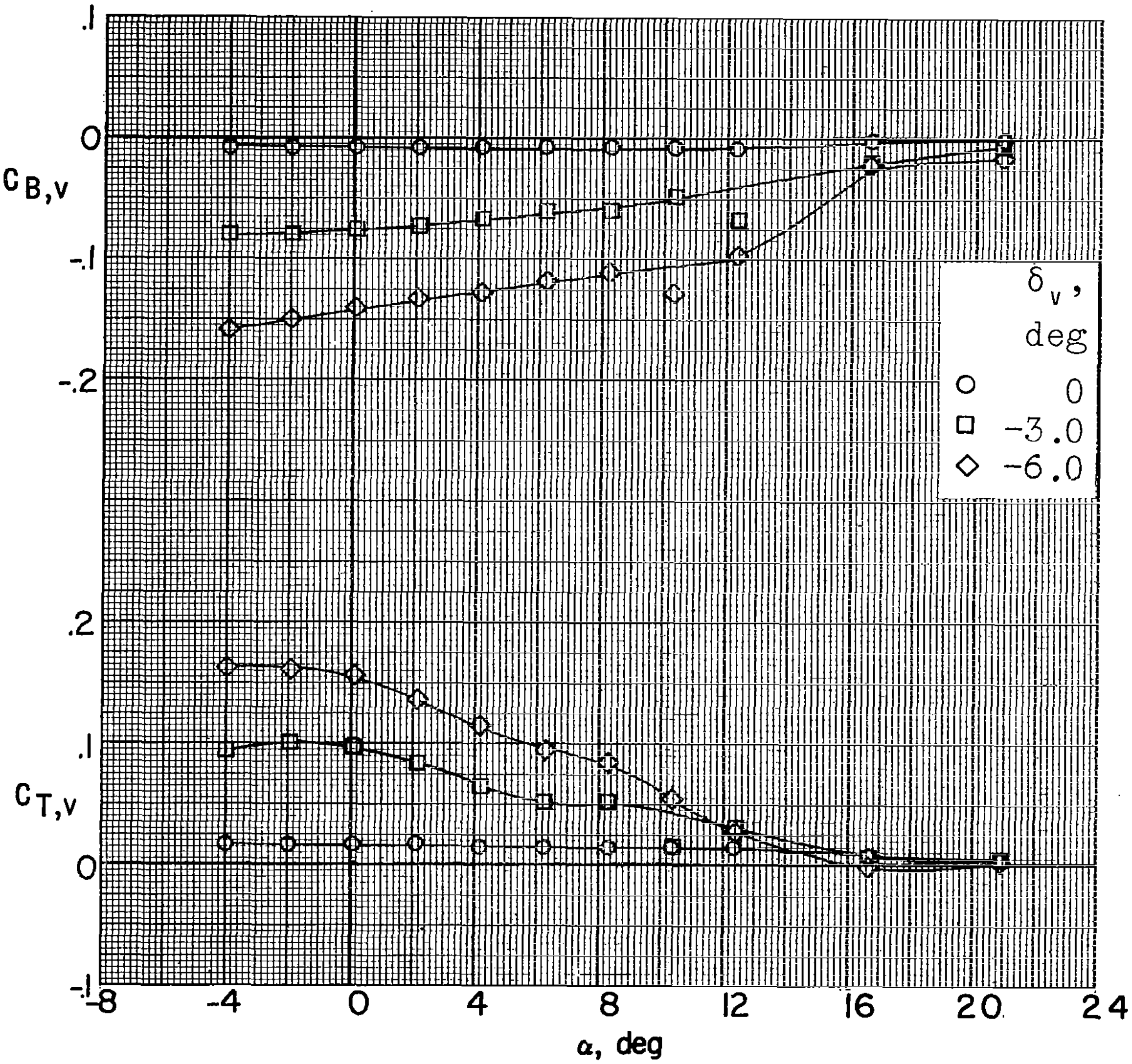

(h) $M = 4.65$; $\beta = 0^{\circ}$.

Figure 45.- Continued.

L-229

[redacted]

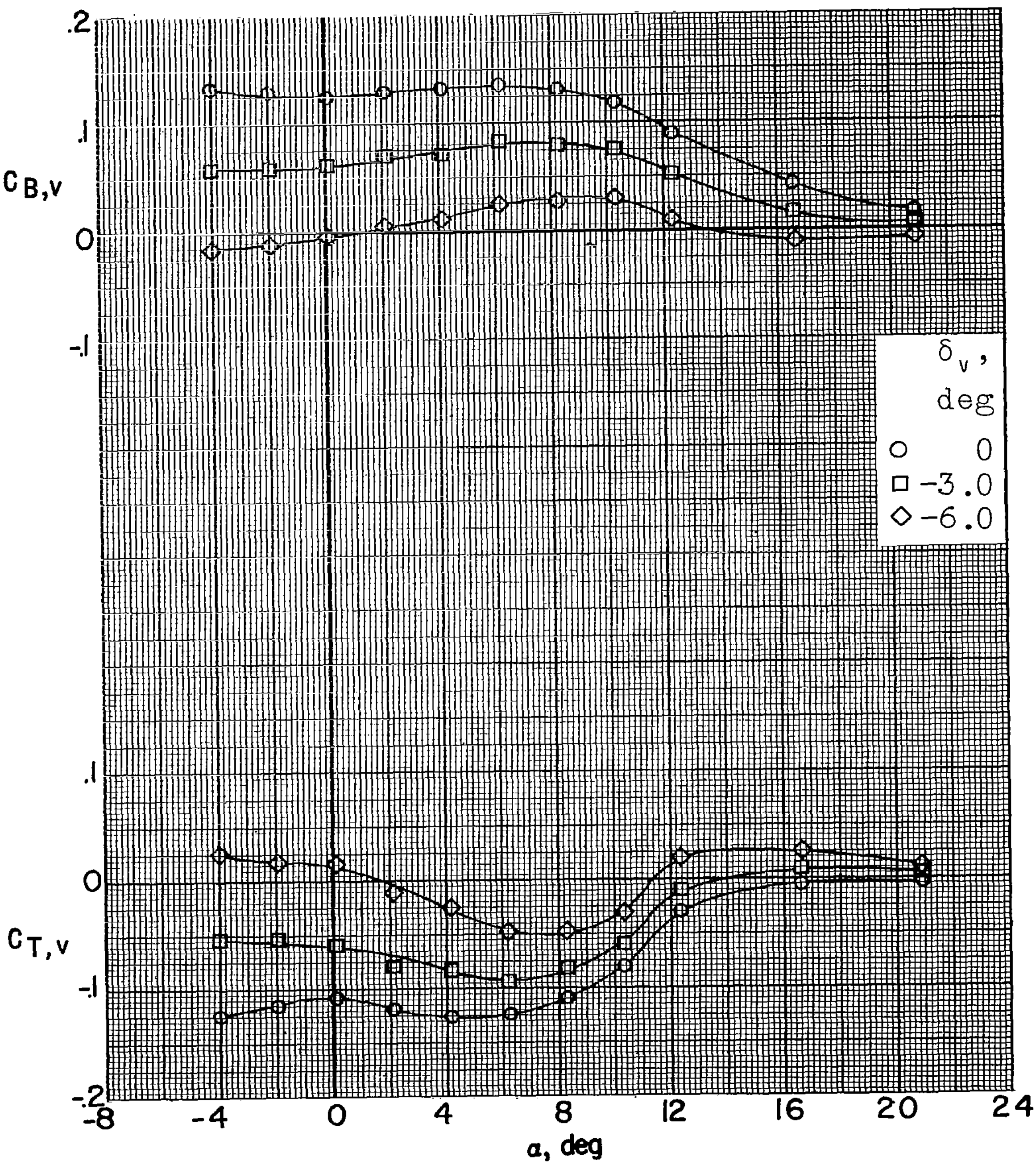

(i) $M = 4.65$; $\beta = -5.1^{\circ}$.

Figure 45.- Continued.

[redacted]

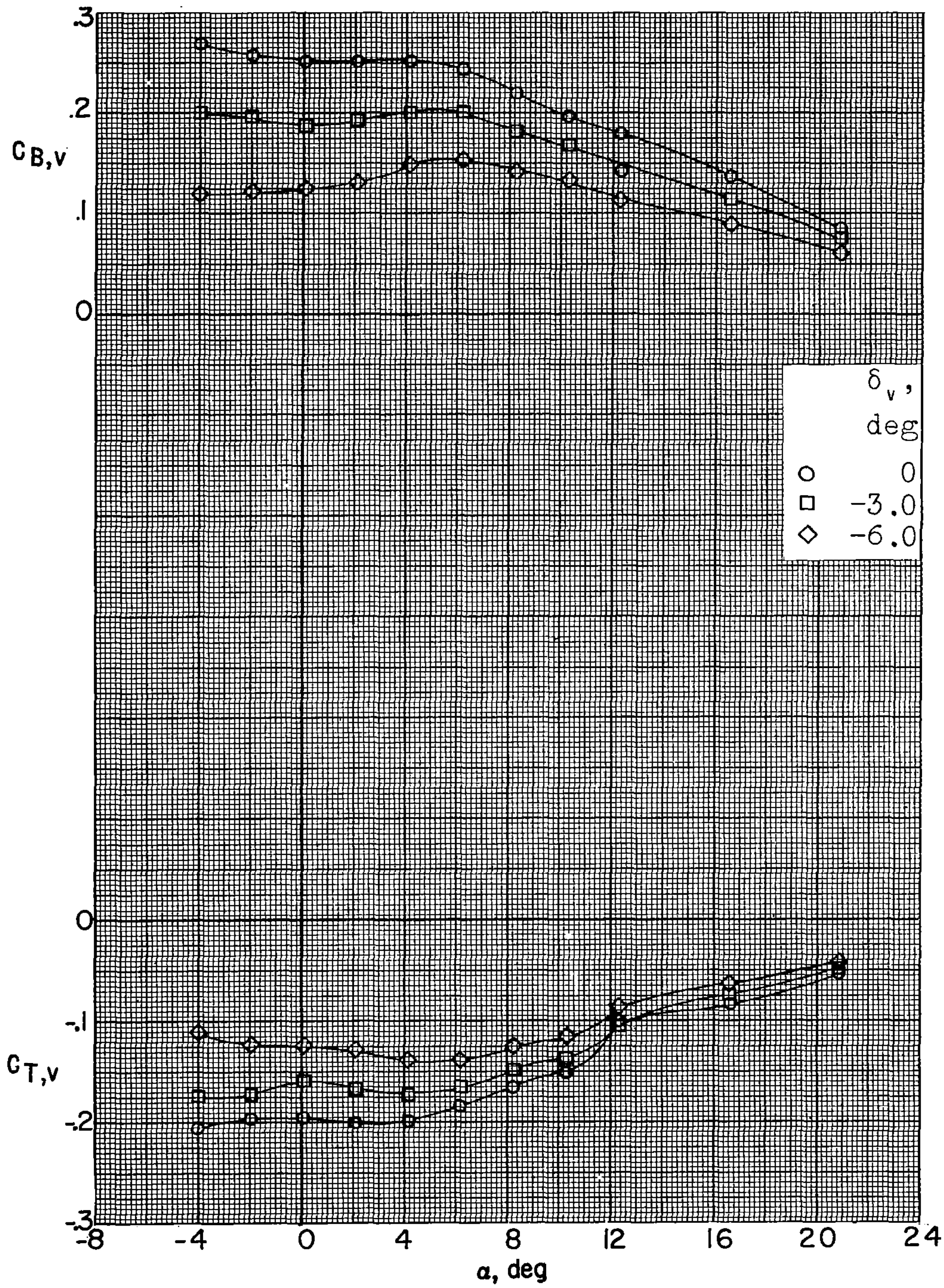

(j) M = 4.65; β = -10.5°.

Figure 45.- Concluded.

[redacted]

[redacted]

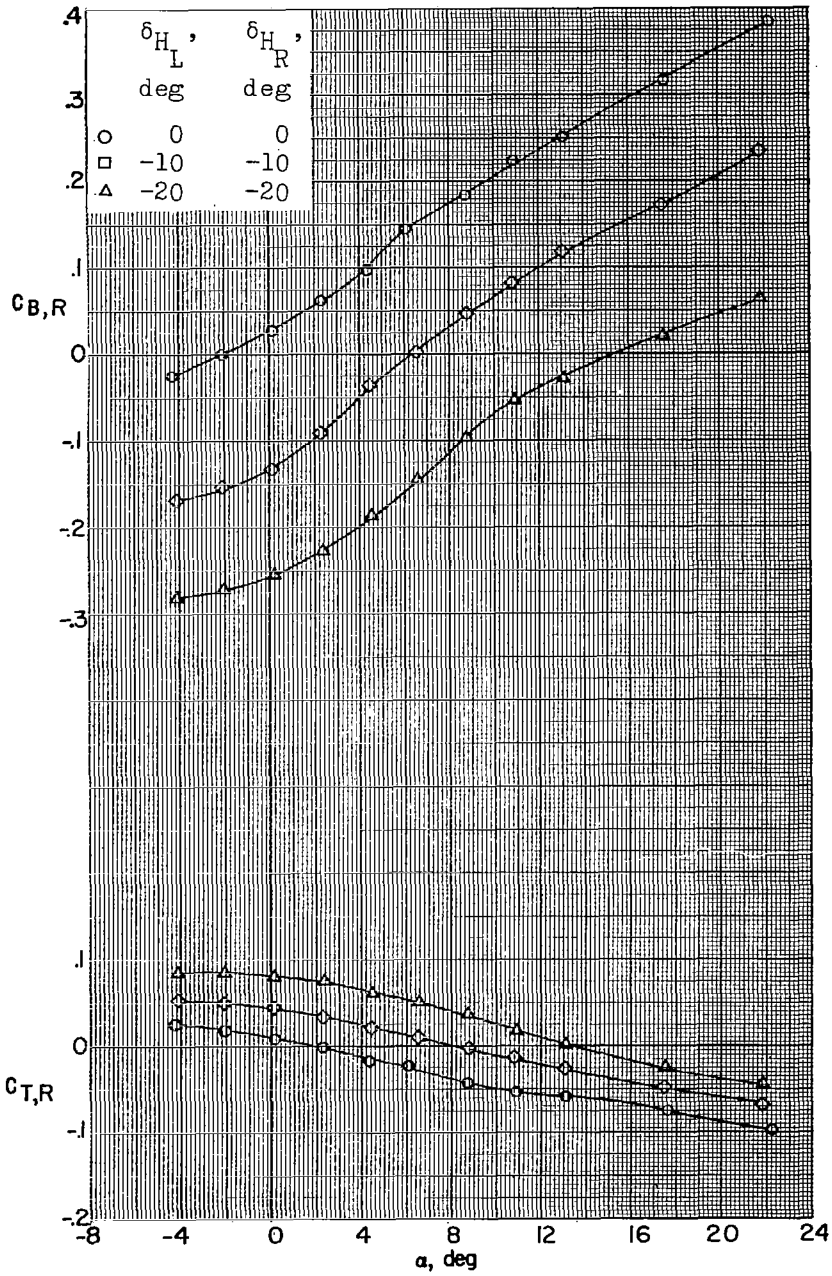

(a) M = 2.29.

Figure 46.- Bending- and torsion-moment characteristics of the right horizontal-tail panel of a 0.067-scale model of the X-15 airplane with pitch-control deflections of the horizontal tail. $\beta = 0^{\circ}$.

[redacted]

[redacted]

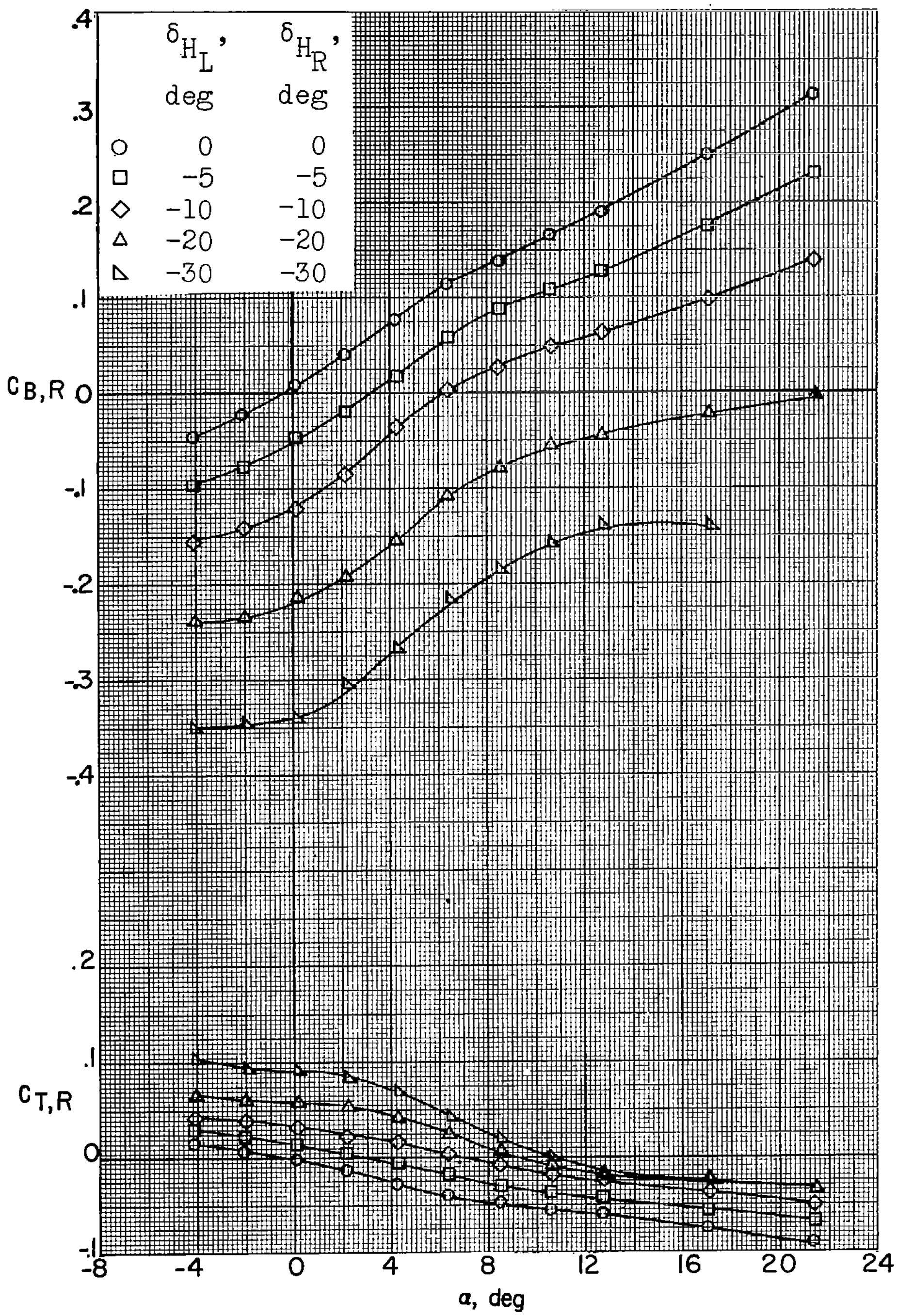

(b) M = 2.98.

Figure 46.- Continued.

[redacted]

L-229

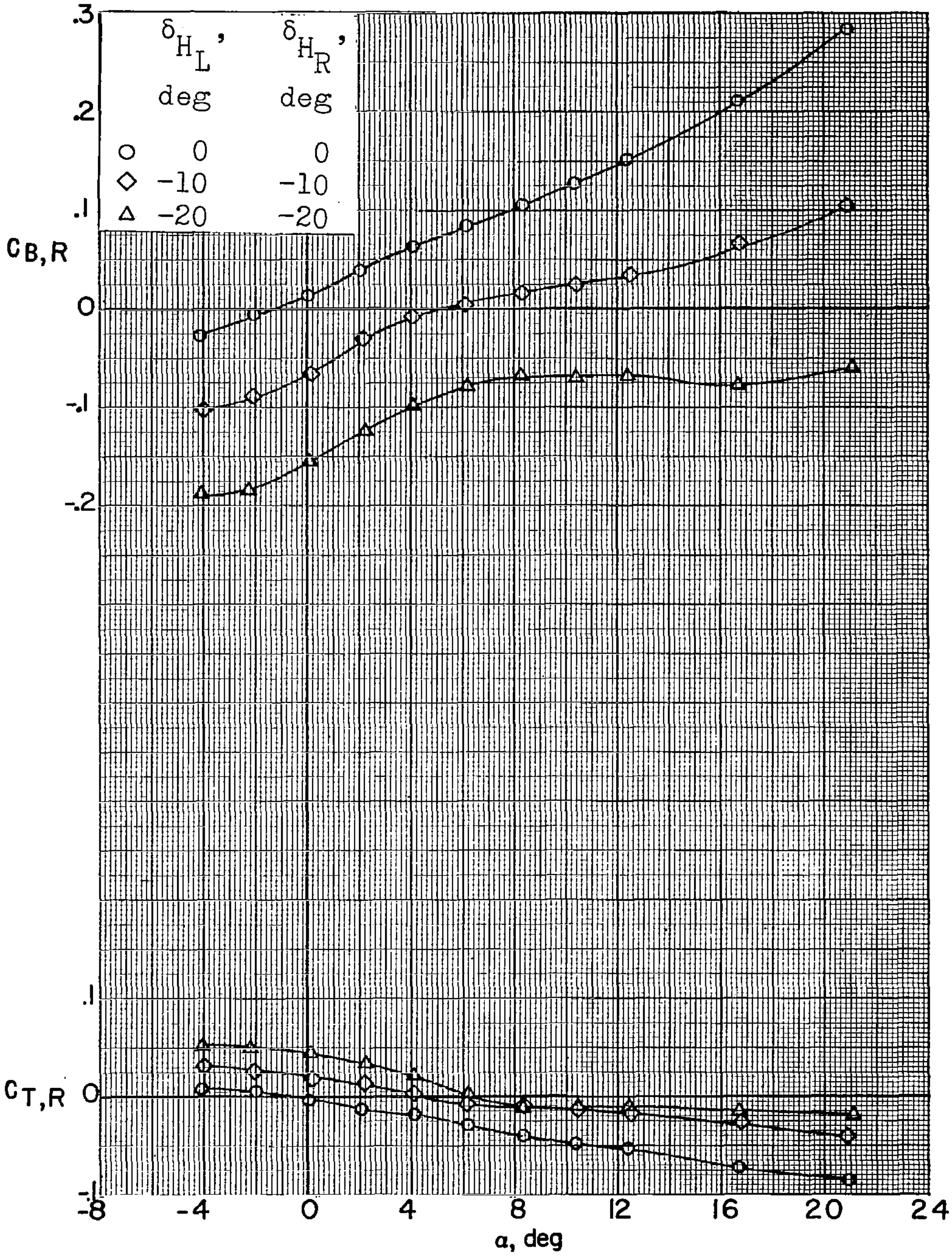

(c) M = 3.96.

Figure 46.- Continued.

[redacted]

[redacted]

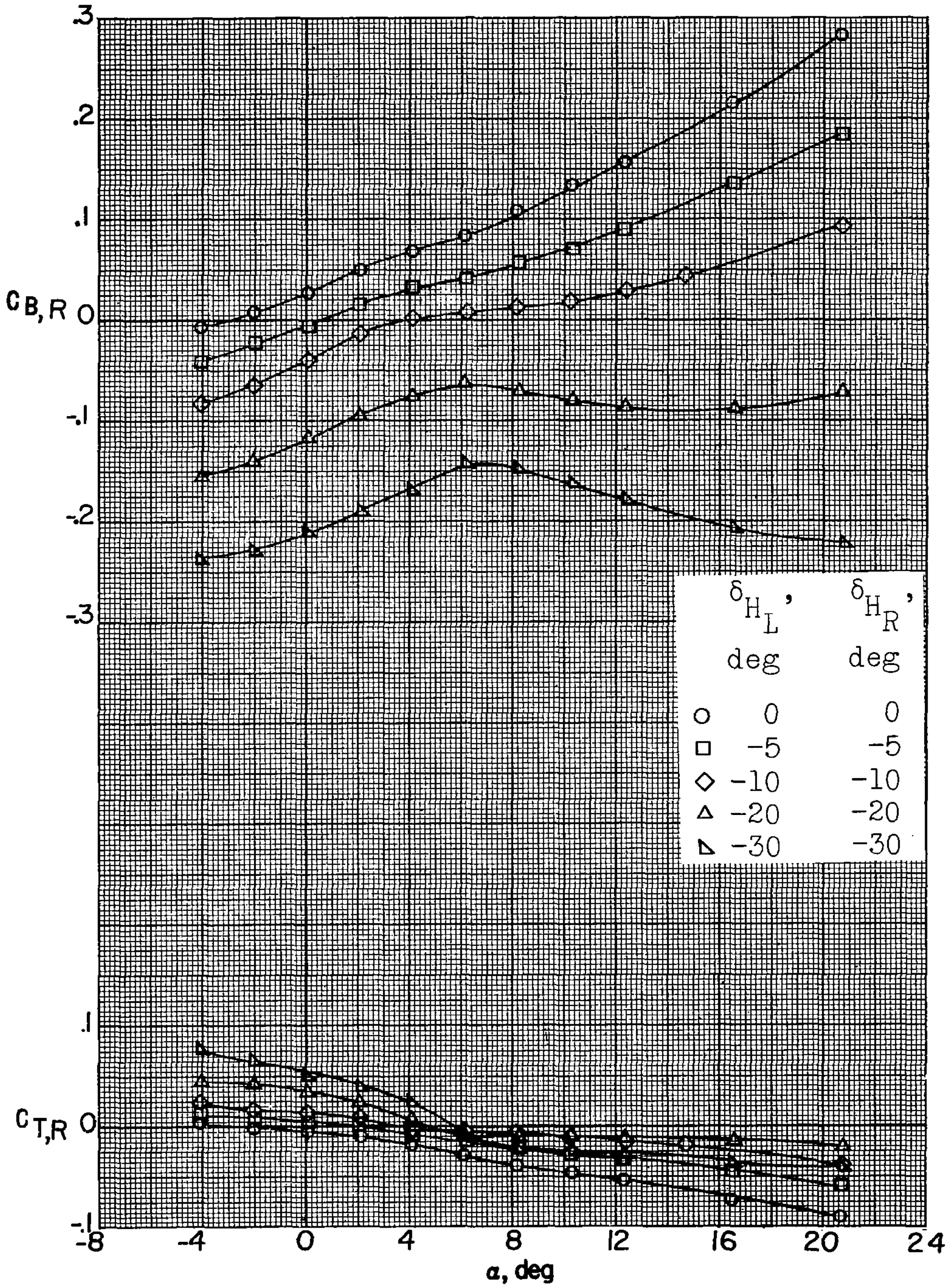

(d) M = 4.65.

Figure 46.- Concluded.

L-229

[redacted]

L-229

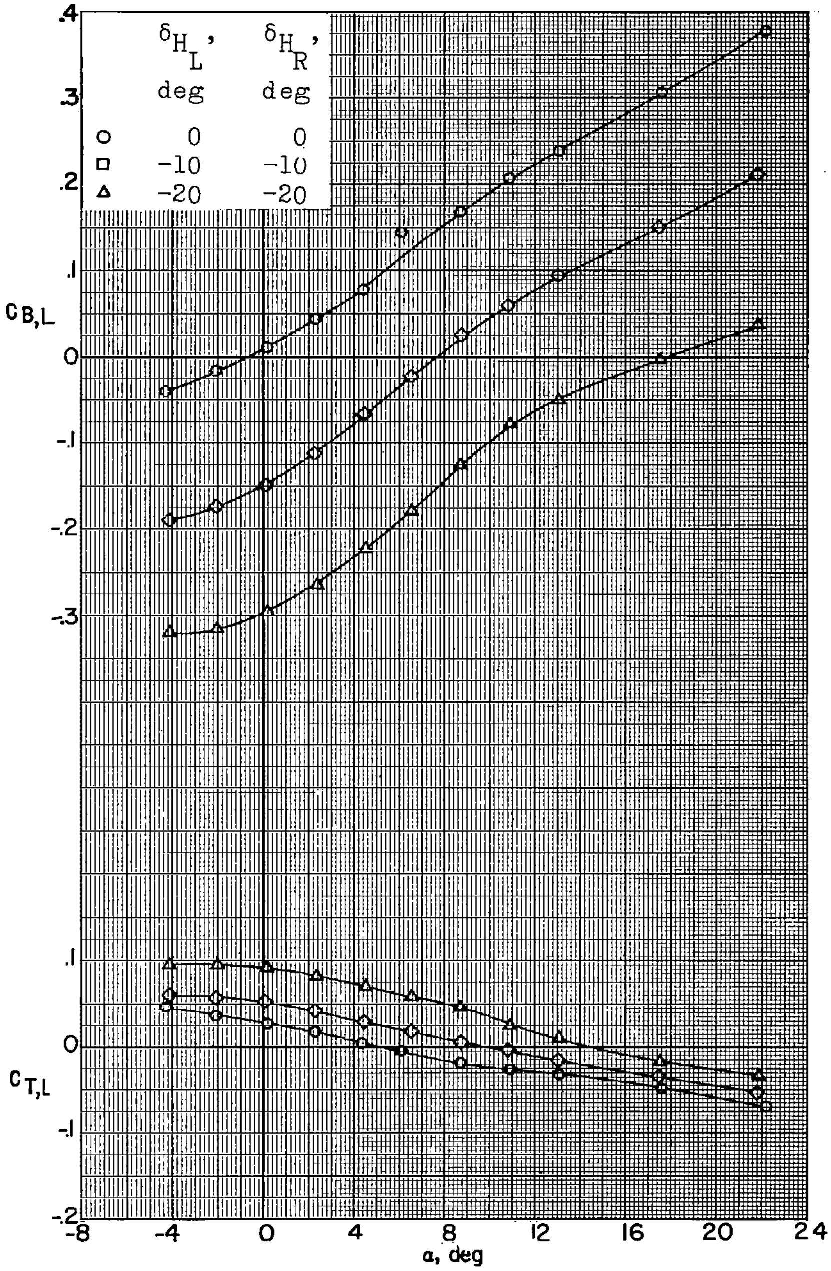

(a) M = 2.29.

Figure 47.- Bending- and torsion-moment characteristics of the left horizontal-tail panel of a 0.067-scale model of the X-15 airplane with pitch-control deflections of the horizontal tail. $\beta = 0^{\circ}$.

[redacted]

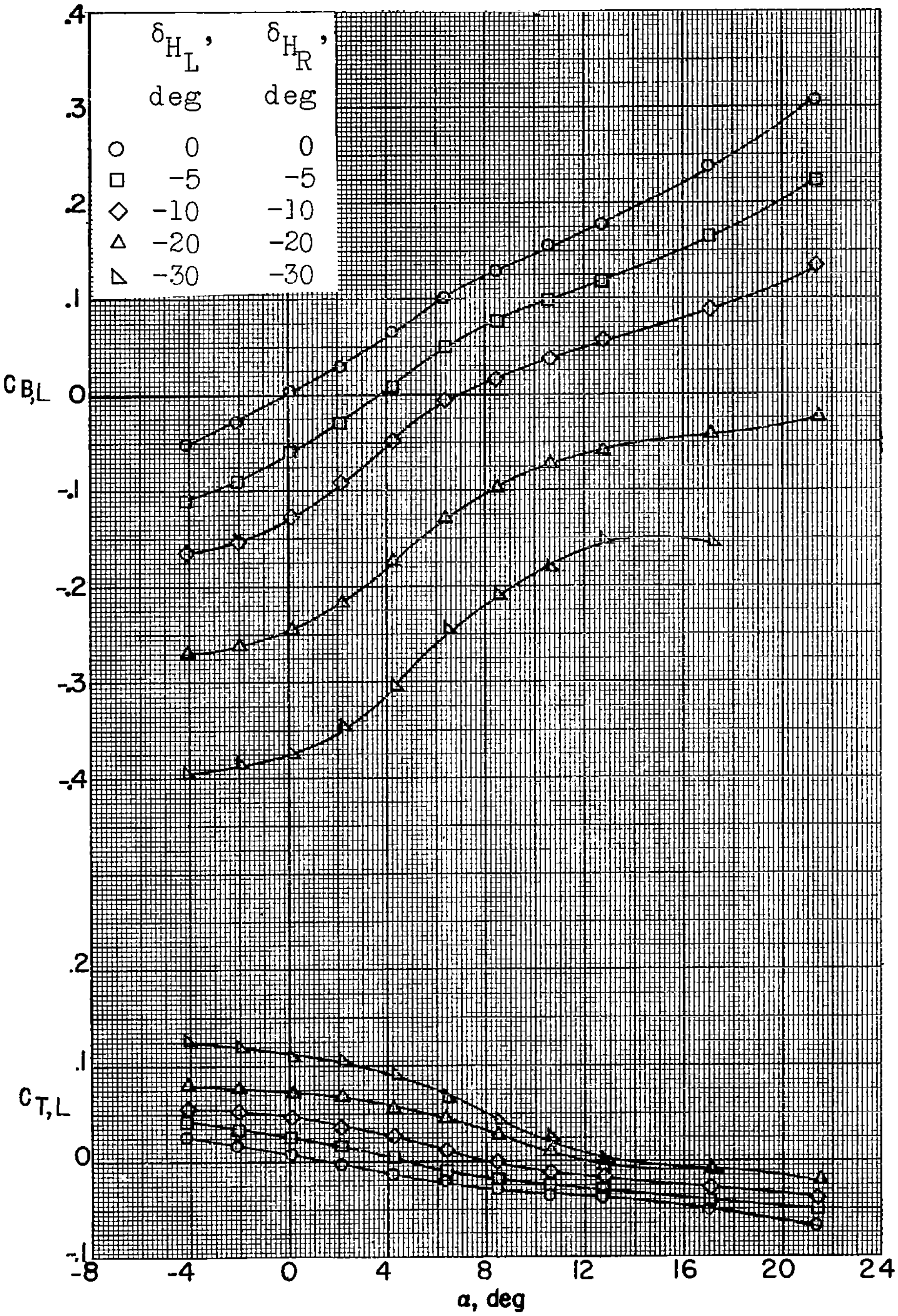

(b) $M = 2.98$.

Figure 47.- Continued.

L-229

[redacted]

[redacted]

L-229

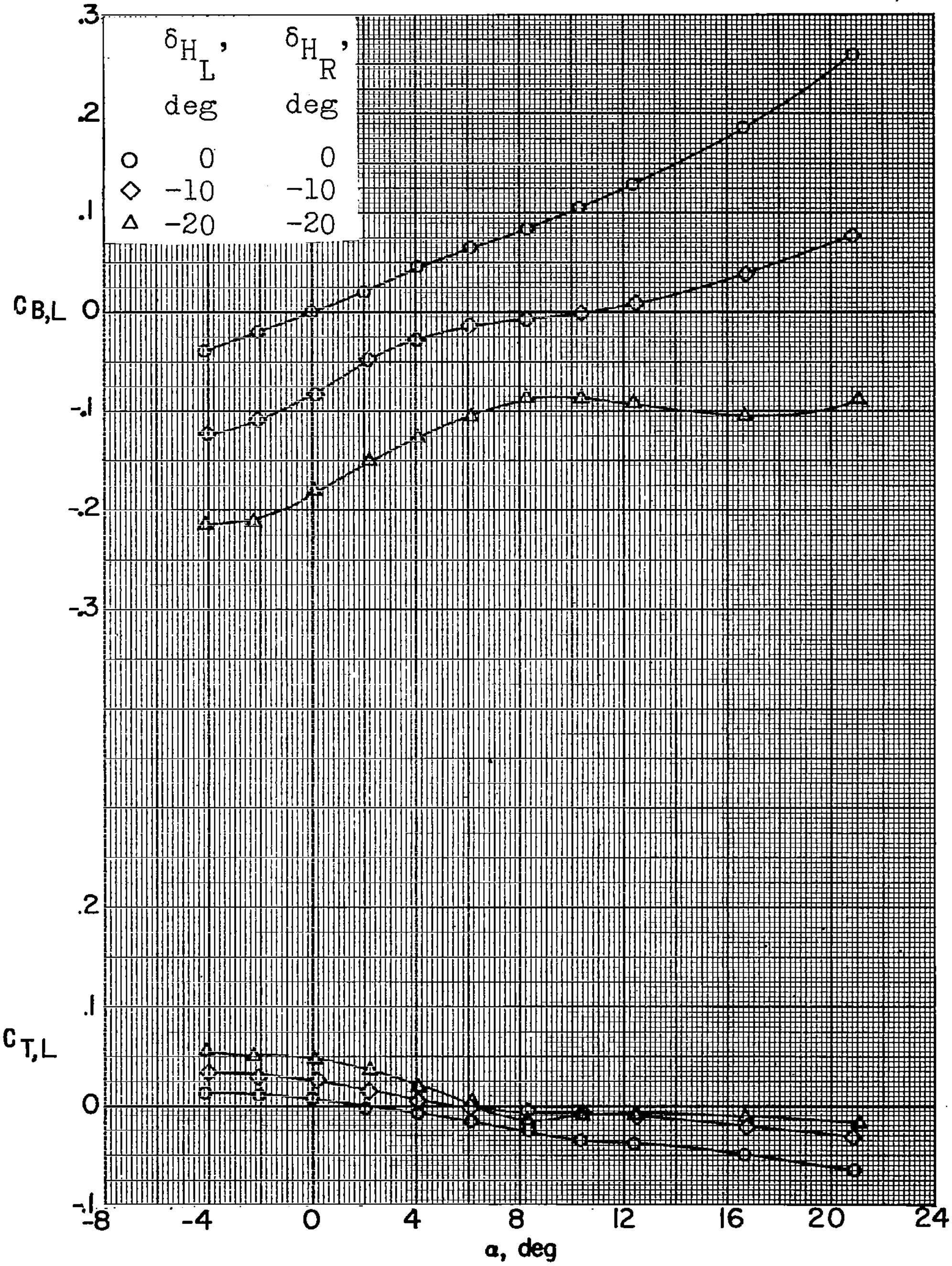

(c) M = 3.96.

Figure 47.- Continued.

[redacted]

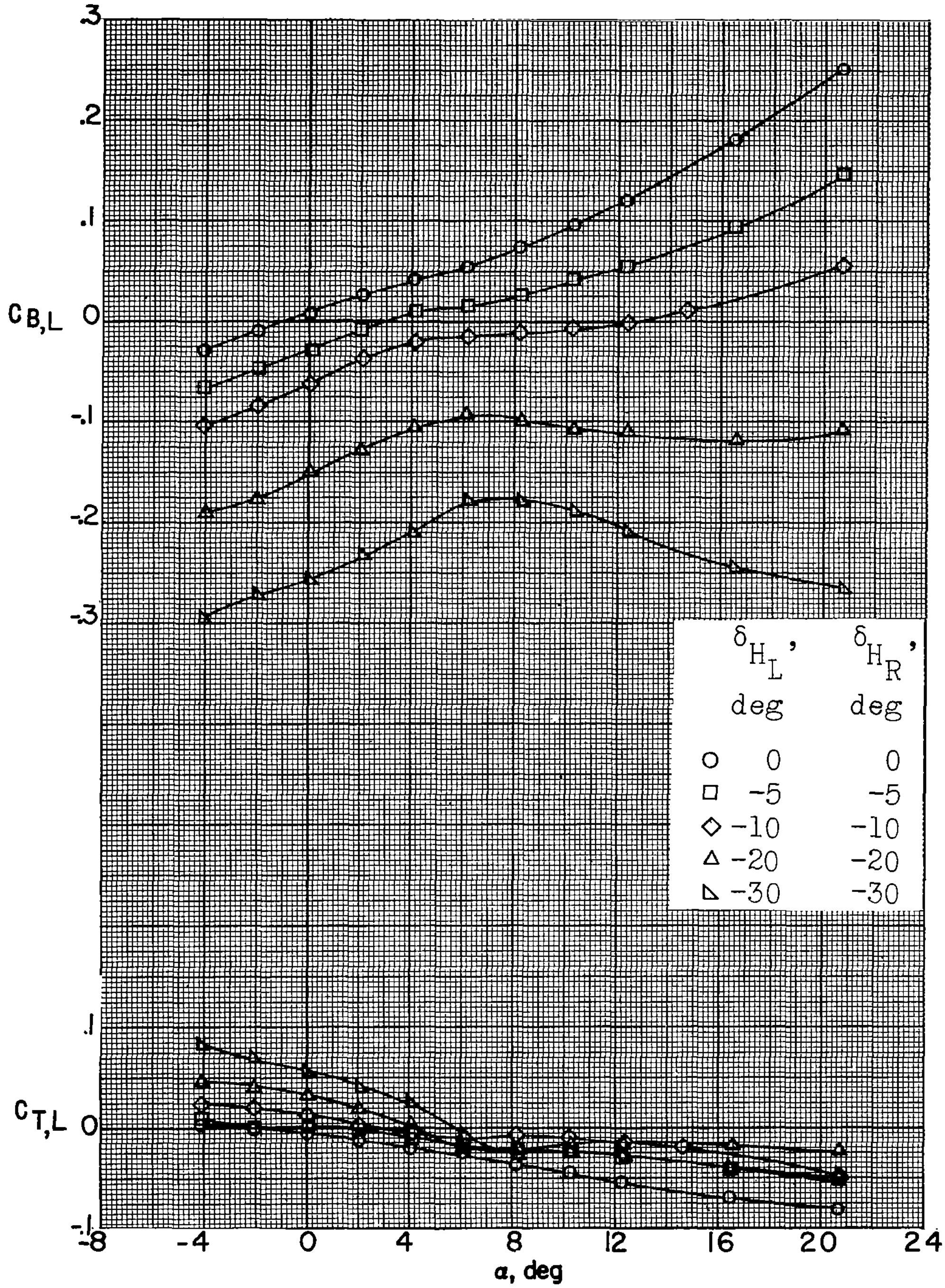

(d) M = 4.65.

Figure 47.- Concluded.

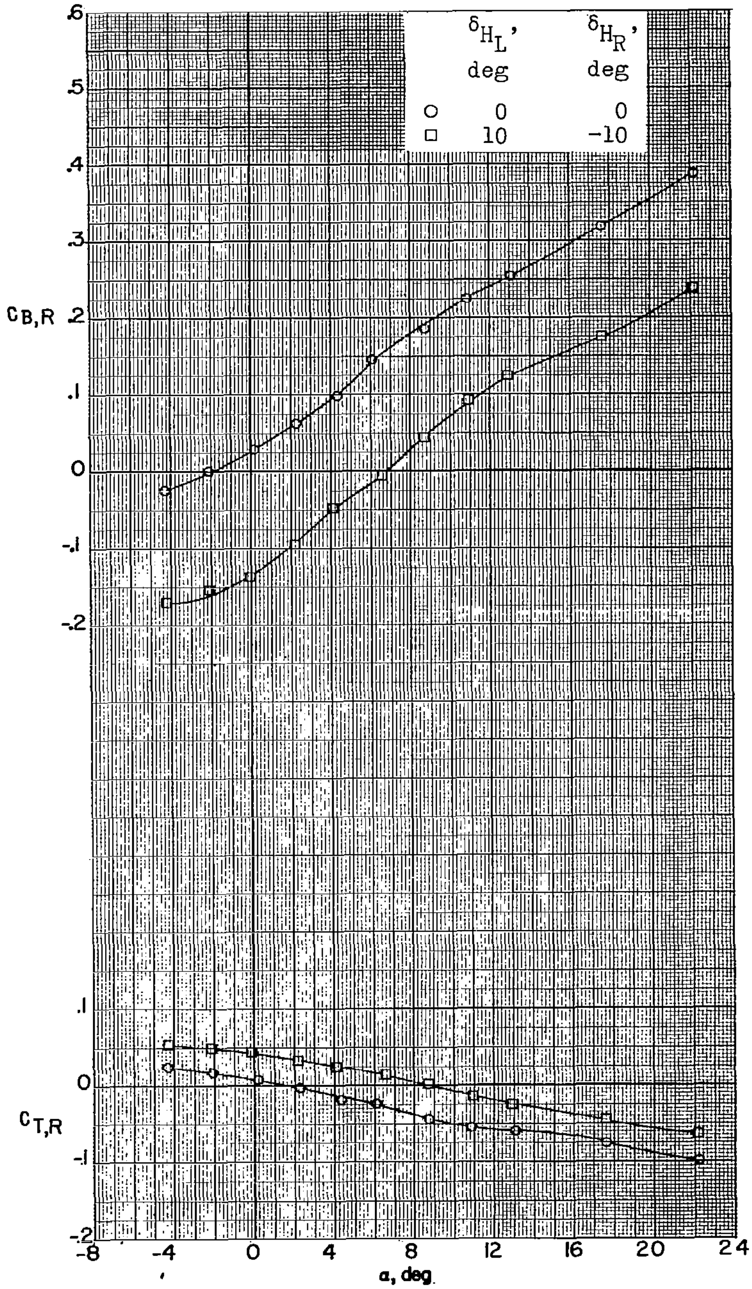

(a) M = 2.29; β = 0°.

Figure 48.- Bending- and torsion-moment characteristics of the right horizontal-tail panel of a 0.067-scale model of the X-15 airplane with roll-control deflections of the horizontal tail.

[redacted]

[redacted]

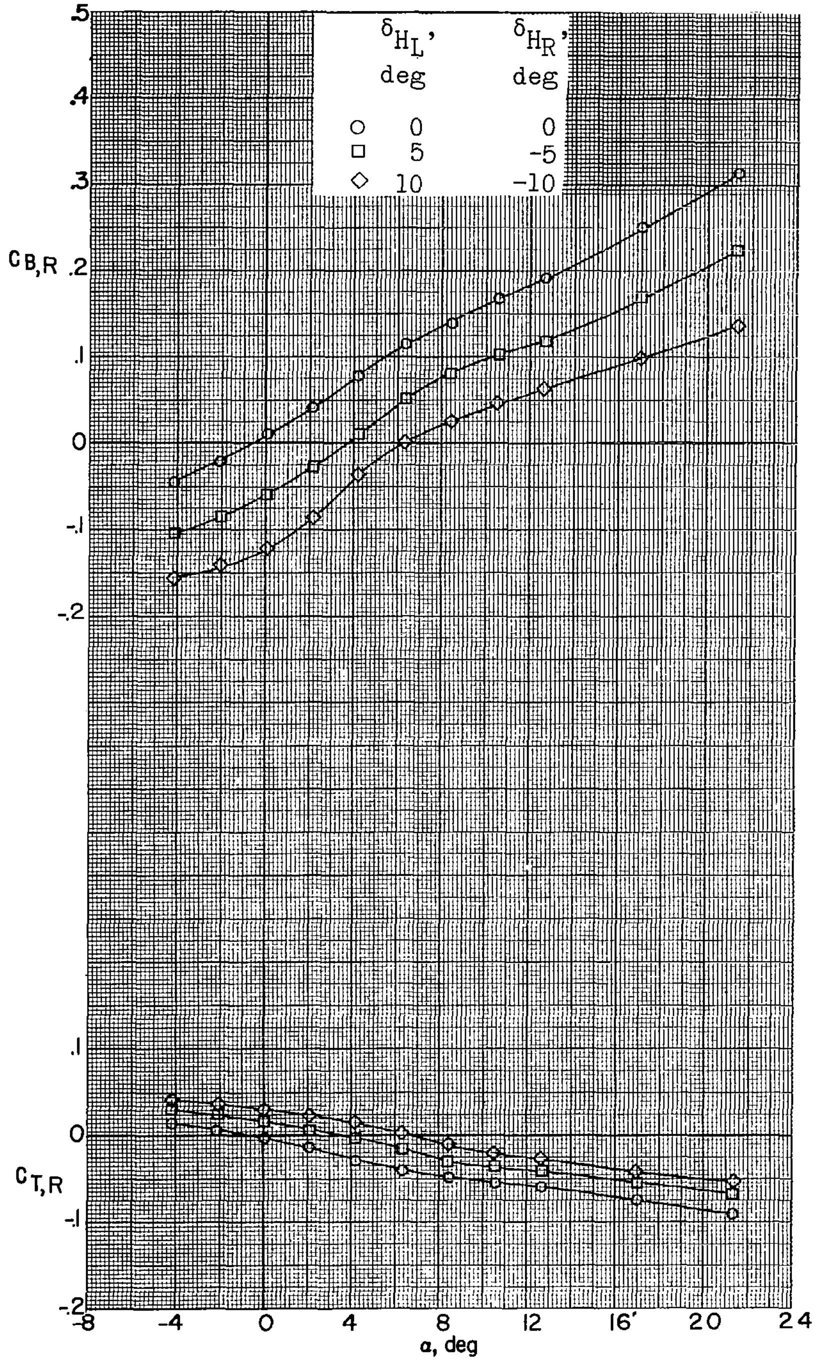

(b) M = 2.98; β = 0°.

Figure 48.- Continued.

[redacted]

L-229

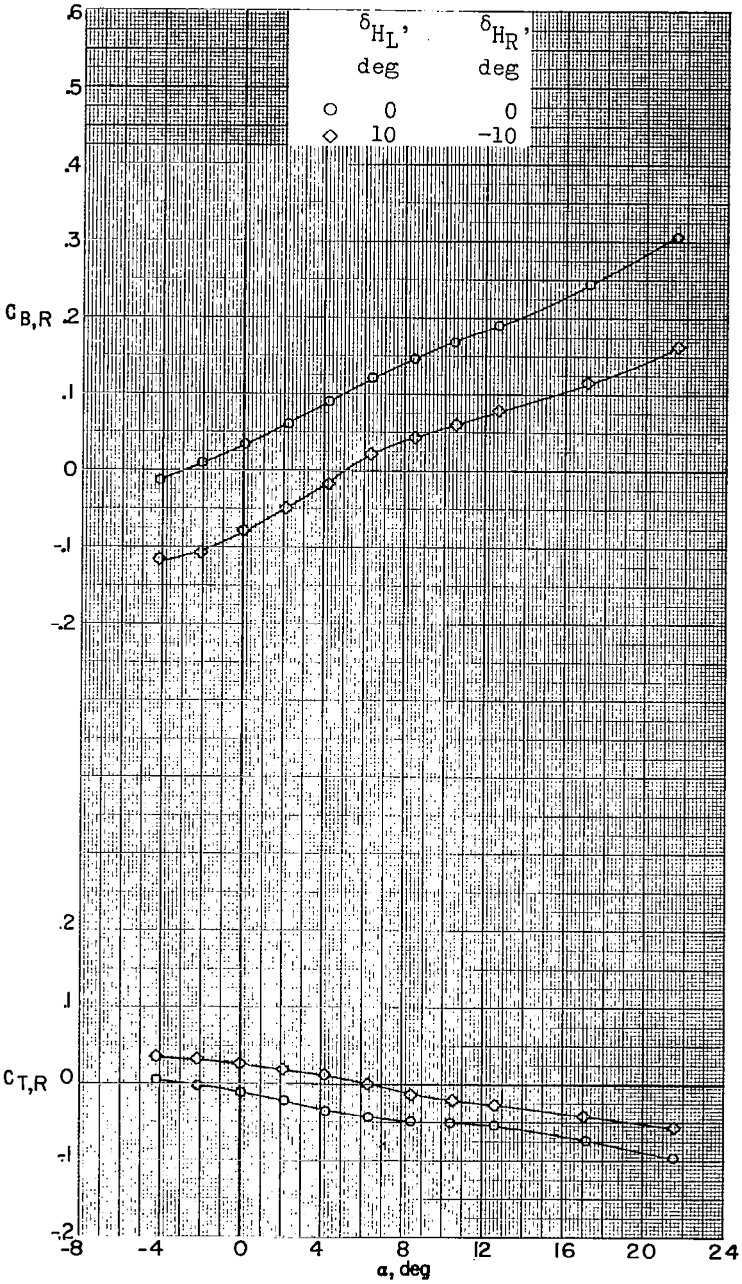

(c) M = 2.98; β = -5.1°.

Figure 48.- Continued.

[redacted]

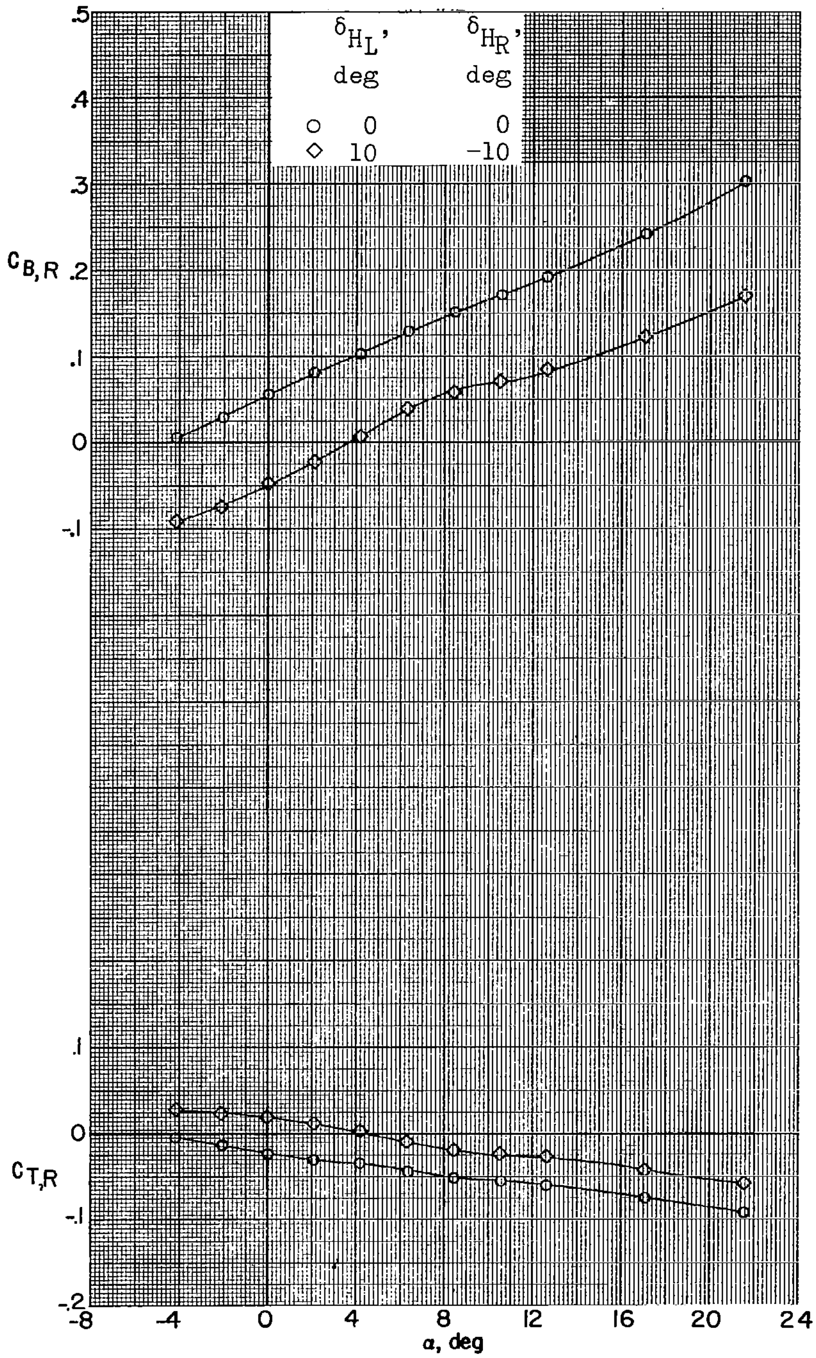

(d) $M = 2.98$; $\beta = -9.7^{\circ}$.

Figure 48.- Continued.

[redacted]

L-229

L-229

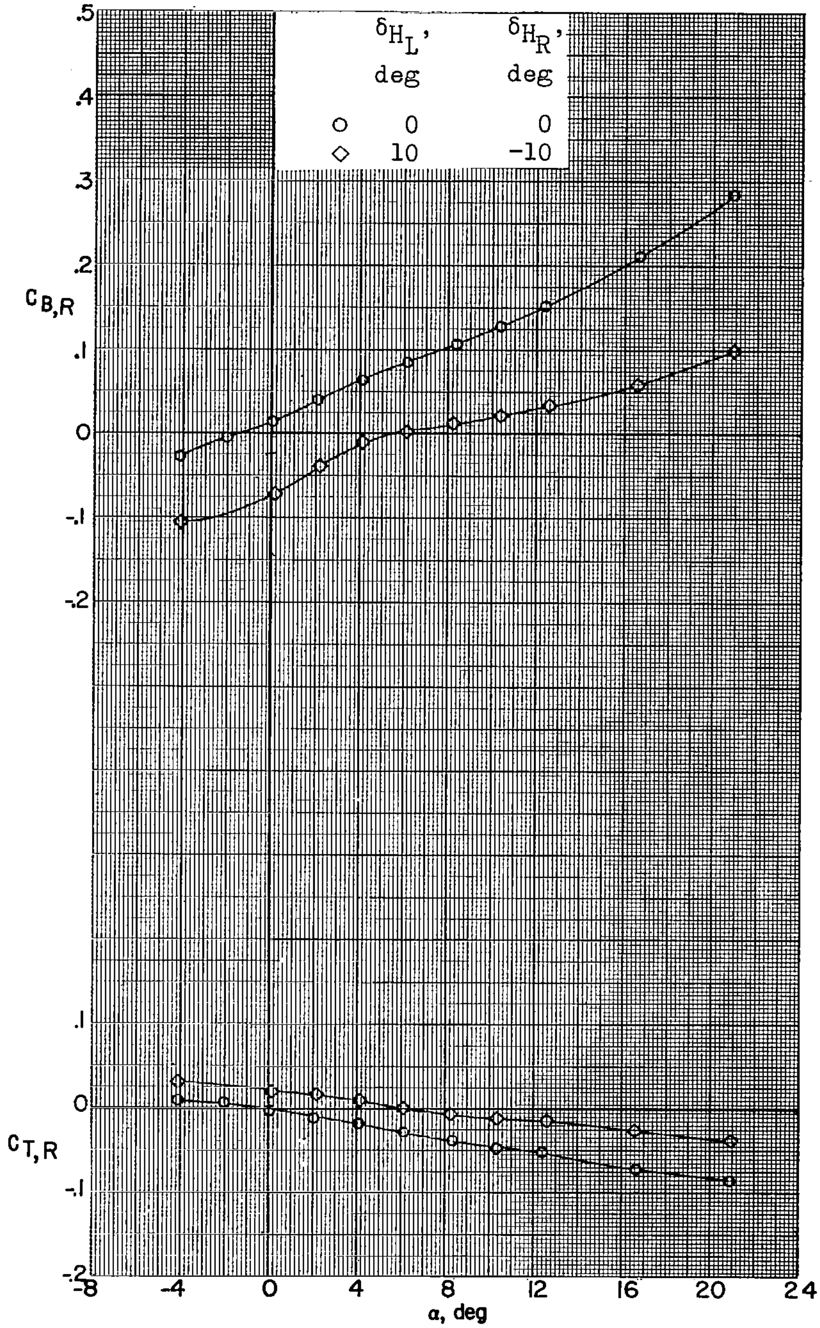

(e) $M = 3.96$; $\beta = 0^{\circ}$.

Figure 48.- Continued.

[redacted]

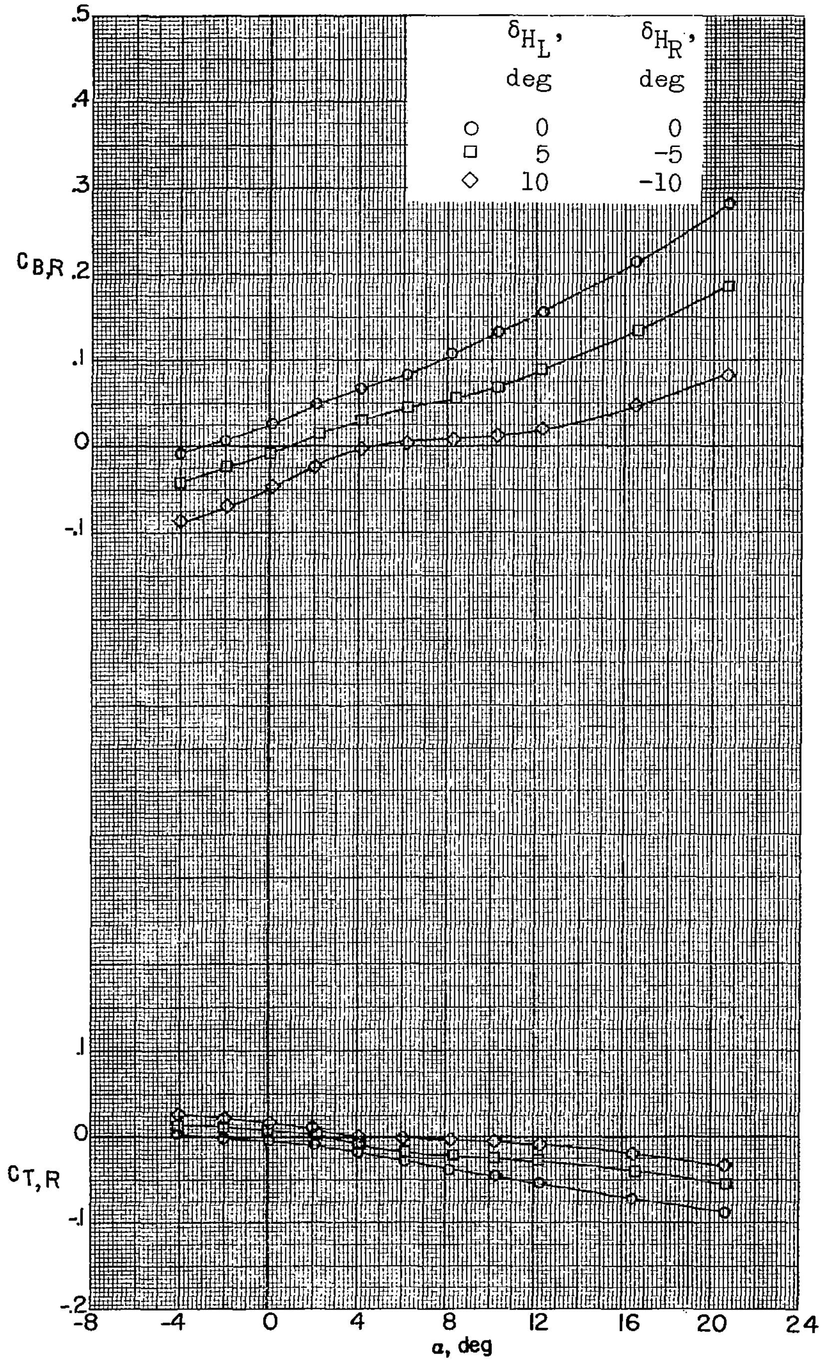

(f) $M = 4.65$; $\beta = 0.1^{\circ}$.

Figure 48.- Continued.

L-229

[redacted]

L-229

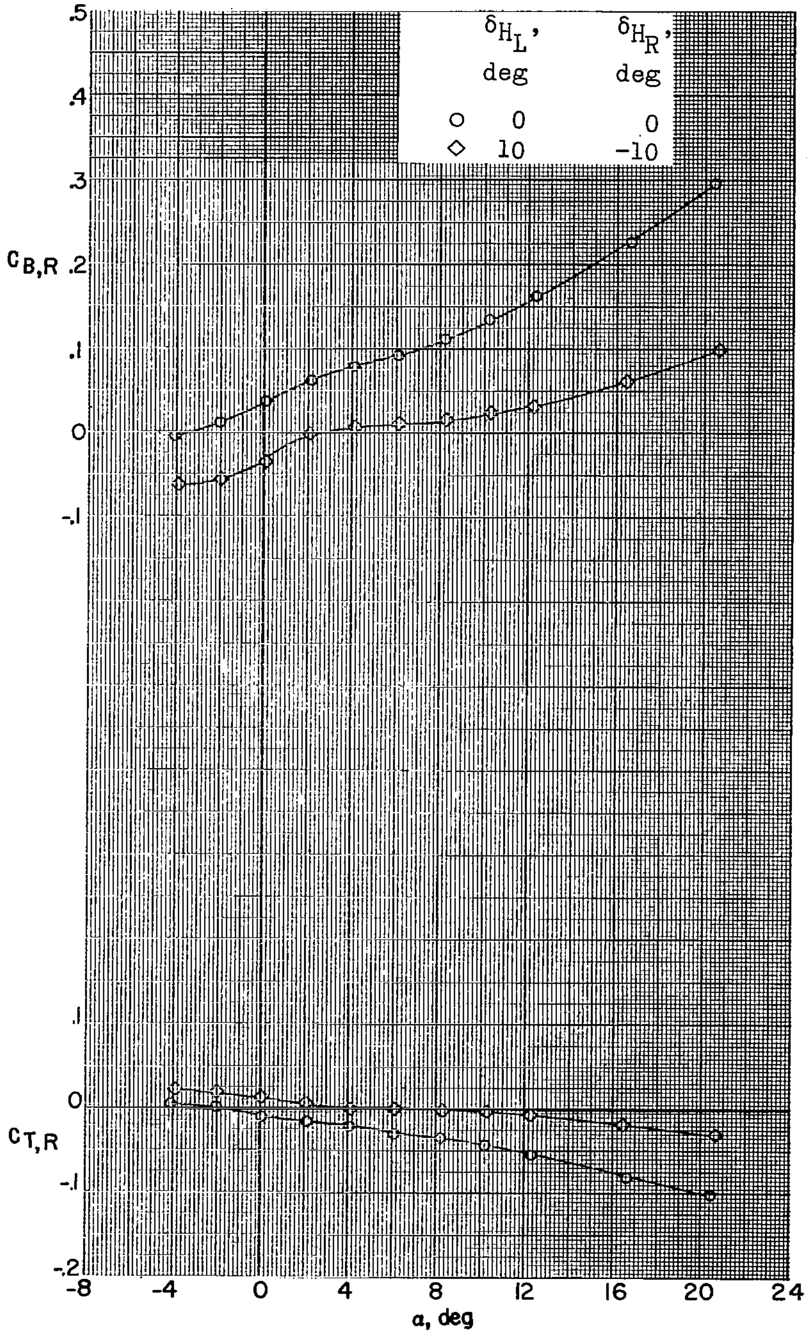

(g) $M = 4.65$; $\beta = -5.1^{\circ}$.

Figure 48.- Continued.

[redacted]

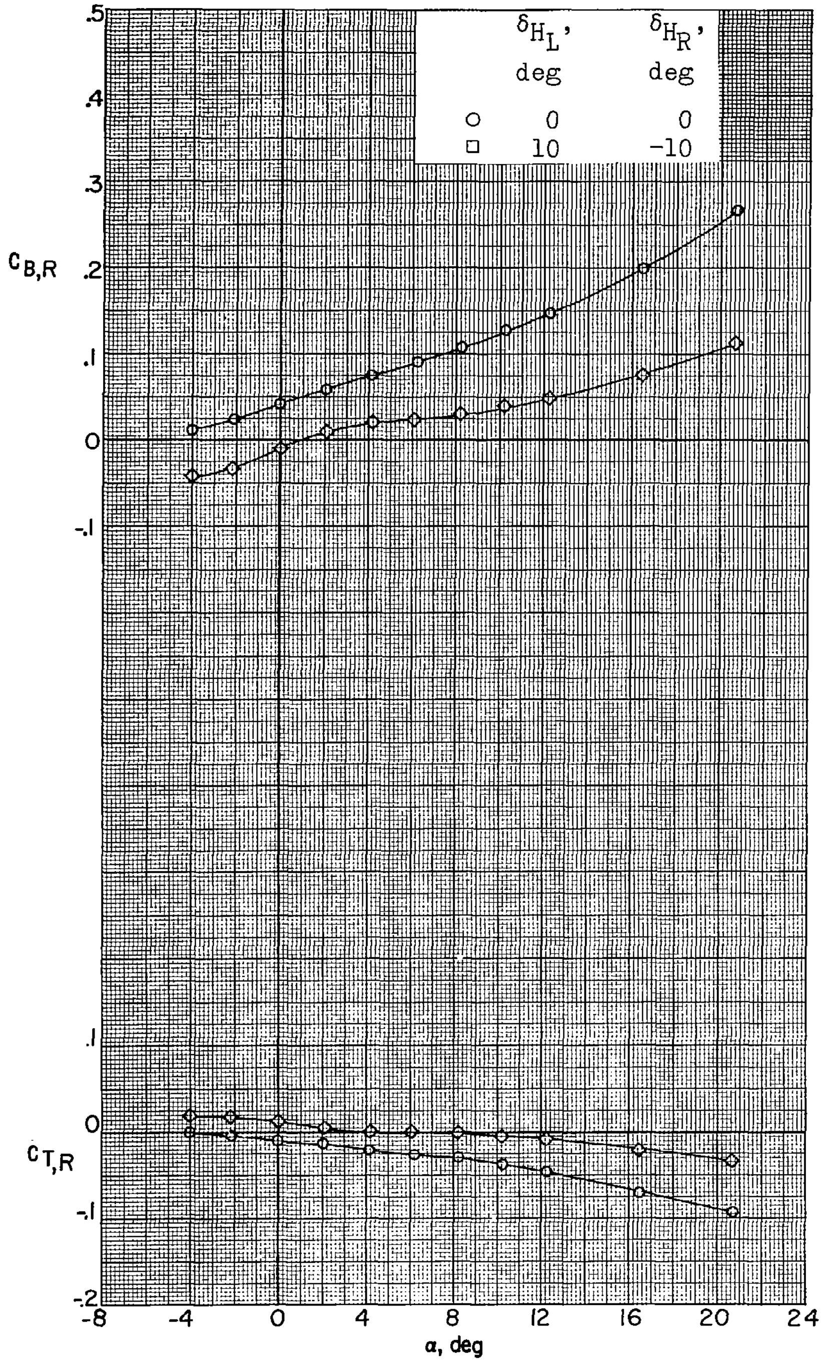

(h) M = 4.65; β = -10.6°.

Figure 48.- Concluded.

[redacted]

L-229

L-229

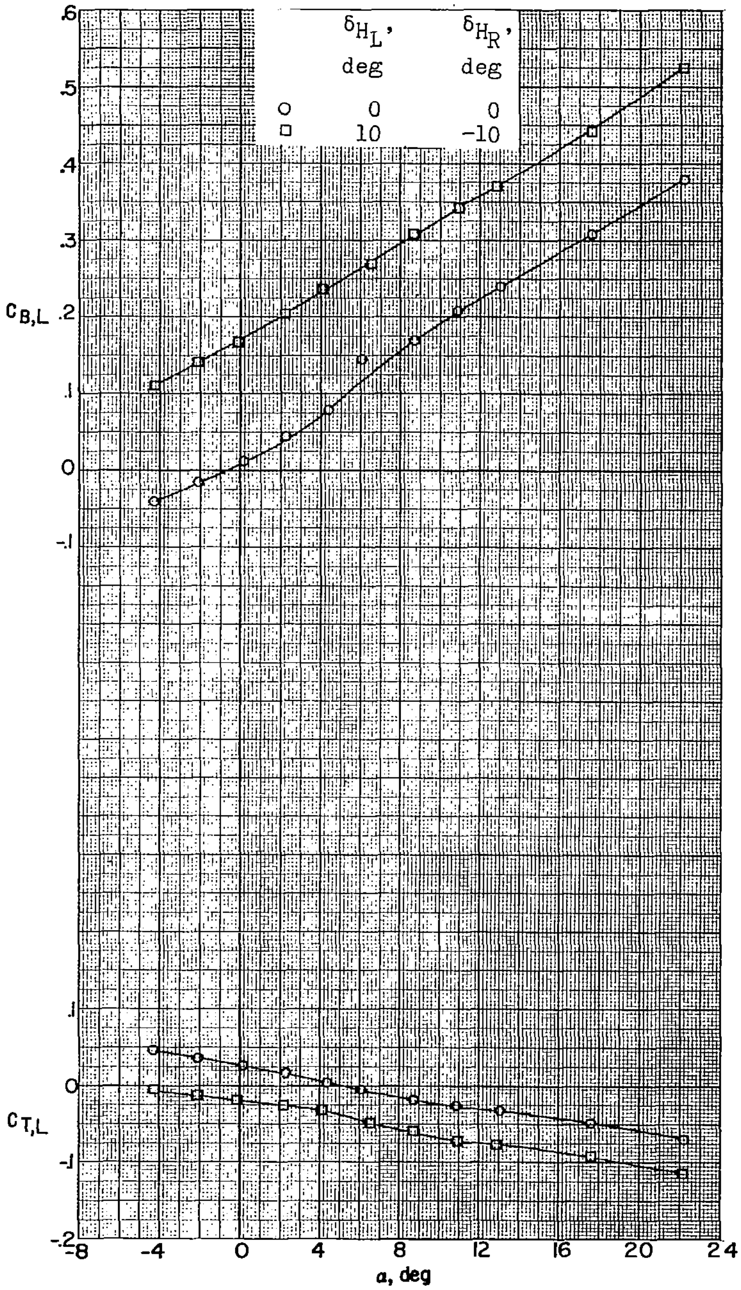

(a) M = 2.29; β = 0°.

Figure 49.- Bending- and torsion-moment characteristics of the left horizontal-tail panel of a 0.067-scale model of the X-15 airplane with roll-control deflections of the horizontal tail.

[redacted]

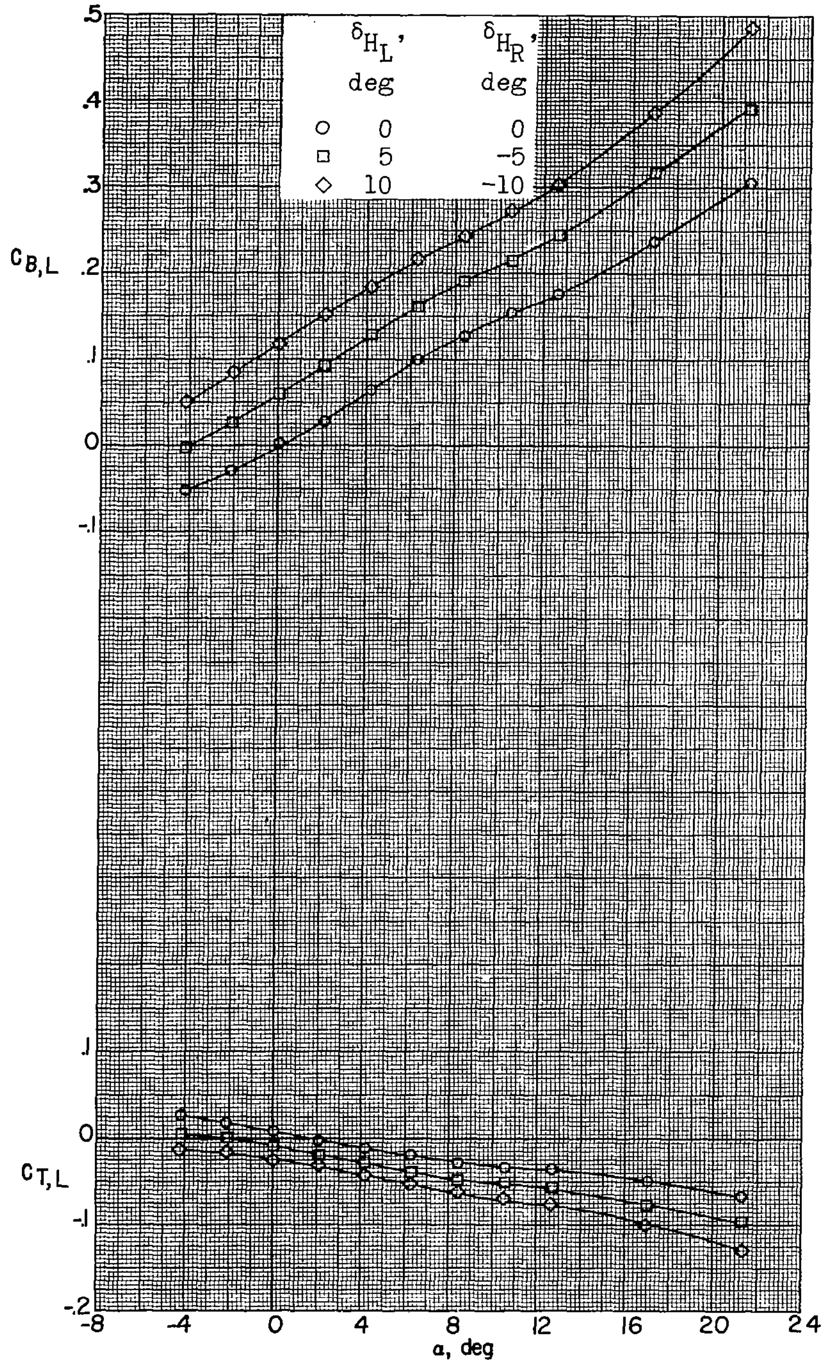

(b) M = 2.98; β = 0°.

Figure 49.- Continued.

L-229

[redacted]

L-229

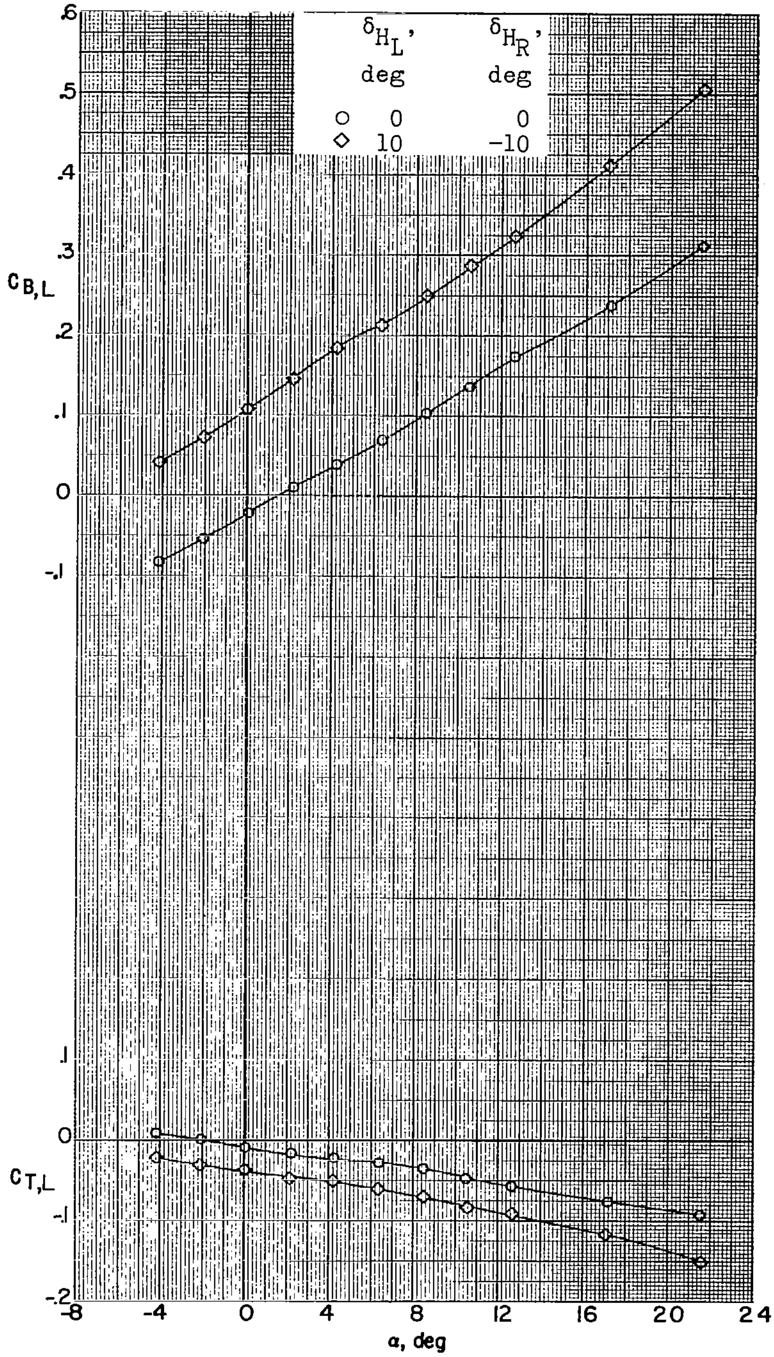

(c) M = 2.98; β = -5.1°.

Figure 49.- Continued.

[redacted]

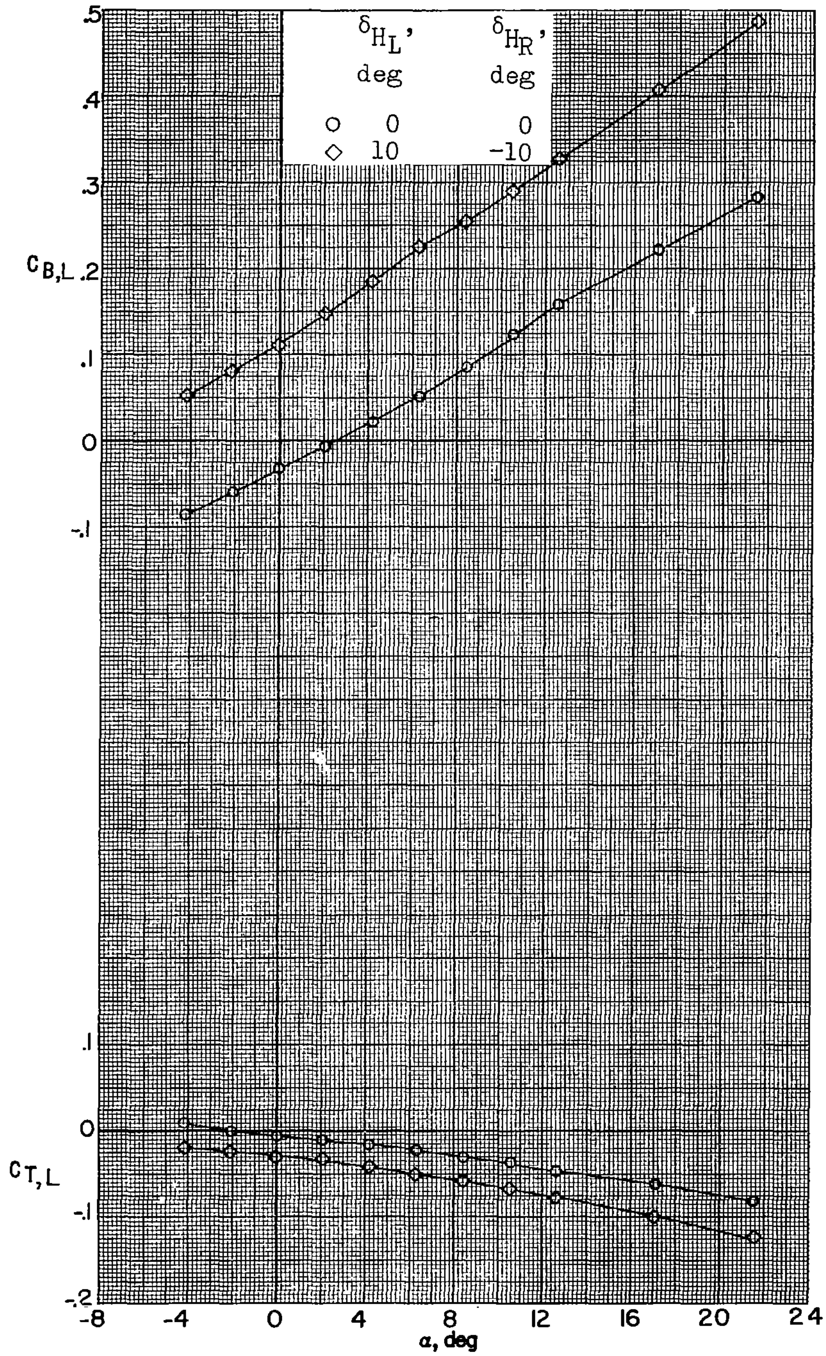

(d) M = 2.98; β = -9.7°.

Figure 49.- Continued.

L-229

[redacted]

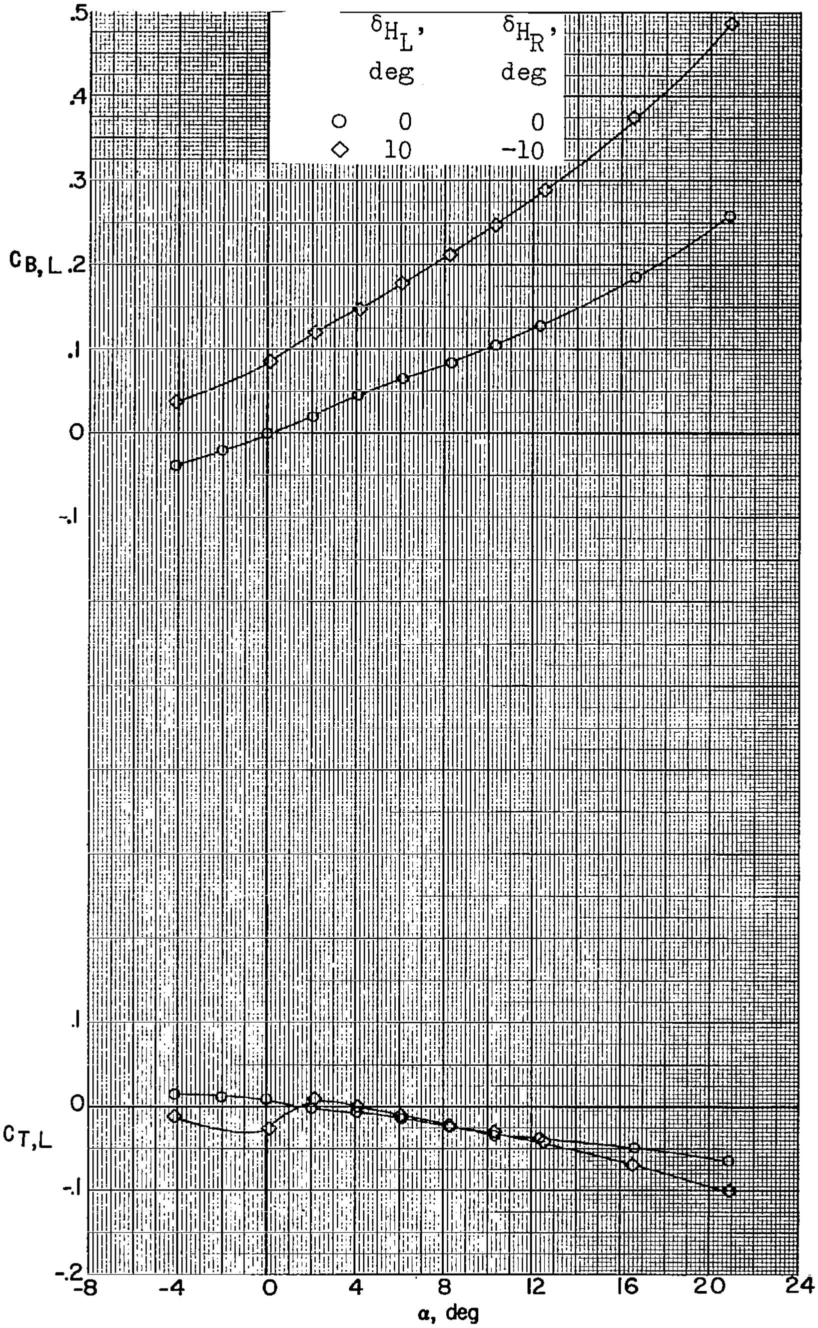

(e) M = 3.96; β = 0°.

Figure 49.- Continued.

[redacted]

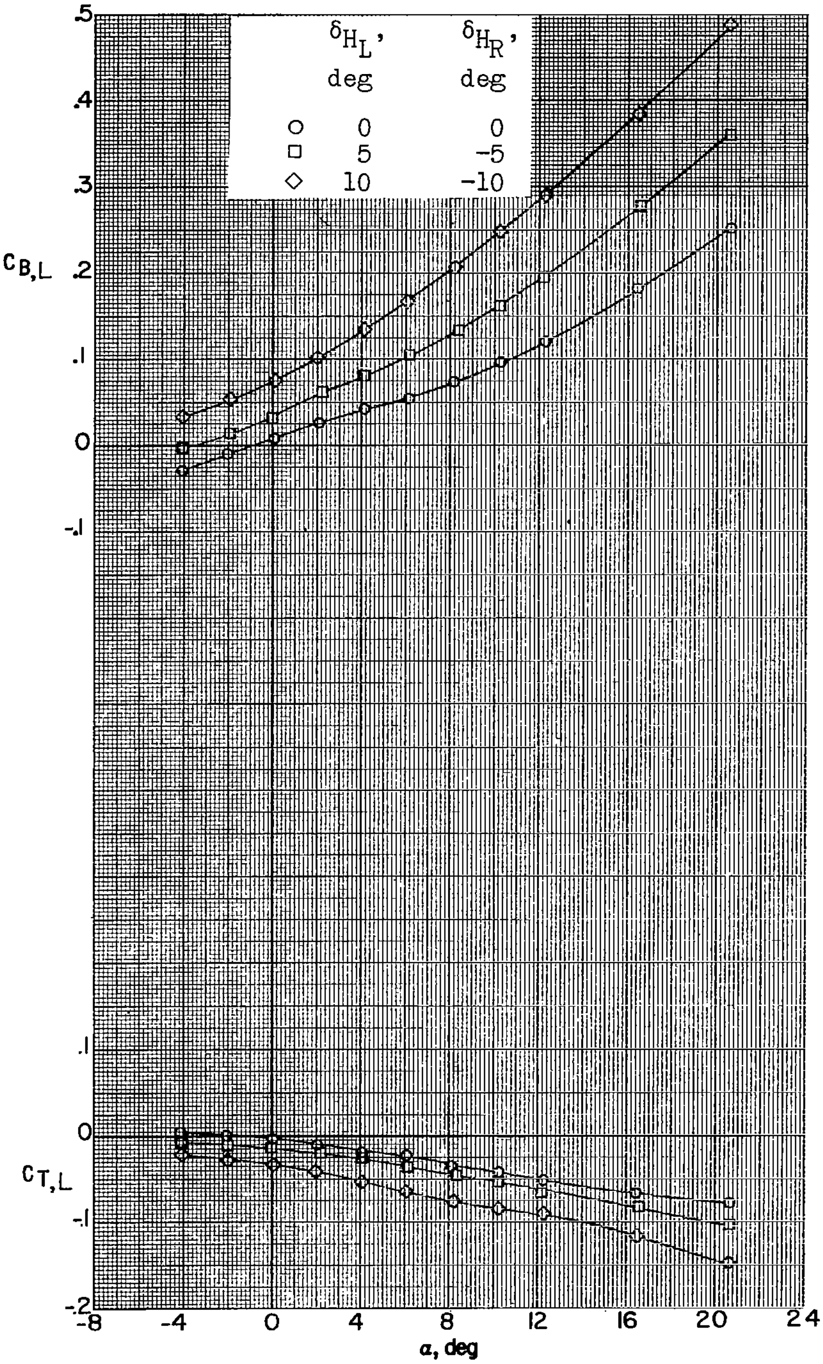

(f) $M = 4.65$; $\beta = 0.1^{\circ}$.

Figure 49.- Continued.

L-229

[redacted]

L-229

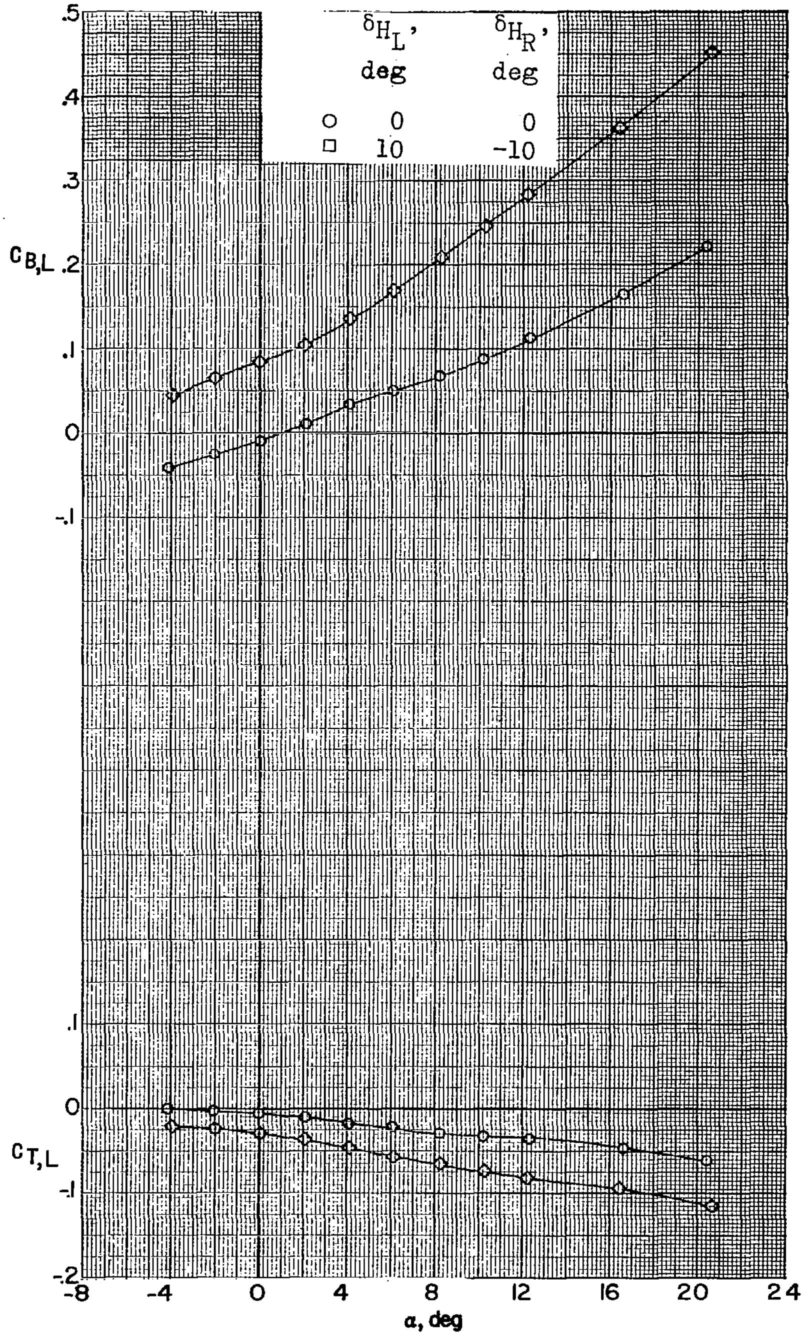

(g) M = 4.65; β = -5.1°.

Figure 49.- Continued.

[redacted]

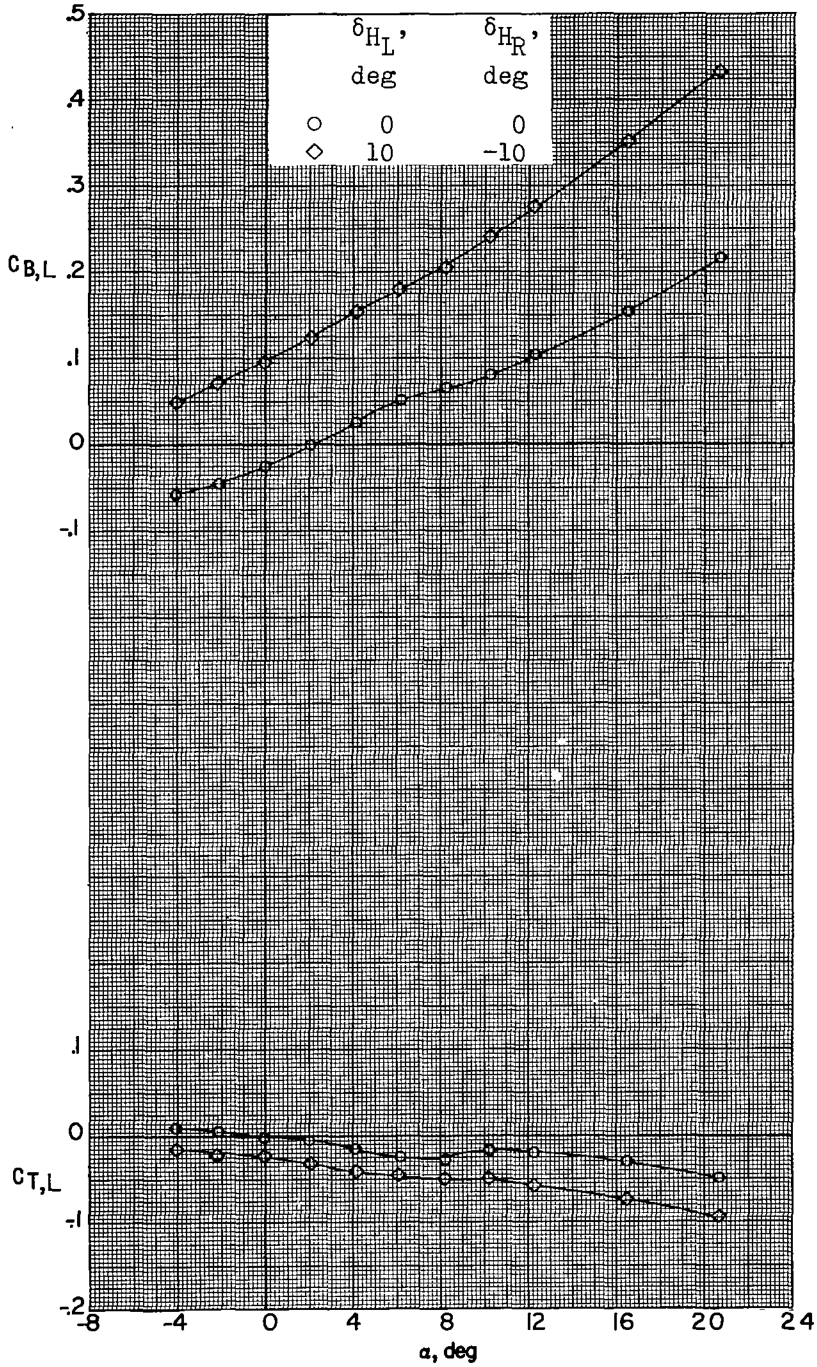

(h) $M = 4.65$; $\beta = -10.6^{\circ}$.

Figure 49.- Concluded.

L-229

[redacted]

[redacted]

L-229

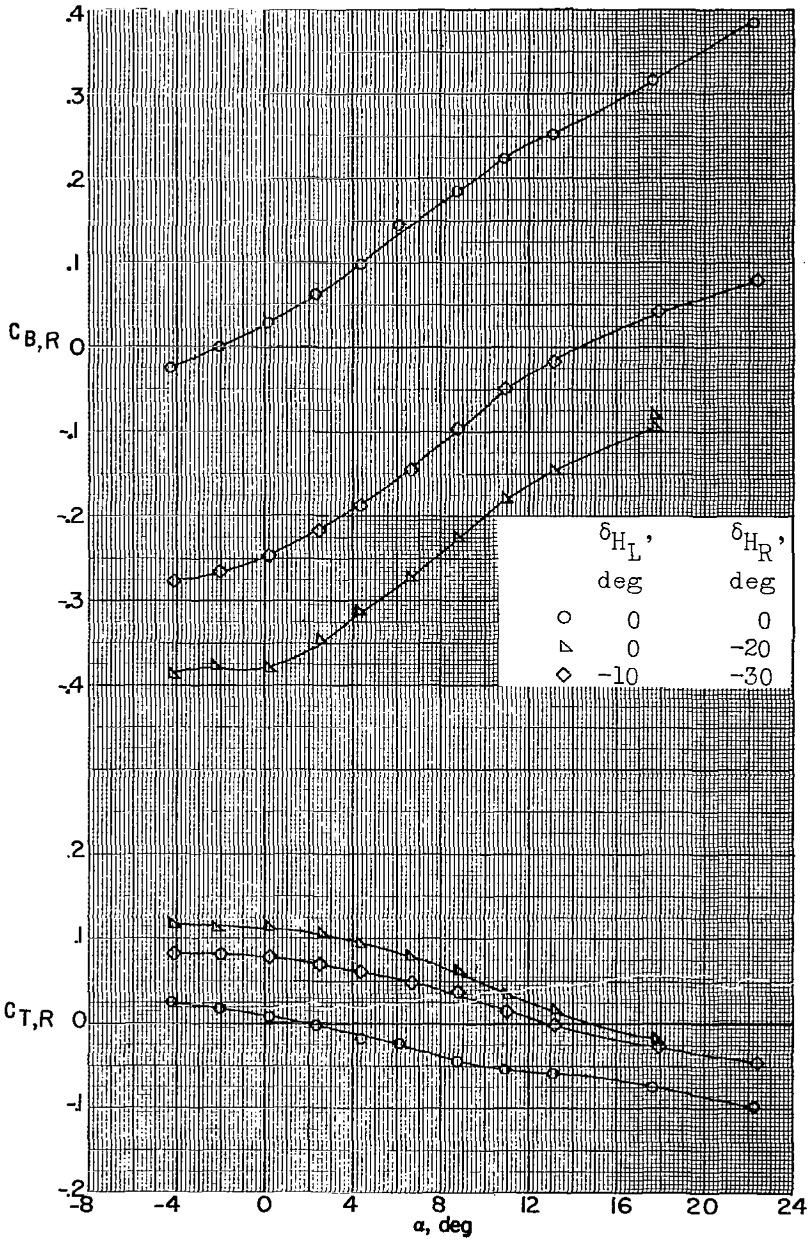

(a) M = 2.29; β = 0°.

Figure 50.- Bending- and torsion-moment characteristics of the right horizontal-tail panel of a 0.067-scale model of the X-15 airplane with roll- and pitch-control deflections of the left and right panels of the horizontal tail.

[redacted]

[redacted]

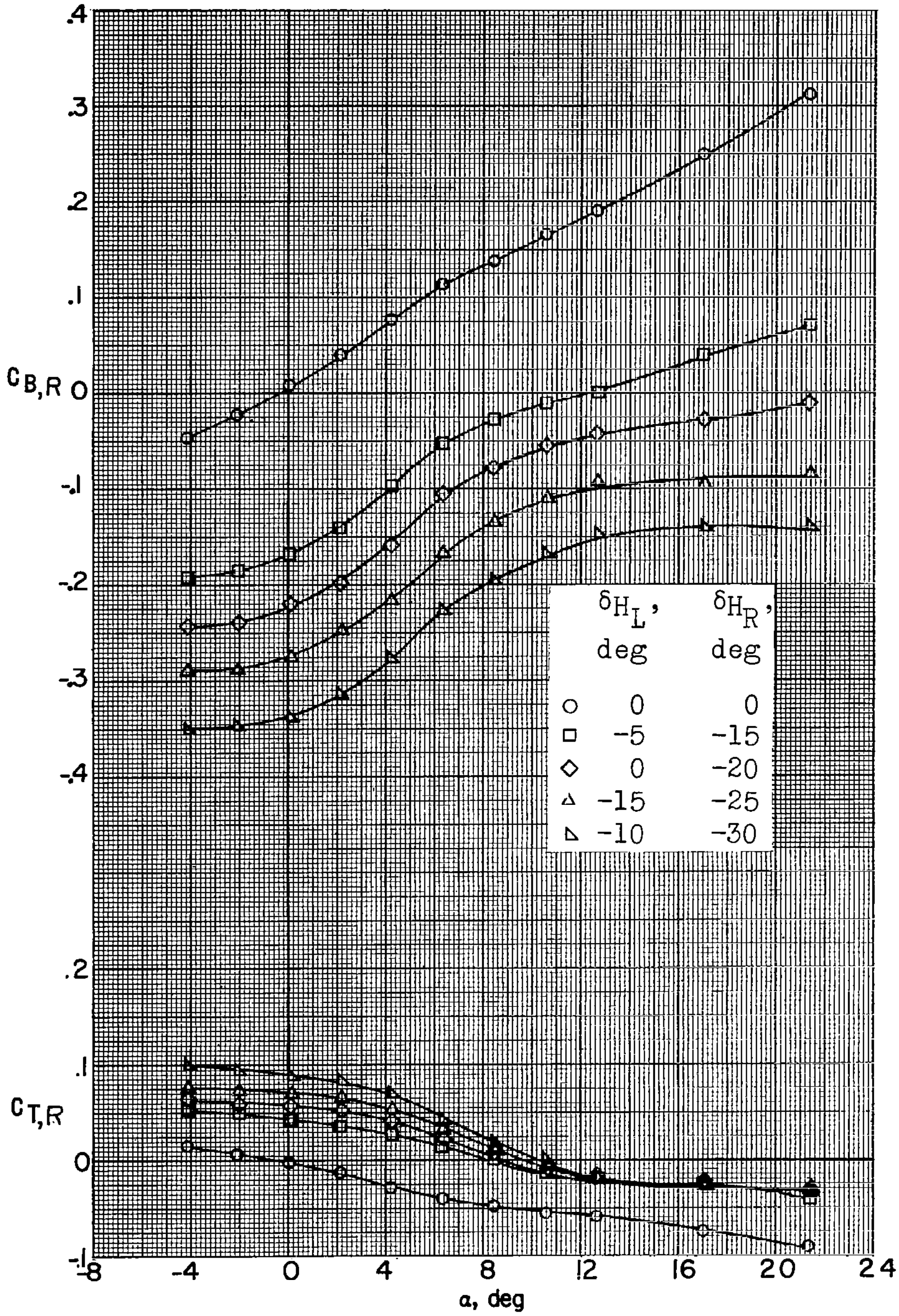

(b) M = 2.98; β = 0°.

Figure 50.- Continued.

[redacted]

L-229

L-229

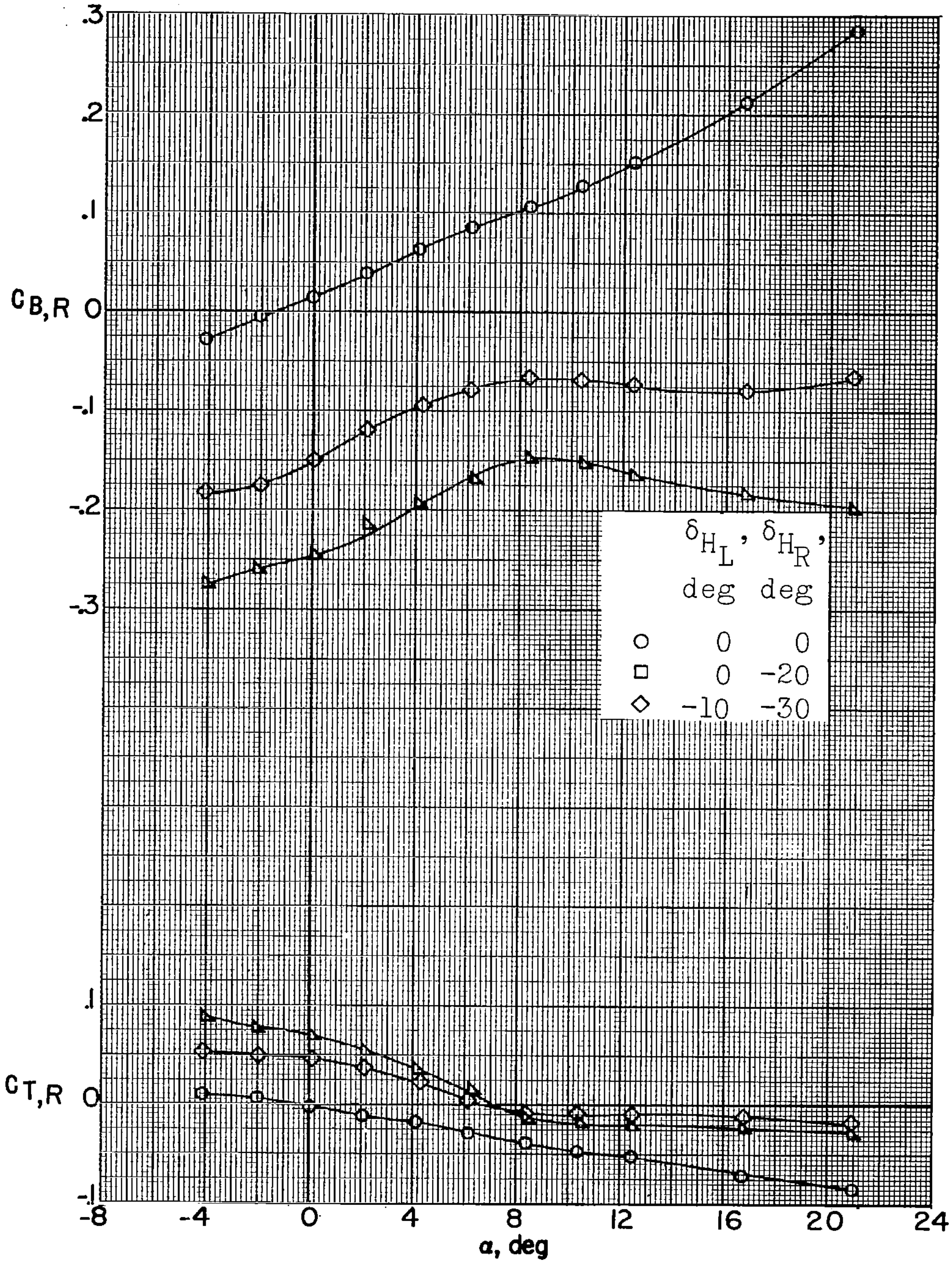

(c) $M = 3.96$; $\beta = 0^{\circ}$.

Figure 50.- Continued.

[redacted]

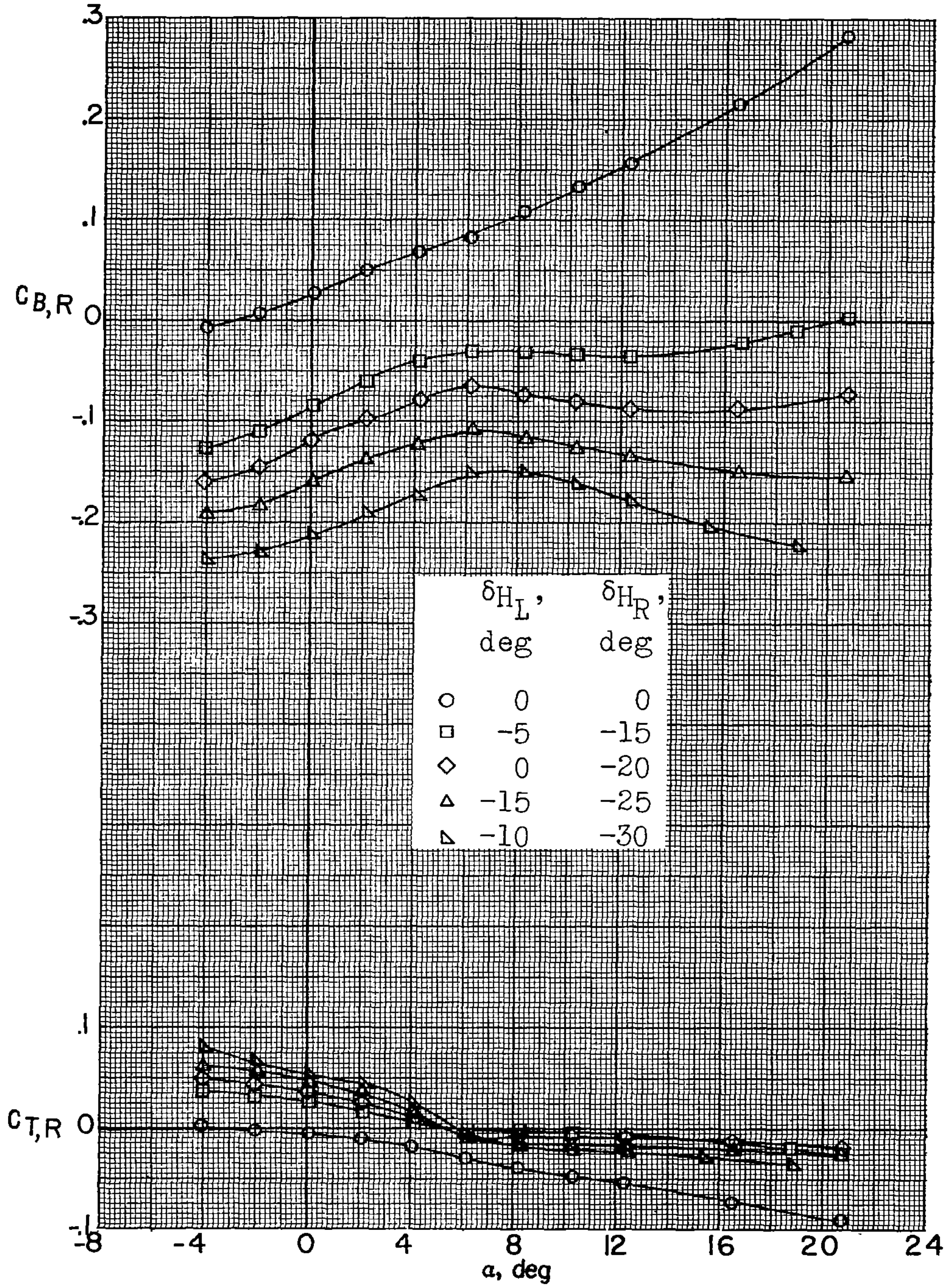

(d) $M = 4.65$; $\beta = 0.1^{\circ}$.

Figure 50.- Concluded.

L-229

[redacted]

[redacted]

L-229

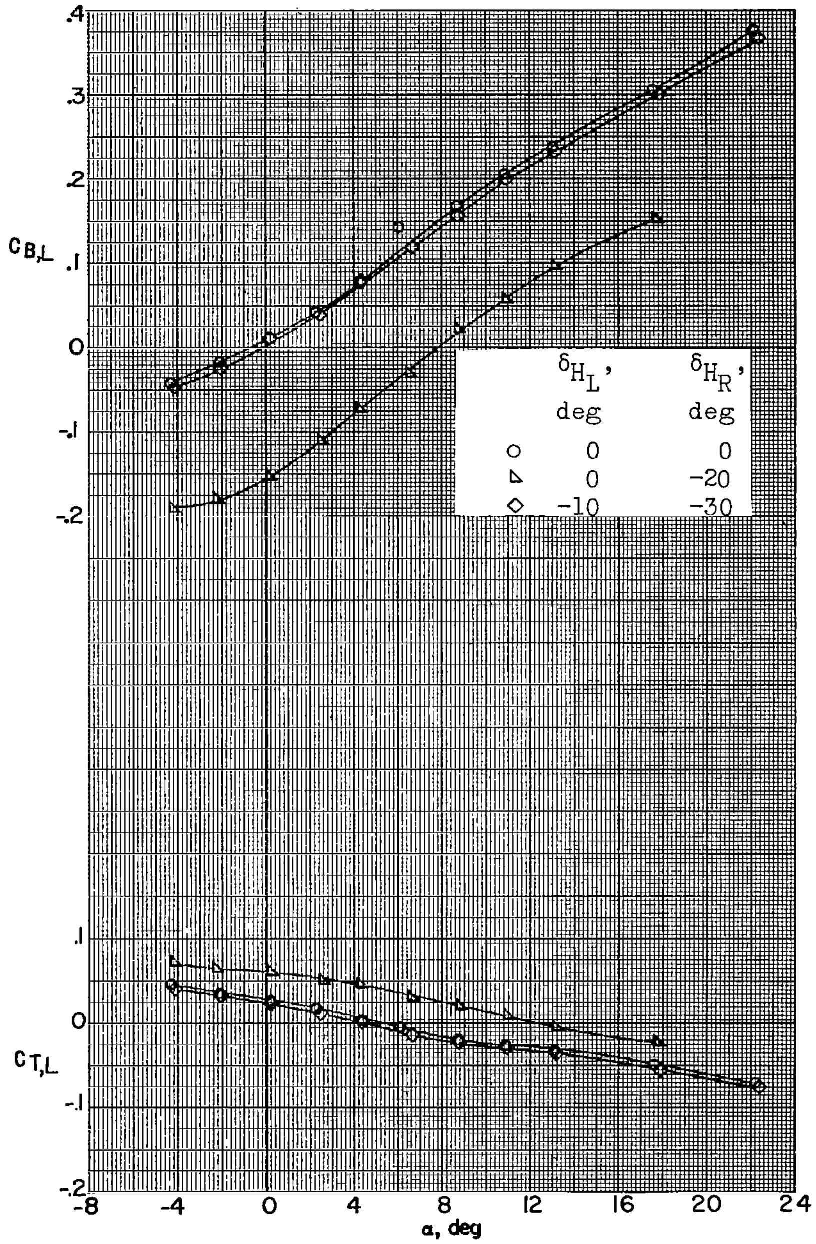

(a) $M = 2.29$; $\beta = 0^{\circ}$.

Figure 51.- Bending- and torsion-moment characteristics of the left horizontal-tail panel of a 0.067-scale model of the X-15 airplane with roll- and pitch-control deflections of the left and right panels of the horizontal tail.

[redacted]

[redacted]

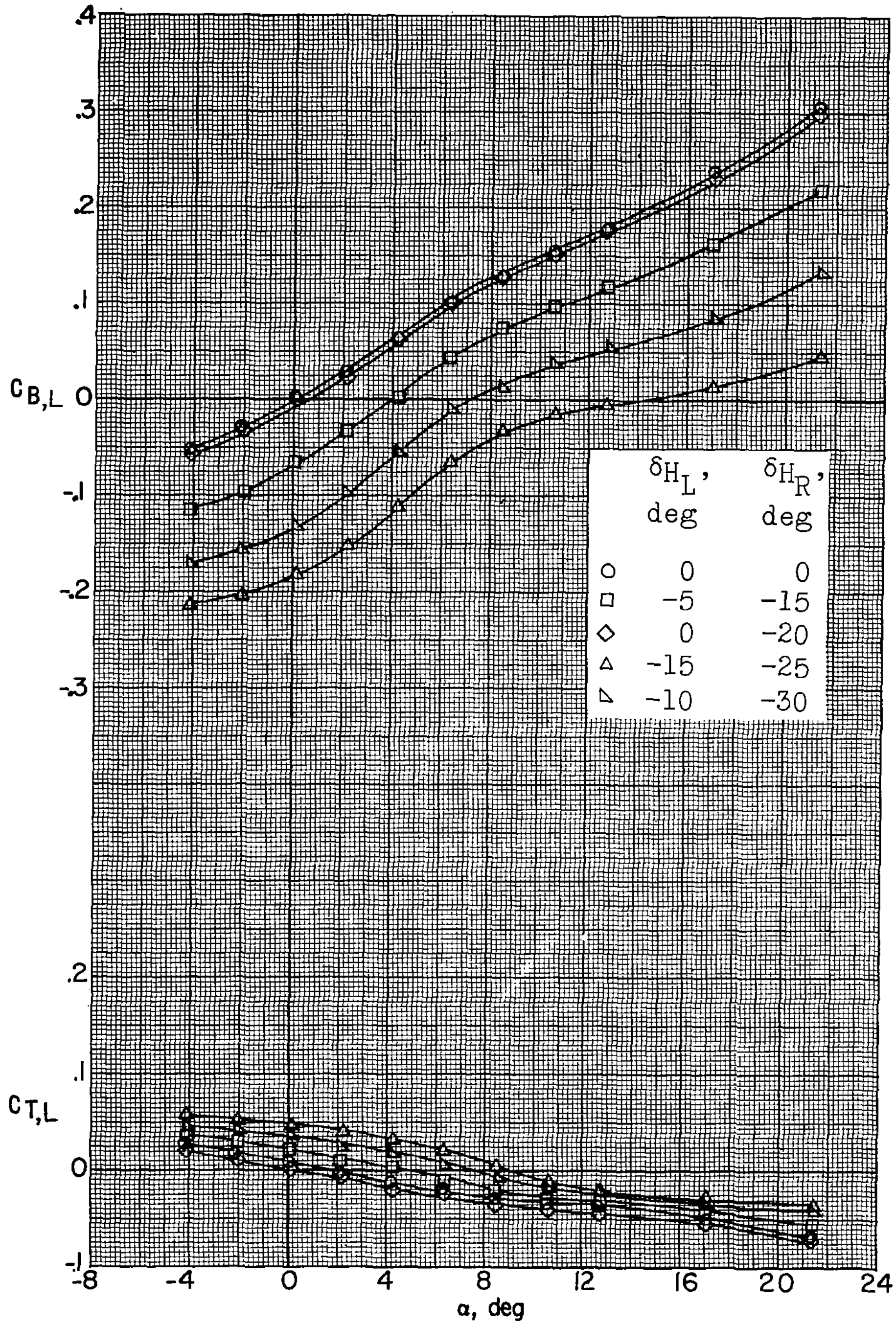

(b) $M = 2.98$; $\beta = 0^{\circ}$.

Figure 51.- Continued.

[redacted]

[redacted]

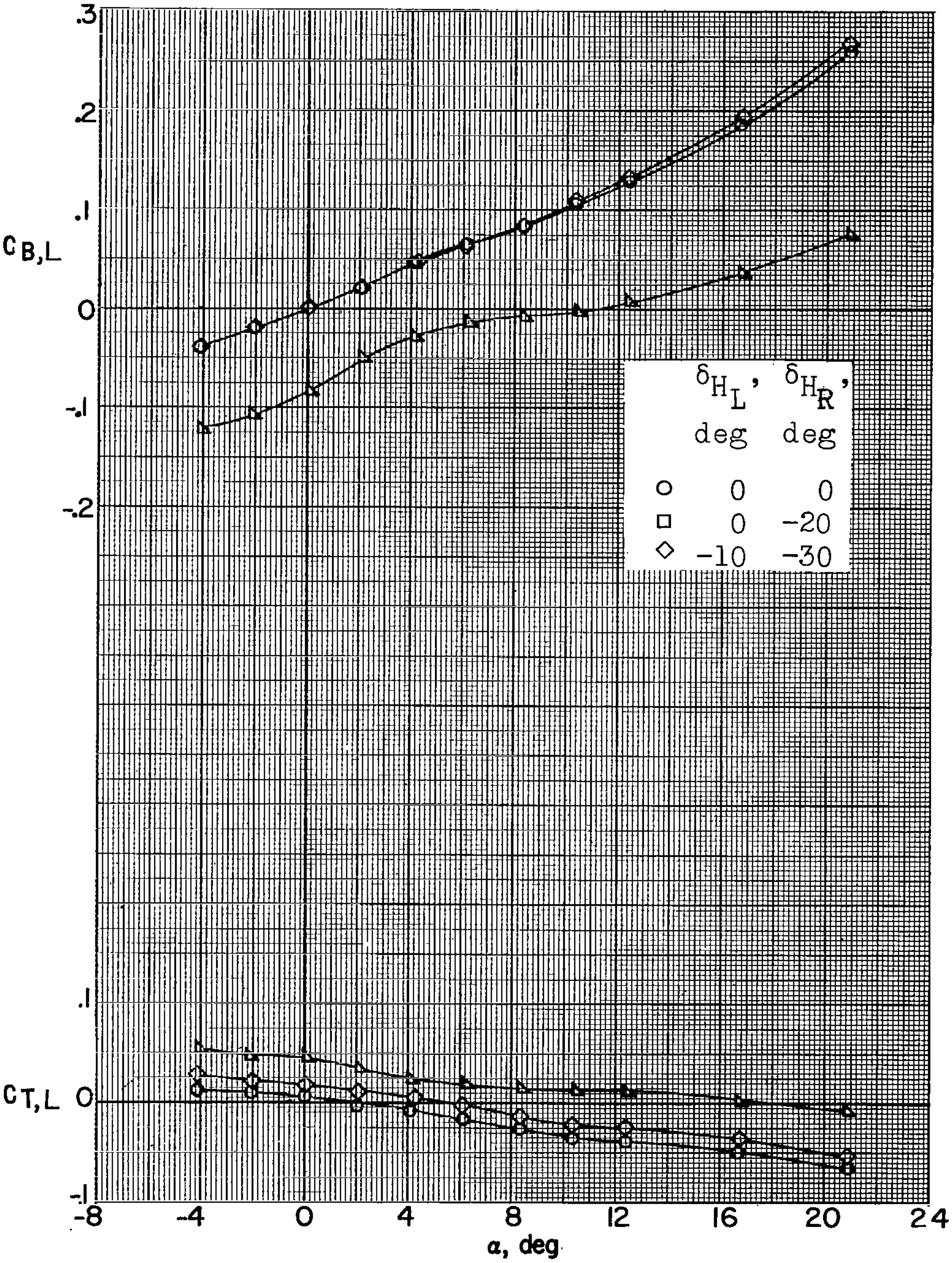

(c) M = 3.96; β = 0°.

Figure 51.- Continued.

[redacted]

[redacted]

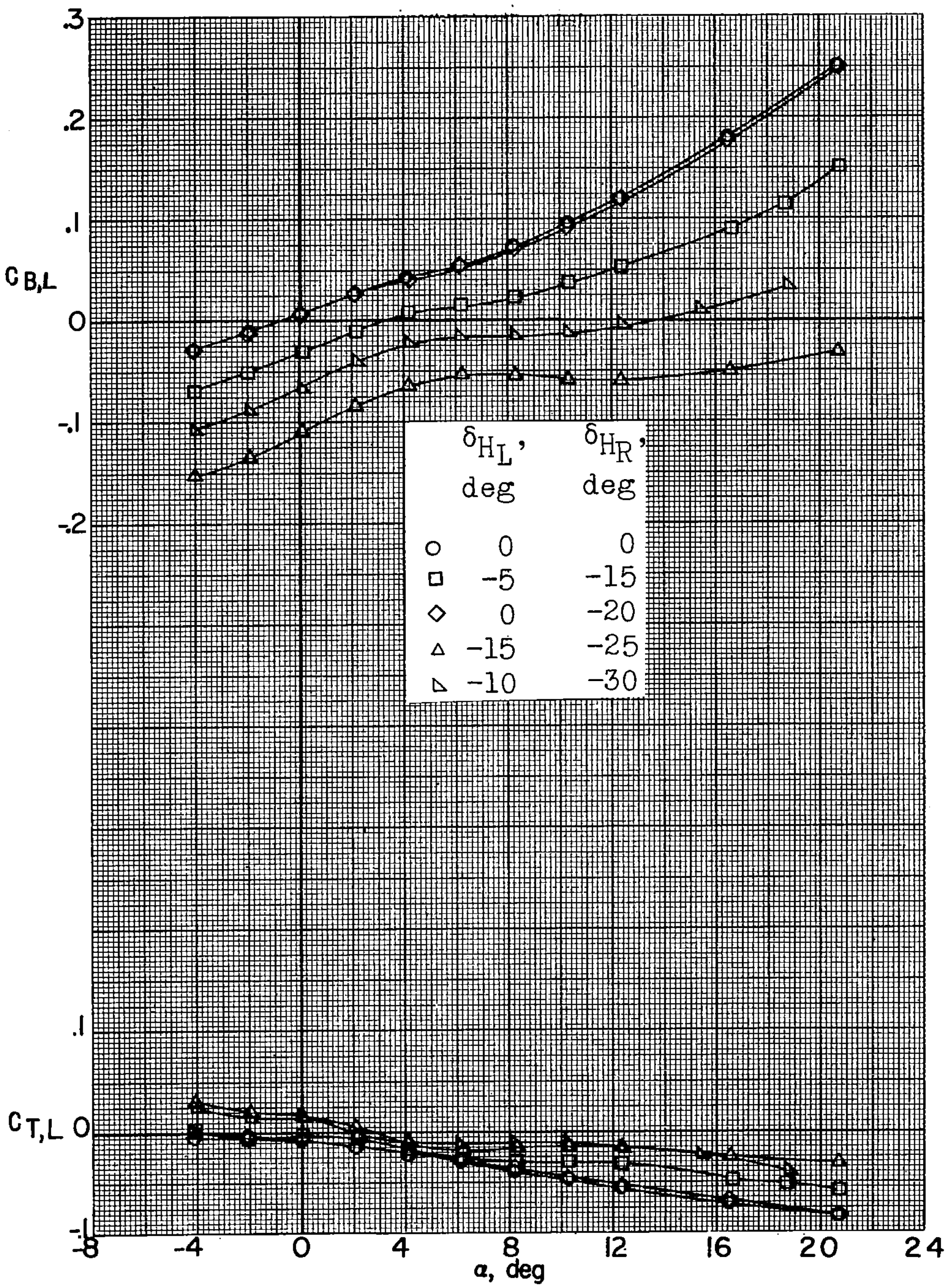

(d) $M = 4.65$; $\beta = 0.1^{\circ}$.

Figure 51.- Concluded.

L-229

[redacted]